# Volatile organic compound fluxes and mixing ratios in two contrasting atmospheric environments: London and the Amazon rainforest

Amy C. Valach

BSc. (Hons)

July 2015

Lancaster Environment Centre

Faculty of Science and Technology

Lancaster University

This thesis is submitted in fulfilment of the requirements for the degree of Doctor of Philosophy.

## Declaration:

I confirm that this work is my own, except where otherwise stated, and has not been submitted for a higher degree elsewhere. Excerpts of this thesis have been published in journals, as indicated within.


Amy Valach


July 2015

# Acknowledgements

First and foremost I would like to thank my supervisors, Nick Hewitt (Lancaster University), Ben Langford and Eiko Nemitz (CEH Edinburgh), and Rob MacKenzie (University of Birmingham) for sharing their vast knowledge and enthusiasm with me, providing guidance, support and for their endless patience: Rob, for his shared love of statistical correctness and his creative expressions, Eiko, for imparting his impressive range of theoretical understanding and practical experience, Ben, for sharing his secrets of LabView and in general how to successfully transition from using a quadrat to a mass spectrometer with all the steps in between, and finally, Nick, for helping me to see the forest for all the trees, his unique ability to explain complex subjects in comprehensible terms and of course his warm encouragement and patience. I'm very lucky to have Nick here to help me complete my thesis. I wish him many more years of exciting and safe expeditions in our shared passion for mountaineering. Berg heil!

I would like to thank Annette Ryan, Brian Davison, Emily House, Marvin Shaw, and Joe Acton, as well as many staff at CEH Edinburgh, University of York (WACL), and colleagues during the ClearfLo, ECLAIRE and CLAIRE-UK campaigns for their technical skills, support, helpful discussions and good company.

Special thanks go to Joe, Marv, Tom Pugh, Paul Young, Andy Jarvis, Robin Frost, Matt Barnes and Oliver Wild and many others in the Atmospheric Science theme group for providing a nurturing and exciting research environment, as well as many members of the Tropical Ecology theme group, Jos, Erika, Bob, Natalie, Fabricio and of course Fillipe, for introducing me to Brazilian Portuguese, culture, expressions, and supporting me with my research in Brazil.

A big thank you goes to all my fellow office mates of LG504 and LG505, Lucas, Matt, Joe, Shane, Anna, Robin, Anni, Victor, Dan, Nicki, Whaley, Nando, Chris, Laura, Jenni and countless more for indulging my office Xmas dinners and for welcome distractions, tea and much cake.

# Volatile organic compound fluxes and mixing ratios in two contrasting atmospheric environments: London and the Amazon rainforest

Amy C. Valach BSc. (Hons)

July 2015

## Abstract

Volatile organic compounds (VOCs) from biogenic and anthropogenic sources are important constituents of the atmosphere with effects on air quality and climate. Current uncertainties in measurements and models relate to their roles in tropospheric ozone and secondary organic aerosol formation, yet there have been few measurements of their fluxes from contrasting chemical environments. Additional measurements with greater spatial and temporal resolutions are required to constrain uncertainties in atmospheric chemistry and climate models.

This thesis presents long-term measurements of VOC fluxes and concentrations in two contrasting environments: central London and the Brazilian Amazon. VOC concentrations were quantified by proton transfer reaction-mass spectrometry and fluxes were calculated using the virtual disjunct eddy covariance method over a period of several months at sites in central London and the Amazon rainforest.

In central London, traffic was found to be the main source of aromatic compounds. Oxygenated compounds and isoprene showed strong correlations with light and temperature, suggesting biogenic, evaporative, or secondary atmospheric origins. The seven VOCs measured in central London had a five-month average total emission rate of 1.4 mg m$^{-2}$ h$^{-1}$. Comparisons with local and national emission inventories showed that modelled emissions were largely underestimated.

Measurements of isoprene and monoterpenes at the remote ZF2 site in the Amazon rainforest showed an 11-month average total emission rate of 2.7 mg m$^{-2}$ h$^{-1}$ with considerable seasonal variation, which could not be accurately reproduced using the light and temperature based MEGAN algorithms.

This thesis presents the first long-term VOC flux measurements providing information at high temporal resolutions on seasonal variability at an urban site and a pristine tropical forest site. They confirm that the Amazon rainforest is an extremely strong source of reactive carbon to the Earth's atmosphere exceeding emissions from a developed megacity, such as London, per unit area.

# Contents

# List of Figures and Tables

\*        \*        \*

# Nomenclature

## Latin alphabet

| | | |
|---|---|---|
| $a$ | Solar angle | ° |
| $c$ | Scalar mixing ratio | ppbv |
| $C_L$ | Dimensionless light adjustment factor | |
| $c_{L1}$ | Light adjustment empirical coefficient | 1.066 |
| $c_P$ | Specific heat capacity of air | 1246 J kg$^{-1}$ K$^{-1}$ |
| $C_T$ | Dimensionless temperature adjustment factor | |
| $c_{T1}$ | Empirical coefficient | 95000 J mol$^{-1}$ |
| $c_{T2}$ | Empirical coefficient | 230000 J mol$^{-1}$ |
| $C_{T1}$ | Empirical coefficient | 80 |
| $C_{T2}$ | Empirical coefficient | 200 |
| $d$ | Displacement height | $2/3 \times z_H$ m |
| $D$ | Molecular diffusion | m$^2$ s$^{-1}$ |
| $D_0$ | Foliar density | kg m$^{-2}$ |
| $E$ | Electric field strength | V cm$^{-1}$ |
| $E_{opt}$ | MEGAN variable | K |
| $F$ | Flux | mg m$^{-2}$ h$^{-1}$ |
| $F_h$ | High frequency flux attenuation scaling factor | |
| $f_m$ | Frequency of the logarithmic cospectral peak | s$^{-1}$ |
| $g$ | Acceleration due to gravity | m s$^{-2}$ |
| $h$ | Planck constant | $6.62606 \times 10^{-34}$ J s$^{-1}$ |
| $H$ | Sensible heat flux | W m$^{-2}$ |
| $i(R^+)$ | Product ion signal | cps |
| $I(RH^+)_{norm}$ | Normalised ion counts | ncps |
| $i_{ox}$ | Concentration ratio of isoprene oxidation products to isoprene | ppbv ppbv$^{-1}$ |
| $k$ | Reaction rate constant | cm$^3$ molecule s$^{-1}$ |
| $K$ | von Karman's constant | 0.4 |
| $L$ | Obukhov length | m |
| $LAI$ | Leaf area index | m$^2$ m$^{-2}$ |
| $N$ | Buffer gas density | molecules cm$^{-3}$ |
| $n_m$ | Normalized frequency of the logarithmic co-spectral peak (neutral and unstable conditions) | 0.085 s$^{-1}$ |
| $P_{ac}$ | Above-canopy PAR flux | μmol m$^{-2}$ s$^{-1}$ |
| $P_{daily}$ | Daily average above-canopy PAR flux | μmol m$^{-2}$ s$^{-1}$ |
| $P_{toa}$ | PAR flux at the top of the atmosphere | μmol m$^{-2}$ s$^{-1}$ |
| $Q$ | Photosynthetically active radiation flux | μmol m$^{-2}$ s$^{-1}$ |
| $R$ | Gas constant | 8.314 J K$^{-1}$ mol$^{-1}$ |
| $[R]$ | Density of neutral compound | cps |
| $RH^+$ | Protonated compound | cps |
| $Re$ | Reynolds number | |
| $S$ | Source and sink terms | |
| $S_N$ | Normalised sensitivity | ncps ppbv$^{-1}$ |
| $t$ | Time | s |
| $T$ | Ambient air temperature | °C, K |
| $T_{daily}$ | Daily average air temperature | K |
| $T_{hr}$ | Hourly average air temperature | K |
| $T_L$ | Leaf temperature | K |

| $t_{lag}$ | Lag time | s |
|---|---|---|
| $T_M$ | Empirical coefficient | 314 K |
| $T_{opt}$ | Optimal temperature variable (MEGAN) | K |
| $T_S$ | Leaf temperature at standard conditions | 303 K |
| $\Delta t_w$ | Vertical wind speed sampling interval | s |
| $u$ | Horizontal (longitudinal) wind velocity component | m s$^{-1}$ |
| $u_*$ | Friction velocity | m s$^{-1}$ |
| $U$ | Average longitudinal wind velocity component | m s$^{-1}$ |
| $U_{cor}$ | Coordinate corrected average longitudinal wind velocity component | m s$^{-1}$ |
| $U_{hor}$ | Horizontal wind speed | m s$^{-1}$ |
| $U_{tot}$ | Total wind speed | m s$^{-1}$ |
| $v$ | Lateral wind velocity component | m s$^{-1}$ |
| $V$ | Average lateral wind velocity component | m s$^{-1}$ |
| $(h)v$ | Frequency (here used in conjunction with $h$ to describe the energy, $E$, of a charged atomic oscillator | s$^{-1}$ |
| $V_{cor}$ | Coordinate corrected average lateral wind velocity component | m s$^{-1}$ |
| $VMR_{stand}$ | Gas standard volume mixing ratio | ppbv |
| $w$ | Vertical wind velocity component | m s$^{-1}$ |
| $W$ | Average vertical wind velocity component | m s$^{-1}$ |
| $W_{cor}$ | Coordinate corrected vertical wind velocity component | m s$^{-1}$ |
| $wd$ | Wind direction | ° |
| $ws$ | Wind speed | m s$^{-1}$ |
| $x$ | Longitudinal Cartesian coordinate | |
| $x_1$ | MEGAN temperature variable | K$^{-1}$ |
| $y$ | Lateral Cartesian coordinate | |
| $z$ | Vertical Cartesian coordinate | |
| $z_0$ | Roughness length | m |
| $z_H$ | Canopy height | m |
| $z_m$ | Measurement height | m |

$$* \quad * \quad *$$

# Greek alphabet

| $\alpha$ | Empirically derived constant | 0.0027 |
|---|---|---|
| $\alpha_1$ | Surface layer stratification constant | 7/8 |
| $\gamma$ | Dimensionless PAR and temperature activity adjustment factor for MEGAN algorithm | |
| $\gamma_0$ | Dimensionless PAR and temperature activity adjustment factor for G95 algorithm | |
| $\gamma_{age}$ | Dimensionless leaf age adjustment factor | |
| $\gamma_{CE}$ | Dimensionless canopy environment activity adjustment factor for MEGAN's PCEEA algorithm | |
| $\gamma_{LAI}$ | Dimensionless leaf area index adjustment factor | |
| $\gamma_P$ | Dimensionless photosynthetically active radiation adjustment factor | |
| $\gamma_{SM}$ | Dimensionless soil moisture adjustment factor | |
| $\gamma_T$ | Dimensionless temperature adjustment factor | |
| $\varepsilon$ | Canopy base emission rate at standard conditions | mg m$^{-2}$ h$^{-1}$ |
| $\varepsilon_0$ | Leaf basal emission rate at standard conditions | µg C g$^{-1}$ dry weight h$^{-1}$ |
| $\varepsilon'$ | Standard deviation of the PTR-MS noise | cps |

| $\zeta$ | Monin-Obukhov stability parameter | m m$^{-1}$ |
| $\eta$ | Deviation angle from x-axis of sonic anemometer | ° |
| $\theta$ | Deviation angle from z-axis of sonic anemometer | ° |
| $\pi$ | Constant ratio of circle's circumference to diameter | |
| $\rho$ | Dimensionless within-canopy production and loss factor | |
| $\rho_0$ | Density of air | 1.01 g m$^{-3}$ |
| $\sigma_v$ | Standard deviation of the lateral wind component | m s$^{-1}$ |
| $\sigma_w$ | Standard deviation of the vertical wind component | m s$^{-1}$ |
| $\tau$ | Momentum flux | N m$^{-2}$ |
| $\tau_c$ | Instrument related characteristic time constant | s |
| $\varphi$ | Dimensionless above-canopy PAR transmission | |

\*      \*      \*

# Abbreviations

| ACTRIS | Aerosols, Clouds, and Trace gases Research InfraStructure network |
| amu | Atomic mass unit |
| AHN | Automatic Hydrocarbon Network |
| AVG | Average lag time method |
| aVOC | Anthropogenic volatile organic compound |
| b/t | Benzene to toluene ratio |
| BC | Black carbon aerosol |
| bVOC | Biogenic volatile organic compound |
| *c-c* | Cross-correlation function |
| CALC | Calculated lag time method |
| CCN | Cloud condensation nuclei |
| CCZ | Congestion Charge Zone |
| CEH | Centre for Ecology and Hydrology |
| CESM | Community Earth System Model |
| CI | Chemical ionisation |
| CLM | Community Land Model |
| $CO_2$ | Carbon dioxide |
| cps | Counts per second |
| DEC | Disjunct eddy covariance |
| Defra | Department for Environment, Food and Rural Affairs |
| DOY | Day of the Year |
| EBL | Equilibrium boundary layer |
| EC | Eddy covariance |
| EI | Electron impact ionisation |
| EU | European Union |
| FIS | Fast isoprene sensor |
| G95 | Guenther *et al.* 1995 algorithm |
| GAW | Global Atmosphere Watch |
| GC | Gas chromatography |
| GC-FID | Gas chromatography-flame ionisation detector |
| GC-MS | Gas chromatography-mass spectrometer |
| GLA | Greater London Area |
| $HO_2$ | Hydroperoxyl radical |
| $H_3O^+$ | Hydronium ion |
| INPA | National Institute for Amazonian Research |
| IPPC | Integrated Pollution Protection and Control |
| IQR | Interquartile range |
| ISOPOOH | Isoprene hydroxy hydroperoxides |

| | |
|---|---|
| K34 | Walk-up tower at km 34 at the ZF2 site |
| KCL | King's College London, Strand |
| LAEI | London Atmospheric Emissions Inventory |
| LAI | Leaf Area Index |
| LBA | Large Scale Biosphere-Atmosphere Experiment in Amazonia |
| LoD | Limit of detection |
| MACR | Methacrolein |
| MAX | Maximum lag time method |
| MEGAN | Model of Emissions of Gases and Aerosols from Nature |
| MEK | Methyl ethyl ketone |
| MID | Multiple ion detection |
| MRd | Marylebone Road |
| MVK | Methyl vinyl ketone |
| $m/z$ | Mass to charge ratio |
| NAEI | National Atmospheric Emissions Inventory |
| ncps | Normalised ion counts per second |
| NK | North Kensington |
| NMVOC | Non-methane volatile organic compound |
| NO | Nitric oxide |
| $NO_2$ | Nitrogen dioxide |
| $NO_x$ | Oxides of nitrogen |
| $O_3$ | Ozone |
| OD | Outer diameter of PFA or PTFE tubing |
| OH | Hydroxyl radical |
| PAR | Photosynthetically active radiation |
| PCEEA | Parameterised canopy environment emission activity |
| PFA | Perfluoroalkoxy alkanes |
| PFT | Plant functional type |
| POCP | Photochemical ozone creation potential |
| POM | Particulate organic matter |
| ppbv | Parts per billion |
| ppmv | Parts per million |
| pptv | Parts per trillion |
| PTR-MS | Proton transfer reaction-mass spectrometer |
| PTR-ToF-MS | Proton transfer reaction- time of flight- mass spectrometer |
| PTFE | Polytetrafluoroethylene |
| RMS | Root Mean Square deviation |
| R | Generic hydrocarbon |
| $RO_2$ | Alkyl peroxy radical |
| sccm | Standard $cm^3 \ m^{-1}$ |
| SD | Standard deviation |
| SEM | Secondary electron multiplier |
| SNAP | Selected Nomenclature for sources of Air Pollution |
| SOA | Secondary organic aerosol |
| spp. | (Multiple) species |
| TT34 | Triangular mast at the ZF2 site |
| TYP | Typical lag time method |
| UK | United Kingdom |
| vDEC | Virtual disjunct eddy covariance |
| VIS | Visual lag time method |
| VMR | Volume mixing ratio |
| VOC | Volatile Organic Compound |
| WMO | World Meteorological Organization |
| WRF | Weather Research and Forecasting |
| ZA | Zero air (VOC-free air) |

ZF2              LBA measurement site near Manaus, Brazil

# Chapter I

## 1 Introduction

Non-methane volatile organic compounds (VOCs) are a group of organic hydrocarbons that have a high vapour pressure at standard conditions which results in a very low boiling point and hence sublimate or evaporate into the atmosphere. VOCs include a wide range of compounds and are ubiquitous, originating from both biogenic and anthropogenic sources. Biogenic sources represent the majority of VOCs globally emitted into the atmosphere. Terrestrial plant foliage is estimated to be the primary source of biogenic VOCs, however there are other minor sources including microbes, animals and aquatic organisms (Wagner *et al.*, 1999). Isoprene is the dominant component of non-methane VOCs with estimated biogenic emissions of approx. 600 TgC a$^{-1}$ globally (Guenther *et al.*, 2006), 90% of which are attributed to tropical and temperate broadleaf tree and shrub species. Monoterpenes account for the second largest contribution of bVOCs to the atmosphere and dominate over boreal forests (Levis *et al.*, 2003).

Anthropogenic VOCs sources constitute a much smaller component of total VOCs. In the urban and suburban environment aVOCs primarily originate from vehicle emissions consisting of either direct emissions from vehicle exhaust or other traffic related sources (Kansal, 2009; Na *et al.*, 2005). The latter are mainly hot-soak emissions during engine cooling (Na *et al.,* 2004; Rubin *et al.*, 2006) and evaporative emissions from petroleum products (Srivastava *et al.*, 2005). Industrial processes such as manufacturing, storage and transport of petroleum and solvent containing products, but also instances of biomass burning for domestic use or agriculture, provide localized emission sources, which combined are important on a global scale (Piccot *et al.*, 1992). Significant anthropogenic compounds include benzene and toluene, but also chlorofluorocarbons and other toxic or banned compounds like MTBE (methyl *tert*-butyl ether).

Many ubiquitous compounds, especially oxygenated VOCs such as acetone and methanol have a variety of anthropogenic and biogenic sources, as well as originating from secondary atmospheric formation since they constitute the oxidation products of other compounds.

VOCs emitted by biogenic and anthropogenic sources affect atmospheric composition and chemistry, and thus have important roles in modifying air quality and climate through various mechanisms. In air quality VOCs can either be directly detrimental to humans and the environment through their toxicity or by acting as a carcinogen (e.g. benzene), or indirectly by forming secondary pollutants such as tropospheric ozone ($O_3$) which causes oxidative damage to human and plant tissues (Lippman, 1993).

Direct and indirect effects of VOCs on climate occur via mechanisms affecting the oxidative capacity of the atmosphere and changing the radiative balance. Many VOCs take part in the formation of secondary organic aerosols (SOA), which affect cloud formation and hence the radiative balance. The oxidative capacity of the troposphere depends on hydroxyl radical (OH) concentrations. Compounds such as $O_3$ and OH determine the oxidation potential, of which VOCs are a key factor, therefore affecting the atmospheric chemistry and its feedbacks on climate. Examples of feedbacks between climate change and atmospheric chemistry include enhanced stratospheric-tropospheric exchange of $O_3$, frequent periods with stable conditions causing pollution accumulation over industrial and urban areas, enhanced temperature-induced biogenic emissions, as well as increasing the lifetime of greenhouse gases by removing OH.

Many biogenic VOC emissions are driven by light and temperature and therefore climate change induced changes in temperature and intercepted radiation will affect VOC emission rates. This example highlights the importance of quantifying VOCs to better understand the possible effects of climate feedbacks (Beerling *et al.,* 2007). VOCs can photolyse forming intermediate radicals, react with OH radicals, $NO_3$ radicals, and $O_3$. Depending on the photochemical regime of the environment, VOCs act as a precursor to net $O_3$ formation when concurrent with oxides of nitrogen ($NO_x$), however in $NO_x$-limited regimes $O_3$ reacts with OH and $HO_2$ radicals which forms

additional loss processes (Atkinson, 2000). The modelling of VOC chemical pathways in the atmosphere is highly complex and although progress has been made using chamber experiments, more field observations are necessary to constrain uncertainties and identify potential gaps in our understanding of VOC chemistry under atmospheric conditions (Lelieveld *et al.,* 2008).

There are large uncertainties in estimating global VOC fluxes; however, there are now methods which allow these estimates to be constrained. These include bottom-up inventories, which are based on computer models and algorithms to scale up local observations to estimate regional or global emissions, and the top-down approaches consisting of direct measurements at larger ecosystem or regional scales, or employing remote sensing techniques.

Bottom-up model predictions depend on accurate input variables such as meteorological and surface exchange processes, which are supplied by emission inventories. Most governments provide a national inventory on a range of pollutants. The National Atmospheric Emissions Inventory (NAEI) provides gridded emission estimates for a range of air pollutants and heavy metals in the UK. Total VOCs are reported with compounds that are directly harmful, i.e. benzene and 1,3-butadiene being given separate attention. Emission estimates for nonpoint sources are calculated by multiplying an emission factor (e.g. kilograms of pollutant per volume of fuel consumed) by an activity statistic (e.g. amount of fuel consumed per year) (NAEI, 2014). There are large uncertainties involved in the estimates which depend on the accuracy of the statistical information used.

Top–down approaches include data acquisition using remote sensing techniques, e.g. the use of formaldehyde observations to constrain isoprene emission estimates (Guenther *et al.*, 2006). Remote sensing techniques are less effective in regard to most VOCs due to the insufficiently strong IR/UV-Vis spectra to be detectable at ambient concentrations. Therefore, direct quantification of ecosystem scale VOC fluxes is necessary to help constrain regional and global models. These data are then used to develop surface parameterizations which provide area-integrated flux estimates on regional to global scales.

Accurately quantifying VOC fluxes using direct measurement techniques requires a good understanding of the transport and surface exchange mechanisms within the boundary layer which has given rise to a variety of methods to quantify a range of different VOC species. The most common are eddy resolving methods which rely on sufficient turbulence for the exchange of VOC fluxes within the boundary layer. The recent development of commercial proton transfer reaction – mass spectrometers (PTR-MS) provided an instrument with sufficient temporal resolution for eddy resolving methods (Lindinger *et al.*, 1998). Virtual disjunct eddy covariance (vDEC) is a recently developed technique using PTR-MS as it requires high frequency measurements of both the micrometeorology and the VOC scalar (Karl *et al.*, 2002; Rinne *et al.*, 2001).

This thesis aims to compare and contrast a suite of anthropogenic and biogenic VOC fluxes and concentrations from fundamentally different environments with contrasting chemical regimes and sources: a European megacity with diverse anthropogenic sources but also with green space that might contribute biogenic VOCs; and a pristine forest canopy in the world's largest tropical biome where anthropogenic influences are minimal. To achieve this, a range of VOC fluxes were measured in London and a remote site in the Amazon basin in Brazil using a PTR-MS in conjunction with the vDEC technique. This thesis is structured into the following chapters/ papers:

I. Application of PTR-MS and validation by direct instrument comparison of VOC concentration measurements by GC-FID in a chemically complex urban environment (Paper I),

II. application of VOC flux measurements over a range of different canopy types such as urban (Paper II) and remote forest (Paper III) using virtual disjunct eddy covariance,

III. comparison of measured fluxes with modelling approaches of biogenic emissions (Papers II and III), urban emissions inventories (Papers I and II), and flux footprints (Papers II and III),

IV.        and comparison and discussion of VOC fluxes and concentrations from anthropogenic versus biogenic sources at the two measurement sites in London and Brazil (Chapter 7).

# Chapter II

# 2 Sources and effects of volatile organic compounds

## 2.1 Introduction to VOCs

Non-methane volatile organic compounds (VOC) are a group of organic compounds that are defined by a high vapour pressure of >0.01 kPa at 20 °C or a low boiling point <250 °C at standard atmospheric pressures of 101.3 kPa, although the classifications in legislation vary between countries (EC Directive 1999/13/EC). This definition includes semi-volatile organic compounds, which have a boiling point higher than water and can begin to vapourise at room temperature (20 °C) (EPA, 2014). These include persistent compounds, such as polycyclic aromatic hydrocarbons and compounds often associated with aerosol formation.

There are thousands of different VOC species in the atmosphere, originating from a range of distinct biogenic and anthropogenic emission sources or resulting from the chemical degradation of parent compounds by photolysis or oxidation (Figure 2.1) (Hewitt and Jackson, 2003). Each will contribute to the chemistry of the atmosphere, to a greater or lesser extent. The atmosphere is a highly energetic and oxidising medium, in which VOCs are oxidised ultimately to $CO_2$ and $H_2O$ if reactive intermediates are not removed by deposition. The dominant chemical reactions in the atmosphere and the precise oxidation routes depend on the presence of co-occurring compounds such as $NO_x$ and other reactive species, as well as environment-dependent variables such as light and temperature. This chapter will compare and contrast the main biogenic and anthropogenic VOC species, sources, emissions, and their importance in two distinct atmospheric environments, namely a pristine background forest environment and a polluted urban environment.
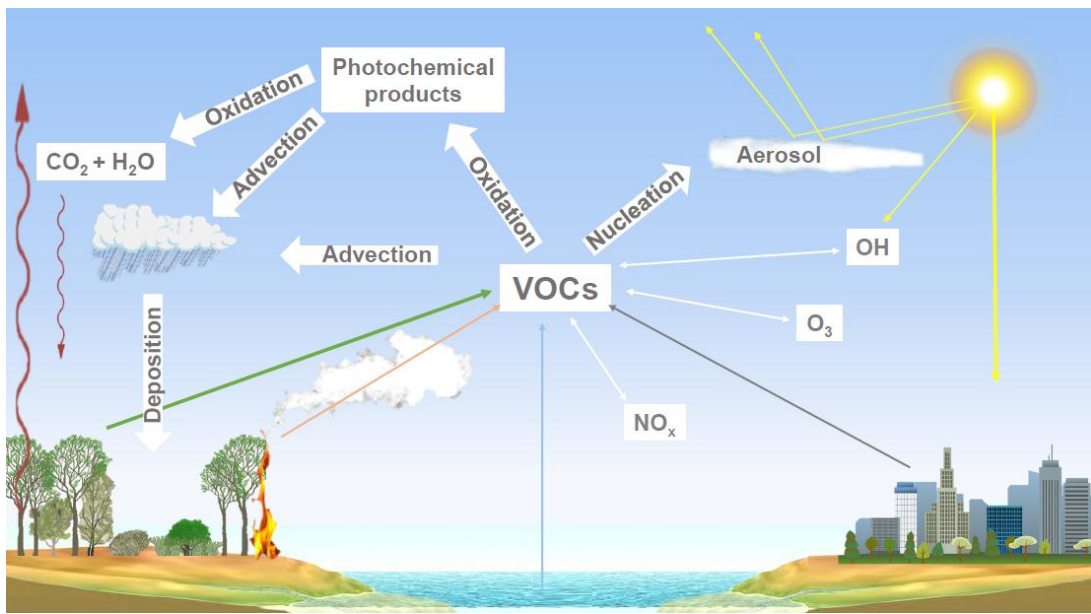
**Figure 2.1.** Diagram showing the main sources and sinks including reactions and processes of volatile organic compounds in the atmosphere with links to their effects in air quality and climate. Image adapted from Monks *et al.* (2009).

## 2.2 Biogenic VOCs

### 2.2.1 Emission sources and estimates

Many plant species emit VOCs into the atmosphere. Although some of these compounds fulfil protective and communication roles within plants and between plants and insect communities, not all the biological functions of bVOCs are clearly understood (Laothawornkitkul *et al.,* 2009).

Global bVOC emissions are believed to far exceed those of anthropogenic VOCs, with estimated emission rates of 1150 TgC $a^{-1}$ and 110 TgC $a^{-1}$, respectively (Guenther *et al.*, 1995; Piccot *et al.*, 1992). However, considerable uncertainties in both these values remain (Arneth *et al.*, 2008). Although bVOCs encompass a wide range of compounds, isoprene is the dominant component of non-methane VOCs both in terms of its mass emission rate and its effects on atmospheric chemistry, because of its considerable chemical reactivity. It has an estimated emission rate of approx. 500-700 TgC $a^{-1}$ globally (Guenther *et al.*, 2006). Terrestrial plant foliage, particularly broadleaf tree and shrub species are the major source of isoprene, accounting

7

for >90% of atmospheric isoprene levels. However, there are other minor sources including microbes, terrestrial animals, and aquatic organisms (Wagner *et al.*, 1999), as well as some anthropogenic sources such as tailpipe emissions from vehicles (Borbon *et al.*, 2001).

Biogenic isoprene emissions are controlled by the circadian rhythm and closely related to photosynthesis in plant biochemistry, but are driven by ambient light and temperature (Hewitt *et al.*, 2011; Monson *et al.*, 2012; Niinemets *et al.*, 1999; Wilkinson *et al.*, 2006). Tropical forests are the regions of largest natural isoprene emissions, although monoculture plantations of high emitting plant species can surpass canopy scale emissions from natural rainforests (Fowler *et al.*, 2011; Langford *et al.*, 2010a; Misztal *et al.*, 2011). Tropical forests experience a combination of high light and temperatures with the occurrence of expansive areas of broadleaf trees, which are, in general, high emitters of isoprene. Global isoprene emission estimate outputs from different models seem to converge around the value of 600 TgC a$^{-1}$. This may be due to significant commonalities in the methodologies used and the lack of observations against which emissions models can be validated and developed.

Monoterpenes account for the second largest contribution of bVOCs to the atmosphere and consist of a wide group of $C_{10}$-terpene compounds. Terpenes are a large group of organic hydrocarbons based on $C_5H_8$ subunits. Isoprene itself is considered a hemi-terpene and together they form the group of isoprenoids. Common monoterpenes include *α*- and *β*-pinenes, limonene, terpinolene, *α*-terpineol, camphene, etc. (Dewick, 1999). Emissions of monoterpenes are dominant above boreal forests and are often associated with natural fragrances (Levis *et al.*, 2003). Generally, monoterpene emissions are primarily temperature dependent, but leaf cuvette measurements (Staudt and Seufert, 1995), and field measurements (Ghirardo *et al.*, 2010; Langford *et al.*, 2010a; Misztal *et al.*, 2010; Taipale *et al.*, 2011) have indicated that for some compounds light is also a driver of emissions. It is not known if *de novo* emissions of monoterpenes are under circadian control, which would result in an indirect control of monoterpene emissions from leaf storage reservoirs. Global emission estimates range from as low as 36 Tg a$^{-1}$ (Arneth *et al.*, 2007a) to 144 Tg a$^{-1}$ (Guenther *et al.*, 1995) with a mean around 103

Tg a$^{-1}$ (Arneth *et al.*, 2008). The large variation in reported monoterpene emission estimates may be because the emission algorithms used are based on an exponential temperature dependency, which consequently becomes more sensitive to the leaf temperatures used. Alternatively, widely diverging values may be reported more openly (Le Quéré, 2006), acknowledging the lack of observational constraints and understanding of emission processes (Arneth *et al.*, 2008).

The emission rates of higher molecular weight biogenic compounds such as C$_{15}$-sesquiterpenes (e.g. *β*-caryophyllene, *β*-farnesene, *α*-bergamotene, etc.) are difficult to estimate on an ecosystem scale, as there are a number of analytical problems related to their very high chemical reactivity and their low vapour pressures. Similar to monoterpenes, sesquiterpene emissions are dominantly temperature dependent. Modelled emission estimates vary widely, as they are often based on leaf level and chamber measurements. Sesquiterpenes are so reactive in the atmosphere that they are not commonly present at concentrations that would make canopy-scale flux measurements possible. Scaled up enclosure measurements have indicated total emission rates of 7 mg m$^{-2}$ during the summer (Ortega *et al.*, 2007) and up to 40 mg m$^{-2}$ per month (Helmig *et al.*, 2007) over coniferous forests during the hottest months.

Other notable compounds of biogenic origin include oxygenated and other reactive species such as methanol, acetone, acetaldehyde, acetonitrile, methacrolein (MACR), methyl vinyl ketone (MVK), and methyl ethyl ketone (MEK) (Kesselmeier and Staudt, 1999). Primary emission sources include terrestrial and marine biota and anthropogenic emissions, which will be discussed separately below (Section 2.3), whereas some compounds (e.g. acetonitrile, MVK and MACR) have greater secondary source contributions such as biomass burning and secondary photochemical production from precursor VOCs, respectively. Methanol and acetone background concentrations can be high due to their long atmospheric lifetimes with respect to hydroxyl radical (OH) concentrations. Highest emissions have been observed from wounded plant material and hence processes such as agricultural harvesting and drying may significantly contribute to their emissions. The characteristic smell of cut grass is due to the emissions of C$_6$ oxygenated VOC compounds. MVK and MACR are reactive primary oxidation products of isoprene and therefore

their measurement can aid our understanding of tropospheric chemistry. Their concentrations are usually around one order of magnitude lower than that of isoprene and recent observations of fluxes over forests indicate a net deposition of MVK and MACR to the canopy (Langford *et al.*, 2010a; Misztal *et al.*, 2011). Unlike methanol and acetone, MVK and MACR have shorter atmospheric lifetimes with respect to OH. Global estimates of oxygenated VOC emissions are poorly quantified with only a few estimates which are around 120 to 340 TgC $a^{-1}$ for methanol (Guenther *et al.*, 1995; Millet *et al.*, 2008) and 260 TgC $a^{-1}$ for other reactive compounds including MVK+ and MACR (Guenther *et al.*, 1995).

## 2.2.2 Effects on atmospheric chemistry and climate

Biogenic VOCs and their oxidation products act as precursors to ground level ozone ($O_3$) and secondary organic aerosol (SOA) formation. The formation of $O_3$ requires the presence of sufficient mixing ratios of oxides of nitrogen (NO + $NO_2$ = $NO_x$) and sunlight. $O_3$ has significant adverse effects on plants and animals, as well as implications for climate change due to its strong radiative forcing. Generally, tropospheric $O_3$ formation or destruction depends on the $NO_x$ mixing ratio relative to that of VOCs and the rate constants for the reactions of both $HO_2$ (hydroperoxyl) and $RO_2$ (alkyl peroxy) radicals with NO. The VOC/$NO_x$ mixing ratio forms a threshold between two contrasting chemical regimes in the atmosphere, i.e. $NO_x$-limited and VOC-limited, whereby high ratios (i.e. >8) equate to $NO_x$-limited chemistry and low ratios (i.e. <4) result in VOC-limited chemistry. It is necessary to mention that the terms "$NO_x$-limited" and "VOC-limited" are loosely defined, because the divide between the chemical regimes is not always linear and the transition between the two is broad with various dependencies and exceptions (see Sillman, 1999, for a more detailed discussion). However, the terms are sufficient to distinguish between the general prevailing atmospheric chemistry that is likely to occur in an urban area compared with that occurring in a remote forest region.

The difficulty in assessing the $O_3$ formation potential of a VOC species depends on uncertainties in the reaction mechanisms and pathways, as well as the amount of NO being converted to $NO_2$ in the VOC degradation mechanism. As the pathway and complexity depends

on the VOC species, they are often poorly understood and can seldom be confirmed in their entirety through observations or laboratory experiments. Derwent *et al.* (1996) developed a photochemical ozone creation potential (POCP) index relative to ethylene using photochemical trajectory models to describe $O_3$ production from the oxidation of 95 individual VOC species in the presence of $NO_x$. The study shows that isoprene is among the species with the highest POCP index. Highest isoprene emissions occur from tropical forests, which are often in areas of low anthropogenic pollution, making the chemical regime $NO_x$-limited. In low $NO_x$ environments VOCs and their products, especially from isoprene oxidation, can react with OH and $O_3$ inhibiting a build-up of tropospheric $O_3$ (Lelieveld *et al.*, 2008). However, as agricultural intensification, urbanization, and industrialization increase in the tropics, high $NO_x$ emissions are more often found concurrently with high VOC emissions. If $NO_x$ levels are sufficient to maintain $O_3$ production, VOCs will control the rate of oxidant production, i.e. VOC-sensitive chemistry dominates resulting in net $O_3$ formation. An example highlighting the potential for significant tropospheric $O_3$ production in the tropics is the conversion of natural rainforest to oil palm monocultures in Malaysia (Hewitt *et al.*, 2009). By introducing additional $NO_x$ emissions, such as from nitrogen fertilizers, the potential maximum $O_3$ levels could exceed 100 ppbv with $NO_x$ concentrations of 3-5 ppbv.

$O_3$ acts as a greenhouse gas with an estimated radiative forcing equating to 25% of that of $CO_2$, although regionally tropospheric $O_3$ could have a forcing effect 1.5 times that of $CO_2$ (Blunden and Arndt, 2014). In addition to the climate forcing of $O_3$, non-methane VOC degradation processes compete with those of more potent greenhouse gases for OH. This can increase the atmospheric lifetime of e.g. methane, thereby increasing their cumulative greenhouse effects. Methane has contributed as much as 40-60% of the climate forcing of $CO_2$ since preindustrial times (Shindell *et al.*, 2005).

Another significant process bVOCs are involved in is the formation of biogenic secondary organic aerosol (SOA). Photooxidation and ozonolysis of isoprene, monoterpenes, sesquiterpenes and their oxidation products lead to the formation of low volatility product species,

which then partition into the condensed phase to produce SOA. Even the small molecule isoprene may oxidize to form SOA in low-$NO_x$ conditions (Claeys *et al.*, 2004). At higher $NO_x$ levels, mesocosm experiments are consistent with no aerosol production from isoprene (Wyche *et al.*, 2014). Depending on season and location SOA contributes a substantial mass to particulate organic matter (POM), which itself can constitute 90% of fine particulate mass over tropical forests (Kanakidou *et al.*, 2005). Fine particulates and their ability to change cloud properties and formation affect the radiative balance and are currently considered the largest uncertainty in climate change predictions. SOA act as cloud condensation nuclei (CCN) producing clouds with higher droplet numbers, thus increasing the cloud albedo. With the exception of black carbon, aerosols and clouds are estimated to constitute the strongest negative climate forcing (Forster *et al.*, 2007).

Atmospheric models show a negative bias in predictions of POM, thus underpredicting organic aerosol mass in the boundary layer (Carlton *et al.*, 2009; Goldstein and Galbally, 2007; Heald *et al.*, 2005), however there has been some improvement in reducing the uncertainty of model predictions (Heald *et al.*, 2010; Spracklen *et al.*, 2011). There are a number of factors that may contribute to errors in estimating aerosol loading. The majority of bVOC-derived SOA result from monoterpenes (19.1 Tg a$^{-1}$ (Kanakidou *et al.*, 2005)), the emissions of which have high uncertainties. Furthermore, the importance of SOA formation from isoprene is still rather unclear (Brégonzio-Rozier *et al.*, 2015; Claeys *et al.*, 2004; Kleindienst *et al.*, 2009; Lin *et al.*, 2012) and it is not always included in aerosol models. Field and laboratory data over the past decade have provided evidence that isoprene is a contributor to SOA formation (see Carlton *et al.*, 2009 and references therein). Although the yield of isoprene-derived SOA is minor, the total contribution to atmospheric POM is substantial (up to 30% of the global POM budget) due to the high global isoprene emissions, which easily surpass contributions from fossil fuel (Heald *et al.*, 2008). Studies have also shown that isoprenoids form highest yields of SOA under low $NO_x$ conditions compared with those formed under high $NO_x$ conditions (Kroll *et al.*, 2005; Presto *et al.*, 2005). These conditions are predominantly found where bVOC emissions are highest, in tropical and

boreal forests. However, chamber investigations have suggested that SOA yields from sesquiterpenes are actually higher under high $NO_x$ conditions (Ng *et al.*, 2007a).

### 2.2.3 Problems with the quantification of bVOC fluxes

There is still a paucity of direct field measurements of bVOC emission rates leading to uncertainties in the assessment of modelled emission estimates. Furthermore, many species and their intermediates are too short lived or require complex measurement installations to quantify accurately. Many or most of the early attempts at quantification of bVOC emission rates and mixing ratios were limited by instrument and technological shortcomings and it is only in the past decade that fast response instruments of high sensitivity have become commercially available. This has allowed the development of micrometeorological flux measurement techniques for VOC flux quantification (Chapter 3). As a result there have been increasing numbers of VOC flux field observations. However, flux measurement techniques are complex and ideal field sites particularly in the tropics that as far as possible fulfil the necessary theoretical and practical requirements are often difficult to access due to the remoteness of the location and/or for political reasons. Specific difficulties in measuring certain VOC species will be discussed along with instrument capabilities in Chapter 3.

## 2.3 Anthropogenic VOCs

### 2.3.1 Emission sources and estimates

Anthropogenic VOCs consist of a wide variety of compound groups with no single dominant species (i.e. there is no single compound equivalent to the importance of isoprene in the case of bVOCs). Direct vehicle exhaust emissions and other traffic-related sources such as hot-soak emissions during engine cooling (Na *et al.*, 2004; Rubin *et al.*, 2006) or evaporative emissions from petrochemical products (Srivastava *et al.*, 2005) are the main aVOC sources in urban centres (Kansal, 2009; Na *et al.*, 2005). For example, in central London, current emission inventories assume that solvents and road transport contribute the most to aVOC emissions (NAEI, 2014). Additionally, industrial processes including manufacturing, storage and transport of petrochemicals, but also waste disposal, biomass burning for domestic use, agriculture or forest

fires constitute local emissions, which cumulatively are important on a global scale (Piccot *et al.*, 1992).

Oxygenated species, alkanes, alkenes, and aromatics are the largest groups of aVOCs in terms of concentrations (Theloke and Friedrich, 2007). VOCs with the highest concentrations in urban areas are often longer lived oxygenated species, e.g. methanol, acetone and acetaldehyde, which have some anthropogenic sources, but also come from biogenic and secondary atmospheric formation. Largest fluxes are commonly from species with strongest urban emissions from either ubiquitous or local point sources such as traffic-related emissions or industrial sites. These mostly aromatic compounds include toluene, $C_2$-benzenes, and $C_3$-benzenes. $C_2$-benzenes constitute ethyl benzene, (*m+p*)-xylene, *o*-xylene and benzaldehyde, whereas $C_3$-benzenes consist of a larger group of $C_9$-aromatics such as propyl benzene, ethyl methyl benzenes, and trimethylbenzenes. Although benzene is the primary constituent of many higher carbon aVOCs and an important component of petrol due to its high octane number, emissions are small and therefore concentrations are low in urban areas. Exceptions are point sources such as petrol station forecourts where concentrations are several orders of magnitude higher (Karakitsios *et al.*, 2007). Additional legislative attention has been given to benzene in order to curb emissions due to its carcinogenicity. Many aVOC species are carcinogenic, such as benzene and 1,3-butadiene, or otherwise toxic, e.g. toluene and xylene, which represent additional adverse effects of aVOCs in the urban environment. The mixing ratios of monitored carcinogenic compounds are usually low, but the combination of certain meteorological conditions can lead to periods of high mixing ratios (Na *et al.*, 2005). For example, during winter when the boundary layer is shallow and photochemical removal is limited, mixing ratios can increase leading to high pollution episodes even though fluxes remain the same.

Global aVOC emissions are estimated to be around 10% of biogenic emissions, i.e. 110 TgC a$^{-1}$ from cities and industrial sources which represent small areas of high local emissions distributed around the world. Emission estimates of aVOCs are often given as total non-methane VOCs with few exceptions where speciated values are provided. Emission rates vary greatly

between countries and even within cities reflecting the diversity of sources and source strengths, as well as differences in national legislation, cultural practices, levels of anthropogenic activity, population size and distribution. Most governments provide detailed emission inventories of estimates of annual aVOC emissions per unit area based on known emission sources from a variety of sectors (see Section 3.2.2.1). The uncertainties involved in producing the estimates can be large as they depend on the accuracy of the information used (i.e. emission source strengths and distributions). In the UK, emissions from point sources such as industrial processes are required to be monitored and reported to the Environment Agency as part of the EU Integrated Pollution Protection and Control (IPPC) Directive (96/61/EC) and are therefore more reliable than nonpoint sources. Total aVOC emissions in the UK were estimated to be around 0.8 TgC in 2013 (NAEI, 2014) which in terms of carbon is much lower than the total UK $CO_2$ emissions of 126 TgC $a^{-1}$ (Department of Energy & Climate Change, 2015). This is in comparison with a reported total aVOC emission estimate of 20.1 TgC $a^{-1}$ (Wei *et al.*, 2008) and a total $CO_2$ emission of 2.45 PgC $a^{-1}$ in China (Carbon Dioxide Information Analysis Center, 2012).

## 2.3.2 Effects on air quality and climate

Apart from their toxicity, many aVOCs contribute to tropospheric $O_3$ and secondary organic aerosol formation. The production of $O_3$ is a nonlinear photochemical process, in which the production rate depends on the ratio of VOC to $NO_x$. The chemical regime in urban areas differs from that of unpolluted environments in that the VOC/$NO_x$ ratio is low and therefore the chemistry is $NO_x$-saturated or VOC-sensitive. Generally, in this instance $O_3$ increases with increasing VOC concentrations and decreases with increasing $NO_x$. The latter is often observed in urban centres, power plants plumes, at night or during winter where the large emissions of NO remove $O_3$ by $NO_x$ titration. This reaction only leads to a net reduction of $O_3$ when there is no photolysis of $NO_2$ to release odd-oxygen (odd-oxygen is the generic term for O atoms and $O_3$ in the atmosphere), since the removal of $O_3$ is smaller (i.e. 1-1.5 $O_3$ per emitted NO) than the rate of production (i.e. >4 $O_3$ per emitted $NO_x$) (Sillman, 1999; Sillman *et al.*, 1998). Additionally, when estimating the VOC/$NO_x$ ratio, it is more appropriate to use a weighted VOC ratio than the sum

of total VOCs, as more reactive VOC species weigh the ratio in favour of $O_3$ production with increasing reactivity in regard to OH. This is especially important in urban areas with a more diverse mix of VOCs, as individual highly reactive species with a higher $O_3$ formation potential, such as isoprene, contribute disproportionally to $O_3$ production (Derwent *et al.*, 1996). This has implications for the planning of green urban infrastructures, i.e. the VOC emission rates of tree species must be considered in the selection process (MacKenzie *et al.*, 1991; Donovan *et al.*, 2005). For example, tree species that emit large amounts of isoprene are less suitable to be planted in urban and suburban areas due to the high $O_3$ forming potential of isoprene. From the integrated POCP values from (Derwent *et al.,* 1996) (see Section 2.2.2) which are relative to ethylene to compare the $O_3$ formation potential of different aVOC species, it is shown that many common aromatics such as *m*-xylene and trimethylbenzene isomers have an even higher POCP value than isoprene (Derwent *et al.*, 1996; Na *et al.*, 2005). Although most compounds including benzene, toluene, most alkanes, and oxygenated species have lower POCP values than ethylene, the diverse mix of VOCs in urban environments can cause difficulties in producing accurate predictions of $O_3$ concentrations in air quality models. VOC emission rates represent the largest uncertainty in photochemical models due to the inaccuracies of emission inventories. Furthermore, the lack of representation of biogenic emissions in urban emission inventories contributes to the generally large underestimation of VOC emissions in cities (Fujita *et al.*, 1992; Langford *et al.*, 2010b).

Advection of pollution and photochemical aging of air masses also play important roles in determining $O_3$ forming potentials. Often new pollution follows a VOC-sensitive regime, but as the air mass ages the pollutants evolve towards $NO_x$-limited chemistry. This evolution depends on the rate at which $NO_x$ reacts in the air parcel (Milford *et al.*, 1994). Even on a regional scale, advected air masses containing high VOC mixing ratios from biogenic emissions from suburban and peri-urban areas can have large effects on urban $O_3$ formation (MacKenzie *et al.*, 1991). Therefore, intercontinental and regional pollution advection become important factors in air quality modelling (Holloway *et al.*, 2003; Zaveri *et al.*, 2010).

As with bVOCs, many aVOCs, especially aromatics (approx. 80%) and their oxidation products contribute to SOA formation. The current global estimate of anthropogenic VOC contributions to SOA formation range from 0.4-2.6 Tg organic matter $a^{-1}$ (Tsigaridis and Kanakidou, 2003). However, observations suggest this to be an underestimation by up to one order of magnitude with updated estimates ranging from 3-25 Tg $a^{-1}$ (Volkamer et al., 2006). The exclusive use of chamber experiments, which do not account for losses of semi-volatile vapours to chamber walls, may be leading to poor understanding of aerosol growth under atmospheric conditions (Zhang et al., 2014). Furthermore, polymers and their highly oxygenated intermediate species have been identified as an important component of aerosol formation from aromatic precursors (de Gouw et al., 2005). A further difficulty is the complexity of oxidation product reaction mechanisms, which increases with higher carbon numbers producing larger SOA yields (Hamilton and Lewis, 2003). Higher carbon compounds such as from diesel emissions have a greater SOA forming potential due to their reactivity, volatility, and higher mass of available carbon (Gros et al., 2007). The SOA formation from these compounds is poorly quantified because of difficulties in measuring speciated higher carbon compounds. Suggestions have been made to improve organic aerosol and thus SOA predictions using species grouped by their volatility (Robinson et al., 2007) and oxidation state (Jimenez et al., 2009).

Like isoprene, aromatic hydrocarbons such as benzene, toluene and xylene produce a higher SOA yield under low $NO_x$ conditions, although the rate of production under high $NO_x$ is faster (Ng et al., 2007b). There are further differences in yield production between individual compounds with toluene and ethyl benzene producing higher SOA yields than xylene and trimethylbenzenes (Odum et al., 1997). Although often not included in climate forcing models, SOA from aVOCs also contribute to climate effects, which could cause up to -0.1 W $m^{-2}$ radiative cooling depending on how much models underestimate SOA yields (Volkamer et al., 2006). On a more local scale, SOA in urban areas can enhance the absorption of radiation by black carbon (Jacobson, 2000) and thus heat the surrounding air affecting atmospheric stability, vertical mixing, precipitation, and incoming radiation (Ramanathan et al., 2001).

Other concerns in urban areas are the effects of SOA on human health and visibility. SOA is part of total fine particulate matter, which has been linked to respiratory and cardiovascular disease. Especially existing conditions such as reduced lung functioning are exacerbated by fine particulates (Seaton *et al.*, 1995). In urban and suburban environments SOA can contribute up to 40% of organic carbon particulate concentrations depending on which VOC precursors are available (Kleindienst *et al.*, 2007).

### 2.3.3 Problems with measuring aVOCs

The number of different aVOCs that play an active role in a variety of adverse effects is vast. Therefore, difficulties in measuring aVOC concentrations lie in the instrument limitations for quantifying speciated VOCs, especially higher carbon compounds, and the number of compounds or compound groups that can be observed simultaneously or at sufficient frequencies. There are additional complications when quantifying aVOC fluxes from urban landscapes. Although the logistical requirements of VOC flux measurements can be easily fulfilled in urban areas, the problem is identifying sites that satisfy the theoretical requirements for micrometeorological flux measurements. The micrometeorological conditions above urban canopies are not ideal due to the high emission source diversity, canopy heterogeneity, and complex urban terrain. Street canyons and building structures increasingly complicate the air flow dynamics creating pollution gradients (Fernando *et al.*, 2001; Pugh *et al.*, 2012; Vardoulakis *et al.*, 2007) and often reducing the representativeness of a measurement site.

## 2.4 Comparison of biogenic and anthropogenic VOCs

VOCs originating from biogenic and anthropogenic sources contribute to SOA and tropospheric $O_3$ formation affecting the climate and the oxidative capacity of the troposphere. However, the source strength, type, emission composition and environment determine the extent of their contributions. Table 2.1 compares and contrasts VOCs from both biogenic and anthropogenic origins and their effects in the atmosphere.

*Table 2.1. Comparison of similarities and differences between biogenic and anthropogenic VOCs in their respective environments, including their contributions and effects in the atmosphere.*

| Category | Biogenic | Anthropogenic |
| --- | --- | --- |
| Dominant compound groups | Isoprene<br>Monoterpenes<br>Oxygenated compounds (methanol, acetaldehyde, acetone) | Alkanes<br>Alkenes<br>Aromatics<br>Oxygenated compounds (methanol, acetaldehyde, acetone) |
| Global emission estimates | 1150[a] TgC a$^{-1}$ (approx. 600[a] Tg a$^{-1}$ isoprene, 103[b] Tg a$^{-1}$ monoterpenes, 230[a,c] TgC a$^{-1}$ methanol, 260[a] TgC a$^{-1}$ other reactive VOCs) | 110[a,d] Tg a$^{-1}$ (33 % alkanes, 30 % oxygenated compounds, 23 % aromatics, 8 % alkenes)[e] |
| Major sources | Direct plant emissions (broadleaf and coniferous trees, shrubs, croplands species)[a]<br>Plants under biotic and abiotic stress<br>Cutting and drying[f]<br>Leaf decomposition[g]<br>Biomass burning[h] | Fossil fuel combustion and vehicle tailpipe emissions[i]<br>Evaporative emissions[j]<br>Solvent use[k]<br>Production processes |
| Environment | Mostly unpolluted, natural;<br>Some urban emissions (urban vegetation, parks, roadside trees), suburban and peri-urban emissions | Mostly polluted, urban;<br>Some emissions in natural environments (resource extraction, transport, agriculture) |
| Typical chemical regime | NO$_x$-limited | VOC-limited |
| Atmospheric lifetime[2] | 1.4 h (isoprene)<br>2.6 h ($\alpha$-pinene)<br>4.1 h (MACR)<br>6.8 h (MVK)<br>12 d (methanol)<br>53 d (acetone) | 9.4 d (benzene)<br>1.9 d (toluene)<br>4.3 h (1, 2, 4-trimethylbenzene)<br>12 d (methanol)<br>53 d (acetone) |
| POCP[3] | 117.8 (isoprene)<br>18.2 (acetone) | 33.4 (benzene)<br>77.1 (toluene)<br>132.4 (1, 2, 4-trimethylbenzene)<br>18.2 (acetone) |

| Global SOA contribution | Ca. 90 %[1] (10-1820 Tg a$^{-1}$)$^{m,n,o}$ | 6 ± 2 %[p] (0.4-2.6 Tg a$^{-1}$) |
|---|---|---|
| | (19.1$^m$ Tg a$^{-1}$ (terpenes), 15$^m$ Tg a$^{-1}$ (other reactive VOCs), 2$^m$ Tg a$^{-1}$ isoprene) | Or <30 %[q] (3-25 Tg a$^{-1}$) |

[1] % contributions of VOC functional groups using the example from Germany.

[2] Atmospheric lifetimes with regard to OH using rate constants at 298 K taken from Atkinson (1997) and assuming a 12 h average daytime OH concentration of $2.0 \times 10^6$ molecule cm$^{-3}$.

[3] Integrated photochemical ozone creation potential (POCP) relative to ethylene from Derwent *et al.*, (1996).

References: a) Guenther *et al.* (1995), b) Arneth *et al.* (2008), c) Millet *et al.* (2008), d) Piccot *et al.* (1992), e) Theloke and Friedrich (2007), f) Guenther *et al.* (2000), g) Warneke *et al.* (1999), h) Lipari *et al.* (1984), i) Borbon *et al.* (2001), j) Srivastava *et al.* (2005), k) Piccot *et al.* (1992), l) Kanakidou *et al.* (2003), m) Kanakidou *et al.* (2005), n) Goldstein and Gallbaly (2007), o) Hallquist *et al.* (2009), p) Tsigaridis and Kanakidou (2003), q) Volkamer *et al.* (2006).

Biogenic and anthropogenic sources of VOCs emit a range of different compounds, although many compounds can have both natural and man-made origins. The source type, distribution and climate determine emission rates and the overall source strength. Often the ambient conditions of the environment in which they are emitted determine the type and magnitude of their effects. The ambient atmospheric concentrations of the OH radical, as well as the local climate conditions establish the oxidative capacity of the troposphere. Furthermore, the dominant chemical regime in the atmosphere is controlled by the co-occurrence of other pollutants, such as $NO_x$, which affect the amount of tropospheric $O_3$ produced by a VOC species. Not always are the conditions right to maximise the potential effects of VOCs, such as $O_3$ or SOA production. Furthermore, these effects are only adverse to human health and climate change when specific conditions are met (Hamilton *et al.*, 2015). It is often the case that maximised potentials occur within or downwind of densely populated areas and concurrent with other adverse influences, resulting in a synergistic effect with damaging consequences. It is therefore vital in terms of both air quality and climate to monitor and be able to accurately model VOC emissions in addition to the more widely monitored pollutants. High uncertainties in VOC emission estimates on a global scale provide a poor basis to model $O_3$ and SOA yields, which in turn reduces the predictive capabilities of climate and air quality models. Therefore, to constrain

modelled emission estimates of both biogenic and anthropogenic VOCs, it is necessary to quantify

direct ecosystem level VOC emissions from both natural and urban environments.

# Chapter III

# 3 Methods of volatile organic compound volume mixing ratio and flux quantification

In this thesis two different, but related, metrics are used with respect to the occurrence of volatile organic compounds (VOCs) in the atmosphere. The first is the volume mixing ratio (expressed in parts per billion, ppb) or concentration ($\mu g\ m^{-3}$). This is used in the calculation of the second metric, the net flux of VOCs with a canopy environment (in units of $mg\ m^{-2}\ s^{-1}$) as determined using micrometeorological techniques. These "top-down" measured fluxes can be compared to VOC emission rates estimated using "bottom-up" emission inventories, methods which are available for both anthropogenic and biogenic VOCs. In this thesis, volume mixing ratios of VOCs were obtained using proton transfer reaction – mass spectrometry (PTR-MS) (Papers I-III), and these data were then used in conjunction with three dimensional wind vector data obtained using a sonic anemometer to calculate fluxes by virtual disjunct eddy covariance (vDEC) (Papers II and III). The measured fluxes were compared with an anthropogenic VOC emissions inventory for London (Paper II) and with modelled biogenic VOC emissions using the Guenther 95 and MEGAN algorithms in both London and over the Amazon tropical forest (Papers II and III).

## 3.1 Quantifying VOC concentrations

### 3.1.1 Proton transfer reaction-mass spectrometry

#### 3.1.1.1 Instrument design and operation

Until the 1990s the quantification of volatile organic compounds (VOCs) was confined to gas chromatographic methods (see Section 3.1.2), which, although able to measure complex mixtures of gas components to the pptv level, do not allow the on-line monitoring of fast changing

concentrations on timescales of a few minutes or seconds. In 1998, Lindinger *et al.* developed a commercial proton transfer reaction-mass spectrometer (PTR-MS) which is an on-line measurement system for trace VOC components with concentrations in the pptv range. The PTR-MS uses a form of chemical ionization (CI) that ionizes molecules, while causing less fragmentation than electron impact ionization (EI), it allows a mixture of multiple compounds to be quantified and characterized by their mass to charge ratio (*m/z*). The chemical ionisation scheme utilised by the PTR-MS is the reaction of VOCs with hydronium ($H_3O^+$) primary reaction ions, which transfer a proton to molecules that have a proton affinity that exceeds that of water (Lindinger *et al.*, 1993). Compounds with proton affinities less than that of water, e.g. $N_2$, $O_2$, $CO_2$ and CO, undergo non-reactive collisions with the reagent ions, thereby reducing the need of prior conditioning of the air sample. When primary ions have enough time to react with the neutral compounds a high sensitivity can be achieved, which is defined by a high ratio of product ion signal $i(R^+)$ to the density of the neutral compound [R], i.e. $i(R^+)/[R]$. Therefore, VOCs (R) in the air sample with proton affinities higher than that of water undergo proton transfer reactions with primary ions as follows

$$H_3O^+ + R \xrightarrow{k} RH^+ + H_2O, \tag{3.1}$$

when the quantity of $H_3O^+$ is greater than *R*, whereby *k* is the reaction rate coefficient. Providing the ambient VOC and $H_3O^+$ concentrations remain stable, the reaction kinetics can be linearized allowing the VOC concentration to be calculated by the ratio of protonated VOCs to $H_3O^+$ ions as

$$R \approx \frac{1}{kt}\frac{[RH^+]}{H_3O^+}, \tag{3.2}$$

where *t* is the reaction time, which corresponds to the transit time of the $H_3O^+$ ions through the drift tube.

The main components of a PTR-MS consist of an ion source, drift tube, quadrupole mass filter and detector (e.g. the secondary electron multiplier, SEM) (Figure 3.1). High purity water

vapour is flushed through a high voltage hollow cathode to provide a stable source of primary reagent ions ($H_3O^+$), which are then focused through a lens into the drift tube where they are combined with the sampled air and react with the compounds present. In the high sensitivity instruments three turbo-molecular vacuum pumps are used to remove the remaining buffer gas to maintain very low pressures in the drift tube (usually around 1.95-2.10 hPa) and the reaction chamber (ca. $1.7 \times 10^{-4}$ hPa).
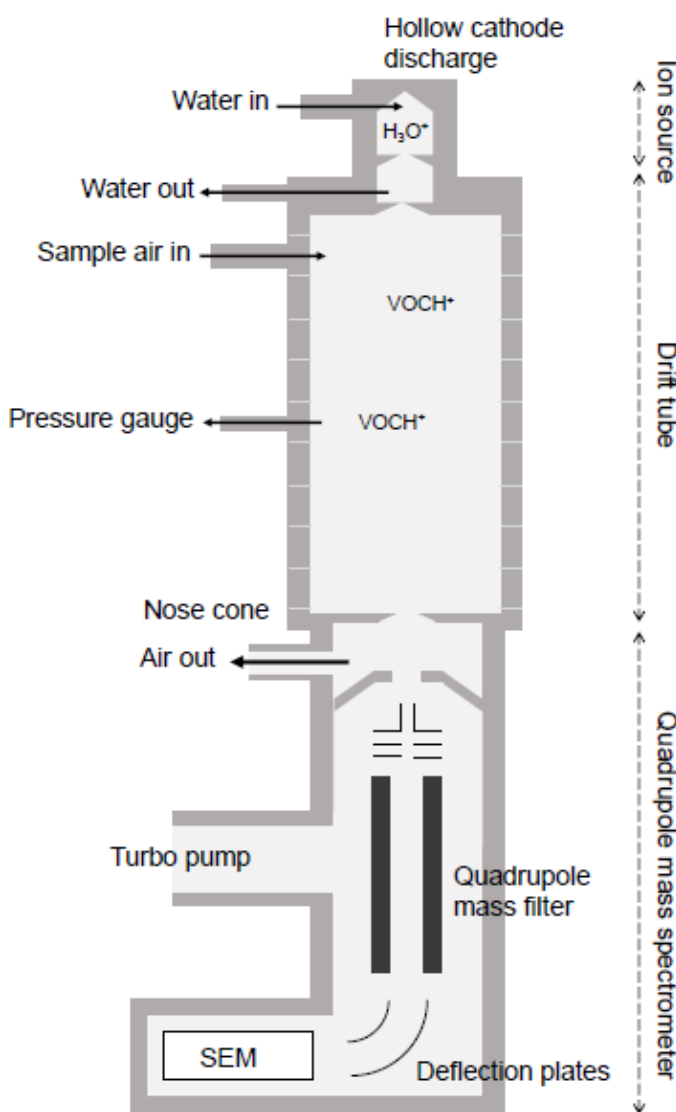


**Figure 3.1.** Schematic of a proton transfer reaction-mass spectrometer (Ionicon Analytik GmbH, Austria) consisting of an ion source, drift tube and quadrupole mass spectrometer. SEM stands for secondary electron multiplier which detects the ions and provides an output in counts per second (cps).

Once analytes have been protonated they are passed through the quadrupole mass filter, which can be set to detect specific *m/z* or scan a section of the mass spectrum (e.g. *m/z* 19-206). The product ions are then detected by an SEM that interprets the signal as an ion count per second (cps). The quadrupole has a unity resolution and therefore can only detect compounds with a similar molecular weight at the same integer atomic mass unit (amu). This requires a cautious interpretation of the resulting mass spectrum, as individual *m/z* may be overestimated due to isobaric interference from other compounds of similar integer mass. An example of this is *m/z* 69 which can include contributions from both isoprene (molar mass of 68.12 g mol$^{-1}$) and, if present, from compounds like furan (molar mass of 68.07 g mol$^{-1}$).

This problem is avoided with the more recently developed proton transfer reaction- time of flight-mass spectrometer (PTR-ToF-MS) by Jordan *et al.* (2009), which is capable of measuring ultra-low VOC concentrations (pptv level) with a high mass resolution. This allows the quantification of the full spectra of compounds by actual mass and elemental composition, therefore distinguishing between isobaric, but not isomeric compounds as there is no structural information given. The drawback of this instrument is the large quantity of data that is produced even during a short deployment making the post-processing procedures extremely time consuming.

### 3.1.1.2 Practical considerations and data handling

#### 3.1.1.2.1 Impurities and compound fragmentation

Most proton transfer processes in the PTR-MS are non-dissociative, resulting in only one product ion species. Dissociation can, however, occur with some compounds, but these follow a certain pattern. Therefore, under controlled conditions the resulting fragments of the neutral reactant can be consistently identified and adequately quantified. The conditions are determined in the drift tube, where ions move through the flowing buffer gas under the influence of an electric field. The ratio of the electric field strength (*E*) and buffer gas density (*N*) controls the drift velocity of the ions and is expressed in units of Townsend, Td = $10^{-17}$ V cm$^2$ molecule$^{-1}$. If a

constant $E/N$ ratio is maintained the fragmentation pattern should be consistent throughout the measurement.

Few studies have attempted to quantify fragmentation patterns of commonly observed compounds as a function of $E/N$ ratio (Hewitt *et al.*, 2003; Misztal *et al.*, 2012; Tani *et al.*, 2004). As the PTR-MS cannot distinguish between compounds of the same integer mass it is possible for fragments of larger compounds to affect the signal of lower masses. In addition, different compounds can result in identical fragments. For example, a range of monoterpenes can all dissociate into fragment ions detectable at $m/z$ 81 and $m/z$ 137. GC-PTR-MS combined analyses can help identify the contribution of individual species to a measured $m/z$, although only few studies are available (de Gouw *et al.*, 2003; Karl *et al.*, 2001ab; Warneke *et al.*, 2003). De Gouw and Warneke (2007) provide a comprehensive overview of expected compound and possible fragment contributions to the most commonly measured masses, as well as a compilation of intercomparison studies between GC-based and PTR-MS methods. Where possible, isobaric interferences and common fragmentation patterns should be investigated for PTR-MS deployment and accounted for during post-processing, as they depend on the suite of compounds emitted in different environments.

High purity water is required to minimize impurities, such as $NO^+$ and $O_2^+$ that can undergo charge-transfer reactions with many VOCs leading to increased fragmentation of the compounds. Although high primary ion counts (2.5-3.5 $\times$ $10^6$ cps) are desirable as they increase the instrument sensitivity, they can increase the number of impurities, therefore the flow rate of the water vapour and the voltages of the ion source are controlled to maintain optimal conditions (de Gouw and Warneke, 2007). $NO^+$ and $O_2^+$ impurities should be monitored at regular intervals to ensure their effects on the analytes are minimal.

### 3.1.1.2.2 Water cluster formation and instrument sensitivity

When $H_3O^+$ ions become hydrated they form water cluster ions ($H_3O^+(H_2O)_n$; $n$ = 1, 2, 3, …) in the reaction chamber depending on the sample humidity. The first water cluster can be quantified directly by monitoring $m/z$ 37 or indirectly via the isotopologue $H_3^{18}O(H_2O)^+$ and

$H_3O(H_2{}^{18}O)^+$ signal at *m/z* 39 as it is typically 0.4% of the signal for $H_3{}^{16}O(H_2{}^{16}O)^+$. These cluster ions can also react with VOCs as reagent ions, therefore, it is important to maintain a cluster ion signal of <5% of the total reagent ion count by dissociating them using the electric field. Too high *E/N* ratios result in increased fragmentation, whereas lower ratios encourage water ion clustering, hence a compromise is necessary, usually in the range of 120-130 Td, to minimize both effects while maintaining a high instrument sensitivity. This can be controlled by altering the drift tube pressure, temperature or voltage. Environmental considerations can also dictate the most suitable operating conditions of the instrument. For example, when measuring in very humid environments (e.g. in the tropics) it may be necessary to increase the *E/N* ratio to >130 Td to minimize the formation of water clusters, but pretreatment to remove the humidity, as is the case in other analytical techniques, is not necessarily required. However, any humidity effects must still be investigated and accounted for in the instrument background signal and sensitivities.

The surface of the SEM progressively degrades during use reducing the instrument sensitivity. Adjusting the SEM voltage can counteract the loss of sensitivity. Regular SEM optimization checks should therefore be undertaken during longer measurements by increasing the voltage stepwise (e.g. by 50 V) until the relative increase in $H_3O^+$ ions to the previous voltage is around 15%. Finding the correct optimum maintains instrument sensitivity and increases the SEM lifetime.

### *3.1.1.2.3 Instrument calibrations and background corrections*

The PTR-MS provides data in raw ion counts per second. As standard, these data are normalized against the primary ion and, if they are humidity dependent, then also against the first water cluster. Normalised ion counts (*I(RH$^+$)$_{norm}$*) are calculated for each mass by

$$I(RH^+)_{norm} = 10^6 \times \left( \frac{I(RH^+)}{I(H_3O^+) + I(H_3O^+(H_2O)_n)} \right), \tag{3.3}$$

where $I(H_3O^+)$ are the primary ion counts (i.e. *m/z* 21 x 500) and $I(H_3O^+(H_2O)_n)$ are the water cluster counts (i.e. *m/z* 37 or *m/z* 39 x 250). Similar to the water cluster, the primary ion counts are monitored via the $H_3{}^{18}O^+$ isotopologue, which is scaled up by the natural isotopic

abundance to estimate the $H_3O^+$ concentration. The principal reagent ion isotopologue ($H_3^{16}O^+$) cannot be monitored directly, because its high signal would overwhelm the SEM. Once ion counts have been normalized they can be converted to a volume mixing ratio (ppbv) using the normalized instrument sensitivity. Calibrations to measure instrument sensitivities should be conducted at regular intervals, especially during longer field deployments. Normalized sensitivities ($S_N$) for each compound can be calculated from the slope of the normalized ion counts (ncps) over a known volume mixing ratio ($VMR_{stand}$) of a calibration gas standard diluted with zero air, which is controlled via a flow controller (Taipale *et al.*, 2008), resulting in

$$S_N = \frac{I(RH^+)_{norm}}{VMR_{stand}},$$ (3.4)

This can then be used to calculate the volume mixing ratio (VMR) of a measured compound by

$$VMR = \frac{I(RH^+)_{norm}}{S_N},$$ (3.5)

where $I(RH^+)_{norm}$ is the ion counts normalized by the primary ions and water clusters. Using normalized counts removes some of the humidity effects on compounds of which the detection is humidity sensitive by taking the water clusters into account (Warneke *et al.*, 2001).

Additionally to calibrations, PTR-MS require regular monitoring of the often high instrument background, which needs to be subtracted from the final measurement. Hourly measurements of VOC-free or zero air (ZA) are needed either from a cylinder containing compressed VOC-free air or from ambient air after removal of VOCs by a scrubber such as a heated platinum catalyst. This enables the current instrument background to be subtracted from the corresponding measurement. Using scrubbers that retain the ambient humidity is desirable, thereby removing the need for humidity dependent background corrections, as ambient humidity can sometimes affect the background measurements of some compounds. If this is not available, the instrument specific response of humidity on the background noise for each measured compound needs to be investigated and accounted for.

Finally, the limit of detection (LoD) should be provided with the final ratified data to allow the user to decide whether to apply the LoD filter or retain all data to avoid bias towards larger values. The instrument detection limit for each compound concentration at the 95% confidence interval is given as two sigma of the mass specific instrument background signal (ppbv) acquired during the respective zero air measurement (Taipale *et al.*, 2008).

As mentioned above, PTR-MS does not allow unambiguous identification of many (or most) detected masses due to the possible occurrence of more than one compound at a given *m/z* value, and the possible formation of mass fragments from larger molecular weight compounds. Hence, complementary measurements using a compound-specific analytical method such as gas chromatography with flame ionization detector (GC-FID) or GC-MS are required in order to confirm the attribution of *m/z* values to specific VOC compounds in ambient air.

### 3.1.2 Gas chromatographic techniques

Gas chromatography is a widespread technique to separate and quantify compounds that are either naturally volatile or do not decompose when vapourised. Instruments consist of a mobile phase, which is an inert carrier gas (e.g. helium or nitrogen), and a stationary phase consisting of a liquid or solid microscopic layer on an inert solid support within a column comprised of glass or metal tubing. The gaseous sample is injected into the head of the column and driven by the carrier gas into the stationary phase. As the analytes interact with the walls of the column, the elution of each compound occurs at different times allowing the construction of a chromatogram based on the retention times of the different compounds. The rate at which the chemical constituents pass through the stationary phase depends on their chemical and physical properties and hence their strength of adsorption to the stationary phase materials. Further parameters controlling retention times and elution order include the flow rate of the carrier gas, the column length and temperature. A detector at the end of the column monitors the outlet stream and therefore the retention time and amounts of each compound can be determined. The nature of the analysis requires discrete samples. Thus, sample acquisition, storage and preparation are necessary prior to analysis. Complex multistage sample handling can be time consuming and

introduce errors, such as storage artefacts for unstable or sticky compounds which is common among VOCs. Automation of sample injection by employing an autosampler is widely used and a variety of column inlet types are available to introduce the sample into the carrier gas flow. Analysis run time can take between several minutes to hours, which does not include the time taken for sample acquisition, resulting in a slow instrument response time.

Further details of the analytical method depend on the type of detector used. Flame ionization detectors (FID) have electrodes that are located adjacent to a hydrogen fuelled flame at the exit of the column. Only organic/ hydrocarbon compounds can be detected, as the carbon forms cations and electrons during pyrolysis, thereby generating a current between the electrodes. This increase in current is interpreted as a peak in the chromatogram. This detector allows very low detection limits (picograms per second), but is limited to hydrocarbons, as it is unable to generate ions from compounds containing carbonyl functional groups (Pavia *et al.*, 2006). Furthermore, it is possible for compounds to co-elute and present similar retention times. Additional steps can be taken to minimize this phenomenon, such as increasing the peak capacity to exceed the number of sample components (Davis and Giddings, 1983). The detector signal is proportional to the number of carbon atoms in the molecule. Thus, the calibration for a single compound can be translated to other compounds.

Gas chromatography – mass spectrometers (GC-MS), as the name implies, use a mass spectrometer as the detector, which breaks the molecules into ionized fragments and detects them using their mass to charge ratio (*m/z*). This allows differentiation of compounds with the same retention time. The combination of gas chromatography and mass spectrometry reduces the probability of erroneous compound identification, as it is highly unlikely that two different compounds will have the same retention time *and* produce a similar pattern of ionized fragments. Different methods of ionization can be used and resulting fragments are detected using an electron multiplier diode, which converts the ionized fragment into an electrical signal (Eiceman, 2000). GC-MS systems need to be calibrated for the range of target compounds to be fully quantitative.

### 3.1.3 Advantages and limitations

The main advantage of PTR-MS is the high time resolution and range of compounds that can be measured virtually concurrently with the same experimental setup. However, for the quadrupole PTR-MS used in this work, the instrument specificity is limited to the integer mass of the compound requiring assumptions or additional verification on compound identification, whereby issues such as fragmentation, isobaric interferences, and humidity dependent responses add further complexity to data interpretation. Using PTR-ToF-MS would reduce this problem, as it is able to distinguish between different fragments with the same nominal, but different exact mass (although not between identical fragments originating from different parent compounds), however, such an instrument was not available for this work. GC methods provide additional information for compound identification, but at a lower time resolution. The long run time of the analysis necessitates acquisition, storage and pretreatment of discrete samples. Table 3.1 compares the main advantages and limitations of both instruments.

*Table 3.1. Comparison of PTR-MS and GC-FID/ GC-MS techniques in VOC volume mixing ratio quantification.*

| Instrument | PTR-MS | GC-FID/MS |
|---|---|---|
| Sampling method | Continuous, on-line acquisition | Accumulation in canisters or in adsorption cartridges requiring storage and pretreatment |
| Response time | Fast (<5 Hz/ 0.2 s) | Slow (>15 min) |
| Detection limits | 10 pptv | pptv-ppqv (1 pg s$^{-1}$ FID, 0.25-100 pg MS) |
| Specificity | Integer mass resolution (mass to charge ratio) | Molecular weight from retention time (mass to charge ratio for MS) |
| Target compound | Analyte proton affinity greater than that of water (using $H_3O^+$ reagent ions) | Organic hydrocarbons (FID only) |

The different advantages of PTR-MS and GC methods complement each other by providing high sensitivity information on a range of temporal and mass resolutions. PTR-MS has

a sufficient response time to show almost real time VOC concentrations and when combined with GC measurements, individual compounds and fragments can be identified and verified.

## 3.2 Quantifying VOC fluxes

### 3.2.1 Ecosystem scale emission measurements: Top-down approaches

The most direct method of making top-down estimates of emission rates is the measurement of fluxes at the canopy-scale. Remote sensing techniques are also considered top down methods, such as the use of formaldehyde observations from space to constrain isoprene emission estimates (Guenther *et al.*, 2006). However, most VOCs cannot be detected directly using earth observation techniques and hence canopy-scale flux measurements have become the preferred technique (Canadell *et al.*, 2000; Geider *et al.*, 2001; Running *et al.*, 1999). Using towers to sample the above-canopy VOC exchange allows the monitoring of ecosystem responses to environmental drivers with minimal disturbance of the environment while maintaining ambient atmospheric conditions.

### 3.2.1.1 Micrometeorological flux measurements: Eddy covariance methods

A number of different methods exist to quantify above-canopy VOC fluxes depending on available resources, targeted VOC species, and desired spatial and temporal resolutions, but the most direct methods are micrometeorological techniques based on eddy covariance (EC). EC methods consist of measuring the fluctuations of the vertical wind speed ($w$) and scalar concentration ($c$) over time ($t$). The technique requires fast response sensors to capture the scalar flux associated with the range of eddy sizes that transport heat momentum and mass within the surface layer. Variations of basic eddy covariance methods have been developed to adapt the technique for VOCs, as originally it was used to quantify fluxes of momentum, sensible heat, $CO_2$ and $H_2O$, for which very fast response sensors have been available for some time (Baldocchi, 2003).

There are a number of theoretical requirements to be fulfilled for all eddy covariance methods, which are related to the conservation of mass equation (Appendix I). For a flux

measured at some measurement height ($z_m$) to accurately reflect the true surface exchange, vertical flux divergence is to be minimized. The conservation equation states that the rate of change of a scalar at a fixed point in space must be balanced by the mean horizontal and vertical advection, divergence or convergence of the flux, molecular diffusion, and by any source or sink. Thus, to minimize vertical flux divergence/convergence, non-zero terms for convergence or divergence of a flux in the horizontal and lateral may present a significant source of error, since they relate to chemical processes associated with the transport of a compound and heterogeneity in the landscape. Chemical reactions, i.e. formation or removal, are a further cause for vertical flux divergence, however when applying EC to calculate VOC fluxes, it is assumed that no reactions take place. This can be problematic, especially for highly reactive VOCs (e.g. sesquiterpenes) when the rate of reaction is equal to or shorter than the time scale of vertical transport, thus leading to under or overestimation of the flux at the measurement point due to divergence or convergence respectively. Under ideal conditions the equation can be simplified to only represent the turbulent exchange of a vertical flux of a compound where storage terms are insignificant. Therefore, ideal conditions exist when:

   i.   The scalar concentration and wind velocities are steady with time,

   ii.   the underlying surface is homogeneous, and

   iii.   the terrain of the upwind fetch area is flat.

When conditions ii and iii are met, an equilibrium boundary layer (EBL) will develop, in which horizontal advection is negligible (Fowler *et al.*, 2001). The layer is considered a Prandtl-Layer in which the compound concentration profiles are in equilibrium with the rate of surface exchange and therefore the flux is constant with height (Figure 3.2) (Denmead *et al.*, 1993). The EBL depth depends on the length of homogeneous fetch (i.e. the distance to the next upwind heterogeneity) and atmospheric conditions. Atmospheric stability represented by the Monin-Obukhov parameter ($\zeta$) affects the ratio of fetch to EBL depth, usually around 100:1, but this can increase when conditions are stable (i.e. $\zeta \geq 0$) as this increases memory effects of upwind obstructions. To attain a reliable representation of the long-term surface flux, statistical averaging

is applied over a time period, usually 30-60 min, which is representative of both high and low frequency turbulent eddies. As long as the mean vertical transport of air over the chosen averaging period equals zero ($\overline{w} = 0$) and fetch requirements have been fulfilled, the flux can be approximated as

$$F_c = \overline{w'c'}, \tag{3.6}$$

where the net flux of a compound ($F_c$) is the time averaged covariance of the instantaneous fluctuations of the vertical wind speed (*w'*) and the scalar (*c'*) around their respective means (Plantaz, 1998). Lateral transport through advection, recorded by changes in the horizontal (*u*) and lateral (*v*) wind speeds, can also occur when there is a horizontal gradient in the measured scalar and can result in advection errors. These can be minimized by sampling over a homogenous canopy which helps to limit horizontal gradients in scalar concentration.
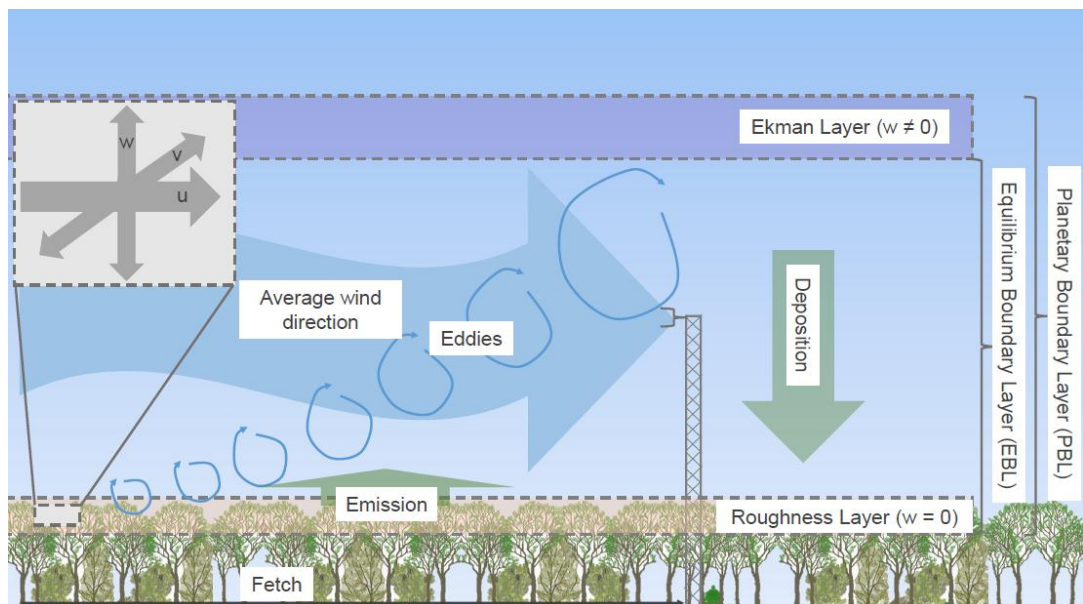


**Figure 3.2.** Diagram showing turbulent transport, compound emission and deposition within the planetary boundary layer as required to measure fluxes using eddy covariance techniques. Image adapted from Langford (2008).

To capture the full flux covariance requires high frequency sampling (at approx. 10 Hz) of atmospheric turbulence and volume mixing ratios, which necessitates fast response instruments for both wind and scalar measurements. Wind vectors are easily measured at this temporal

resolution using a sonic anemometer but analyte detection at this resolution is more difficult. If the sensor has a slow response time, a long sensor path (e.g. through an extended inlet tube), a low sampling rate, or a large distance between sensor placements, then low pass filtering of the turbulence signals (i.e. $w$ and $c$) can occur causing the attenuation of high frequency contributions to the flux (Aubinet *et al.*, 1999). Conversely, high pass filtering occurs when the sampling duration is too short or the averaging period fails to include contributions from large, slow moving eddies (Massman, 2000). Additional difficulties arise when measuring over heterogeneous surfaces such as forest canopies and urban areas, as the surface roughness of the tree crowns and buildings generates wake turbulence which disrupts the constant flux layer. Reliable measurements over these terrains are still possible when the measurement site is at a sufficient height above the tree crowns or street level, as the small scale heterogeneities blend together to form a homogeneous net flux. Furthermore, elevated sensor positioning enables the measurement of surface fluxes over larger areas to increase the spatial representation of heterogeneous terrain as long as the sensor is within the equilibrium layer. Urban areas can be more complex due to the multitude of street canyons and varying building structures and heights. However, aerosol and trace gas fluxes have been successfully quantified when measuring at sufficiently high elevations (Dorsey *et al.*, 2002; Grimmond *et al.*, 2002; Karl *et al.*, 2009a; Langford *et al.*, 2009; 2010b; Nemitz *et al.*, 2002; Velasco *et al.*, 2005; 2009).

### 3.2.1.1.1 Virtual disjunct eddy covariance

Ultrasonic anemometers are widely used in EC setups to measure the wind components at a high frequency. However, there are very few instruments to measure VOCs that have a sufficient response time for flux quantification by EC. The notable exception is the fast isoprene sensor (FIS) developed by Guenther and Hills (1998) which is based on chemiluminescence but is only effective for measurements of isoprene. Consequently, Rinne *et al.* (2001) developed a grab sampling system that filled canisters with air samples at a fast rate (e.g. 5 Hz response) every few seconds. This approach allowed the stored air sample to be analyzed during the few seconds (typically between 10 to 15 s) between grab samples using FIS or PTR-MS and resulted in a

discontinuous time series of VOC measurements and corresponding vertical wind velocities, i.e. a flux measurement that is based on a subset of the values that enter a standard eddy-covariance calculation (Lindinger *et al.*, 1993). The technique, dubbed disjunct eddy covariance (DEC), has been successfully used to measure VOC fluxes over crop and forest canopies (Grabmer *et al.*, 2004; Warneke *et al.*, 2002). Although validation studies have shown good agreement (within 10%) between DEC and EC data, there are still a number of impracticalities and uncertainties (Turnipseed *et al.*, 2009). The main drawbacks of DEC are i) the incomplete evacuation of the canisters which leads to a carry-over effect, ii) the practicalities of mounting the system close to the sonic anemometer, as it can disturb the air flow around the sonic anemometer, and iii) the potential chemical interaction (i.e. losses) of VOCs with each other and with the sampling system walls. The carry-over effect can be corrected for using the VOC concentrations and pressures in the current and previous storage reservoirs (Langford *et al.*, 2009). Otherwise, removing the grab sampling system reduces the system complexity and any interference of the air flow around the sonic anemometer. This was the basis for the development of an adapted version of DEC by Karl *et al.* (2001b), termed virtual disjunct eddy covariance (vDEC), which bypasses the necessity of sample canisters by utilizing the relatively fast response time of PTR-MS. This technique has been used several times for measuring VOC fluxes over forest (Davison *et al.*, 2009; Karl *et al.*, 2002; Langford *et al.*, 2010a; Misztal *et al.*, 2011; Spirig *et al.*, 2005) and urban canopies (Langford *et al.*, 2009; 2010b; Velasco *et al.*, 2005; 2009).

Capable of high frequency measurements (up to 5 Hz) a PTR-MS can sequentially measure a set of pre-determined VOC masses creating a discontinuous time series. Due to the size and complexity of the instrument it cannot be co-located with the sonic anemometer on the tower. This, as well as the discontinuous measurements, introduces different problems requiring the measurement setup to be adapted. As the PTR-MS can only measure individual masses sequentially, the measurement time of each compound must be sufficiently fast (approx. 0.2 s) in order to capture the flux carried by high frequency eddies. Furthermore, the length of the duty cycle, which depends on the number of compounds measured, must be limited to a few seconds

in order to maximise the number of data points used in the flux calculation, as this provides stronger statistics and reduces the random error in the flux. The distance between the sonic anemometer at the top of the tower and the PTR-MS at the foot of the tower introduces a significant lag time between the wind speed and the corresponding compound concentration measurements. A cross-correlation (*c-c*) function can help identify the temporal lag by finding a maximum correlation between the vertical wind speed and the compound concentration, which should occur at the moment of zero lag. Taking the above adjustments into consideration the vDEC flux calculation is expanded to

$$F = \frac{1}{n} \sum_{i=1}^{n} w' \left( \frac{i - t_{lag}}{\Delta t_w} \right) \times c'(i), \tag{3.7}$$

where *w'* and *c'* are the instantaneous fluctuations around the mean vertical wind ($w - \overline{w}$) and the mean VOC concentration ($c - \overline{c}$), *n* is the number of VOC concentration measurements per 30-60 min averaging period, $t_{lag}$ is the lag time between the wind and PTR-MS measurements due to the transit through the sampling line, and $\Delta t_w$ is the sampling interval of the vertical wind speed measurements of the sonic anemometer. The typical setup for this technique requires the sonic anemometer and extended instrument inlet line to be located together at the top of a mast or tower above the canopy. The minimum measurement height should be at least twice the mean height of the roughness elements when over more heterogeneous canopies ensuring it is outside the surface roughness layer (Grimmond and Oke, 1999). The sample air is pumped at a high flow rate (60-80 L min$^{-1}$) through a chemically inert tube (made from PTFE or PFA) to the PTR-MS, which is usually located in a container at the bottom of the tower. The instrument subsamples from the main line using a short tube at a lower flow rate (0.25-0.3 L min$^{-1}$). Sampling at a high flow rate ensures turbulent flow (Reynolds number, $Re > 4000$) is maintained which limits the attenuation of VOC signals by the tube walls.

There are different methods to determine the appropriate lag time between the wind and VOC measurements. Taipale *et al.* (2010) tested the most common methods including the calculated (CALC), typical (TYP), maximum (MAX), average (AVG), and visual (VIS) methods.

Both the CALC and TYP methods keep the lag time constant, which is either calculated using the sampling flow and line dimensions (CALC) or by deducing a typical daytime value from the median of several measurements (TYP). The maximum and average methods rely on the *c-c* function and use the absolute maximum point (MAX) or the value at the time-lag at which a running average of the *c-c* function peaks (AVG). The VIS method is based on manual assessment of the correlation function and visually determining the lag time for each flux period. We further investigated the effects of different lag time methods for data with poor signal-to-noise ratios, which is often found when VOC concentrations are low or analyzer noise is high (Langford *et al.*, 2015) (Appendix II). Methods that systematically search for a maximum in the *c-c* function within a given window (MAX method) can bias the calculated fluxes towards more extreme (positive or negative) values. The study recommends using a prescribed lag time determined either through the use of a monitored sample flow rate or by using the typical lag time derived by searching for a maximum as this results in a random flux error but does not cause a systematic bias. Different compounds interact with the walls of the sampling lines in different ways (i.e. they have different adsorbtion/desorption properties). For example, compounds such as water vapour or methanol are stickier, which results in longer time-lags. Consequently, where appropriate, time-lags should be independently calculated for each compound measured. Failure to account for these effects may result in a systematic underestimation of the flux. Further aspects of data post-processing and quality control are outlined below.

### *3.2.1.1.2 Sonic anemometer data corrections*

Usually, the horizontal or streamwise (*u*), lateral (*v*), and vertical (*w*) wind velocity components are aligned with respective longitudinal (*x*), lateral (*y*), and vertical (*z*) directions of a Cartesian coordinate system. A mathematical rotation of the coordinate system is applied in which $\bar{w}$ is forced to zero as the tilting of the sonic anemometer can cause the vertical wind component (*w*) to deviate from zero. A conventional rotation method of the coordinate frame is around the z-axis, aligning the x-axis with the mean horizontal wind direction ($\bar{v} = 0$) (Stull, 1988), and then rotating the x-axis to align *w* with the z-axis ($\bar{w} = 0$) (Baldocchi, 2003).

Processing of the sonic data and calculations of accompanying variables such as sensible heat ($H$) and momentum ($\tau$) fluxes, friction velocity ($u_*$), Obukhov length ($L$), wind speed ($ws$) and direction ($wd$) are found in Appendix I.

### 3.2.1.1.3 Fulfilment of basic eddy covariance criteria and attenuation corrections

Theoretical requirements for eddy covariance flux calculations include sufficiently developed turbulence and stationarity. Periods of insufficient turbulence, during which gases emitted by soil and vegetation may not reach the measurement height but be advected horizontally below the measurement height (drainage flow), can be filtered by applying a minimum threshold based on the friction velocity ($u_*$), whereby in this study a cut-off of $u_* \leq 0.15$ m s$^{-1}$ is applied as a typical value found during $u_*$ filter tests for $CO_2$. The stationarity requirement states that the statistical properties between the flux averaging periods are comparable and time independent. They must represent those of the measured process and not be a result of the averaging period (Dabberdt *et al.*, 1993). A test developed by Foken and Wichura (1996) declares that a time series fulfils stationarity when the flux equals the mean of its components (i.e. the 30 min flux $\approx$ the average of fluxes calculated over five minute intervals) within predefined error bounds. Therefore, if the mean of the flux components is >60% different to the respective 30-60 min averaged flux, the time series is considered to breach stationarity and must be rejected. A problem with this approach is that it tends to flag small fluxes as non-stationary and care needs to be taken that the remaining dataset does not get biased towards larger flux values.

Flux losses due to high and low frequency attenuation can be estimated and corrected for using the methods of Horst (1997) and Moncrieff *et al.* (2004), respectively. High frequency flux attenuation can be estimated by

$$F_h = 1 - \frac{1}{(1 + (2\pi f_m \tau_c)^{\alpha_1})}, \tag{3.8}$$

where $\tau_c$ is the instrument related characteristic time constant (i.e. PTR-MS dwell time), $\alpha_1$ is $\frac{7}{8}$ for neutral to unstable stratification within the surface layer, and $f_m$ is the frequency of the peak of the logarithmic cospectrum. The frequency $f_m$ can be estimated by

$$f_m = \frac{n_m \bar{u}}{z_m - d},$$

(3.9)

in which $n_m$ is the normalized frequency of the logarithmic co-spectral peak and equals 0.085 for neutral and unstable stratification, $\bar{u}$ is the mean horizontal wind speed, $z_m$ is the measurement height, and $d$ the displacement height which equals ⅔ of the canopy height ($d = $ ⅔$z_h$) (Horst, 1997).

Attenuation from low frequency fluctuations for the averaged flux period (e.g. 30 min) can be investigated by analyzing the sensible heat fluxes with progressively longer averaging periods, e.g. 60, 90, 120 and 150 min. The coordinate rotation is applied to the joined files individually, which acts as a high pass filter to the three wind vectors, confirming that fluctuations of eddies with a longer time period than the 30 min averaging time do not contribute to the flux measurement (Moncrieff *et al.*, 2004). The fluxes are then compared back to the 30 min averaged fluxes, which have the coordinate rotation applied before joining, again to ensure only turbulent fluctuations of ≤30 min contribute to the flux.

### 3.2.1.1.4 Flux precision and limits of detection

One approach to estimating the limit of detection (LoD) of a flux measurement is to quantify the noise of the cross-correlation (*c-c*) function. This is calculated using the method of Spirig *et al.* (2005), where one standard deviation of the *w'c'* covariance at a sufficient distance away from the true lag time (3-4 times the integral timescale) is then multiplied by three to give the flux precision with a 99.7% confidence interval. Unlike concentration LoDs, flux measurement LoDs are derived from the fluctuations in the covariance function and are not constant, due to the correlating characteristics of the sensors (i.e. sonic anemometer and PTR-MS) and the instantaneous atmospheric conditions during each flux period. Furthermore, the range of LoDs for different compounds does not only depend on the instrument sensitivities, but also varies with ambient concentrations and background signals at a specific mass, since non-turbulent fluctuations increase the general noise of the covariance function. In Langford *et al.* (2015), we discuss the use of the root mean square deviation (RMS) method from Nemitz *et al.*

(in preparation) to calculate the flux detection limit that can be applied to data with different signal-to-noise ratios.

The effect of the instrument noise on the flux detection limit can also be isolated from other effects: for this purpose, a white noise flux with a sigma matching the instrument noise is generated and applied to the $c$-$c$ function with $w'$ to obtain the instrumental random noise. This allows the separation of the instrument noise and genuine variability of VOC concentrations that both contribute to the $c$-$c$ function variability, and thus an approximation of the total random error of a flux (Langford *et al.*, 2015).

## 3.2.2 Modelled estimates and small-scale measurement techniques: Bottom-up methods

Bottom-up estimates are widely used to report city-scale, ecosystem-scale, national or global emissions of anthropogenic (aVOC) and biogenic VOCs. Estimates of aVOCs are based on the emission intensity of various anthropogenic activities, which produces an emission estimate per unit area and can be aggregated to form an emissions inventory. Emission estimates of bVOCs are derived from models based on temperature and/or light modification factors, but there are also physiological models of isoprene emissions, which include the budgets of isoprene synthesis and photosynthesis. However, most models combine the light and temperature activity adjustment factor with a term for ecosystem properties such as foliage density, seasonal variability, species composition, and a species-specific or plant functional group-specific VOC "base" emission rate at a given set of standard conditions of temperature and PAR. The key component is often this base emission rate, which depends on the plant species or functional type. The average base emission rate estimated for a particular biome is based on measurements from leaves, chamber enclosures, or canopies from the respective ecosystem. Both types of estimates can be compared with measured VOC fluxes or scaled up to produce regional or global VOC emission budgets.

**3.2.2.1 Emission estimates of aVOCs using emission inventories**

Anthropogenic VOC emissions are estimated using detailed emission inventories, which provide biannual estimates of pollutants per unit area (e.g. 1 km$^2$) based on known emission sources from a variety of sectors. The UK National Atmospheric Emissions Inventory (NAEI), which is commissioned by the Department for Environment, Food and Rural Affairs (Defra), provides emission estimates for total non-methane VOCs in addition to which the priority pollutants benzene and 1,3-butadiene are listed separately. The NAEI separates emission contributions into 11 SNAP (Selected Nomenclature for sources of Air Pollution) sectors consisting of industrial, commercial and residential combustion and other processes, energy production, fossil fuel extraction, road and other transport, waste treatment, solvent use, agriculture, nature, and point sources. SNAP sector distributions are constructed using statistics appropriate to the type of sector. Information on large point sources are retrieved from official UK bodies, such as the Environment Agency, whereas area sources are represented by a distribution map generated from surrogate statistics appropriate for that sector. In the latter case emission estimates are calculated by multiplying an emission factor with an activity statistic representative of that particular sector. Using the example of road transport, the mass of a pollutant emitted per volume of fuel consumed is multiplied by the amount of fuel consumed per year. There are large uncertainties associated with the estimates depending on the accuracy of the statistical information used to construct the activity statistic. Each estimate is accompanied by a quality rating calculated from each source emission and overall emissions for each pollutant (NAEI, 2014). Emission estimates are available for non-methane VOCs in kg km$^{-2}$ a$^{-1}$ based on the 1 km resolution Ordinance Survey grid and a total annual emission for the UK is reported. Limited information on indirectly speciated VOCs is available, whereby species profiles are used to describe the chemical components of total VOC emissions from each source type. Contributions of individual VOC species are shown as a percentage of the total emissions of the respective source. There are large uncertainties associated with the speciated emission estimates, as i) minor emission sources lack species profiles, ii) emission sources may contain unspeciated components, iii) emission sources are speciated using species profiles from different sources on

the assumption that emission characteristics are similar, and iv) species profiles are assumed to be realistic, but may not be accurate (Bush *et al.*, 2006; Passant, 2002).

At the national level air quality models using inventory emission estimates generally compare well with measured ambient concentrations by automatic air quality monitoring sites (van Loon *et al.*, 2007; Williams *et al.*, 2011). Currently 27 NMVOC mixing ratios are monitored across four sites in the UK by the Automatic Hydrocarbon Network (AHN). These sites use an automated GC-FID system providing hourly average concentrations. In areas where emissions have high spatial and temporal variability, such as in urban centres, hourly averages fail to capture short term (<1 h) changes in mixing ratios including high frequency maxima. Furthermore, emission estimates require comparisons with direct canopy-scale flux measurements, which the AHN is unable to provide. Although AHN sites most of the time fulfil the data quality objectives set out by the Global Atmosphere Watch (GAW) of the World Meteorological Organization (WMO), they performed poorly using the more demanding quality controls within the framework of the European infrastructure ACTRIS (Aerosols, Clouds, and Trace gases Research InfraStructure Network). Measurement performance in terms of uncertainty and repeatability of measurement results from a multicomponent VOC mixture in whole air using standardized operation procedures are as high as 20% and 15% respectively for GAW, but are set to 5% and 2% respectively in ACTRIS (Hoerger *et al.*, 2014).

### 3.2.2.2 Modelled bVOC emission estimates

Emissions of dominant bVOCs, i.e. isoprene and monoterpenes, are species specific and depend on environmental conditions, primarily temperature and photosynthetically active radiation (PAR). In order to develop a bVOC emission model, these drivers and their effects on emissions, as well as the emission rates themselves, must be quantified.

The base algorithm to model foliar isoprene and monoterpene emissions was developed by Guenther *et al.* (1995), which was

$$F_{95} = \varepsilon_0 \times D_0 \times \gamma_0, \tag{3.10}$$

where $\varepsilon_0$ is the leaf base emission rate at standard conditions (30 °C and 1000 μmol m$^{-2}$ s$^{-1}$ PAR) in μgC g$^{-1}$ dry weight h$^{-1}$, $D_0$ is the foliar density in kg dry matter m$^{-2}$, and $\gamma_0$ is a dimensionless activity adjustment factor accounting for variations in PAR and temperature. An additional canopy radiative transfer model can be used as part of $\gamma_0$ to simulate the variability in solar radiation fluxes within a vegetation canopy by computing the PAR flux density on sunlit and shaded leaves (see Appendix I for detailed equations). The further development of this algorithm led to the Model of Emissions of Gases and Aerosols from Nature (MEGAN) (Guenther *et al.*, 2006), which expands the previous equation to

$$F_{06} = \varepsilon \times \gamma \times \rho, \tag{3.11}$$

where $\varepsilon$ is the canopy emission factor at standard conditions (30 °C and 1500 μmol m$^{-2}$ s$^{-1}$) in mg m$^{-2}$ h$^{-1}$, which in this version includes the previously separate foliar density ($D_0$), $\gamma$ is the emission activity factor that accounts for emission changes because of deviations from standard conditions, and $\rho$ represents a within-canopy production and loss factor.

At the regional and global scale the emission factor $\varepsilon$ can be calculated from the dominant plant functional types (PFT). Ideally, at the local to regional scale canopy flux measurements should be used to determine the net ecosystem emission rate. However, before direct canopy-scale measurements were developed, only leaf level cuvette measurements of bVOC emission rates were available. This approach requires an understanding of the community composition of the biome, as well as obtaining base emission rates for each plant species in order to produce an accurate ecosystem-scale emission rate. Large uncertainties with both requirements lead to biased model outputs. The main issues are related to (i) the measurement technique and (ii) the low sample number and representativeness of the measurements. In the first instance the presence of the cuvette or enclosure introduces additional complications such as changes to the immediate environment of the leaves, which could alter emissions, as well as providing surfaces or condensation for VOCs to react with. Even using improved measurement techniques such as light and temperature controlled leaf cuvettes to maintain ambient conditions, other problems relating to VOC chemistry and plant physiology remain. For example, as bVOCs are often light and

temperature dependent there are physiological differences in sun and shade leaves and therefore emissions, making the selection of leaves to be monitored a primary concern. However, sun leaves are often at the top of the canopy and are not easily accessible.

Using branch enclosures with either static or dynamic air through-flows captures some of the natural variability in emission rates between leaves, but it is not always possible to reach ideal branches. The second issue concerns the representativeness of the measurements due to the species composition of ecosystems. Often there are dominant species that emit high amounts of either isoprene and/or monoterpenes, e.g. oak (*Quercus* spp.) and poplar (*Populus* spp.) species in temperate deciduous forests or pine (*Pinus* spp.) species in boreal coniferous forests, which have an average of 3-4 tree species $km^{-2}$ (Perry, 1994). Assuming intra-species differences in base emission rates are minimal and dominant emitting species have been identified, leaf level measurements may suffice to accurately model total ecosystem emissions. However, in areas of high biodiversity such as the Amazon tropical forest with an average of 250 tree species $ha^{-1}$ (Valencia *et al.*, 2004), which is a major source of bVOCs, the task of providing detailed species inventories, as well as obtaining a sufficient sample size of representative leaf level emissions becomes exceedingly difficult. Even in monocultures intra-species differences may be large (Hakola *et al.*, 2006; Tarvainen *et al.*, 2005).

Terms describing the effects of environmental drivers on bVOC emissions (i.e. $\gamma$) have been adapted and improved over time based on measured emission responses to PAR and temperature, but also factors such as wind speed, humidity, and soil moisture. In the initial versions of emission models these responses were based on investigations using temperate plants under temperate conditions. However, this is not representative of the majority of isoprene emissions, as the largest emissions are from tropical forests. In recent years the database has expanded to include responses in tropical climates as data of direct canopy emissions have become increasingly available for a range of different environments with the emergence of eddy covariance techniques. Moreover, the importance of past light and temperature conditions has been recognized and newer algorithms include terms which take the 24 h and 240 h prior PAR

and temperature levels into consideration. This highlights the necessity for accurate measurements of PAR and temperature to improve modelled emissions at the local scale. MEGAN offers a range of methods to calculate the variables necessary for the calculation of $\gamma$. Options include the standard method, which uses a full canopy environment model to estimate leaf level PAR and temperature for sun and shade leaves at various canopy depths as a function of several ecosystem parameters, as well as the current and past canopy climate. Alternative methods provide a means with which a simple canopy environment model can be implemented requiring less detailed meteorological and environmental measurements. The least complex version consists of simplified parameterized canopy environment emission activity (PCEEA) algorithm for $\gamma$ and further assumptions, wherein many variables are assigned a constant value. Newer versions of MEGAN v2.0 and v2.1 are now integrated in more widely used chemistry transport and Earth systems models such as the Weather Research and Forecasting (WRF-Chem) model and the Community Land Model (CLM) of the Community Earth System Model (CESM).

Overall, models using leaf or branch-level measurements, mechanistic models of leaf emissions, or a combination thereof to extrapolate emissions have provided good insights in bVOC fluxes for a range of ecosystems at the regional to global scale, but most are still associated with large uncertainties (Arneth *et al.*, 2007b; 2011; Guenther *et al.*, 1995; 2006; Niinemets *et al.*, 1999; Owen and Hewitt, 2000; Räisänen *et al.*, 2009; Simpson *et al.*, 1995; Sitch *et al.*, 2003). At the local scale, modelled isoprene emissions using MEGAN over undisturbed forest canopies generally compare well with canopy-scale flux measurements, even when simpler model versions such as PCEEA are implemented (see Paper III, and Karl *et al.*, 2007, Langford *et al.*, 2010a, and Misztal *et al.*, 2011). When deriving basal emission rates from canopy-scale flux measurements, care needs to be taken to use algorithms that are compatible with those used for the forward calculations of the modelled fluxes, i.e. when deriving the base emission rate from the slope of the regression with $\gamma$, the same version of $\gamma$ must be used to model the fluxes.

# Chapter IV

# 4 Paper I: Concentrations of volatile organic compounds at kerbside and background sites in central London

This chapter details the first deployment of the PTR-MS to measure a range of anthropogenic VOC concentrations at two contrasting urban sites, i.e. an urban background site and a kerbside site. The measurements were taken during the winter intensive observation period of the NERC-funded ClearfLo project in London during January and February 2012. The PTR-MS was placed at the urban background site at the Sion Manning School in North Kensington between 16 January - 25 January before being moved to the urban kerbside site at Marylebone Rd during 25 January until 7 February, which is a site used for the Automatic Hydrocarbon Network (AHN) in central London. The results at the kerbside site were compared with those made by the AHN which employs a GC-FID. The comparison between sites showed that mixing ratios were higher at the kerbside site. The instrument comparison indicated that the PTR-MS captured high resolution fluctuations in VOC concentrations, but measurements were higher than GC-FID measurements and therefore the instrument may suffer from humidity dependencies, for which corrections were attempted, and isobaric interference due to additional compounds or fragments.

The following work was submitted to the journal Atmospheric Environment on 25 January 2014 and accepted for publication on 25 June 2014. The authors' contributions were as follows:

**Amy C. Valach (Lancaster University):** Operated the instrument during the field campaign, processed the data, performed the analyses, and wrote the manuscript.

**Ben Langford (CEH):** Assisted with instrument operation, provided guidance on data processing and analysis, and helped compile the manuscript.

**Eiko Nemitz (CEH):** Helped with data processing, analysis, and compilation of the manuscript.

**A. Rob MacKenzie (University of Birmingham):** Helped with interpretation of the results and compilation of the manuscript.

**C. Nick Hewitt (Lancaster University):** Devised the research, obtained funding, helped with interpretation of the results and compilation of the manuscript.

## Concentrations of selected volatile organic compounds at kerbside and background sites in central London

A.C. Valach [a], B. Langford [b], E. Nemitz [b], A.R. MacKenzie [c], C.N. Hewitt [a,*]

[a] Lancaster Environment Centre, Lancaster University, Lancaster, LA1 4YQ, United Kingdom
[b] Centre for Ecology & Hydrology, Bush Estate, Penicuik, Midlothian, EH26 0QB, United Kingdom
[c] School of Geography, Earth and Environmental Sciences, University of Birmingham, Edgbaston, Birmingham, B15 2TT, United Kingdom

### HIGHLIGHTS

- Volatile organic compound concentrations were measured in central London.
- Measurements were compared with the automatic hydrocarbon network.
- Vehicle emissions were the main source at both urban background and kerbside sites.
- Some effects of temperature on compound correlations were observed.
- Excellent qualitative agreement was seen between the measurement instruments.

### ABSTRACT

Ground-level concentrations of nine volatile organic compounds (VOCs) were measured using a proton transfer reaction-mass spectrometer (PTR-MS) in central London at an urban background (North Kensington, NK, during 16th–25th Jan 2012) and a kerbside site (Marylebone Rd, MRd, during 25th Jan–7th Feb 2012) as part of the winter intensive observation period of the ClearfLo project. Site comparisons indicated that VOC concentrations at the urban background site were significantly lower than at the kerbside site (ratio MRd/NK of 2.3). At the kerbside site PTR-MS measurements of aromatics (benzene,

# 4 Concentrations of volatile organic compounds at kerbside and background sites in central London

A. C. Valach[a], B. Langford[b], E. Nemitz[b], A. R. MacKenzie[c] and C. N. Hewitt[a]

[a]{Lancaster Environment Centre, Lancaster University, Lancaster, LA1 4YQ, United Kingdom (a.valach@lancaster.ac.uk; n.hewitt@lancaster.ac.uk)}

[b]{Centre for Ecology & Hydrology, Bush Estate, Penicuik, Midlothian, EH26 0QB, United Kingdom (benngf@ceh.ac.uk; en@ceh.ac.uk)}

[c]{School of Geography, Earth and Environmental Sciences, University of Birmingham, Edgbaston, Birmingham, B15 2TT, United Kingdom (a.r.mackenzie@bham.ac.uk)}

Correspondence to: C. N. Hewitt (n.hewitt@lancaster.ac.uk)

## Abstract

Ground-level concentrations of nine volatile organic compounds (VOCs) were measured using a proton transfer reaction-mass spectrometer (PTR-MS) in central London at an urban background (North Kensington, NK, during 16th - 25th Jan 2012) and a kerbside site (Marylebone Rd, MRd, during 25th Jan - 7th Feb 2012) as part of the winter intensive observation period of the ClearfLo project. Site comparisons indicated that VOC concentrations at the urban background site were significantly lower than at the kerbside site (ratio MRd/NK of 2.3). At the kerbside site PTR-MS measurements of aromatics (benzene, toluene, $C_2$- and $C_3$-benzenes) were compared with the gas chromatography – flame ionization detector data from the UK Government's Automatic Hydrocarbon Network. Very good qualitative agreement was observed between the two methods ($r = 0.90 - 0.91$, $p < 0.001$, $N = 260$), although there was a significant offset between the instruments. This was partly due to issues with humidity dependent background measurements, but possibly also from isobaric interference of other compounds and their fragments, giving a positive bias to the PTR-MS data. Most compounds showed strong indications of traffic-related sources with double rush hour peaks in diurnal profiles and high correlations with known traffic-related compounds ($r = 0.68 - 0.97$ at NK , $0. 48 - 0.87$ at MRd, $p < 0.001$, $N_{NK} = 2202-2227$, $N_{MRd} = 2705-2720$) and CO ($r = 0.80-0.96$ at NK, $0.65-0.84$ at MRd, $p < 0.001$, $N_{NK} = 223$, $N_{MRd} = 256-274$). Polar plots agreed with statistical analysis of wind direction dependency and identification of potential emission sources was attempted.

## 4.1 Introduction

Anthropogenic sources of volatile organic compounds (VOCs) are of particular importance in urban areas due to the intensity of fossil fuel combustion and the relative paucity of biogenic sources in cities. A wide range of VOCs are emitted directly by the evaporation of fuels and solvents, as unburnt fuel and as partially oxidized compounds from combustion processes, mostly vehicle emissions (Kansal, 2009). Some VOCs can directly affect human health (e.g. benzene, which is a known carcinogen) while others contribute to the formation of ozone

and aerosol particles in the atmosphere (Derwent, 1995). Both have detrimental effects on human health and the environment (Kim *et al.*, 2001). In winter elevated VOC concentrations are observed due to the shallow daytime boundary layer with limited dilution and mixing. In the UK, VOC emissions are subject to control under European Commission Directive 2008/50/EC. Monitoring networks such as the Automatic Hydrocarbon Network (AHN) provide a running annual mean concentration for a suite of pollutants. Emissions are estimated as part of the National Atmospheric Emission Inventory (NAEI) activity (Yardley *et al.*, 2012).

A wide range of studies focus on VOC concentrations and air quality in cities around the world using diverse measuring techniques (Baker *et al.*, 2008; Jobson *et al.*, 2010). Due to the variety of emission sources, meteorological conditions, and often short atmospheric lifetimes of the compounds, VOC volume mixing ratios can be associated with large variability. Slow response instruments have identified seasonal patterns of urban VOC concentrations (Kim *et al.*, 2001), however only fast response instruments have been shown to record short term temporal variability.

The aim of this study was to:

i.    Quantify a suite of VOCs at an urban background and a kerbside site in winter and;

ii.   Compare VOC volume mixing ratios from fast response PTR-MS measurements with the GC-FID measurements from the Automatic Hydrocarbon Network.

This study was part of the winter intensive observation period of the Clean Air for London project (ClearfLo, www.clearflo.ac.uk), aimed to research boundary layer pollution over London in 2011-2012 (Bohnenstengel *et al.*, 2015). Here we report measurements of nine VOC species measured at high temporal resolution at a kerbside and a background site in central London (16th January - 7th February 2012).

## 4.2 Methods

### 4.2.1 Measurement sites and meteorology

Details of both the North Kensington (NK) background and Marylebone Rd (MRd) kerbside sites are compared (Supplementary content Table 4.A1). Air was pumped through a PTFE inlet (and PTFE filter at MRd) attached to 1/4" OD PTFE tubing to a high sensitivity proton transfer reaction-mass spectrometer (PTR-MS; Ionicon Analytik GmbH, Innsbruck, Austria).

Meteorological measurements were co-located with the inlet at NK (Figure 4.1 and Supplementary content Table 4.A1). The mean UK temperature in January was 6.0 °C, i.e. 1.3 °C above the 1971-2000 average (Met Office UK, 2012), although February experienced low temperatures and snowfall, which is uncommon in London.
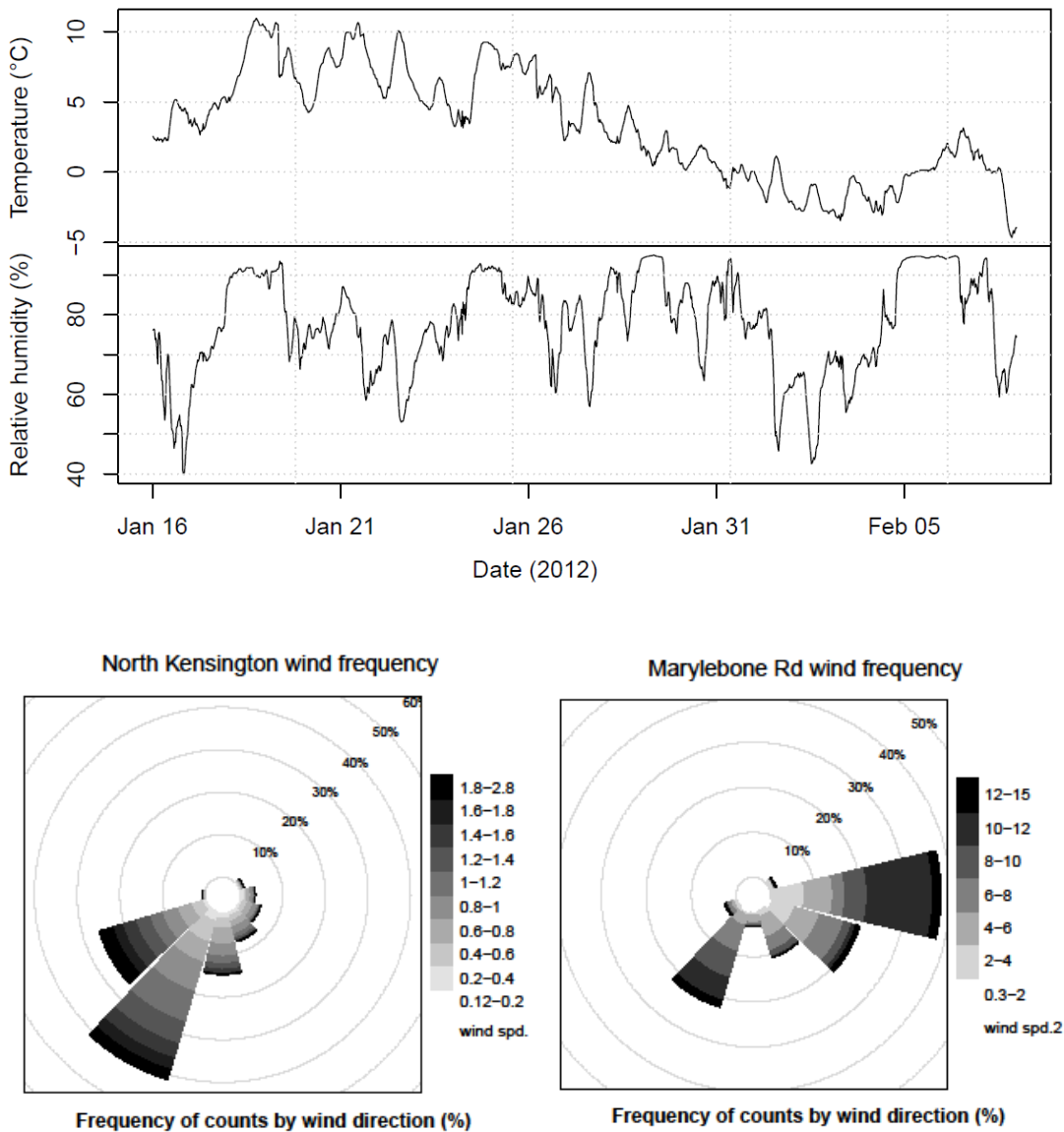
**Figure 4.1.** *Top*: 5 min means of ambient air temperature (°C) and relative humidity (%) during the campaign 16th Jan – 7th Feb 2012. *Bottom*: Frequency plots of mesoscale wind direction (%) with subcategories of wind speed (m s^{-1}) using 30 min mean data from the WXT520 (Vaisala Ltd) at 190 m on the BT tower at NK (16th – 25th Jan 2012) (*left*) and MRd (25th Jan – 7th Feb 2012) (*right*).

### 4.2.2 VOC sampling

VOC mixing ratios were measured on-line using a PTR-MS (de Gouw and Warneke, 2007; Lindinger *et al.*, 1998). The instrument was operated in multiple ion detection (MID) and mass scan (SCAN) modes (Supplementary content 4.5.A1). In MID mode the quadrupole mass spectrometer scanned through 11 pre-determined masses, to which the following compounds were

ascribed: $m/z$ 21 (indirect quantification of $m/z$ 19 primary ion count [$H_3O^+$] via isotopologue [$H_3^{18}O^+$]), $m/z$ 33 (methanol), $m/z$ 39 (indirectly quantified $m/z$ 37 first cluster [$H_3O^+.H_2O^+$]), $m/z$ 42 (acetonitrile), $m/z$ 45 (acetaldehyde) $m/z$ 59 (acetone/propanal), $m/z$ 69 (cycloalkanes/isoprene), $m/z$ 79 (benzene), $m/z$ 93 (toluene), $m/z$ 107 ($C_2$-benzenes) and $m/z$ 121 ($C_3$-benzenes).

The UK national Automatic Hydrocarbon Network (AHN) station at MRd measures 29 different hydrocarbons using a gas chromatography-flame ionization detector (GC-FID, AutoSystem XL; PerkinElmer Inc., USA). This method complies with standards set out by the European Air Quality Directive (Broadway and Tipler, 2008). A 40 min continuous sampling period provides hourly means (Supplementary content 4.5.A2).

PTR-MS measures in unit mass resolution and a fragment may derive from several parent compounds, therefore each detected mass may relate to one or more compounds. Where possible, measurements should be verified by more specific analytical techniques, such as GC-FID. Unfortunately, only benzene, toluene, some $C_2$- and $C_3$-benzenes were verified by the AHN.

### 4.2.3 Quality analyses and data handling

The PTR-MS was calibrated over a range of concentrations using a certified multi-component VOC gas standard (Ionimed Analytik GmbH, Austria). The measured instrument sensitivities were then used to convert normalized count rates of $RH^+$ to volume mixing ratios (Langford *et al.*, 2010a). The instrument background was quantified using a platinum catalyst and subtracted from the ambient measurements. Since the background was determined for dry air, corrections for humidity effects on some compounds had to be applied and were associated with large uncertainties (Supplementary content 4.5.B).

A low pass filter was applied to smooth the data and reduce instrumental noise. Spearman's rank correlation coefficients and Wilcoxon rank sum tests were used in statistical analyses due to the data distributions.

## 4.3 Results and Discussion

### 4.3.1 VOC concentrations

VOC concentrations measured by the PTR-MS at the North Kensington (NK) background site (Figure 4.2a) and at the Marylebone Rd (MRd) kerbside site (Figure 4.2b) are summarized in Table 4.1a and 4.1b. At both sites methanol, acetaldehyde and acetone, all oxygenated compounds, were the most abundant. Methanol has a variety of biogenic, anthropogenic and atmospheric sources (Cady-Pereira *et al.*, 2012). Acetone has some biogenic contributions but solvents and tailpipe emissions were most likely the main sources (de Gouw *et al.*, 2005; Reissell *et al.*, 1999; Warneke *et al.*, 1999). Both have a low photochemical reactivity with OH resulting in longer atmospheric lifetimes, which also contributed to the relatively high mixing ratios. The compounds with the lowest mixing ratios at both sites were acetonitrile and cycloalkanes/isoprene. Although these are emitted from vehicle exhaust, their volume mixing ratios were much lower than other traffic-related compounds. The isoprene component of *m/z* 69 was estimated at 22% and presumably from traffic as the biogenic component was absent due to the season (Borbon *et al.*, 2001). Comparison with GC-FID isoprene concentrations at NK inferred that cycloalkanes provided a significant contribution to *m/z* 69 (Supplementary content 4.5.C) (Erickson *et al.*, 2014 ;Yuan *et al.*, 2014). Although globally biomass burning is the main source of acetonitrile (Holzinger *et al.*, 2001), in urban areas emissions from vehicle exhaust are prominent as diurnal profiles resembled a double rush hour pattern (Section 4.3.4) with some increased acetonitrile emissions occurring at low temperatures possibly from solid fuel burning (Section 4.3.3).
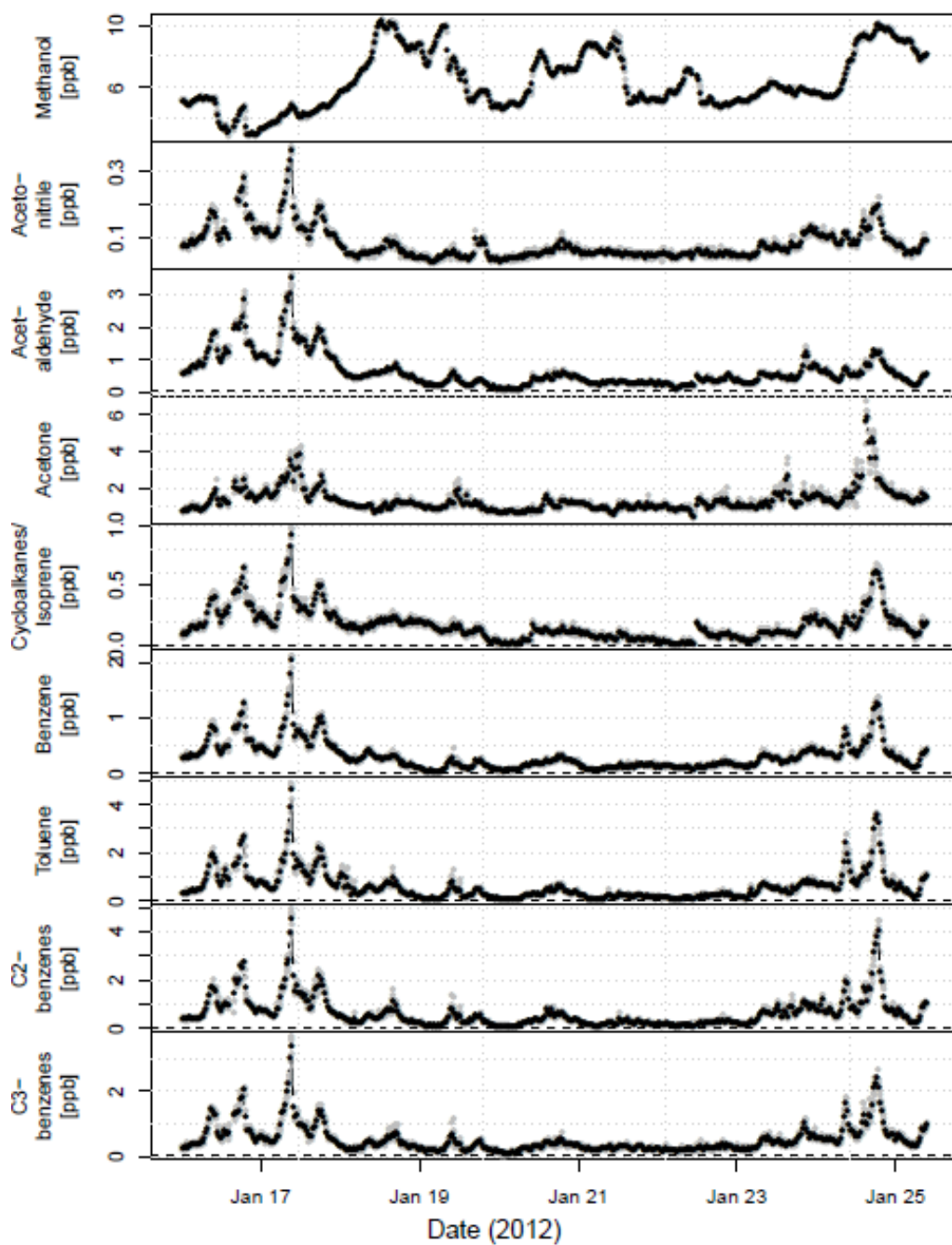
**Figure 4.2a.** 5 min mean (grey) and 25 min means (black) with detection limits (dashed line) for all measured VOCs (ppb) at North Kensington. *M/z* are 33 (methanol), 42 (acetonitrile), 45 (acetaldehyde), 59 (acetone), 69 (cycloalkanes/isoprene), 79 (benzene), 93 (toluene), 107 ($C_2$-benzenes) and 121 ($C_3$-benzenes).
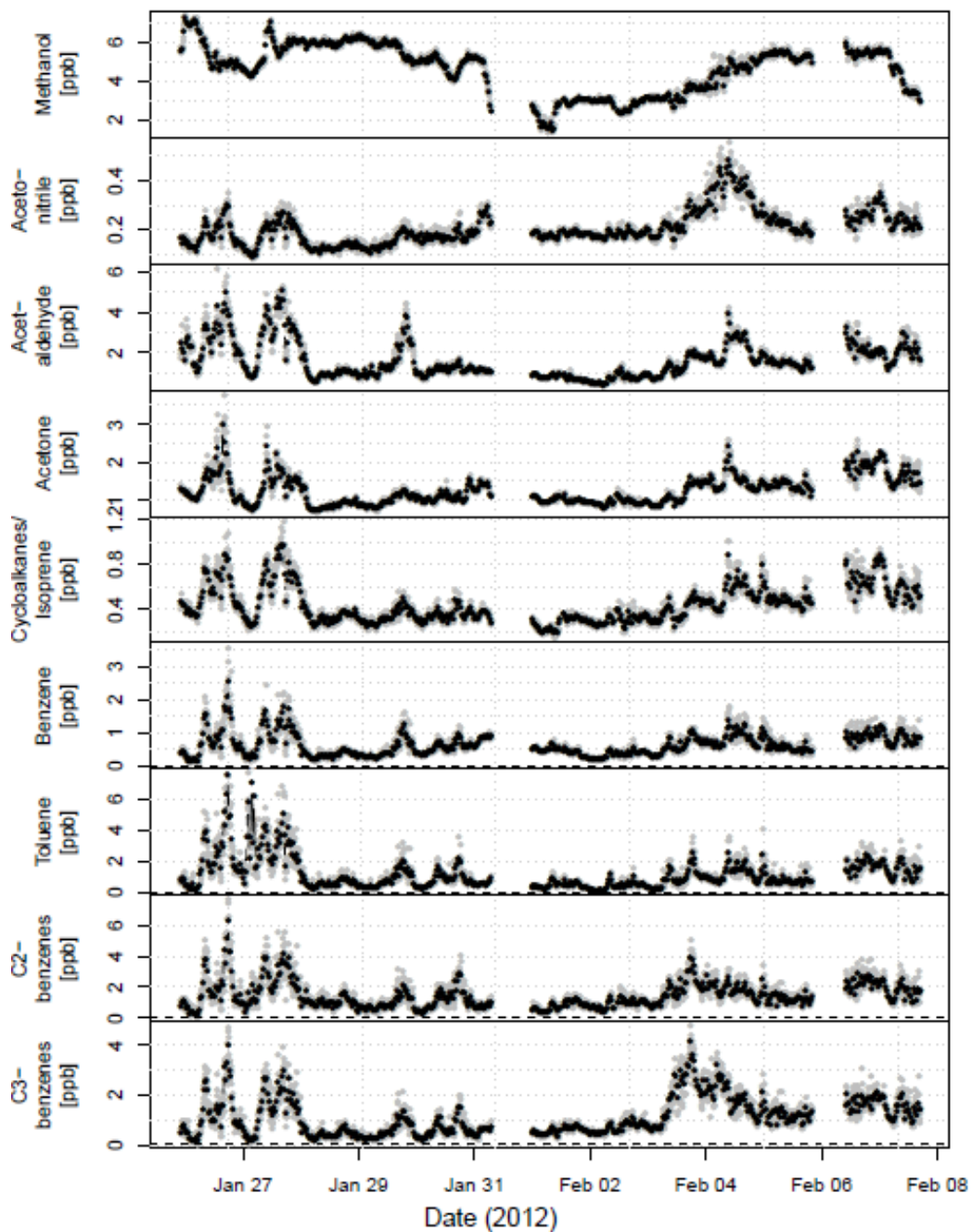
**Figure 4.2b.** 5 min mean (grey) and 25 min means (black) with detection limits (dashed line) for all measured VOCs (ppb) at Marylebone Rd. *M/z* are 33 (methanol), 42 (acetonitrile), 45 (acetaldehyde), 59 (acetone), 69 (cycloalkanes/isoprene), 79 (benzene), 93 (toluene), 107 ($C_2$-benzenes) and 121 ($C_3$-benzenes).

*Table 4.1a. Summary of 5 min averages of VOC mixing ratios (ppb) at North Kensington, London (16th - 25th Jan 2012). b. Summary of 5min averages of VOC mixing ratios (ppb) at Marylebone Rd, London (25th Jan - 7th Feb 2012).*

| Mixing ratios (ppb) | Methanol m/z 33 | Aceto-nitrile m/z 42 | Acetal-dehyde m/z 45 | Acet-one m/z 59 | Cyclo-alkanes/ Isoprene m/z 69 | Benzene m/z 79 | Tol-uene* m/z 93 | C2-benzenes m/z 107 | C3-benzenes m/z 121 |
|---|---|---|---|---|---|---|---|---|---|
| Lifetime (OH[a]) | 12 d | 1.5 yr | 8.8 h | 53 d | 1.4 h | 9.4 d | 1.9 d | 5.9 h[b] | 4.3 h[c] |
| N | 2219 | 2202 | 2211 | 2213 | 2199 | 2227 | 2226 | 2225 | 2226 |
| LoD | 0.37 | 0.04 | 0.18 | 0.06 | 0.005 | 0.04 | 0.01 | 0.08 | 0.03 |
| Min. | 2.86 | <LoD | <LoD | 0.37 | <LoD | <LoD | 0.03 | <LoD | 0.04 |
| 1st quartile | 5.06 | 0.05 | 0.29 | 0.95 | 0.08 | 0.14 | 0.21 | 0.23 | 0.24 |
| Median | 5.77 | 0.06 | 0.46 | 1.16 | 0.14 | 0.24 | 0.42 | 0.44 | 0.37 |
| Geom. mean | 6.17 | 0.07 | 0.50 | 1.25 | 0.13 | 0.24 | 0.42 | 0.45 | 0.40 |
| Arithm. mean | 6.40 | 0.08 | 0.62 | 1.34 | 0.17 | 0.31 | 0.60 | 0.63 | 0.50 |
| 3rd quartile | 8.00 | 0.07 | 0.75 | 1.51 | 0.21 | 0.39 | 0.74 | 0.79 | 0.59 |
| Max. | 10.4 | 0.10 | 3.67 | 6.79 | 0.98 | 2.13 | 4.92 | 4.89 | 3.65 |
| SD | 1.84 | 0.05 | 0.51 | 0.67 | 0.13 | 0.26 | 0.61 | 0.62 | 0.42 |
| Skew | 0.39 | 2.09 | 2.08 | 3.02 | 1.90 | 2.19 | 2.53 | 2.62 | 2.61 |
| Kurtosis | -0.89 | 6.03 | 5.25 | 13.5 | 4.85 | 6.96 | 8.71 | 9.45 | 9.36 |
| | | | | | | | | | |
| N | 2712 | 2718 | 2716 | 2705 | 2720 | 2715 | 2713 | 2708 | 2715 |
| LoD | 0.37 | 0.04 | 0.18 | 0.06 | 0.005 | 0.04 | 0.01 | 0.08 | 0.03 |
| Min. | 1.34 | 0.08 | 0.38 | 0.70 | 0.15 | 0.06 | 0.02 | <LoD | 0.05 |
| 1st quartile | 3.47 | 0.16 | 0.92 | 0.95 | 0.31 | 0.38 | 0.49 | 0.81 | 0.50 |
| Median | 5.00 | 0.19 | 1.34 | 1.15 | 0.39 | 0.56 | 0.80 | 1.21 | 0.86 |
| Geom. Mean | 4.48 | 0.19 | 1.39 | 1.20 | 0.41 | 0.55 | 0.85 | 1.21 | 0.85 |
| Arithm. Mean | 4.67 | 0.20 | 1.61 | 1.25 | 0.44 | 0.63 | 1.18 | 1.45 | 1.11 |
| 3rd quartile | 5.61 | 0.24 | 2.07 | 1.47 | 0.53 | 0.81 | 1.50 | 1.87 | 1.52 |
| Max. | 7.39 | 0.56 | 6.18 | 3.78 | 1.18 | 3.57 | 10.0 | 7.60 | 4.76 |
| SD | 1.27 | 0.07 | 0.92 | 0.38 | 0.17 | 0.35 | 1.13 | 0.9 | 0.79 |
| Skew | -0.47 | 1.33 | 1.29 | 1.21 | 1.05 | 1.68 | 2.8 | 1.62 | 1.21 |
| Kurtosis | -0.72 | 2.28 | 1.53 | 2.04 | 0.65 | 5.36 | 11.6 | 0.02 | 1.20 |

[a] Atmospheric lifetimes with regard to OH for a 12 h daytime average OH radical concentration of $2.0 \times 10^6$ molecule $cm^{-3}$ (Atkinson, 2000).

[b] Example using *m*-xylene.

[c] Example using 1,2,4-trimethylbenzene.

Mixing ratios for most of the compounds agreed with or were lower than observations from other urban areas, but benzene and C2-benzene concentrations were slightly higher at MRd compared with previous observations in UK cities (Langford *et al.*, 2009, 2010b). The

measurement proximity to the source emissions must be considered; for example, Langford *et al.* (2010b) reported concentration measurements from tall towers where the effects of dilution and photochemical loss are greater. During both measurement periods the beginnings and ends were marked by high pollution episodes (16th -18th, 24th -28th Jan and 3rd -7th Feb).

### 4.3.1.1 Site comparison

The volume mixing ratios of all compounds were significantly different ($p$ <0.001) between NK and MRd, except for acetone ($p$ = 0.26). Acetone has a relatively long atmospheric lifetime (Table 4.1a) and therefore mixing ratios are often homogenous over larger areas. Apart from methanol, which was 1.5 times higher at NK, the remaining compounds were up to 3 times higher at the MRd site with a mean site ratio (MRd/NK) of 2.3. This difference is related to the proximity to sources and differences of source strengths. Comparison of both time periods using the AHN data from MRd showed that aromatic compounds were significantly higher ($p$ <0.001) during the first period indicating that the differences between the sites were indeed due to the location. These compounds are found in tailpipe emissions, which so close to a heavily trafficked road was the main source. In general, NK represents an urban location away from major sources and broadly representative of city-wide background concentrations, e.g. urban residential areas, whereas MRd, an urban kerbside site next to a major arterial route, represents central urban areas such as surrounding the congestion charge zone in London.

## 4.3.2 Comparisons with the Automatic Hydrocarbon Network and PTR-MS quantification limitations

Benzene, toluene, $C_2$- and $C_3$-benzenes from PTR-MS measurements were compared with the same compounds or sum of compounds with similar masses measured by GC-FID in the framework of the Automatic Hydrocarbon Network (AHN). Due to isobaric interference within the PTR-MS measurements the sum of available GC-FID measurements was used for compounds with a protonated mass of *m/z* 107 and *m/z* 121. Direct comparisons of 1 h mean (±2.9-5.9% SE) PTR-MS and GC-FID measurements (Figure 4.3) are summarized in Table 4.2. The PTR-MS data for these compounds corresponded to within a factor of 1.3 for *m/z* 79, 93 and 107, and a

factor of 2.5 for $m/z$ 121 ($p$ <0.001). Comparison of the time series showed that the PTR-MS

measurements closely followed the diurnal variations of the GC-FID measurements (Figure 4.3).

*Table 4.2. Summary of 1h averages of compounds (ppb) measured by both PTR-MS and GC-FID at Marylebone Rd, London (25th Jan – 7th Feb 2012).*

| | PTR-MS | | | | GC-FID | | | |
|---|---|---|---|---|---|---|---|---|
| *Mixing ratios (ppb)* | *Benz-ene* $m/z$ 79 | *Tol-uene* $m/z$ 93 | *$C_2$-benzenes* $m/z$ 107 | *$C_3$-benzenes* $m/z$ 121 | *Benz-ene* $m/z$ 79 | *Tol-uene* $m/z$ 93 | *$C_2$-benzenes* $m/z$ 107 | *$C_3$-benzenes* $m/z$ 121 |
| *N* | 274 | 274 | 274 | 256 | 302 | 302 | 302 | 302 |
| *LoD* | *0.04* | *0.01* | *0.08* | *0.03* | *0.01* | *0.01* | *0.01* | *0.01* |
| *Min.* | 0.17 | 0.13 | 0.29 | 0.13 | 0.14 | 0.07 | 0.03 | 0.01 |
| *1st quartile* | 0.39 | 0.52 | 0.87 | 0.46 | 0.30 | 0.38 | 0.57 | 0.13 |
| *Median* | 0.57 | 0.82 | 1.23 | 0.91 | 0.42 | 0.61 | 0.83 | 0.24 |
| *Geom. mean* | 0.58 | 0.95 | 1.30 | 0.81 | 0.41 | 0.66 | 0.86 | 0.24 |
| *Arithm. mean* | 0.63 | 1.17 | 1.44 | 1.07 | 0.47 | 0.87 | 1.01 | 0.33 |
| *3rd quartile* | 0.82 | 1.53 | 1.89 | 1.51 | 0.58 | 1.09 | 1.32 | 0.46 |
| *Max.* | 2.26 | 6.42 | 5.12 | 3.71 | 1.42 | 5.17 | 4.51 | 1.45 |
| *SD* | 0.32 | 1.01 | 0.81 | 0.74 | 0.23 | 0.83 | 0.63 | 0.29 |
| *Skew* | 1.30 | 2.06 | 1.38 | 0.93 | 1.53 | 2.33 | 1.39 | 1.27 |
| *Kurtosis* | 2.65 | 5.21 | 2.53 | 0.39 | 2.98 | 6.36 | 2.13 | 1.16 |

As the PTR-MS cannot distinguish between compounds with similar masses, isobaric interference can occur, e.g. benzaldehyde can produce mass interferences for $C_2$-benzenes (Warneke *et al.*, 2003). The $m/z$ 107 likely has four contributing species: ethyl benzene, ($m+p$)-xylene, $o$-xylene, and some benzaldehyde. $C_3$-benzenes may include a wider range of compounds: propyl benzene, two ethyl methyl benzenes and three trimethylbenzene isomers. The AHN measurements included all of the above for $m/z$ 107, but only three trimethylbenzene isomers at $m/z$ 121.
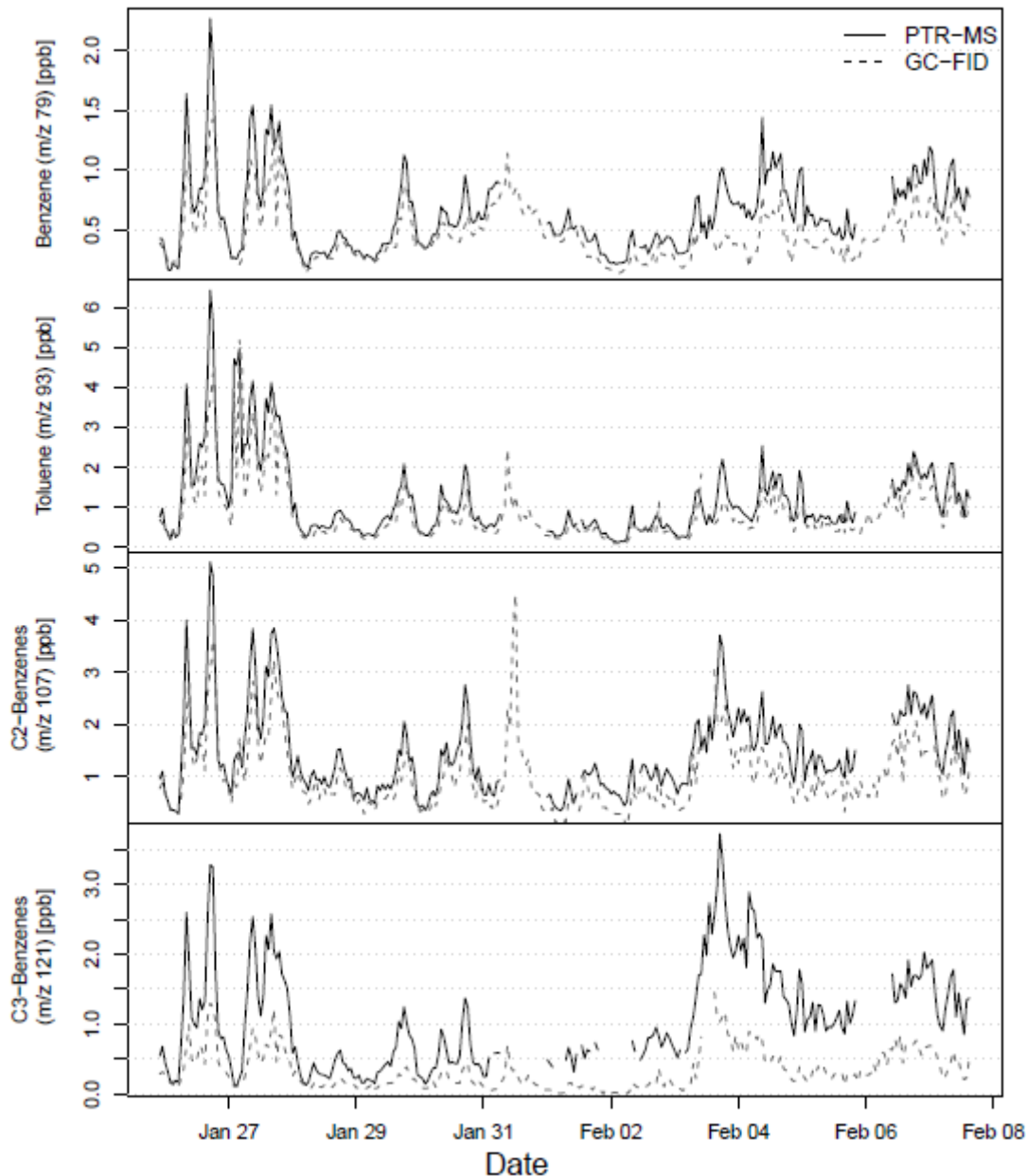
**Figure 4.3.** 1 h means for benzene, toluene, $C_2$- and $C_3$-benzenes mixing ratios (ppb) measured by the PTR-MS (solid line) and GC-FID (dashed line) at Marylebone Road ($25^{th}$ Jan – $7^{th}$ Feb 2012).

Humidity dependencies on instrument sensitivities and backgrounds were thoroughly investigated in the laboratory after the campaign. Calibrations showed no significant variations of sensitivity with humidity. Corrections were applied to compounds showing humidity effects on instrument background, but not all effects could be recreated and accounted for, such as humidity effects on inlet impurities affecting aromatics (Supplementary content 4.5.B).

61

Fragmentation can become a concern at higher $E/N$ ratios (de Gouw and Warneke, 2007; Maleknia *et al.*, 2007; Warneke *et al.*, 2003). An $E/N$ ratio of 125 Td was used in this study as this represents a compromise between reagent ion clustering and fragmentation suppression (Hewitt *et al.*, 2003). Some fragmentation can still occur, as several studies using a coupled GC-PTR-MS with a range of $E/N$ ratios have identified various fragment ions. Benzaldehyde, ethyl benzene and xylene isomers with $m/z$ 107 may produce fragments of about 30-40% at $m/z$ 79 with higher $E/N$ ratios (Maleknia *et al.*, 2007), as well as propyl benzene isomers and smaller contributions of fragments of butyl benzene (Warneke *et al.*, 2003). As only *o*-xylene was present in the calibration standard, fragments from other compounds at that mass cannot be accounted for and are likely to have contributed to the increased PTR-MS signal. It is estimated that with an electrical field strength of 125 Td around 15% $C_2$-benzenes may have contributed to $m/z$ 79. Interference from fragments at $m/z$ 93 could include a range of biogenic terpenes and their isomers (Maleknia *et al.*, 2007).

Previous studies have shown that there is good correlation between PTR-MS and GC-FID, however the quantitative agreement can be poor with differences of up to a factor of 2 (de Gouw and Warneke, 2007; Kato *et al.*, 2004). The value for $m/z$ 121 is somewhat higher than cited in the literature, which may be due to humidity effects on inlet impurities which could not be accounted for after the campaign, as well as isobaric interference from compounds and fragments not measured by the AHN. All four $m/z$ showed very good correlations (Figure 4.4) with $r = 0.90\text{-}0.91$ ($p < 0.001$) in agreement with literature values (Kuster *et al.*, 2004; Langford *et al.*, 2010b).
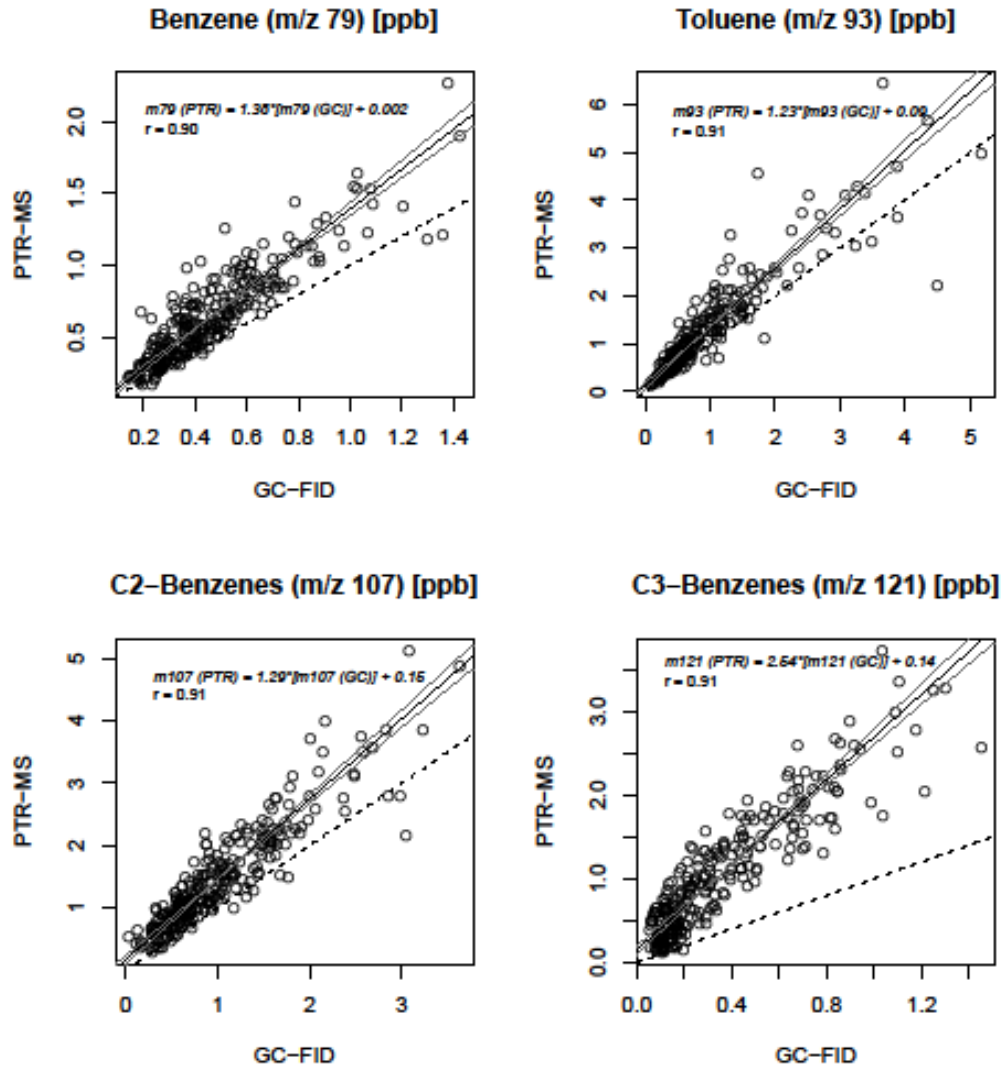
**Figure 4.4.** Scatter plots of 1h mean VOC concentrations (ppb) (benzene, toluene, $C_2$- and $C_3$-benzenes) of PTR-MS against GC-FID measurements at Marylebone Road ($25^{th}$ Jan – $7^{th}$ Feb 2012) with Reduced Major Axis (RMA) linear regressions, $\pm\ 99^{th}$ confidence intervals, 1:1 line (dotted) with $r$ values.

### 4.3.2.1 Correlations with carbon monoxide

Carbon monoxide (CO) concentrations were used for correlations and ratios with VOCs to determine whether the VOC sources were from fuel combustion (Table 4.3), as CO is a suitable marker for anthropogenic combustion emissions.

*Table 4.3. Mean VOC/CO ratios for volume mixing ratios (ppbv/ppbv) at NK and MRd, London (16th Jan - 7th Feb 2012).*

| Compound | NK[a] | | MRd | | | |
|---|---|---|---|---|---|---|
| | PTR-MS | | PTR-MS[b] | | GC-FID[c] | |
| | [VOC]/[CO] | r | [VOC]/[CO] | r | [VOC]/[CO] | r |
| Methanol | 2.13E-02 | 0.28 | 1.20E-02 | 0.27 | | |
| Acetonitrile | 2.70E-04 | 0.87 | 5.21E-04 | 0.55 | | |
| Acetaldehyde | 2.14E-03 | 0.93 | 4.14E-03 | 0.84 | | |
| Acetone | 4.53E-03 | 0.62 | 3.18E-03 | 0.74 | | |
| Cycloalkanes/ Isoprene | 5.74E-04 | 0.80 | 1.13E-03 | 0.82 | | |
| Benzene | 1.08E-03 | 0.96 | 1.59E-03 | 0.75 | 1.58E-03 | 0.68 |
| Toluene | 2.07E-03 | 0.93 | 3.09E-03 | 0.72 | 3.33E-03 | 0.65 |
| C2-benzenes | 2.16E-03 | 0.89 | 3.69E-03 | 0.66 | 4.70E-03 | 0.58 |
| C3-benzenes | 1.72E-03 | 0.86 | 2.60E-03 | 0.65 | 1.61E-03 | 0.68 |

[a]$N = 226$, [b]$N = 256-274$, [c]$N = 302$.

High correlations for acetonitrile against CO indicate that fuel burning was likely the primary source at NK. Correlations with CO were higher for PTR-MS than GC-FID ($r = 0.65 - 0.75$, $p < 0.001$ for PTR-MS; $r = 0.58-0.68$, $p < 0.001$ for GC-FID). Possibly the higher temporal resolutions and the longer sampling time of the PTR-MS allowed the detection of short-term variations in emission patterns.

### 4.3.3 VOC correlations and ratios

Correlations between the different VOCs yielded coefficients ($r$) ranging between -0.23 and 0.97 at NK and -0.20 and 0.87 at MRd ($p < 0.001$). The poorer correlations involved methanol ($r = -0.23 - 0.35$). Methanol has a variety of different sources, which in this case had little commonality with the other compounds. Strong linear correlations ($r = 0.67 - 0.97$ at NK, $0.48 - 0.87$ at MRd) indicate that the other compounds shared some or almost all sources, however, bimodal distributions can relate to multiple separate sources. In winter, vehicle exhaust and, to a small extent, evaporative emissions account for a majority of the sources. The *r*-values at MRd were lower than at NK showing more scatter (Figure 4.5). This may reflect a sequential sampling artefact due to the instrument continuously cycling through the different *m/z*, combined with highly variable concentrations at this site. Alternatively, it may represent true variability in the nearby emission source; within traffic emissions, diverse types of vehicles, fuels, and driving

patterns result in different traffic related VOC ratios (Figure 4.5), which can be detected by online methods as the compounds reach the inlet with little mixing (C.-C. Chan *et al.*, 1991; C. Y. Chan *et al.*, 2002).
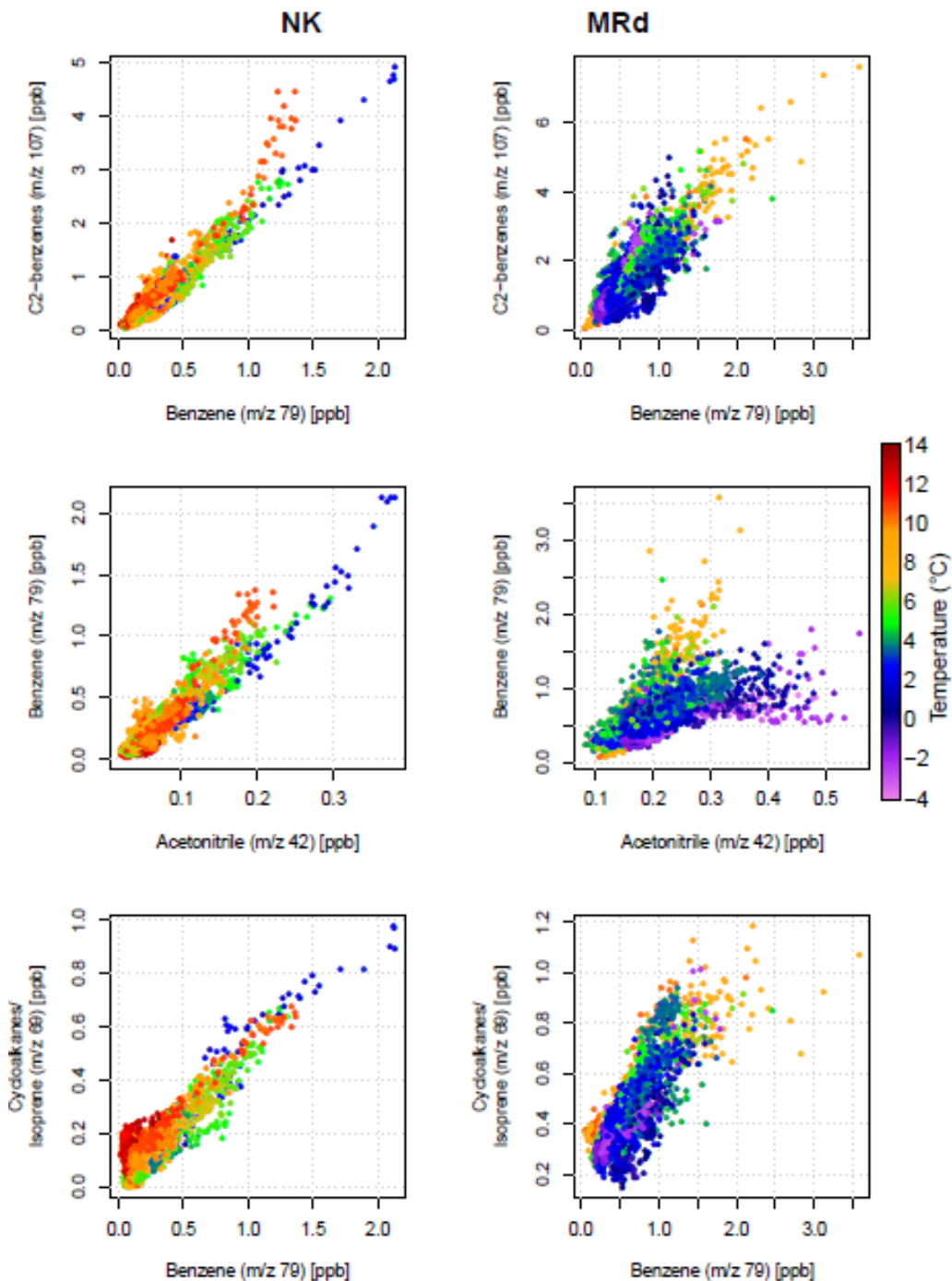


**Figure 4.5.** Scatter plots of representative VOC correlations measured at North Kensington (left) and Marylebone Rd (right) (16th Jan – 7th Feb 2012) using 5 min means (ppbv) with ambient air temperature (°C) at time of sampling (colour bar).

Biomass burning for heating may explain a secondary source contribution to acetonitrile at MRd, as it mostly occurs with cold temperatures and is not shared with benzene, hence is not related to traffic emissions (Figure 4.5).

Using temperature as a third variable can illustrate temperature dependencies of source contributions. Cycloalkanes/isoprene and benzene show a good correlation ($r = 0.77$ and $0.80$) as they are present in tailpipe emissions (Park *et al.*, 2011) with a seasonally low biogenic component (Figure 4.5). The main source of most $C_2$- and $C_3$-benzenes are motor vehicle emissions (Heeb *et al.*, 2000) which was reflected in the high correlations ($0.72$ to $0.97$, $p < 0.001$). These aromatics have a shorter atmospheric lifetime making them important factors in urban photochemical smog production (Table 4.1a).

Benzene-to-toluene (b/t) ratios can indicate the photochemical age of the pollution carried by air masses (Warneke *et al.*, 2001 and references therein). Due to seasonally low OH concentrations, only changes in b/t ratios over longer periods were considered to be representative of air mass transport.

The median (IQR) b/t ratios were around 0.6 (0.43-0.80) at both sites and agreed with previous values (Chan *et al.*, 2002; Heeb *et al.*, 2000; Langford *et al.*, 2009), as well as with those from the AHN at MRd with a median of 0.6 (0.48-0.76) ($r = 0.90$, $p < 0.001$). These b/t ratios are consistent with the air mass footprints derived from the UK Met Office's Numerical Atmospheric-dispersion Modelling Environment (NAME) (Jones *et al.*, 2007) using Unified Model (UM) Met data (Figure 4.6). This model simulates the origin of the air masses affecting the ClearfLo sites within the previous 24 h (Bohnenstengel *et al.*, 2015). Shifts between high and low pollution episodes often are correlated with changes in wind direction and intensity. For the low pollution periods (19th-23rd Jan and 31st Jan-2nd Feb) strong westerlies brought air masses with regional influences and high b/t ratios of 0.91 (0.64-1.31). The high pollution episodes (24th -25th Jan and 4th Feb) showed low wind speeds resulting in shorter travel distances of the air masses and stronger local London influences (up to 87%, campaign average 37%) and corresponding low b/t ratios of 0.48 (0.39-0.58).
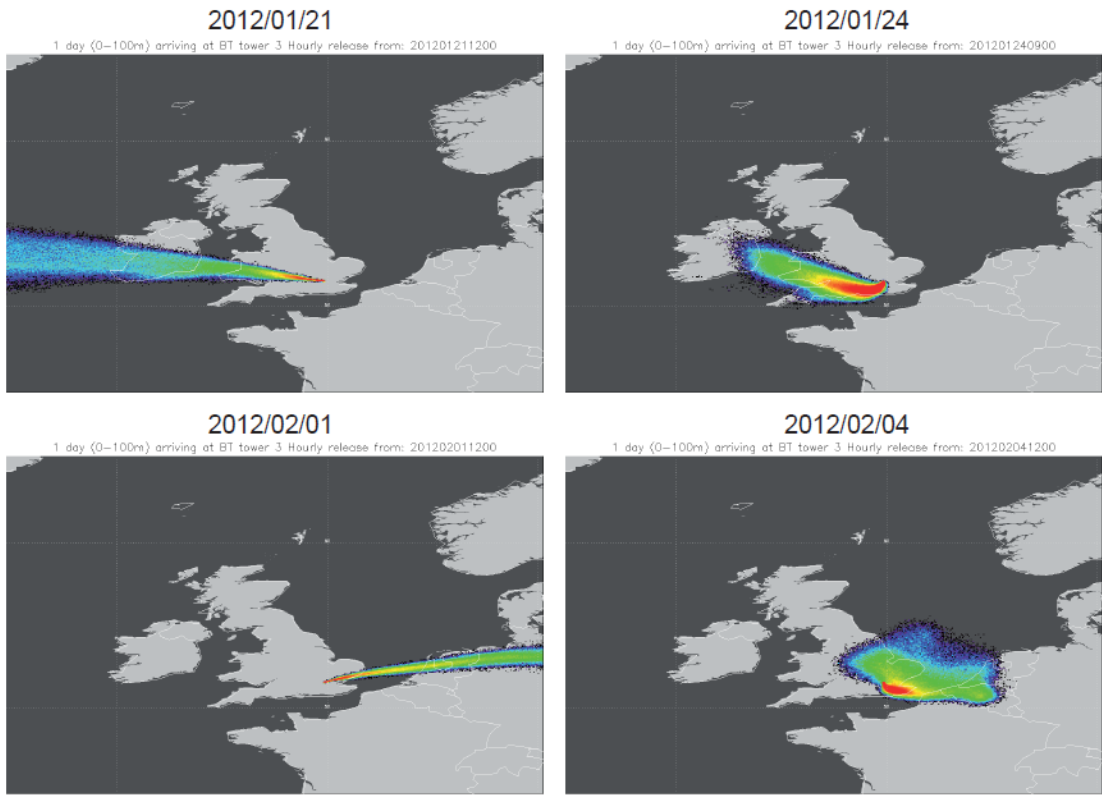
**Figure 4.6**. 24 hour back trajectories from the Met Office NAME dispersion model at North Kensington (16th Jan-7th Feb 2012). Daily release for 3 hours from midday (20 m height) tracking the surface layer only (0-100 m) for the 24 hours prior. Colours indicate particle concentrations ranging from 6 x 10^{-7} g m^{-3} (blue) to 1 x 10^{-4} g m^{-3} (red). Reproduced with permission from Zoë Fleming (NCAS, University of Leicester).

### 4.3.4 Diurnal averages

Meteorological conditions can mask emission patterns, therefore diurnal averages are used to aid in their identification (Figure 4.7). Concentrations can depend on the mixing height in the boundary layer, however LIDAR measurements showed little diurnal variation in the seasonally shallow mixing height (500-1000 m) (Bohnenstengel *et al.*, 2015). All compounds, bar methanol, showed a double rush hour peak during weekdays (07:00-10:00 and 17:00-20:00 GMT) and lower concentrations with less variability on weekends (Figure 4.7, E - H), suggesting vehicle exhaust as a major source. At MRd, rush hour peaks were less pronounced due to the continuously high daytime traffic density (68002 vehicles per day; Department for Transport, 2012), which causes the road to saturate for prolonged periods during the day.

NK                    MRd
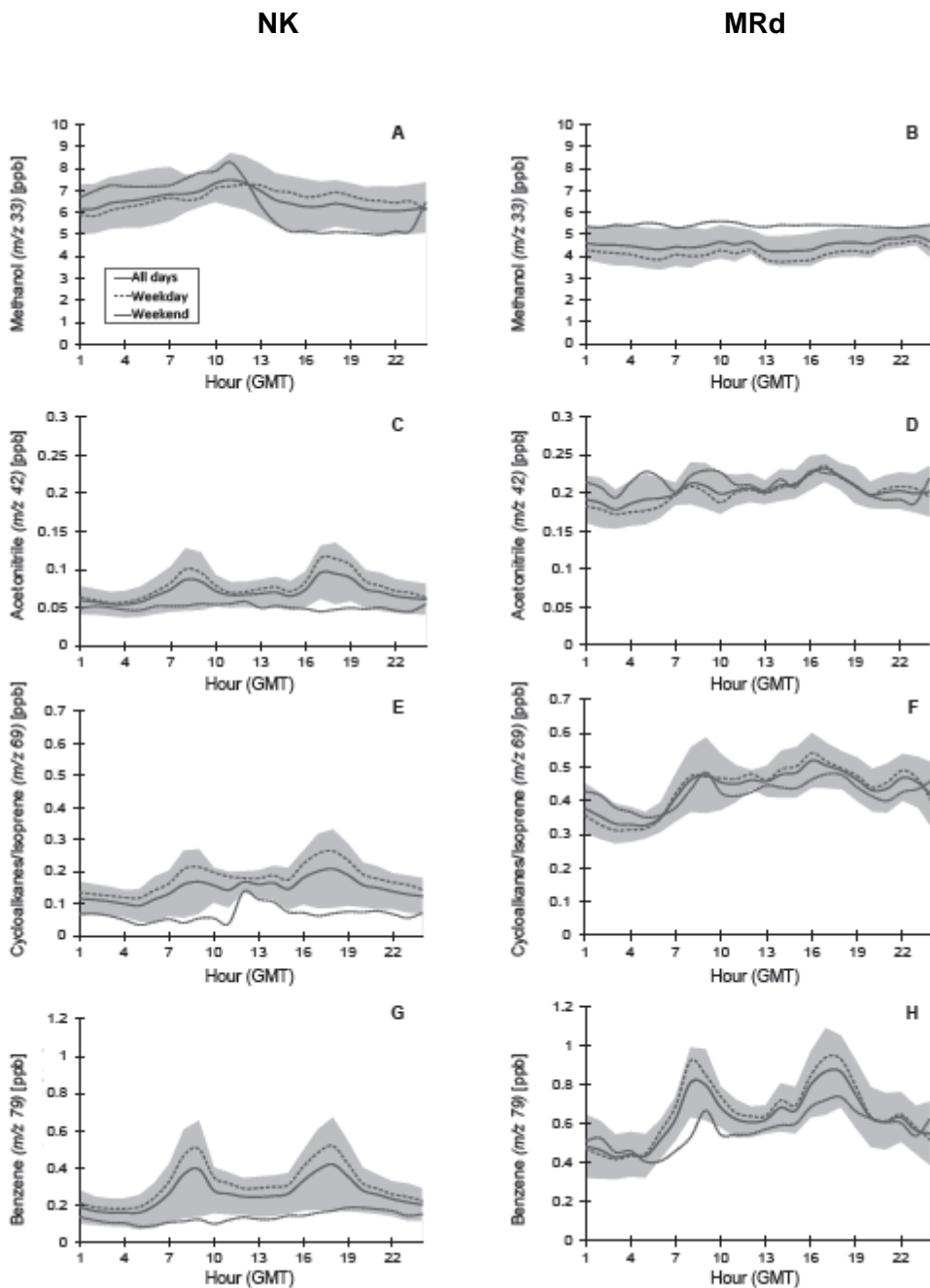
**Figure 4.7.** Diurnal plots of 25 min averages (ppb) for representative VOCs at North Kensington (*left column*) and Marylebone Road (*right column*) (16th Jan – 7th Feb 2012) with the 95% confidence interval (shaded areas), all days (solid line), weekdays (dashed line) and weekends (dotted line).

The early morning minima (04:00 – 06:00 GMT) can be attributed to reduced human activity which sharply increases during the morning rush hour peak (07:00-10:00 GMT) (Figure

4.7, F – H). Methanol and acetone have numerous sources and longer atmospheric lifetimes resulting in no clear diurnal pattern (Figure 4.7, A and B).

### 4.3.5 Analyses of wind direction dependence

### 4.3.5.1 Synoptic polar plots

Using wind speed and direction measurements from the BT tower (190 m a.g.l.), polar plots were constructed for compound mixing ratios (Figure 4.8) using a generalized additive model (GAM) (Hastie and Tibshirani, 1990; Wood, 2006) to interpolate between averaged data points in the R package OpenAir (Carslaw, 2012; Carslaw and Ropkins, 2012). At NK high concentrations for most compounds were associated with low wind speeds (i.e. $<5$ m s$^{-1}$) indicating local emission sources. Methanol showed high concentrations with WSW wind directions and speeds $>5$ m s$^{-1}$ possibly representing pollution transported to the site from a biodiesel production facility located 1 km SW of the site. Biodiesel production from waste cooking oil by transesterification often involves evaporating methanol.

At MRd methanol showed high concentrations with S and N winds $>10$ m s$^{-1}$, whereas benzene is representative of the other compounds with patches of increased concentrations at speeds of 5-10 m s$^{-1}$. The WSW and ENE patches coincide with the directional layout of Marylebone Rd, while the SSW source may originate from traffic in the Marble Arch/Hyde Park Corner area, which boasted the highest annual mean traffic count of 100574 motor vehicles per day in all of Westminster, London (Department for Transport, 2012).
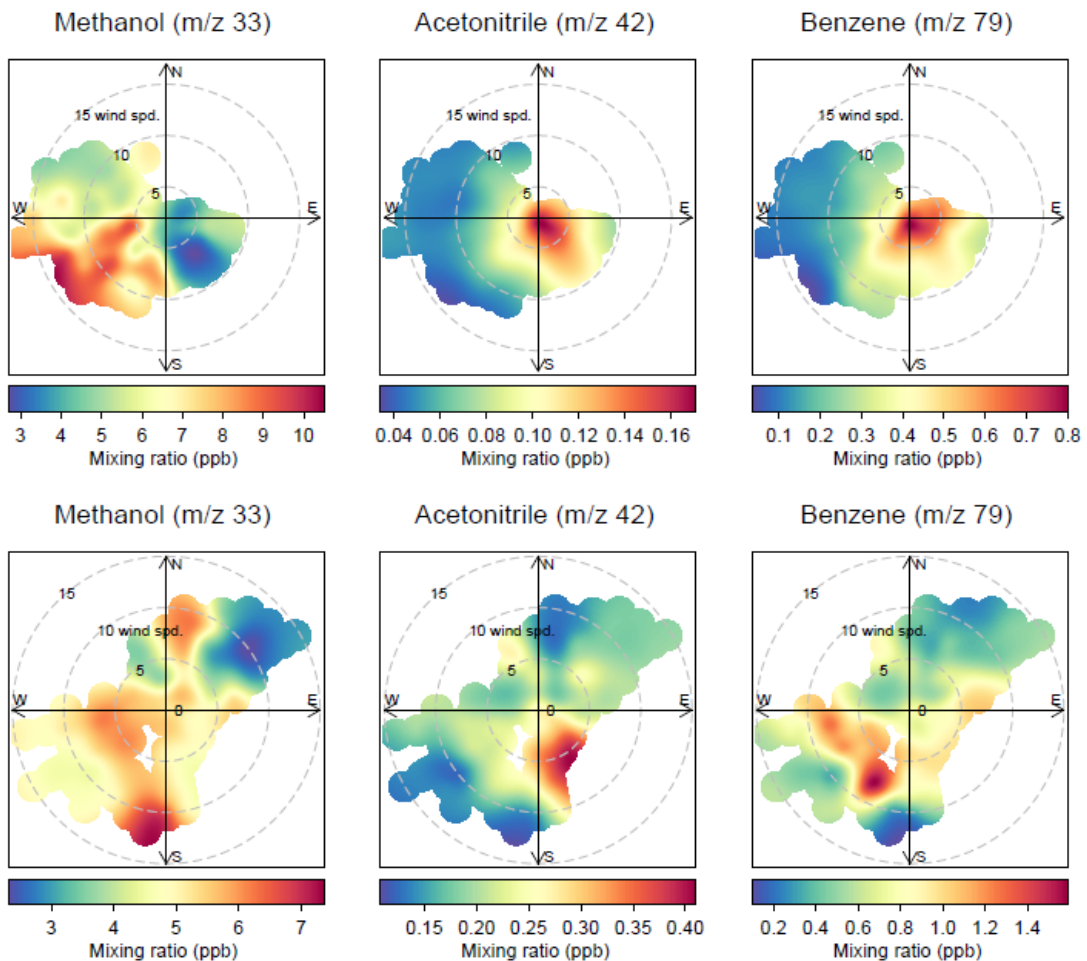
**Figure 4.8.** Representative selection of polar plots of synoptic wind speed (m s$^{-1}$) against wind direction (°) from the BT tower (190 m) with VOC mixing ratios (ppb) as a third variable (colour bar) for methanol (*m/z* 33), acetonitrile (*m/z* 42) and benzene (*m/z* 79) at North Kensington (16$^{th}$ -25$^{th}$ Jan 2012) (*top*) and Marylebone Rd (25$^{th}$ Jan – 7$^{th}$ Feb 2012) (*bottom*).

### 4.3.5.2 Synoptic wind direction dependencies and comparison with NAEI

To quantify wind direction dependencies (Section 4.3.5.1) and compare measured VOC mixing ratios at MRd with the National Atmospheric Emissions Inventory (NAEI) for estimated emissions, general linear models were used for each compound concentration against the four wind direction categories. There was no significant difference in wind speed with direction. Correlations of VOC concentrations with wind speed showed weak negative relationships ($r = -0.38$ to $-0.14$, $p <0.05$) indicating that a dilution effect depending on wind speed from above-canyon air mass mixing may play a small role in street canyon concentrations.

All species showed significant differences in mixing ratios with wind direction (*F* statistic 6.73 - 41.8, *p* <0.001 for measured compounds; *F* statistic = 4.48, *p* <0.01 for estimated benzene) and agreed with the polar plots. Differential source density within the four sectors and fetch variability over the city are likely reasons.

Estimated emissions and observed concentrations for benzene agreed that low emission source densities to the N resulted in low observed mixing ratios. The largest estimated emissions were to the E, whereas measurements indicated the S. Regent's Park to the N and Hyde Park to the S have large areas of low emissions reducing the estimates in these sectors. Emission estimates also ignore background values from greater fetch across London. High localized emission sources seen in the polar plots (Figure 4.8) could be responsible for higher measured VOC concentrations to the W and S, which partially agrees with the high estimated emissions from the nearest westerly grid cell. Estimated emissions from the NAEI are integrated over 1 km$^2$ grid resolution, but localized sub-grid scale effects may be masked by the grid averaging area. It must be emphasized that the volume mixing ratios were measured at ground-level within the street canyon, whereas the wind data are representative of synoptic winds above the street canyons.

## 4.4 Conclusion

High VOC concentrations during the winter in urban locations are mostly from traffic emissions. This was reflected at both sites in diurnal profiles, VOC/VOC and VOC/CO correlations and ratios, wind sector dependence analyses and polar plots. Measurements at the NK background site indicated significantly lower mixing ratios than at the MRd kerbside site, even though AHN data showed that kerbside concentrations were higher during the first measurement period, suggesting site differences due to the location with different source strengths and proximity.

Comparison of PTR-MS and GC-FID data from MRd for aromatics showed good correlation and qualitative agreement. However, PTR-MS data were significantly higher possibly due to some isobaric interference from additional compounds and fragments, and possibly

systematic errors introduced during instrument background corrections. Short term variations in the ratio of traffic related compounds from differences in traffic density, driving style, vehicle and fuel types were observed by PTR-MS at the MRd site and higher correlations with CO for PTR-MS than the GC-FID measurements were likely due to the fast response and longer sampling times of the PTR-MS. The AHN can only report hourly arithmetic means due to the methods employed, possibly leading to a reporting bias and a loss of information on short term variability.

Elevated concentrations were mostly observed when synoptic-scale wind speeds were low at NK as dispersion of localised emissions was reduced. However, some non-local emission sources were detected using polar plots and possible sources were identified. There were significant differences in VOC concentrations with wind direction. When compared with estimated benzene emissions by the NAEI, estimates were less representative when VOC concentrations were high, as they are unable to capture the influence of city background emissions and reduced local sub-grid emission source contributions.

## Acknowledgements

## 4.5 Supplementary content

### 4.5.A. Details on measurement sites, instrument parameters and duty cycles for both PTR-MS and GC-FID

Extensive comparisons of the measurement sites and the mean meteorological measurements during the two measurement periods are summarised in Table 4.A1.

*Table 4.A1. Summary of site descriptions for measurements sites at North Kensington and Marylebone Rd, London and campaign average meteorology.*

|  | North Kensington | Marylebone Road |
| --- | --- | --- |
| Time period | 16 - 25 January 2012 | 25 January - 7 February 2012 |
| Site category [a] | Urban background (class A) | Urban kerbside (class A) |
| Area | Sion Manning School courtyard | Automatic Hydrocarbon Network[c] cabin |
| Coordinates (altitude) | 51°31'15.18" N; 0°12'48.85" W (25 m.s.l.) | 51°31'21.14" N; 0°09'16.59" W (35 m.s.l.) |
| Surroundings | Residential, <10 m buildings to N and W, main road 95 m E and A40 Westway 500 m S (70 000-100 000 vehicles per day) | Commercial, A501 Marylebone Rd (70 000 vehicles per day) 1.5 m N, intersection Luxborough Street, Regent's Park (green area of 166 ha) 200 m N |
| Oke 2006 (UCZ[b]) category | 3 | 2 |
| Inlet height (m) | 4.7 | 2.5 |
| Tube length (m) | 7 | 4 |
| Mean temperature (°C) | $7.8 \pm 2.9$[d1] | $3.0 \pm 2.8$[d2] |
| Mean RH (%) | $71.8 \pm 12.2$ [d1] | $68.4 \pm 12.0$ [d2] |
| Precipitation (mm) | 3 [d1] | 11 [d2] |
| Mean wind speed (m s$^{-1}$) | 1 (at 4.7 m) [d1] | 6.4 (at 191 m) [d2] |
| Mean wind direction (°) | 205 (SSW) [d1] | 62 (ENE) [d2] |

[a]Site classification: Category A indicates sites highly representative of emissions for intended areas.

[b] Urban Climate Zone classifications by Oke (2006).

[c] Permanent measurement site run by the Department for Environment, Food and Rural Affairs (Defra).

[d1] Data from WXT520 weather sensor (Vaisala Ltd, Finland) at NK.

[d2] Data from WXT520 weather sensor at BT tower near MRd.

### 4.5.A1. PTR-MS

A high-sensitivity proton transfer reaction- mass spectrometer (PTR-MS) fitted with three Varian turbo-molecular pumps and a 9.5 cm long drift tube was used for online measurements VOC mixing ratios. During each deployment of the PTR-MS, drift tube pressure, temperature and voltage were kept constant at 2.06 mbar, 48 °C and 550 V respectively to maintain an *E/N* ratio of 125 Td. Air was subsampled from the main line with an inlet flow rate of 0.25-0.3 l min$^{-1}$. The

primary ion count ($m/z$ 19) ranged between 6 - 14 $\times$ $10^6$ cps with a mean of $11 \times 10^6$ cps. The $H_3O^+.H_2O^+$ water cluster ions ranged between $6.5 \times 10^4 - 2.6$ x $10^5$ cps with a mean of $1.4 \times 10^5$ cps which represented on average 1.7% of the primary ion signal, while the $O_2+$ signal ($m/z$ 32) was <2% of the primary ion signal. The 1 h measurement protocol consisted of 5 min zero air measurements using a zero air generator (Parker Balston, UK), then 25 min MID mode, followed by 5 min mass scans and another 25 min in MID mode (Figure 4.A1). During the MID mode, 11 selected masses were measured with a dwell time of 2 s per mass and 0.5 s for the primary ion, resulting in a 20.5 s cycle time, whereas SCAN modes cycled through the mass range $m/z$ 21 – 206 with a dwell time of 0.5 s each.
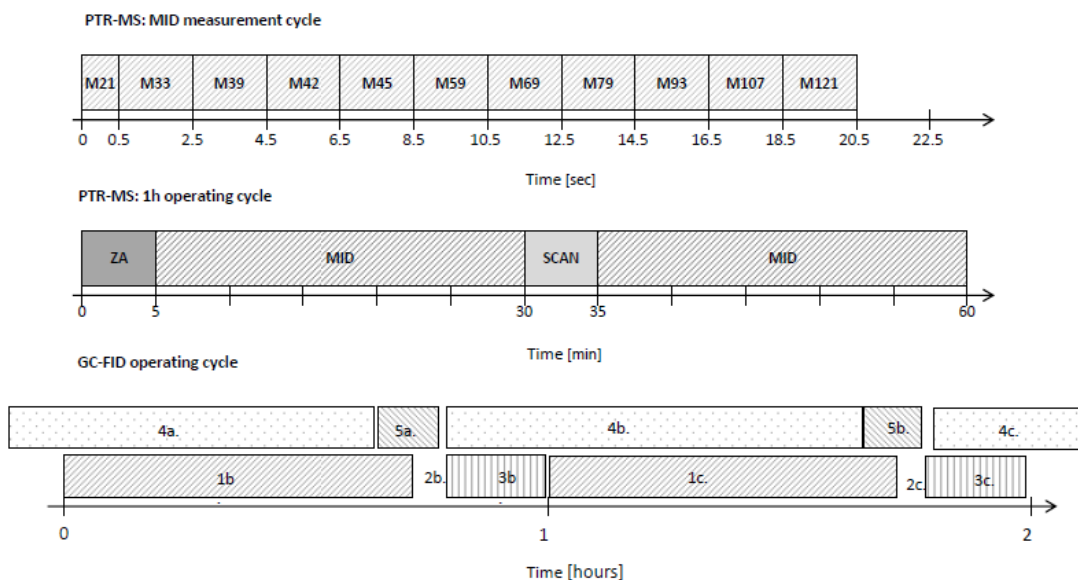


**Figure 4.A1.** *Top*) Representation of the PTR-MS measurement cycle used at both North Kensington and Marylebone Rd sites. The multiple ion detection (MID) cycle lasted 20.5 s and was repeated during 25 min. *Bottom*) Approximation of the measurement cycle used by the Automatic Hydrocarbon Network GC-FID at the Marylebone Rd measurement site. Multiple sample analyses are indicated by *a* (previous hour), *b* (hour 1) and *c* (hour 2). Each cycle consists of the following stages: *1*. Sample acquisition (40 min), *2*. Analytes are injected into GC columns, *3*. Trap cooling in preparation for the next sample acquisition (15 min), *4*. GC analysis (50 min), and *5*. GC cooling in preparation for the next sample analysis (Yardley *et al.*, 2012).

**4.5.A2. GC-FID**

The GC-FID method used by the AHN has recently been linked to the QA/QC procedures of the EU Infrastructure Project ACTRIS (www.actris.net). The method includes a TurboMatrix thermal desorption (TD) unit with an online sampling accessory to gather samples directly from ambient air. The TD extracts the compounds onto an adsorbent trap, which is cooled to -30°C. The analytes are then thermally desorbed and transported through a heated transfer line by a carrier gas to the GC. The GC contains two columns and compounds are separated by volatility into two fractions. The flame ionization detector (FID) monitors the chromatography on two columns. After a 40 min sampling period the sample is injected into the GC and the trap automatically begins collecting the next sample after 20 min ensuring hourly sample acquisition.

Inter-comparisons with the VOC standards used by the AHN were not possible, therefore uncertainties associated with the AHN standards cannot be discounted and may have contributed to the offsets between the two methods. Especially in areas of high pollution, datasets from automated monitoring systems using GC-FID can also be susceptible to high variability, as was shown in Fortin *et al.* (2005), which would introduce additional uncertainty.

The GC-FID data were converted to ppbv using ambient pressure and temperature measurements which may also have introduced some uncertainty in the AHN data.

**4.5.B. Calibrations and instrument background determination of the PTR-MS**

The multi-component VOC gas standard (Ionimed Analytik GmbH, Austria, 1 ppmv ± 5% uncertainty for all compounds) contained all VOCs selected for quantification by PTR-MS except *m/z* 121. After the campaign it was independently validated against another multi-component VOC standard (Apel Riemer Environmental Inc., CO, USA) containing the same compounds with the addition of a 1,2,4-trimethylbenzene. Uncertainties for all compounds were quantified in the Ionimed standard to be <10%, apart from methanol which was 15%.

The standard was diluted with air from the zero air generator. Normalized sensitivities were between 1.4 (*m/z* 121) and 11.9 (*m/z* 45) ncps ppbv$^{-1}$. The original instrument used for the

measurements had been substantially upgraded, therefore a very similar instrument with similar specifications and performance indicators was used to investigate relative changes in background and sensitivity against humidity. These were thoroughly investigated in the laboratory using a range of relative humidites and all variations in sensitivity were within the overall calibration uncertainty (20% for methanol and <15% for all other compounds, see Figure 4.B1). Sensitivities were comparable between instruments, although those of the original instrument started to decrease towards the higher masses. However, overall sensitivities correlated well ($r = 0.94$, $p < 0.001$) and since the same instrument parameters and conditions as during the campaign were maintained, it is assumed that instrument responses are comparable.

PTR-MS sensitivities of benzene and toluene in particular have been shown to depend on changes in relative humidity, i.e. when the fraction of $H_3O^+ \cdot (H_2O)$ ions in the reactor change (Warneke *et al.*, 2001). For these two compounds the reaction with $H_3O^+ \cdot (H_2O)$ ions is energetically not permitted and does not occur (Spaněl and Smith, 2000). However, PTR-MS sensitivities have a less pronounced humidity dependency at higher *E/N* ratios because the reagent ions are dominated by $H_3O^+$ (de Gouw and Warneke, 2007). Although the absence of the reaction with *m/z* 37 for these two compounds was taken into account when normalising the signals, some humidity effects on background counts may have contributed to the offset, as humidity effects were determined post-calibration and had to be extrapolated resulting in large uncertainties.
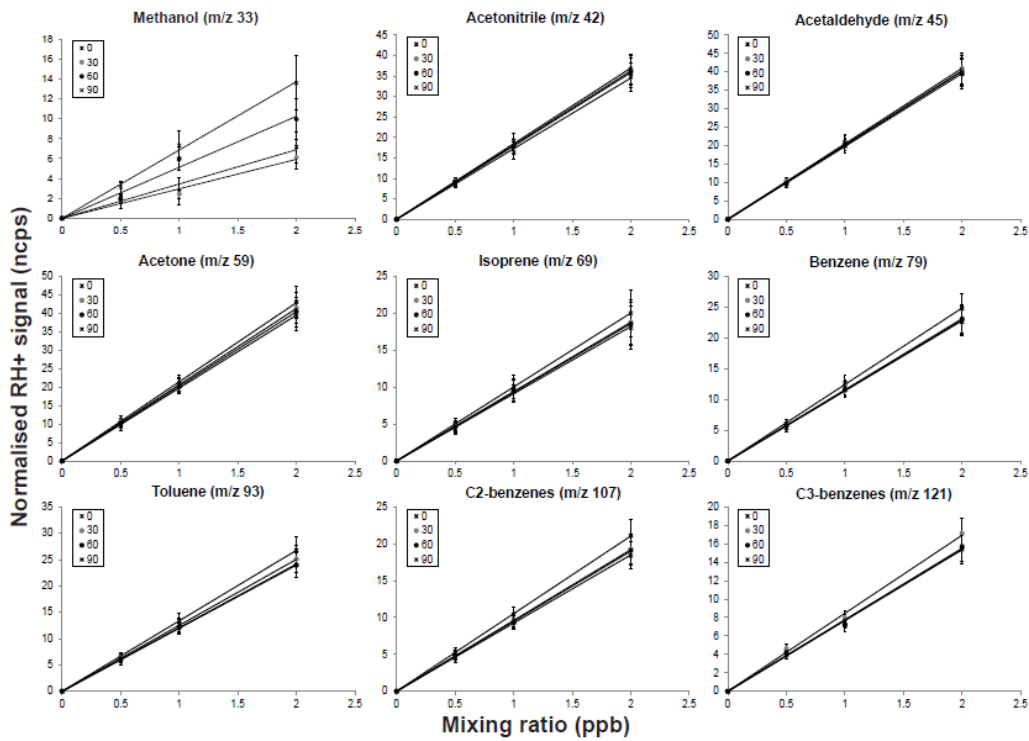
**Figure 4.B1.** Post-campaign calibrations over a range of relative humidities (0, 30, 60, 90% ± 5%) for all nine selected compounds (methanol [*m/z* 33], acetonitrile [*m/z* 42], acetaldehyde [*m/z* 45], acetone [*m/z* 59], isoprene [*m/z* 69], benzene [*m/z* 79], toluene [*m/z* 93], *o*-xylene [*m/z* 107], and 1,2,4-trimethylbenzene [*m/z* 121]).

A custom built zero air generator consisting of a platinum catalyst and charcoal heated to 200 °C was used to determine instrument background values. During the campaign dry air was used, however this was insufficient in accounting for variations due to humidity. Therefore, humidity effects were determined by humidifying the zero air over a range of relative humidities in the laboratory after the campaign. The instrument background for the campaign average relative humidity (72% with IQR 64-83%) was subtracted for compounds showing moderate humidity dependency. For compounds with stronger humidity effects a running correction based on the *m/z* 37/ *m/z* 19 ion ratio, which is a proxy for humidity, was applied. These corrections produced a minimal difference due to the low variability of *m/z* 37 counts during the campaign (0.8-2.6% with a mean of 1.7% of primary ion signal). Impurities in the inlet system during the campaign may have caused additional humidity dependency for aromatic species. These could

not be accurately recreated when investigating humidity effects in the laboratory, hence this may have resulted in the remaining background offset for $m/z$ 79, 93, 107 and 121. The largest offset was seen in $m/z$ 121, which may be due to a number of factors (discussed in Section 4.3.2 in more detail) including the fact that the instrument was only calibrated against one trimethylbenzene, as standards for many of the other contributing compounds were unavailable to calibrate separately. Correlations of the compound against relative humidity showed low coefficients ($r$ between 0.08 and 0.3, $p > 0.05$), which suggests most humidity effects were sufficiently accounted for, although a large uncertainty associated with the quantitative measurements remains, especially for the higher $m/z$.

Isobaric interferences from $O_2+$ ions on $m/z$ 33 due to the $^{16}O^{17}O+$ isotope were accounted for, as this reacts with the water cluster in the drift tube causing a decrease in the instrument background signal with higher humidities. During the campaign, however, the $O_2+$ counts were always <2% of the primary ion count. Additionally, interference of a $CCl_4$ isotope at $m/z$ 121 was subtracted. Since the Montreal Protocol the addition of this compound in fire extinguishers, cleaning agents, and precursors for refrigerants is prohibited and it is uniformly distributed throughout the atmosphere at around 0.1 ppbv. This provides a constant contribution to $m/z$ 121 in PTR-MS which can be subtracted.

**4.5.C. Comparison of $m/z$ 69 with isoprene concentrations measured by GC-FID**

Globally isoprene is the dominant component of $m/z$ 69, however due to the season and the urban location, the biogenic contribution was absent. Comparison of the PTR-MS data for $m/z$ 69 against isoprene concentration measurements from a GC-FID at NK (courtesy of J. Hopkins and R. Holmes) showed that the isoprene signal of $m/z$ 69 was around 22% after correcting for the instrument background signal (Figure 4.C1). However, correlations with the isoprene concentrations were high ($r = 0.94$, $p < 0.001$). The remaining offset could be from isobaric interference from other compounds such as cyclic alkanes, which share emission sources with anthropogenic isoprene, in which case they represent a considerable contribution to $m/z$ 69 (Yuan *et al.*, 2014). Alternatively, it may be possible that, as seen in the aromatic compounds, the large

uncertainties associated with the calibration (15% total uncertainty) or the background corrections

of the PTR-MS resulted in the offset.
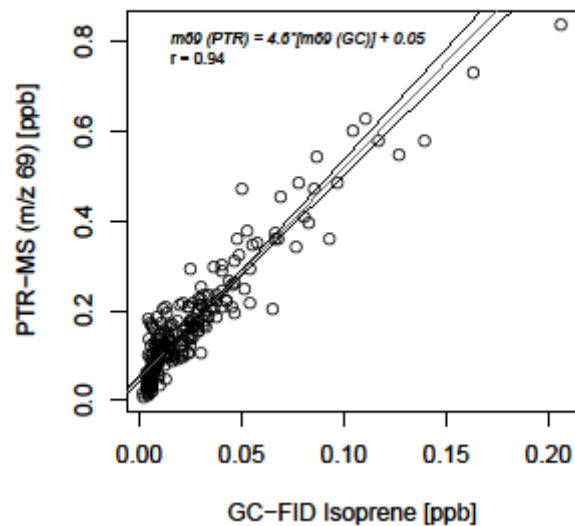


**Figure 4.C1.** Comparison of 1 h averages of *m/z* 69 (ppb) measured by PTR-MS against isoprene concentrations measured by GC-FID (ppb) at North Kensington during 16th – 25th Jan 2012 showing the linear regression with correlation coefficient (*r*). We gratefully acknowledge James Hopkins and Rachel Holmes (University of York) for making the data available for analysis.

# Chapter V

## 5 Paper II: Seasonal and diurnal trends in concentrations and fluxes of volatile organic compounds in central London

This chapter details the use of the PTR-MS to measure VOC fluxes using virtual disjunct eddy covariance in an urban environment. Measurements were made from a tower on the roof of King's College in the Strand, central London starting on 7 August 2012 during the summer ClearfLo IOP and continued through to 19 December 2012. Analysis of seasonal fluxes and concentrations suggested various source contributions and meteorological effects. The Guenther *et al.* (1995) algorithm was used to model urban isoprene emissions of biogenic origin during August and September. The flux footprint was modelled using the Kormann-Meixner-based model and confirmed that measurements were well connected to the surface layer and included emissions from within a radius of ca. 1 km of the measurement site. VOC fluxes were compared to emissions estimates from the London and the National Atmospheric Emissions Inventories.

The work was submitted to the journal Atmospheric Chemistry and Physics on 6 February 2015 and accepted for publication on 30 June and published on 16 July 2015. The authors and their contributions are listed below:

**Amy C. Valach (Lancaster University and CEH):** Set up the system and operated the instrument during the field campaign, processed the data, performed the analyses, and wrote the manuscript.

**Ben Langford (CEH):** Assisted with instrument setup and operation, provided guidance on data processing and analysis, and helped compile the manuscript.

**Eiko Nemitz (CEH):** Helped with data processing, analysis, and compilation of the manuscript.

**A. Rob MacKenzie (University of Birmingham):** Helped with interpretation of the results and compilation of the manuscript.

**C. Nick Hewitt (Lancaster University):** Devised the research, obtained funding and helped with interpretation of the results and compilation of the manuscript.

Atmospheric
Chemistry
and Physics

Open Access

# Seasonal and diurnal trends in concentrations and fluxes of volatile organic compounds in central London

A. C. Valach[1,2], B. Langford[2], E. Nemitz[2], A. R. MacKenzie[3], and C. N. Hewitt[1]

[1]Lancaster Environment Centre, Lancaster University, Lancaster, LA1 4YQ, UK
[2]Centre for Ecology & Hydrology, Bush Estate, Penicuik, Midlothian, EH26 0QB, UK
[3]School of Geography, Earth and Environmental Sciences, University of Birmingham, Edgbaston, Birmingham, B15 2TT, UK

*Correspondence to:* C. N. Hewitt (n.hewitt@lancaster.ac.uk)

# Seasonal and diurnal trends in concentrations and fluxes of volatile organic compounds in central London

A. C. Valach[1,2], B. Langford[2], E. Nemitz[2], A. R. MacKenzie[3] and C. N. Hewitt[1]

[1]{Lancaster Environment Centre, Lancaster University, Lancaster, LA1 4YQ, United Kingdom (a.valach@lancaster.ac.uk; n.hewitt@lancaster.ac.uk)}

[2]{Centre for Ecology & Hydrology, Bush Estate, Penicuik, Midlothian, EH26 0QB, United Kingdom (benngf@ceh.ac.uk; en@ceh.ac.uk)}

[3]{School of Geography, Earth and Environmental Sciences, University of Birmingham, Edgbaston, Birmingham, B15 2TT, United Kingdom (a.r.mackenzie@bham.ac.uk)}

*Correspondence to: C. N. Hewitt (n.hewitt@lancaster.ac.uk, +44 1524 593931)

## Abstract

Concentrations and fluxes of seven volatile organic compounds (VOCs) were measured between August and December 2012 at a rooftop site in central London as part of the ClearfLo project (Clean Air for London). VOC concentrations were quantified using a proton transfer reaction mass spectrometer (PTR-MS) and fluxes were calculated using a virtual disjunct eddy covariance technique. The median VOC fluxes, including aromatics, oxygenated compounds and isoprene, ranged from 0.07 to 0.33 mg m$^{-2}$ h$^{-1}$. Median mixing ratios were 7.3 ppb for methanol and <1 ppb for the other compounds. Strong relationships were observed between the fluxes and concentrations of some VOCs with traffic density and between the fluxes and concentrations of isoprene and oxygenated compounds with photosynthetically active radiation (PAR) and temperature. An estimated 50-90% of the fluxes of aromatic VOCs were attributable to traffic activity, which showed little seasonal variation, suggesting that boundary layer effects or possibly advected pollution may be the primary causes of increased concentrations of aromatics in winter.

Isoprene, methanol and acetaldehyde fluxes and concentrations in August and September showed high correlations with PAR and temperature, when fluxes and concentrations were largest suggesting that biogenic sources contributed to their fluxes. Modelled biogenic isoprene fluxes from urban vegetation using the Guenther *et al.*, (1995) algorithm agreed well with measured fluxes in August and September. Comparisons of estimated annual benzene emissions from both the London and the National Atmospheric Emissions Inventories agreed well with measured benzene fluxes. Flux footprint analysis indicated emission sources were localised and that boundary layer dynamics and source strengths were responsible for temporal and spatial VOC flux and concentration variability during the measurement period.

## 5.1 Introduction

Currently over 50% of the global population lives in urban areas and with increasing migration to urban centres, air quality remains a high public health priority. In the European Union, including in the UK, volatile organic compound (VOC) emissions are subject to control under the European Commission Directive 2008/50/EC and emission reducing technologies have been implemented, yet urban air pollution continues to be a concern. VOCs from both anthropogenic and biogenic sources impact urban air quality and climate through their contribution to tropospheric ozone and aerosol particle formation. Some VOCs, including benzene and 1,3-butadiene are also carcinogens that can directly affect human health (Kim *et al.*, 2001). Most VOCs in urban areas are assumed to come from fuel combustion or evaporative emissions (Kansal, 2009; Srivastava *et al.*, 2005). However, in summer urban vegetation may act as an additional source of VOCs such as methanol, isoprene and monoterpenes, even in cities with a temperate climate and little green space such as London or Manchester (Langford *et al.*, 2009; 2010b).

Emission inventories such as the London Atmospheric Emissions Inventory (LAEI, http://www.cleanerairforlondon.org.uk/londons-air/air-quality-data/london-emissions-naei/road-traffic-emissions) and the National Atmospheric Emissions Inventory (NAEI, http://naei.defra.gov.uk/data/) use a "bottom-up" approach based on activity data and emission

factors to estimate emission rates from pollutant sources. Micrometeorologically based eddy covariance techniques allow a "top-down" approach to quantify fluxes and these measurements can be compared with modelled emission inventory estimates. Such comparisons are essential as "bottom-up" emission inventories may inadvertently not include specific pollutant sources or may use unrepresentative emission factors or activity profiles. "Top-down" approaches using Earth observation data from satellites are also available for a few chemicals (Lamsal *et al.*, 2011) but not for primary VOCs. There have been few studies on VOC fluxes in urban areas, and these have been limited in spatial and temporal extent (Langford *et al.*, 2009; 2010b; Park *et al.*, 2010; 2011; Velasco *et al.*, 2005; 2009). Due to the high technical demands of VOC flux measurements, it is difficult to increase spatial coverage or to make measurements for long periods of time. Making further measurements of this kind is therefore a high priority in studies of air quality.

In this study we present flux and concentration measurements of seven selected volatile organic compounds made over 5 months in central London using the virtual disjunct eddy covariance method. The aims of this study were to i) quantify VOC fluxes above an urban canopy using proton transfer reaction mass spectrometry and virtual disjunct eddy covariance; ii) investigate seasonal, diurnal and spatial differences in VOC fluxes and concentrations; iii) examine possible major source contributions of speciated VOCs in central London; and iv) compare measured fluxes with those estimated by both the LAEI and the NAEI.

These observations were made as part of the ClearfLo (Clean air for London) project, which provided integrated short-term and long-term measurements of meteorology, gas phase and particulate pollutants over London and surrounding areas during 2011 and 2012 (Bohnenstengel *et al.*, 2015).

## 5.2 Methods

### 5.2.1 Measurement site

Micrometeorological flux measurements were made during the period 7$^{th}$ August - 19$^{th}$ December 2012 from a flux tower located on the roof of a building belonging to King's College,

University of London (51.511667° N, 0.116667° W; ground altitude 30 m a.s.l.), on the Strand in central London. Although the site is within the London Congestion Charge Zone (an area encompassing central London requiring road tolls to be paid and hence an area with reduced traffic density), surrounding roads supported a medium to high traffic volume (annual average of 50000-80000 vehicles per day, (Department for Transport, 2014)) with the River Thames situated 200 m to the south. This site is classified as a local climate zone class 2 compact midrise according to Stewart and Oke (2012) (i.e. dense mix of midrise buildings; 3–9 stories; few or no trees; land cover mostly paved; stone, brick, tile and concrete construction materials). Land cover types (in %) were calculated based on the Ordnance Survey map for the surrounding 9 km$^2$ area (Figure 5.1) encompassing the site and are roads (37%), buildings (31%), other paved areas (14%), unpaved/ vegetation (11%) and water bodies (7%).

The sampling inlet and sonic anemometer were mounted on a triangular mast (Aluma T45-H) at approx. 60.9 m (2.3 times mean building height, $z_H$) above ground level. The mean building height was around 25 m and the mast was located on an elevated area in the centre of the roof. A street canyon was located to the NW and an enclosed parking area to the SE, but generally surrounding buildings were of equal height. The sampling point (which we call KCL) is located 37 m west of a sampling point (KSS) that has been used for long-term energy and $CO_2$ flux measurements (Kotthaus and Grimmond, 2012). Although the site is not optimal for micrometeorological flux measurements due to the heterogeneity of the urban canopy, its suitability has been assessed in detail by Kotthaus and Grimmond (2014ab). This study describes in detail the measurement area and investigates the influence of source area characteristics on long-term radiation and turbulent heat fluxes for the KSS site. They conclude that the site can yield reasonable data on surface-to-atmosphere fluxes.

The weather in 2012 was somewhat cooler than the 1981 to 2010 long-term mean for London during summer and autumn, with several cold fronts bringing up to twice as much precipitation and associated winds as average, suppressing pollution levels. However, during the period of the Olympic and Paralympic games (27th July – 12th August and 29th August – 9th

September 2012) the weather was hot and dry causing sustained pollution peaks. Winter 2012/2013 was generally warmer and drier in London than the 1981-2010 mean (Met Office, 2013).

### 5.2.2 Instrumentation and data acquisition

The CSAT3 sonic anemometer (Campbell Scientific Inc., Utah, USA) and inlet were faced toward the predominant wind direction (SW) to minimise flow distortion. Data from the sonic anemometer were logged at a frequency of 10 Hz and flux measurements were calculated using 25 min averaging periods. The rotation angle theta ($\theta$), used to correct measurements of the vertical wind velocity for minor misalignment of the sonic anemometer, showed no significant disturbance of the turbulence from interactions with the building when plotted against wind direction. Data were recorded in UTC (universal time coordinated), which is 1 h earlier than local time in summer and coincident with Greenwich mean time in winter. However, all analyses used local time.

VOC concentrations were measured using a high-sensitivity proton transfer reaction (quadrupole) mass spectrometer (PTR-MS) (Ionicon Analytik GmbH, Innsbruck, Austria) with three Varian turbomolecular pumps (see for example de Gouw and Warneke, 2007, Hayward *et al.*, 2002, and Lindinger *et al.*, 1998 for more detailed description of the instrument). Air was drawn through an inlet co-located with the sonic anemometer. Sample air was purged through a ~ 30 m ½" OD (3/8" ID) PTFE tube at a flow rate of 81 L min$^{-1}$ to the PTR-MS, which was housed in a utility room below. The high flow rate ensured turbulent flow was maintained and signal attenuation minimised (Reynolds number, $Re$ = 11177). During the campaign, PTR-MS operating parameters were maintained at 1.95 mbar, 510 V and 50 °C for drift tube pressure, voltage and temperature respectively to achieve an $E/N$ ($E$ is the electric field strength and $N$ is the buffer gas number density) ratio of 123 Td (1 Td = $10^{-17}$ V cm$^2$). This field strength forms a compromise between reagent ion clustering and fragmentation suppression (Hewitt *et al.*, 2003). Further instrument parameters and meteorological conditions are summarised in Table 5.1. The inlet flow rate into the instrument was 0.25-0.3 L min$^{-1}$.

The logging program was written in LabVIEW (National Instruments, Austin, Texas, USA) and operated the PTR-MS in multiple ion detection (MID) and SCAN modes for VOC concentrations of nine selected masses and a range of the protonated mass spectrum $m/z$ 21-206 respectively. The sonic anemometer was not directly interfaced with the LabVIEW logging program, requiring the measurements to be synchronised during post-processing through the use of a cross-correlation function between the vertical wind velocity $w$ and the VOC ion counts $c$. A valve system controlled the measurement cycle, which consisted of 5 min zero air (ZA), 25 min MID followed by 5 min SCAN of sample air and 25 min MID mode. During the ZA cycle, air was pumped through a custom-made gas calibration unit fitted with a platinum catalyst heated to 200 °C to provide instrument background values at ambient humidity. In MID mode the quadrupole scanned nine predetermined protonated masses with a dwell time of 0.5 s each, to which the following compounds were ascribed: $m/z$ 21 (indirectly quantified $m/z$ 19 primary ion count via [$H_3^{18}O^+$]), $m/z$ 33 (methanol), $m/z$ 39 (indirectly quantified $m/z$ 37 first cluster [$H_3O^+(H_2O^+)$]), $m/z$ 42 (acetonitrile, results not shown), $m/z$ 45 (acetaldehyde), $m/z$ 59 (acetone/propanal), $m/z$ 69 (isoprene/furan), $m/z$ 79 (benzene), $m/z$ 93 (toluene), $m/z$ 107 (C$_2$-benzenes), and $m/z$ 121 (C$_3$-benzenes, results not shown). The total cycle time was 5.5 s. Secondary electron multiplier voltage, as well as $O_2^+$ ($m/z$ 32) and photon "dark counts" ($m/z$ 25) signals were monitored weekly.

*Table 5.1. Summary of instrument operating parameters and average meteorological conditions during the measurements in central London, August – December 2012.*

| Parameter | Unit | Mean (range) |
|---|---|---|
| *Normalised sensitivity* $(S_N)^a$ | ncps ppb$^{-1}$ | 11.5 (*m/z 33*), 13.3 (*m/z 45*),10 (*m/z 59*), 4 (*m/z 69*), 3.6 (*m/z 79*), 2.5 (*m/z 93*), 1.5 (*m/z 107*) |
| *Primary ion (m/z 19)* | cps | $8.31 \times 10^6$ ($6.14 \times 10^6$ – $1.15 \times 10^7$) |
| *Water cluster (m/z 37)* | cps | $1.92 \times 10^5$ ($9.15 \times 10^4$ – $3.86 \times 10^5$) |
| | % of *m/z 19* | 2.3 (1.5-3.4) |
| $O_2^+$ | % of *m/z 19* | <1.45 (1.11-2.01) |
| *Temperature*$^b$ | °C | 14.0 (-1.81-30.39) |
| *Relative humidity* | % | 76 (50-97) |
| *Pressure* | mbar | 1004.27 (968.71-1023.27) |
| *Wind speed*$^b$ | m s$^{-1}$ | 3.35 (0.12-14.96) |
| *Friction velocity* $(u_*)^b$ | m s$^{-1}$ | 0.5 (0.01-1.50) |
| *SD of vertical wind speed* $(\sigma_w)^b$ | m s$^{-1}$ | 0.65 (0.15-1.62) |

[a]$S_N$: Normalised sensitivity as calculated using Taipale *et al.* (2008).

[b]Derived from measurements from the CSAT3 sonic anemometer (Campbell Scientific).

The PTR-MS cannot distinguish between different compounds with the same integer mass; therefore, isobaric interference can occur. For example, *m/z* 107 may result from several contributing $C_8$ aromatics: ethyl benzene, (*m+p*)-xylene, *o*-xylene and some benzaldehyde (Warneke *et al.*, 2003). Further interferences at measured *m/z* from additional compounds and fragmentation for this instrument in an urban environment are discussed in Valach *et al.* (2014). Although the $O_2^+$ and water cluster ions were kept <2% of the primary ion, interferences from $^{17}O^+$ isotopes at *m/z* 33 were taken into account.

Single point calibrations were performed on-site once a month using a certified multiple component VOC gas standard (Ionimed, part of Ionicon Analytik GmbH, Austria), which was validated by cross-calibration with a second independent VOC standard (Apel Riemer Environmental Inc., CO, USA). Before and after the campaign, multistep calibrations were

performed with both standards. Standards were diluted with catalytically converted zero air, since cylinder concentrations were approx. 1 ppm ± 5% uncertainty (Ionimed Analytik) and 0.5 ppm ± 10% (Apel Riemer). Error propagation resulted in a total calibration uncertainty of <20%. Measured normalised instrument sensitivities ($S_N$, Table 5.1) based on Taipale *et al.* (2008) were used to convert normalised count rates (ncps) of protonated masses ($RH^+$) to volume mixing ratios (Langford *et al.*, 2010a). Only the *o*-xylene isomer was present in the Ionimed standard, which was used to determine instrument sensitivities for *m/z* 107, but sensitivities agreed well when compared with sensitivities for *p*-xylene present in the Apel Riemer standard. Any remaining humidity effects on calibrations were previously investigated for this instrument and were found to be within the overall calibration uncertainty (Valach *et al.*, 2014). Detection limits of VOC concentrations (Table 5.2) were calculated according to Taipale *et al.* (2008).

### 5.2.3 Flux calculations and quality assessment

Fluxes were calculated according to Karl *et al.* (2002) and Langford *et al.* (2009; 2010a) using

$$F = \frac{1}{n} \sum_{i=1}^{n} w'^{\left(\frac{i-t_{lag}}{\Delta_{tw}}\right)} \times c'^{(i)}, \tag{5.1}$$

where *w'* and *c'* are the instantaneous fluctuations around the mean vertical wind ($w - \overline{w}$) and mean VOC concentration ($c - \overline{c}$), *n* is the number of VOC concentration measurements per 25 min averaging period (*n* = 273), $t_{lag}$ is the lag time between the wind and PTR-MS measurement due to the transit through the sampling line and $\Delta_{tw}$ is the sampling interval of the vertical wind speed measurements of the sonic anemometer (10 Hz = 0.1 s). Langford *et al.* (2015) recently demonstrated that the method used to determine the time lag becomes important where the signal-to-noise ratio of the analyser is poor, showing that methods that systematically search for a maximum in the cross-correlation function within a given window (MAX method) can bias the calculated fluxes towards more extreme (positive or negative) values. Their study recommends the use of a prescribed lag time determined either through the use of a monitored sample flow rate or by using the typical lag time derived by searching for a maximum. Here the prescribed lag

times were determined by fitting a running mean to the time series of daytime lag times calculated using the MAX method for acetone, which had large fluxes and the clearest time lags. Prescribed lag times for all other compounds were set relative to that of acetone, accounting for the offset introduced by the sequential sampling of the PTR-MS.

Flux losses due to the attenuation of high and low frequency eddies were estimated for our measurement setup. High frequency flux attenuation was estimated to be on average 11% using the method of Horst (1997), and a correction was applied. Attenuation from low frequency fluctuations for a 25 min flux period was investigated by reanalysing the sensible heat fluxes for longer averaging periods of 60, 90, 120 and 150 min. The coordinate rotation was applied to the joined files, which acted as a high pass filter to the three wind vectors, confirming that fluctuations of eddies with a longer time period than the averaging time did not contribute to the flux measurement (Moncrieff $et$ $al.$, 2004). The fluxes were compared to the 25 min average fluxes, which had the coordinate rotation applied before joining, again to ensure only turbulent fluctuations of ≤25 min contributed to the flux (Supplementary information Figure 5.A1). Flux losses due to low frequency attenuation were estimated to be <1.5% and, therefore, no corrections were deemed necessary. The error due to the disjunct sampling was estimated by comparing the sensible heat fluxes calculated from the continuous data series with those calculated from a disjunct data series using a set sampling interval of 5.5 s. The continuous data were averaged to match the sampling frequency of the disjunct data (i.e. 2 Hz). The difference between the eddy covariance and DEC sensible heat fluxes was minimal (0.01%) and thus no additional corrections were applied.

Many of the 25 min resolved flux measurements were close to the limit of detection (LoD), based on 1 standard deviation using the method of Spirig $et$ $al.$ (2005), with an average fail rate of 82%. Various techniques to statistically analyse or replace values below the LoD have been developed (Clarke, 1998). However, they often result in significant bias, either high or low depending on the value substituted, because values tend to be below the LoD when fluxes are indeed small (Helsel and Hirsch, 1992). In this study, our analysis focused on diurnally averaged

flux profiles and we decided not to filter out individual flux values on the basis of being <LoD in order to avoid this bias. When averaging the 25 min flux data it is appropriate to also average the LoD which, as shown by Langford *et al.* (2015), decreases with the square root of the number of samples averaged (*N*). Therefore, although the majority of the individual 25 min flux measurements were below the LoD, their diurnal average profiles may exceed the LoD for the average and thus still yield important data on the net exchange of VOCs above the city.

$$\overline{LoD} = \frac{1}{N} \sqrt{\sum_{i=1}^{N} LoD^2}. \tag{5.2}$$

The following describes the additionally applied filter criteria. 25 min flux values with a friction velocity ($u_*$) <0.15 m s$^{-1}$ were rejected (3.4% of total data) due to insufficient turbulence. The stationarity test and data quality rating methods of Foken and Wichura (1996) and Velasco *et al.* (2005) were used, and 47% of the data files were rejected on this basis. The high number of files rejected in the stationarity test is to be expected for eddy covariance measurements over highly heterogeneous canopies, although horizontally averaged canopy morphology recovers some surface homogeneity. Furthermore, the low measurement height used can cause an increased sensitivity towards canopy roughness features resulting in non-stationarity. Since urban environments are inherently not ideal for micrometeorological flux measurements due to their heterogeneity, integral turbulence characteristics of this site were assessed by comparing the measured standard deviation of the vertical wind velocity ($\sigma_w$) normalised by $u_*$ to the parameters of a modelled ideal turbulence (Foken *et al.*, 2004). Results showed that 99.6% of all the data was rated category six or better and 0.4% was rejected using the criteria of Foken *et al.* (2004). This large pass rate gives further confidence that the measurements were not unduly affected by wake turbulence generated from the structure of the building. Erroneous meteorological data (2.6% of total) were removed around wind directions of 14-15° due to minor turbulence interferences from the presence of other sensors on the mast. Depending on the compound, between 40 and 61% of flux data (*N* = 1934–2949) passed all of the above quality controls. Exactly 2014 h of

concentration data ($N$ = 4834) was obtained. For consistency, regression coefficients ($R^2$) were used throughout.

The traffic densities used for the analysis were obtained from a nearby site at Marylebone Road (approx. 3 km to the NW) and consisted of hourly vehicle counts covering the period 7th - 22nd August 2012. The major roads of the Strand and the Thames Embankment surrounding the measurement site support a comparable traffic volume with an annual average of 50000 - 80000 vehicles per day (Department for Transport, 2014) and diurnal patterns in traffic are likely to be similar across central London.

Photosynthetically active radiation (PAR) and $CO_2$ measurements used in the analysis were part of the long-term micrometeorological measurements at the same site and covered the period from August to September for PAR and from August to December for $CO_2$. Average diurnal profiles were calculated for the boundary layer mixing height, which was measured using three LiDARs located on rooftops within central London during an approx. 2-week period in summer and winter 2012 (Bohnenstengel *et al.*, 2015).

### 5.2.3.1 Flux footprint calculations

Although there are no operational footprint models for urban environments that take the complex topography and spatial variability in building height and surface heat fluxes into account, the analytical footprint model of Kormann and Meixner (2001) has previously been applied in non-homogeneous terrain (Helfter *et al.*, 2011; Neftel *et al.*, 2008). The Kormann-Meixner (KM) model determines the 2D footprint density function explicitly from micrometeorological parameters, which are provided by the eddy covariance measurements, i.e., friction velocity ($u_*$), measurement height ($z_m$), Obukhov length ($L$), horizontal wind velocity at the measurement height ($u(z_m)$), and standard deviation of the lateral wind ($\sigma_v$). The flux footprints were calculated for each 25 min flux period. Neftel *et al.* (2008) developed a Microsoft Excel-based tool that allows the footprint contributions (%) of user-defined spatial elements to be mapped. In this case we used a total of nine 1 $km^2$ grid squares to match the Ordnance Survey (OS) grid (Figure 5.1), centred on the measurement site. This grid resolution was validated using a simple

parameterisation model (Kljun *et al.*, 2004) with average diurnal cycle parameters for $\sigma_w$, $u_*$ and

boundary layer height ($z_i$) during the campaign, which calculated the distance of the maximum

flux contribution ($X_{max}$) and the extent of the 90% flux footprint ($X_{90}$).

The KM footprint calculation requires the Monin-Obukhov stability parameter ($\zeta$) to be

within the interval [-3, 3], where

$$\zeta = \frac{z_m - d}{L},$$ 
(5.3)

with $d$ ($d = \frac{2}{3}z_H = 16.7$ m) being the displacement height estimated as a fraction of the canopy

height (Garrat, 1992). The footprint estimation for cases of extreme stability is of lower quality

but still provides useful information. The vertical turbulent flux $F_c(0,0,z_m)$ measured at the height

$z_m$ is related to the corresponding surface flux area $F_c(x,y,0)$, which is upwind of the measurement

point, such that

$$F_c(0,0,z_m - d) = \int_{\infty}^{-\infty} \int_{0}^{\infty} F_c(x,y,z_m - d)\Phi(x,y,z_m - d)dxdy,$$
(5.4)

where $z_m$ is the measurement height and the x-axis is aligned with the mean horizontal wind

direction. $\Phi(x, y, z_m - d)$ is the footprint function and includes a weighting function to describe

the influence of a unit point source on the flux from any surface location *(x,y)*. In order to compare

VOC fluxes with estimated emissions from the London Atmospheric Emissions Inventory

(LAEI), a 9 km$^2$ section of the 1 km$^2$ resolution OS grid system was used, which on average

included 90% of the footprint contribution to all measured fluxes. This area was limited to central

London and partially included the following boroughs: Westminster (squares 1, 4, 5 and 7),

Southwark (2, 3 and 6), Camden (8) and the City of London (9) (Figure 5.1).
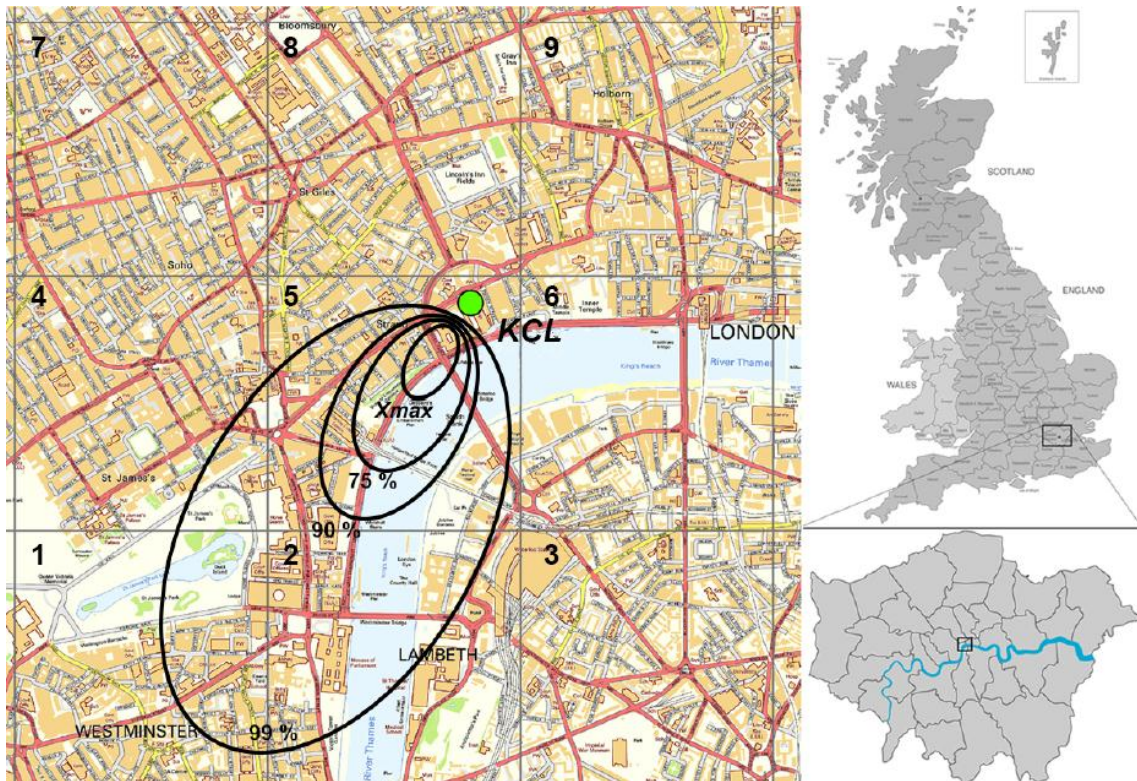
**Figure 5.1**. Map of central London overlaid with the Ordnance Survey grid including the measurement site (KCL) at King's College (green point) with references to the geography of Greater London and Great Britain. Grid squares correspond to the numbers (1-9) in Section 5.3.3 starting bottom left to top right. Outlines of the areas that contribute the maximum ($X_{max}$), as well as 75%, 90%, and 99% to the flux footprint using overall median meteorological values are shown as black contour lines with their respective labels laid out according to the median wind direction. © Crown Copyright. Reproduced by permission of Ordnance Survey®.

## 5.3 Results and Discussion

### 5.3.1 Diurnal profiles of VOC fluxes and concentrations

Average diurnal cycles of measured VOC fluxes and mixing ratios are shown in Figure 5.2a and 5.2b with descriptive statistics for all the data summarised in Table 5.2. Largest median (interquartile range in parenthesis) fluxes per day were from $C_2$-benzenes and toluene, with 7.86 (0.92-21.8) kg km$^{-2}$ d$^{-1}$ and 7.26 (1.83-15.3) kg km$^{-2}$ d$^{-1}$ respectively, followed by oxygenated compounds, i.e. methanol with 6.37 (2.99-10.0) kg km$^{-2}$ d$^{-1}$, acetaldehyde 3.29 (1.52-5.62) kg km$^{-2}$ d$^{-1}$ and acetone 5.24 (2.33-9.62) kg km$^{-2}$ d$^{-1}$. Isoprene and benzene showed the smallest median fluxes with 2.14 (0.56-4.85) kg km$^{-2}$ d$^{-1}$ and 1.78 (0.06-4.34) kg km$^{-2}$ d$^{-1}$ respectively. The highest median mixing ratios were of the oxygenated compounds methanol (7.3 (6.8-7.9) ppb),

acetone (0.95 (<LoD-1.36) ppb) and acetaldehyde (0.82 (0.59-1.13) ppb), followed by aromatics ($C_2$-benzenes, toluene and benzene), and isoprene.

Oxygenated compounds commonly have relatively long atmospheric lifetimes and widespread origin including anthropogenic and biogenic sources and photochemistry, resulting in elevated concentrations and less pronounced diurnal profiles (Atkinson, 2000). Most VOC fluxes and concentrations were comparable to or lower than those previously observed in London (Langford *et al.*, 2010b) and other UK cities (Langford *et al.*, 2009), although $C_2$-benzene fluxes and concentrations, as well as isoprene and benzene concentrations were slightly higher. The discrepancy in isoprene and benzene concentrations is consistent with photochemical loss during transport to the higher measurement height of the previous studies. Compared to other cities such as Houston Texas (Park *et al.*, 2010) and Mexico City (Velasco *et al.*, 2005), VOC fluxes and concentrations were lower with the exception of $C_2$-benzenes, which were comparable or higher; however, it must be noted that $C_2$-benzenes in this study represent the sum of multiple VOC species. Unlike the other studies cited, Park *et al.* (2010) use relaxed eddy accumulation to measure VOC fluxes and hence the data obtained are not directly comparable with measurements made by EC-based methods.

Diurnal profiles of aromatic fluxes and concentrations presented two clear rush hour peaks during the morning and evening (07:00-10:00 and 17:00-20:00 local time). Concentration peaks are thought to be linked to additional advection of traffic-related pollution from larger commuter roads outside of the city centre, as well as boundary layer effects and photochemistry. VOC concentration measurements at canopy height can be affected by boundary layer depth (Vilà-Guerau de Arellano *et al.*, 2009). The rush hour emission peaks mostly coincide with the boundary layer expansion and collapse and therefore the effect of each factor cannot be separated. The morning concentration peak was slightly higher than the evening peak across traffic-related species even though fluxes tended to be larger during the evening rush hour. Morning emissions enter a shallow nocturnal boundary layer leading to relatively larger concentrations compared to higher afternoon emissions entering a developed boundary layer leading to relatively lower

concentrations. This enhanced dilution effect is found more often during summer when the boundary layer mixing height is higher (Figure 5.2). Therefore, the regression analyses below only refer to data from August (cf Section 5.3.1.2 for comparisons with winter). Furthermore, increased photochemical degradation during the day removes VOCs, further contributing to the midday minimum in mixing ratios. The diurnal flux profiles of methanol, acetone, isoprene and to a smaller extent acetaldehyde showed one large peak just after midday (approx. 13:00 local time), which was only reflected in the concentration profiles of acetone and isoprene. Acetaldehyde concentrations presented a slight double peak similar to mixing ratios of aromatics. Methanol has a relatively long atmospheric lifetime and therefore high background concentrations, and hence mixing ratios showed no distinct diurnal profile.

*Table 5.2. Summary of 25 min VOC fluxes and mixing ratios above central London during August-December 2012.*

| Compound (m/z) | Methanol (m/z 33) | Acet-aldehyde (m/z 45) | Acetone/propanal (m/z 59) | Isoprene/furan (m/z 69) | Benzene (m/z 79) | Toluene (m/z 93) | C₂-benzenes (m/z 107) |
|---|---|---|---|---|---|---|---|
| *Fluxes (mg m⁻² h⁻¹)* | | | | | | | |
| *Lifetime (OH[a])* | 12 d | 8.8 h | 53 d | 1.4 h | 9.4 d | 1.9 d | 5.9 h |
| *N* | 2920 | 2811 | 2945 | 2119 | 1908 | 2315 | 2053 |
| *Min.* | -2.91 | -0.28 | -1.74 | -0.35 | -0.64 | -2.31 | -3.27 |
| *1. quartile* | 0.12 | 0.06 | 0.10 | 0.02 | 0.002 | 0.08 | 0.04 |
| *Median* | 0.27 | 0.14 | 0.22 | 0.09 | 0.07 | 0.30 | 0.33 |
| *Mean* | 0.29 | 0.16 | 0.31 | 0.13 | 0.09 | 0.41 | 0.54 |
| *3. quartile* | 0.42 | 0.23 | 0.40 | 0.20 | 0.18 | 0.64 | 0.91 |
| *Max.* | 3.36 | 1.09 | 2.85 | 1.16 | 0.59 | 4.86 | 8.63 |
| *SD* | 0.25 | 0.15 | 0.34 | 0.16 | 0.15 | 0.53 | 0.86 |
| *Skew* | 0.86 | 1.27 | 2.08 | 1.18 | 0.32 | 1.75 | 2.33 |
| *Kurtosis* | 20.37 | 2.85 | 7.57 | 2.81 | 0.76 | 8.04 | 14.48 |
| *Mixing ratios (ppb)* | | | | | | | |
| *N* | 4834 | 4834 | 4834 | 4834 | 4834 | 4834 | 4834 |
| *Min.* | 5.73 | <LoD (0.14) | <LoD (0.02) | <LoD (0.03) | <LoD (0.04) | <LoD (0.05) | <LoD (0.14) |
| *1. quartile* | 6.82 | 0.59 | <LoD (0.65) | <LoD (0.16) | <LoD (0.18) | <LoD (0.38) | <LoD (0.57) |
| *Median* | 7.27 | 0.82 | 0.95 | <LoD (0.22) | <LoD (0.24) | <LoD (0.54) | 0.75 |
| *Mean* | 7.53 | 0.94 | 1.10 | 0.25 | 0.29 | <LoD (0.65) | 0.87 |
| *3. quartile* | 7.90 | 1.13 | 1.36 | 0.30 | 0.34 | 0.77 | 1.03 |
| *Max.* | 17.06 | 5.17 | 6.07 | 1.86 | 1.71 | 5.30 | 4.96 |
| *SD* | 1.12 | 0.53 | 0.66 | 0.14 | 0.19 | 0.45 | 0.50 |
| *Skew* | 2.21 | 2.14 | 1.65 | 1.97 | 2.80 | 3.07 | 2.79 |
| *Kurtosis* | 7.22 | 7.83 | 4.06 | 7.27 | 12.37 | 15.89 | 12.99 |
| *LoD[b]* | 0.96 | 0.45 | 0.66 | 0.25 | 0.28 | 0.66 | 0.71 |

[a]Atmospheric lifetimes with regard to OH for a 12 h daytime average OH concentration of $2.0 \times 10^6$ molecules cm⁻³ (Atkinson, 2000).

[b]LoD: Limit of detection calculated using Taipale *et al.* (2008).
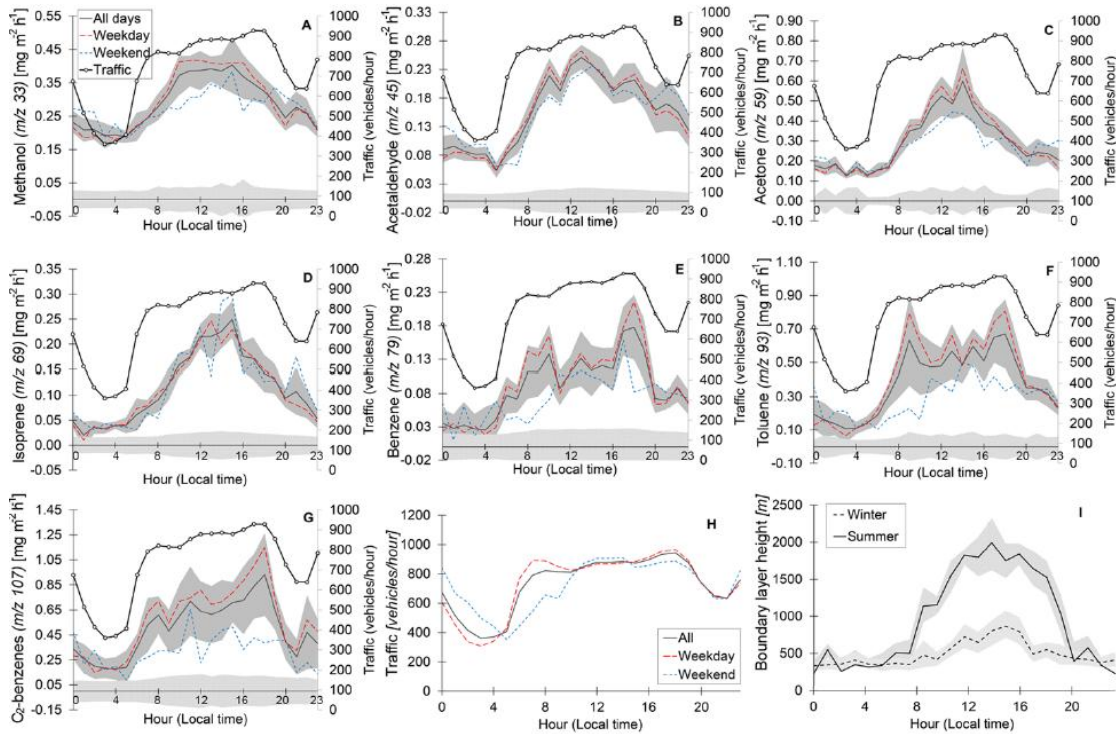
**Figure 5.2**. *Part 1*: average diurnal profiles in local time for selected VOC fluxes (mg m$^{-2}$ h$^{-1}$) separated into all days, weekdays (red dashed line) and weekends (blue dotted line) with traffic density (vehicles h$^{-1}$), detection limit (patterned area) and upper and lower confidence intervals (shaded area). Traffic density (with weekday and weekend) and boundary layer mixing height (for summer and winter) are shown in separate panels. Compounds are *m/z* 33 (methanol), *m/z* 45 (acetaldehyde), *m/z* 59 (acetone/propanal), *m/z* 69 (isoprene/furan), *m/z* 79 (benzene), *m/z* 93 (toluene) and *m/z* 107 (C$_2$-benzenes).
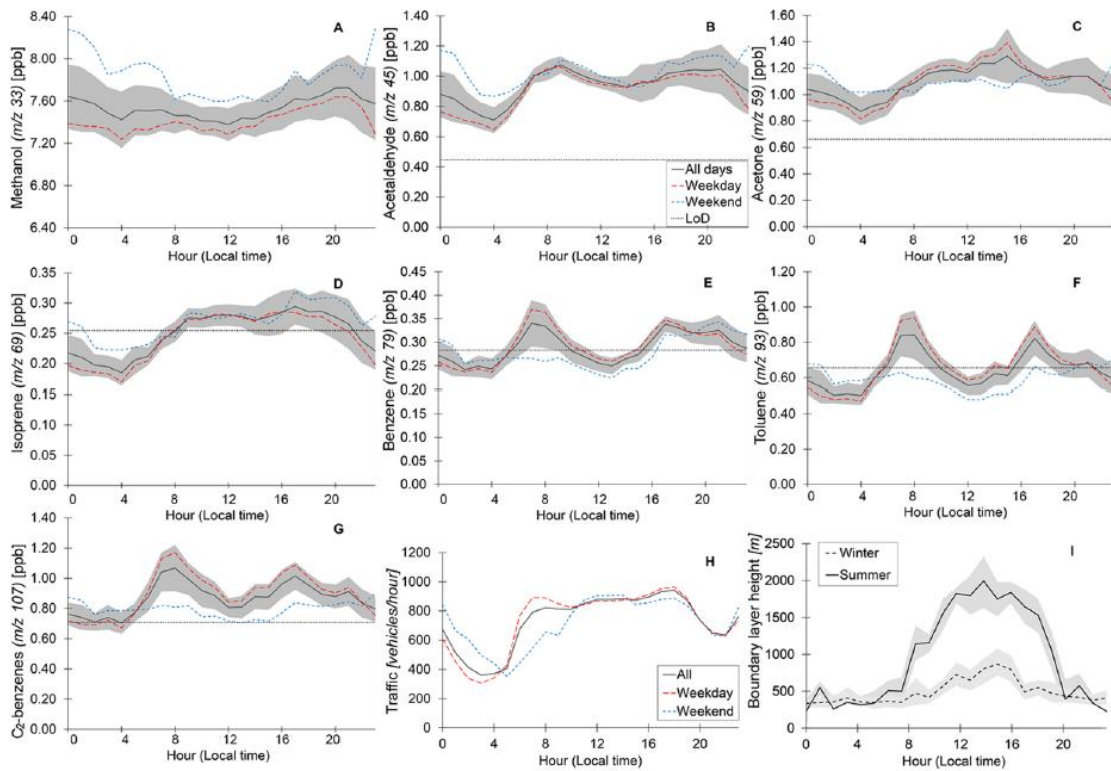
**Figure 5.2**. *Part 2*: average diurnal profiles in local time for selected VOC mixing ratios (ppb) separated into all days, weekdays (red dashed line) and weekends (blue dotted line) with detection limit (dotted line) and upper and lower confidence intervals (shaded area). Traffic density (with weekday and weekend) and boundary layer mixing height (for summer and winter) are shown in separate panels. Compounds are *m/z* 33 (methanol), *m/z* 45 (acetaldehyde), *m/z* 59 (acetone/propanal), *m/z* 69 (isoprene/furan), *m/z* 79 (benzene), *m/z* 93 (toluene) and *m/z* 107 (C$_2$-benzenes). The mixing ratio axes start from 0 apart from that of methanol, which begins at 6.4 ppb due to the high atmospheric background.

### 5.3.1.1 Correlations with possible controlling variables of VOC fluxes and concentrations

Aromatic compound fluxes closely followed the diurnal profile of traffic density with good correlations ($R^2 = 0.51$-$0.92$, $p < 0.05$) and slightly lower fluxes observed on the weekends. In central urban areas in the UK, traffic densities — and therefore traffic-related VOC fluxes — increase steadily throughout the day, with discernible peaks during morning, midday and evening (Nemitz *et al.*, 2002), which was also observed in this study. Previous studies have shown that the Marylebone Road traffic count can be used as a proxy representative of traffic flows throughout central London (Helfter *et al.*, 2011).

The aforementioned concentration dilution due to boundary layer expansion resulted in negative correlations between boundary layer height and aromatic mixing ratios in August ($R^2$ = 0.33-0.56, $p$ <0.01). As aromatic compound fluxes slightly dipped around midday, the mixing ratios were further diluted by the deep boundary layer. The above evidence suggests that traffic-related emissions were the main contributors to fluxes and mixing ratios of aromatic compounds. Acetone and isoprene showed peak midday fluxes, which maintained daytime mixing ratios and produced positive correlations with boundary layer height ($R^2$ = 0.16 and 0.59 respectively; $p$ <0.01). De Gouw *et al.* (2005) reported that changes in boundary layer meteorology could result in greater effects on observed concentrations of methanol and acetone due to their high background values. The mixing ratios of these compounds are, therefore, likely dominated by advected pollution rather than the local flux. Possibly a combination of boundary layer and photochemical effects were seen with methanol mixing ratios wherein correlations with mixing height were negative ($R^2$ = 0.70, $p$ <0.01), whereas acetone and isoprene fluxes seemed to be sufficiently high during the day to maintain peak midday mixing ratios (Figure 5.3 example of isoprene). Vehicle emissions may have contributed to acetaldehyde and isoprene levels directly or indirectly (Figure 5.3 example of isoprene), because correlations of fluxes with traffic density were fairly high ($R^2$ = 0.60 and 0.46 respectively; $p$ <0.05). The diurnal concentration profile of acetaldehyde to some degree mimicked those of traffic-related compounds reflecting a slight double peak.
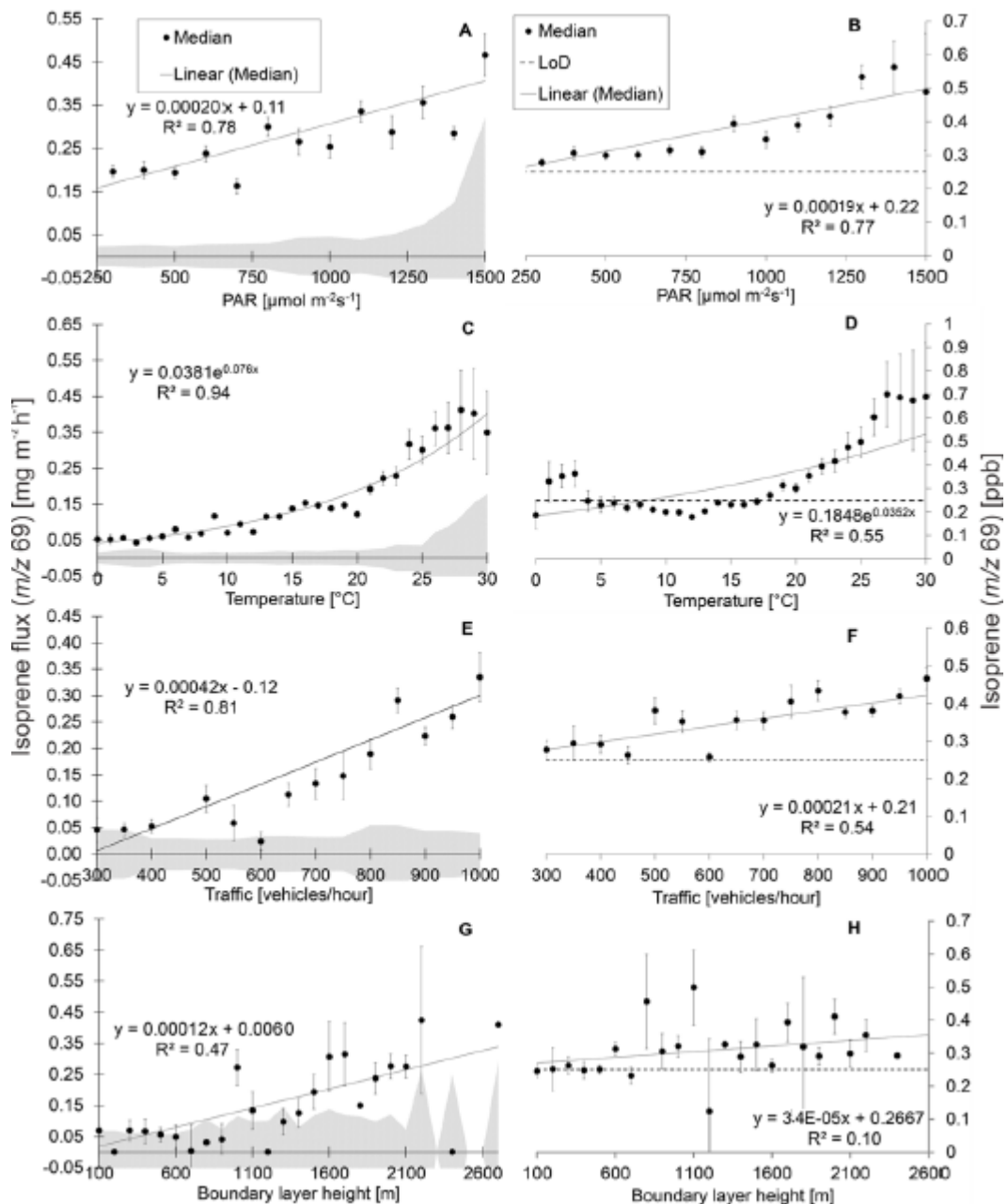
**Figure 5.3**. Examples, using isoprene, of averaged VOC fluxes (*left*) and mixing ratios (*right*) as a function of photosynthetically active radiation (PAR) ($\mu$mol m$^{-2}$ s$^{-1}$), temperature (°C), traffic density (vehicles h$^{-1}$) and boundary layer mixing height (m) based on 25 min VOC means with linear or exponential regressions, formulae, $R^2$ values and detection limit (shaded area for fluxes and dashed line for mixing ratios).

VOC fluxes and concentrations plotted as a function of PAR showed strong daytime (defined as 06:00 to 18:00 local time) correlations for methanol, acetaldehyde and isoprene fluxes ($R^2 = 0.71$-$0.78$, $p < 0.001$) and concentrations ($R^2 = 0.66$-$0.83$, $p < 0.001$). Plotted as a function of

temperature, high correlations with methanol, acetaldehyde and isoprene fluxes were seen ($R^2 =$ 0.75, 0.63 and 0.94 respectively; $p$ <0.001), whereas only methanol and acetone concentrations showed higher correlations with temperature ($R^2 = 0.64$ and 0.81 respectively; $p$ <0.001 respectively). Methanol fluxes correlated linearly with temperature ($R^2 = 0.75$, $p$ <0.001), but acetaldehyde and isoprene fluxes ($R^2 = 0.64$ and 0.94; $p$ <0.01) and mixing ratios ($R^2 = 0.45$ and 0.55; $p$ <0.01) had exponential relationships with temperature (Figure 5.3 example of isoprene). The relationships of mixing ratios with PAR and temperature for these compounds improved greatly when night-time values were excluded (defined as PAR <100 μmol m$^{-2}$ s$^{-1}$) and when times of low temperature (<5 °C) were excluded. This indicates either separate source contributions or effects of boundary layer meteorology in these instances, whereby increased mixing ratios of these compounds with low PAR and temperature likely result from reduced dilution within a shallow boundary layer, e.g. at night or in winter, or from possible contributions of anthropogenic sources such as exhaust emissions, which are largely independent of light and temperature. Increases in concentrations due to high PAR and temperature suggest biogenic sources, increased evaporative emissions and/or secondary atmospheric formation driven by oxidation of precursor hydrocarbons (Singh *et al.*, 1994). Oxygenated compounds have a variety of different source contributions such as tailpipe emissions, evaporative emissions from fuel and solvents, direct emissions from plants, leaf decomposition and secondary atmospheric production (Langford *et al.*, 2009 and references therein).

Modelling studies have indicated that the contribution of secondary atmospheric formation to VOC concentrations could be more significant, especially in urban areas, during summer, i.e. with high PAR and temperatures (de Gouw *et al.*, 2005; Harley and Cass, 1994). Acetone fluxes reached a maximum when PAR and temperature were around 1000 μmol m$^{-2}$ s$^{-1}$ and 15-20 °C respectively before declining, whereas mixing ratios increased exponentially with light and temperature. These observations resemble measurements over forest canopies (e.g. Schade and Goldstein, 2001). Aromatic compound concentrations and fluxes showed no correlations with PAR. Weak negative correlations were seen between aromatic concentrations

and temperature, and weak positive correlations were seen between fluxes and temperature likely due to increased thermal mixing. The observed light and temperature responses associated with isoprene fluxes and mixing ratios in August and September can be explained by biogenic sources (cf Section 5.3.1.3).

### 5.3.1.2 Seasonal variability of VOC sources and meteorology

Most compounds showed larger fluxes in August and September than in October, November and December with the exception of acetaldehyde, which also showed increased fluxes in December (Figure 5.4 *top*). Increased acetaldehyde fluxes in December may have resulted from an additional source, such as domestic biomass burning (Andreae and Merlet, 2001; Lipari *et al.*, 1984), although there are only few residential buildings in this area of London. Only toluene fluxes in September were significantly higher than in other months and benzene fluxes showed no significant seasonal differences. Seasonal variability in fluxes was likely due to increased emissions in summer, especially for compounds with biogenic and secondary atmospheric sources. Average monthly meteorological parameters are summarised in Table 5.3.
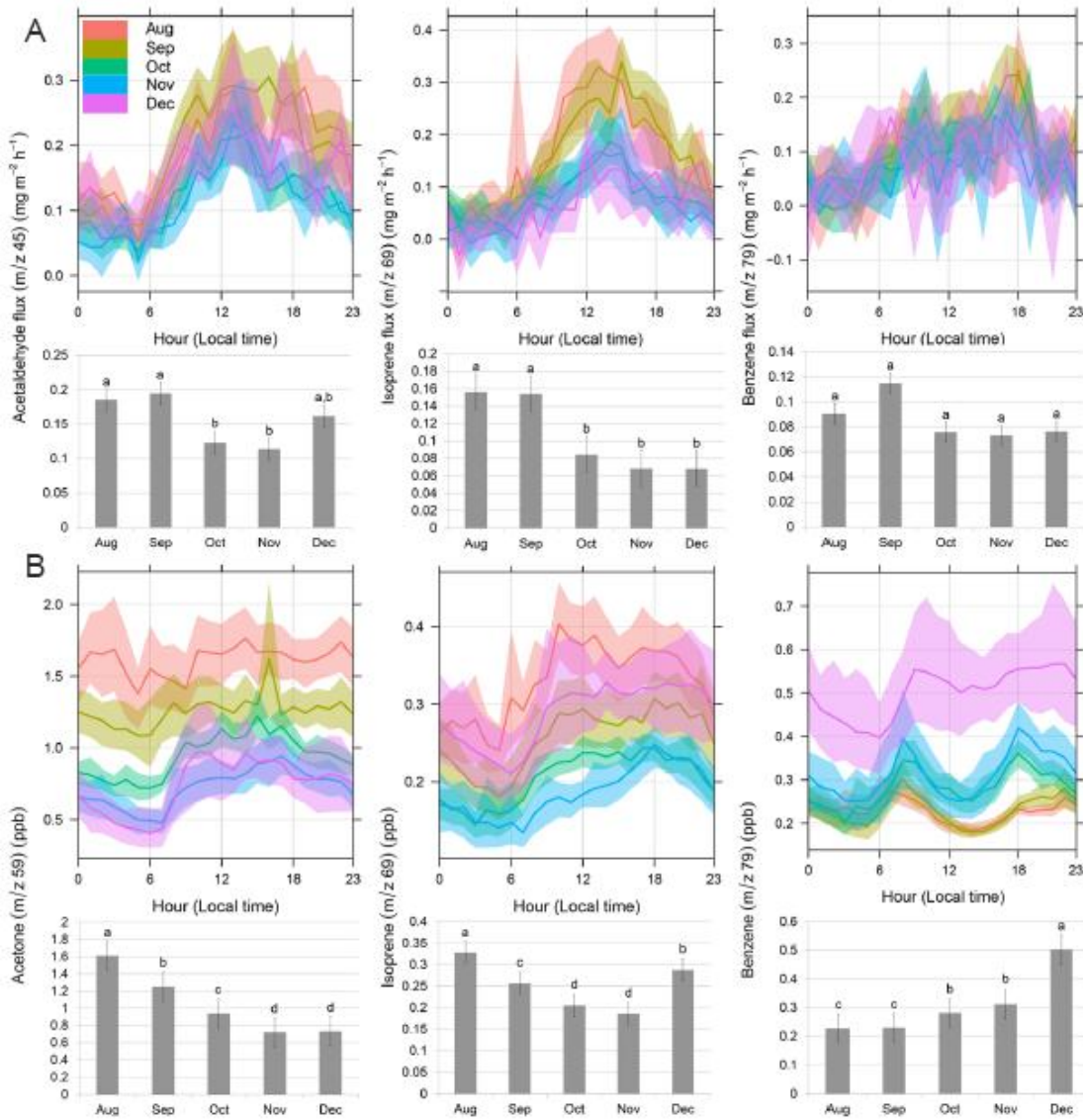
**Figure 5.4**. Diurnal profiles by month with confidence intervals and bar charts showing hourly averages for the respective month and representative compound (top) fluxes (mg m$^{-2}$ h$^{-1}$) (m/z 45, 69 and 79) and (bottom) mixing ratios (ppb) (m/z 59, 69 and 79). Letters (a-d) indicate statistically significant subgroups using Tukey's Honestly Significant Difference post hoc test.

Mixing ratios of aromatics were generally lower in summer and highest in December (Figure 5.4 *bottom*). This is likely due to less dilution effects in winter when the boundary layer is shallow or from advection of additional sources such as heating, since there was no increase in fluxes. Generally, in summer the boundary layer mixing height is higher and collapses later in the evening which maintains the dilution effect for VOC concentrations. In winter the average

boundary layer mixing height is lower. It develops later in the morning and collapses earlier in the afternoon, which could increase not only overall VOC mixing ratios but also individual maxima, e.g. during rush hours. Comparing average diurnal profiles of compound mixing ratios with boundary layer height during summer and winter shows that aromatic compound concentrations were associated with negative correlations in summer (cf Section 5.3.1.1) which became positive during winter ($R^2 = 0.10\text{-}0.33$, $p < 0.01$), while fluxes maintained positive correlations with boundary layer height regardless of season. This suggests that boundary layer effects may be an important driver of increased concentrations in winter. Furthermore, traffic counts for the Congestion Charge Zone in central London indicate lower monthly average vehicle counts in December (Department for Transport, 2014). Oxygenated compounds and isoprene mixing ratios were highest in summer with the exception of acetone, which increased in December likely from boundary layer effects, reduced photochemical degradation or advection. Correlations of mixing ratios and fluxes with boundary layer height were positive for acetone and isoprene during summer and winter, whereas methanol and acetaldehyde presented negative correlations during summer, indicating stronger dilution effects (cf Section 5.3.1.1).

*Table 5.3. Summary of site meteorology by month in central London during 2012.*

| Parameter | Data coverage (%) | Median stability ($\zeta$) | Wind speed (m s$^{-1}$) | Dominant wind direction (%) | Footprint[a] length (m) | Footprint width (m) |
|---|---|---|---|---|---|---|
| *Aug* | 67 | -0.0086 | 3.3 | S (54) | 2417 | 1355 |
| *Sep* | 83 | -0.0154 | 3.2 | W (48) | 1285 | 880 |
| *Oct* | 89 | -0.0006 | 3.5 | S (29) | 2624 | 1327 |
| *Nov* | 51 | -0.0037 | 3.4 | S (53) | 2329 | 1156 |
| *Dec* | 40 | 0.0047 | 3.4 | N (32) | 1804 | 990 |

[a]Calculated two-dimensional description of the oval footprint according to the KM model. Length parameter is the length between the point nearest to the sensor where the crosswind-integrated footprint function reaches 1% of its maximum value to the point where it drops below 1% of the maximum value.

Increased summer mixing ratios of oxygenated compounds and isoprene indicated a temperature-dependent, possibly biogenic source contribution. While biogenic emissions may be advected from outside of the city, the concurrent increase in isoprene fluxes suggests the source to be largely local to the flux footprint. The temperature-dependent fraction of observed isoprene mixing ratios, which may include advected pollution, was estimated using the isoprene temperature response function from Figure 9 in Langford *et al.* (2010b), which estimated a 30% and 20% contribution in August and September respectively. These values were significantly higher than for isopentane, a non-biogenic compound available from the Automatic Hydrocarbon Network, to which the same analysis was applied. The temperature-dependent component of isoprene in October, November and December showed no significant difference to that of isopentane, suggesting the biogenic component was reduced or absent at lower temperatures. High correlations of *m/z* 69 with light and temperature during August and September indicate that isoprene was the likely major component during these months; however, during the rest of the period the contribution of additional compounds such as furan and other alkenes at that mass may have increased, thereby overestimating the isoprene signal (Yuan *et al.*, 2014).

### 5.3.1.3 Modelling the biogenic isoprene contribution in London

An attempt was made to model the biogenic isoprene component during August and September using the light and temperature algorithms of Guenther *et al.* (1995), hereafter termed G95. The foliar-emissions-based model calculates VOC fluxes as follows:

$$F = D \times \varepsilon \times \gamma, \tag{5.5}$$

where $D$ is the foliar density (kg dry matter m$^{-2}$), $\varepsilon$ is an ecosystem-dependent base emission rate (μg C m$^{-2}$ s$^{-1}$ normalised to a PAR flux of 1000 μmol m$^{-2}$ s$^{-1}$ and leaf temperature of 303.15 K) and $\gamma$ is a dimensionless activity adjustment factor accounting for the effects of PAR and leaf temperature. Ambient air temperature and PAR measurements were used to calculate the light- and temperature-controlled parameters $C_L$ and $C_T$ for $\gamma$, where

$$\gamma = C_L \times C_{T.} \tag{5.6}$$

The slope of the linear regression of the measured total isoprene flux and $\gamma$ provided an emission factor in mg m$^{-2}$ h$^{-1}$, which was converted to µg g$^{-1}$ h$^{-1}$ by dividing by the foliar density ($D$ = 0.129 kg m$^{-2}$). The foliar density was estimated using the total tree leaf area as seen from visible satellite imagery within the flux footprint and tree leaf dry weight for representative species commonly planted in the area, such as *Platanus x acerifolia* (City of Westminster, 2009)*,* that are also high isoprene emitters (Geron *et al.*, 1994). The resulting base emission rate $\varepsilon$ from the measured fluxes was 6.5 µg g$^{-1}$ h$^{-1}$, which compares well with the figure given in the literature (5 µg g$^{-1}$ h$^{-1}$) for cities in a cool climate (Guenther *et al.*, 1995). For details of this calculation, see the Supplementary Information 5.5.B. These estimates are representative of the biogenic isoprene fluxes from a highly heterogeneous canopy within the flux footprint, including both high- and low-isoprene-emitting species as well as low average foliar density due to the sparse distribution of urban roadside and park trees. Green areas, as defined on the OS map, comprised 9% of the total grid area and were evenly distributed across the 9 km$^2$. Only grid square 1 included a large green area of 23 ha (St. James' Park). The National Forest Inventory (NFI, http://www.forestry.gov.uk/forestry/hcou-54pg9u) of England only included 4.4% green areas within the grid selection. The NFI excluded individual trees in parks and avenues, which can encompass up to 50% of trees maintained by the local authority in central London (City of Westminster, 2009).

Figure 5.5 shows that the modelled isoprene fluxes using the calculated base emission rate compared well with the measured fluxes by wind direction. Linear regressions from wind directions that have a strong anthropogenic component are lower, e.g. W ($R^2$ = 0.13, $p$ <0.001), than from those areas dominated by biogenic sources, e.g. SE ($R^2$ = 0.81, $p$ <0.001) due to the nearby Temple Gardens. Modelled emissions seemingly underestimated observed isoprene fluxes since these included the traffic component; however, it appears that biogenic isoprene represents a detectable source contribution in summer.
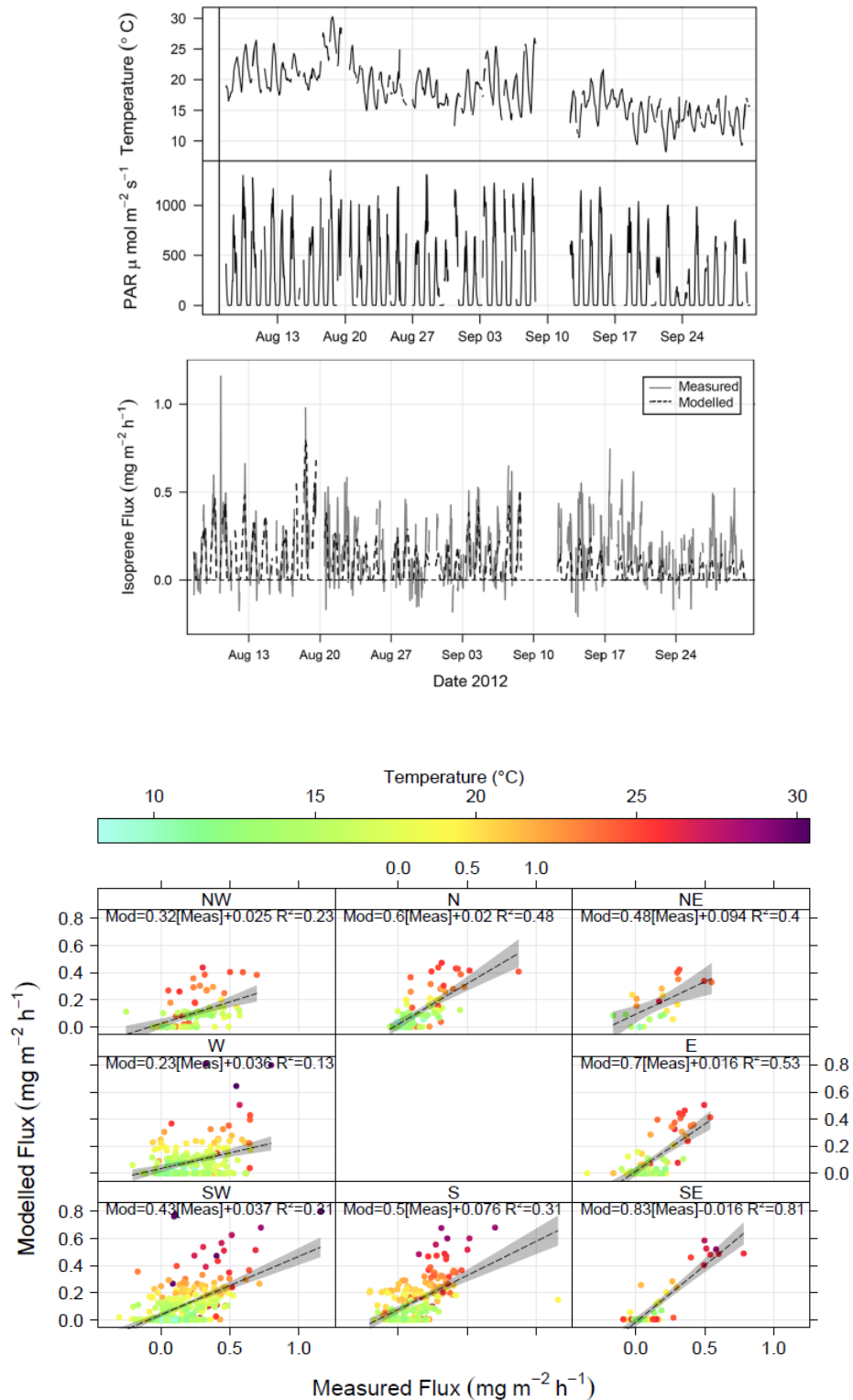
**Figure 5.5.** (*Top*) Time series of both measured (grey) and modelled (black) fluxes, as well as PAR and temperature measurements for August and September 2012, and (*bottom*) correlation between modelled and measured isoprene fluxes (mg m$^{-2}$ h$^{-1}$) by wind direction using the G95 algorithm with temperature as a third variable, ordinary least squares regression lines, 99th confidence intervals, formulae and $R^2$ value.

**5.3.2 VOC/VOC correlations and ratios**

Correlations of VOC/VOC fluxes ($R^2$ = 0.40-0.62, $p$ <0.001) indicated two groups of compounds with good correlations within each group, i.e. compounds related to traffic sources, such as aromatics, and oxygenated and biogenic compounds, such as methanol, acetone and isoprene (Figure 5.6 *top*). Correlations of VOC/VOC concentrations ($R^2$ = 0.13-0.84, $p$ <0.001) showed the highest correlations between traffic-related compounds ($R^2$ = 0.45-0.84, $p$ <0.001) and good correlations between the oxygenated and biogenic compounds ($R^2$ = 0.55-0.69, $p$ <0.001) (Figure 5.6 *bottom*). High correlations between oxygenated VOCs could indicate source commonality or formation mechanisms that depend on similar environmental factors. Scatter plots between aromatic compounds and isoprene/oxygenated compounds tend to show bimodal distributions indicating separate source contributions. Using temperature or, to a smaller extent, PAR as a third variable highlights a temperature or light dependency of the second source supporting the existence of additional biogenic and/or atmospheric sources. In the example of isoprene against benzene the relationship changes with temperature from 2:1 to 1:2.
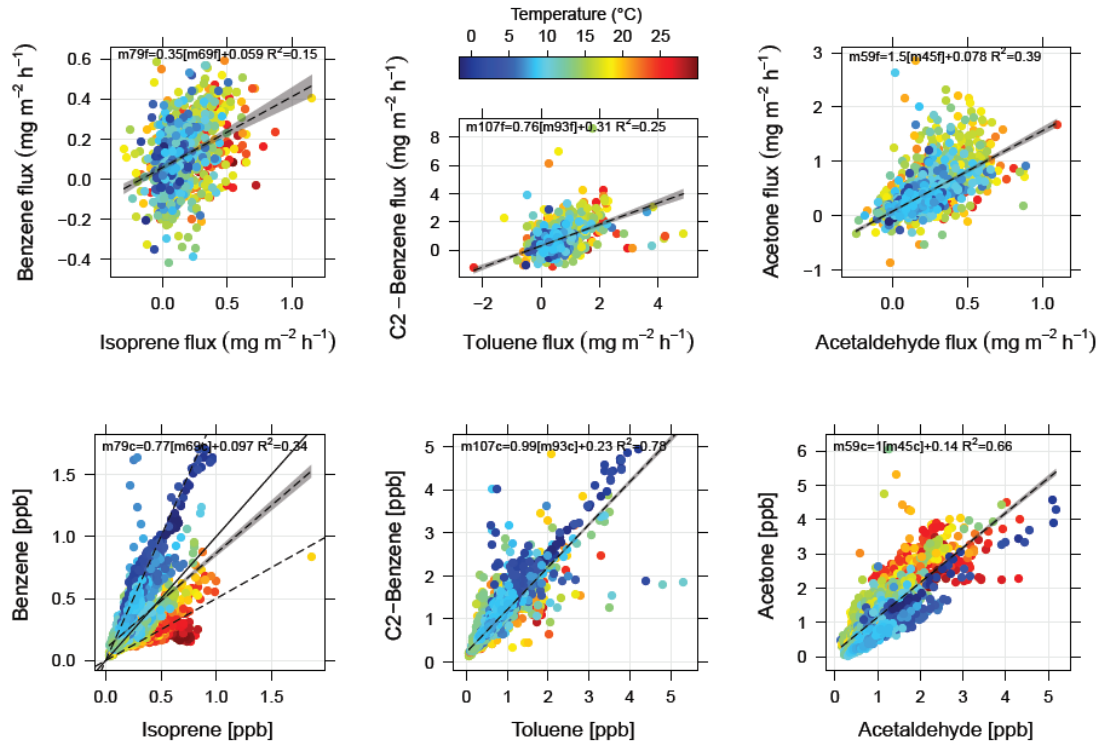
**Figure 5.6**. Selected scatter plots of representative correlations of VOC/VOC fluxes (*top*) and mixing ratio (*bottom*) with temperature as a third variable showing an example of bimodal, strong linear and medium linear correlations as commonly seen in the mixing ratio correlations with $R^2$ values, 1:1 line, 1:2 and 2:1 lines for the bimodal example in the bottom left panel.

### 5.3.2.1 Benzene to toluene ratios

Benzene to toluene (*b/t*) ratios can help identify source types and changes in ratios can indicate the photochemical age of an air mass as toluene reacts at a faster rate with OH in the atmosphere, assuming sufficient OH concentrations to drive the reaction (Warneke *et al.*, 2007). Median (and interquartile range, IQR) *b/t* flux ratios were 0.21 (0.02-0.43) and median (IQR) *b/t* concentration ratios were 0.45 (0.39-0.48). Individual maxima and minima were seen in the *b/t* concentration ratios, examples of which are discussed below.

The observed ratios compared well with those of other European cities, which showed *b/t* concentration ratios of 0.35 in Zurich (Heeb *et al.*, 2000), 0.57 in Manchester (Langford *et al.*, 2009), 0.57-0.63 in London (Valach *et al.*, 2014) and 0.1 at 190 m above London (Langford *et al.*, 2010b). Traffic-related emissions are considered to be an important source of benzene and toluene in London. *B/t* exhaust emission ratios based on derived yearly emissions in other

megacities, such as Mexico City, were found to be 0.4 (Zavala *et al.*, 2006), which agreed well with observed *b/t* concentration ratios in this study. Airborne flux measurements over Mexico City have shown average *b/t* flux ratios of 0.31 with lower ratios of 0.07 to 0.1 over industrial areas due to increased toluene emissions from industrial processes (Karl *et al.*, 2009a; Velasco *et al.*, 2007). Evaporative emissions from gasoline or direct industrial toluene emissions may have contributed to the lower *b/t* flux ratios in London. Furthermore, low *b/t* concentration ratios of 0.26 from diesel emissions have been reported (Corrêa and Arbilla, 2006). The widespread use of diesel fuel in London (buses, taxis and some cars and trains) and diesel emissions from roads which exclude passenger cars, such as Oxford Street (approx. 1.3 km W from the measurement site), or central railway nodes, such as Waterloo railway station (1 km S), may have affected *b/t* ratios.

Wind speed and direction can play a role for *b/t* concentration ratios by transporting pollution over longer distances allowing more time to react with or exposure to higher OH concentrations, thus increasing the ratio. An example of this (Figure 5.7) was seen on 12th August when median (IQR) *b/t* concentration ratios reached 0.5 (0.45-0.56) with stronger SE winds (mean 3.67 m s^{-1}) possibly advecting pollution from Benelux/northern Europe, whereas on 9th August median b/t ratios were 0.34 (0.30-0.38) with low wind speeds (mean 1.28 m s^{-1}) indicating higher contributions of local sources (i.e. 60% London influence) (Bohnenstengel *et al.,* 2015). On both days OH concentrations above London were around $1.25 \times 10^6$ molecules cm^{-3} and *b/t* flux ratios were not significantly different making pollution advection a likely cause of the observed difference (L. Whalley, personal communication 2014). Calculated back trajectories using the HYSPLIT trajectory model (Hybrid Single Particle Lagrangian Integrated Trajectory Model (Draxler and Rolph, 2008)) were run at 3 h intervals starting at ground-level (10 m) from London and propagated 24 h backwards in time. During periods of high *b/t* ratios the back trajectories indicated that air had passed over continental Europe in the past 24 h, during which freshly emitted pollution would have been entrained.
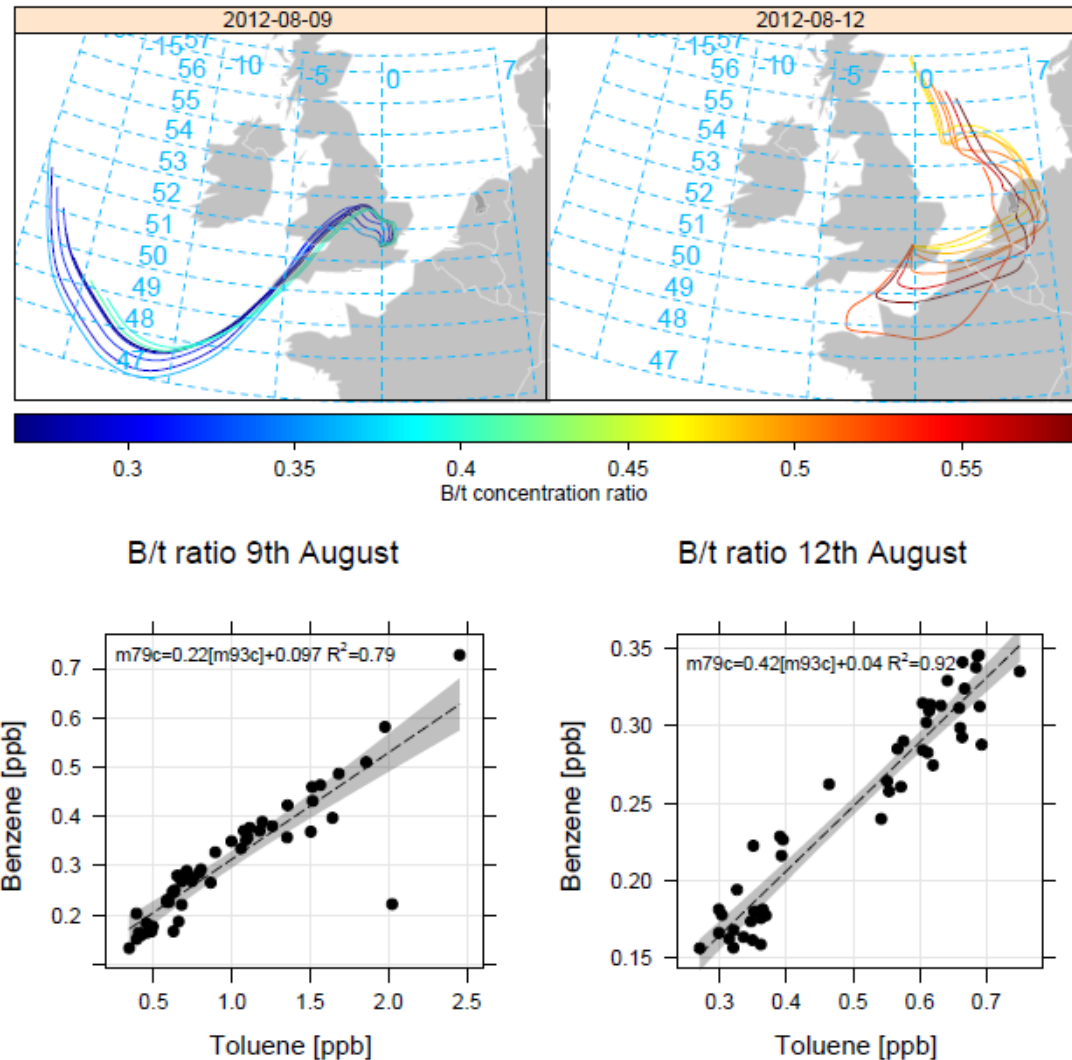
**Figure 5.7**. *Top*: 24 h back trajectories from the NOAA HYSPLIT trajectory model during selected days in August 2012 corresponding to periods of low (*left*) and high (*right*) benzene/toluene concentration ratios. Daily release in 3 h intervals (10 m height) for 24 h prior. *Bottom*: Scatter plots showing benzene-to-toluene concentration ratios during 9th August 2012 (*left*) and 12th August 2012 (*right*) with linear regression with 95th confidence interval, regression equation and coefficient ($R^2$).

The median monthly *b/t* flux ratio during the measurement period stayed between 0.18 and 0.26, which is to be expected since only local fluxes were detected; however, the median (IQR) monthly *b/t* ratio for concentrations steadily increased from 0.41 (0.36-0.47) to 0.62 (0.55-0.70) from August to December. Advected pollution from mainland Europe may be common in

winter or biomass burning may play a greater role in colder months, as this is associated with higher *b/t* ratios, e.g. 1.67 (Lemieux *et al.*, 2004), due to the different fuel combustion emission profile. Furthermore, OH concentrations in London are often below the detection limit during winter (Bohnenstengel *et al.*, 2015), resulting in less local photochemical removal during the winter months.

Median (IQR) concentration ratios for benzene to $C_2$-benzenes were 0.31 (0.28-0.33) and toluene to $C_2$-benzenes were 0.72 (0.63-0.81), which both agree with previous values and suggest that these masses are indeed the ascribed traffic-related compounds (Heeb *et al.*, 2000; Warneke *et al.*, 2001).

### 5.3.2.2 VOC-to-$CO_2$ correlations and ratios

Good correlations were found among averaged VOC fluxes plotted as a function of averaged $CO_2$ fluxes, which were measured concurrently at the site ($R^2 = 0.03\text{-}0.81$, $p < 0.001$). Traffic-related compounds were initially among the lowest correlations with $CO_2$ fluxes ($R^2 = 0.03\text{-}0.48$, $p < 0.01$). However, when points of peak $CO_2$ fluxes were removed, the correlations with traffic-related VOC fluxes increased significantly to $R^2 = 0.65\text{-}0.91$ ($p < 0.001$). Presumably, the initial poor correlations resulted from an additional strong $CO_2$ source, such as vents from gas-fired boilers in nearby buildings, which have a lower source commonality with aromatic VOCs, i.e. a lower VOC/$CO_2$ emission ratio than that of traffic emissions for aromatic compounds. The LAEI indicates that VOC/$CO_2$ flux ratios for benzene are higher for traffic emission sources (i.e. $2 \times 10^{-5}$) than gas sources (i.e. $0.6 \times 10^{-5}$) within the flux footprint. The improved correlations are greater for traffic-related compounds due to the limited range of source types contributing to this group compared with oxygenated/biogenic compounds. The regression coefficient ($R^2$) of benzene with $CO_2$ fluxes increased from 0.48 to 0.91, whereas for isoprene fluxes the increase was small, i.e. 0.68 to 0.70 (Figure 5.8), as isoprene has a range of different sources of which only a few are commonly shared sources with $CO_2$.
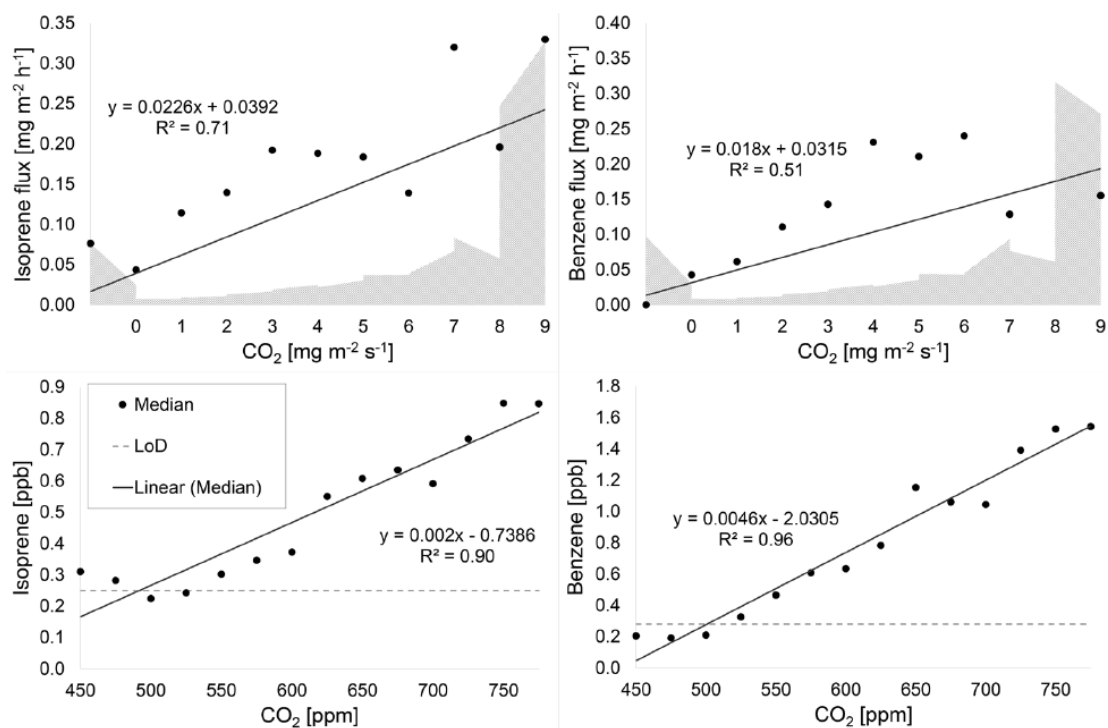
**Figure 5.8**. Scatter plots showing averaged flux and concentration regressions of isoprene and benzene as a function of $CO_2$ fluxes and concentrations based on 25 min VOC means with linear regressions, formulae, $R^2$ values and detection limit (shaded area for fluxes and dashed line for mixing ratios).

The presence of a strong separate $CO_2$ source within the flux footprint is supported by the high averaged VOC-to-$CO_2$ concentration correlations for traffic-related compounds ($R^2 = 0.92$-$0.96$, $p < 0.001$). This differs from the fluxes, which are influenced only by sources in the flux footprint, where one strong point source with a different emission ratio may have a larger effect on emission rates of one compound but not the other. Concentrations are influenced by advected pollution from outside the flux footprint for both $CO_2$ and VOCs, where shared emission sources with relatively higher VOC/$CO_2$ ratios are more widespread. Averaged VOC to $CO_2$ concentration correlations were lower with the oxygenated/biogenic compounds ($R^2 = <0.71$-$0.90$, $p < 0.05$).

Median VOC/$CO_2$ flux ratios ranged from $1.7 \times 10^{-5}$ to $7.7 \times 10^{-5}$ (mg m$^{-2}$ h$^{-1}$/ mg m$^{-2}$ h$^{-1}$) with isoprene and benzene showing low ratios due to their low fluxes and toluene and $C_2$-benzenes showing high ratios. Highest flux ratios for all compounds were with W winds, whereas

lowest for biogenic compounds with N and for traffic-related compounds S wind directions. Flux ratios declined towards December as $CO_2$ fluxes increased and VOC fluxes decreased. Similarly, VOC/$CO_2$ concentration ratios were between $0.45 \times 10^{-6}$ and $14.6 \times 10^{-6}$ (ppb/ppb) with isoprene and benzene representing the lowest and methanol and acetone the highest ratios. Highest concentration ratios were seen in August for oxygenated compounds/isoprene and December for traffic-related species.

### 5.3.3 Wind direction and flux footprint analysis

Polar annulus and polar plots were constructed for VOC fluxes and mixing ratios respectively and representative compounds are shown (Figure 5.9). Polar plots use a generalized additive model to interpolate between wind direction and wind speed averaged data points within the OpenAir package in R (see Carslaw and Ropkins, 2012, Hastie and Tibshirani, 1990, and Wood, 2006). Polar annulus plots averaged by time of day instead of wind speed show diurnal variability with wind direction. The majority of the time (83%), unstable and near neutral conditions prevailed ($\zeta < 0.2$), although the frequency varied between months with 87%, 89%, 82%, 84% and 69% during August, September, October, November and December respectively. Wind directions with mostly unstable conditions were with W and S winds and near neutral with N or E winds. Mixing ratios were on average highest with low wind speeds (showing a negative correlation) when pollutants accumulate due to reduced mixing, indicating local emissions (Figure 5.9, *bottom*).

## Isoprene (m/z 69)

## Benzene (m/z 79)



## Isoprene (m/z 69)
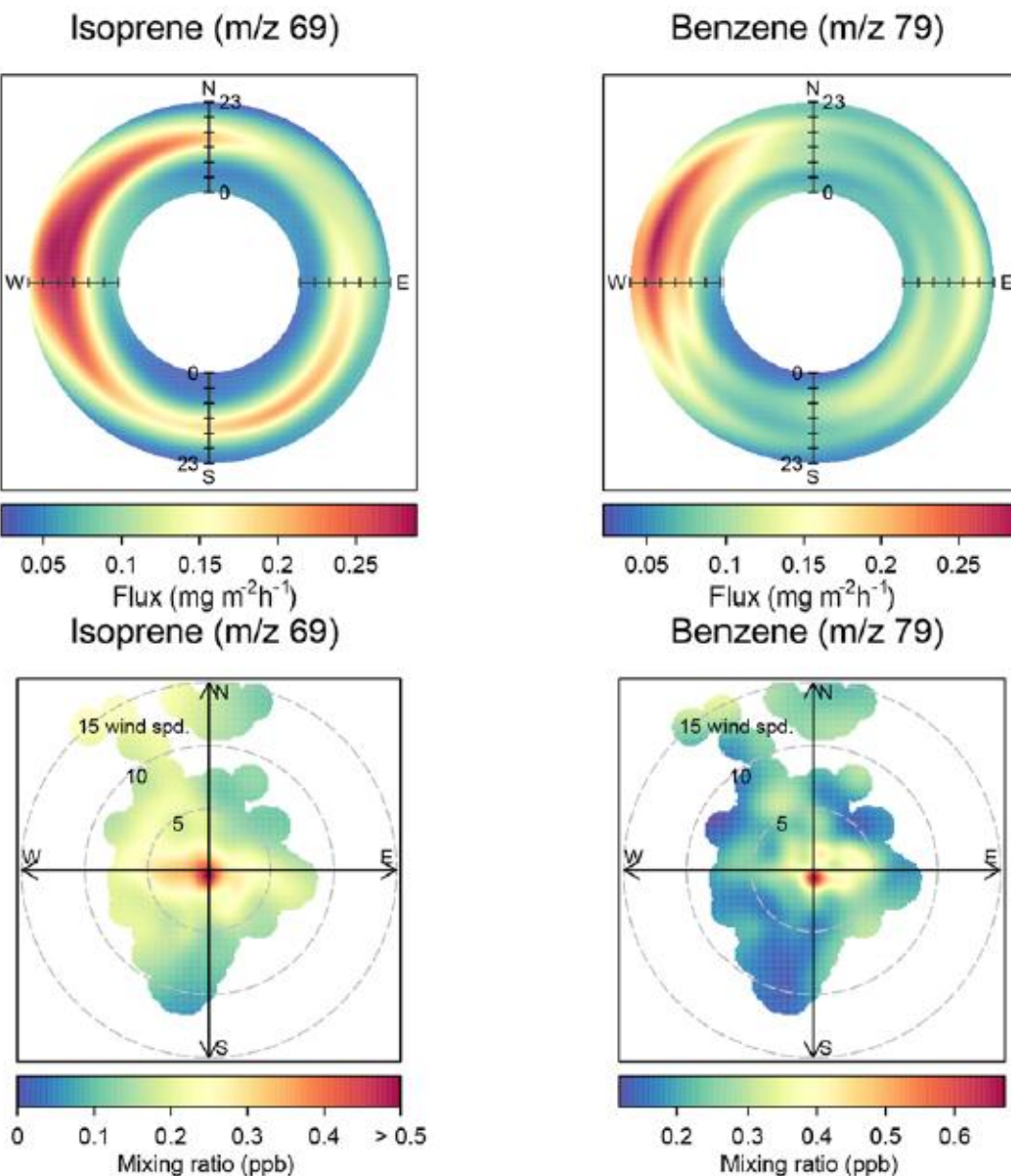
## Benzene (m/z 79)



**Figure 5.9**. Polar annulus and polar plots for isoprene (*m/z* 69) and benzene (*m/z* 79) fluxes (*top*) and mixing ratios (*bottom*) (colour scale) by time of day (*top*), wind speed (*bottom*) and wind direction.

Largest fluxes for all compounds were from the NW with either one daytime peak (e.g. isoprene) or two distinct rush hour peaks (e.g. benzene) (Figure 5.9, *top*). On average, fluxes were largest from the W>E$\geq$N>S (*F* statistic = 60.37-227.06, *p* <0.001) because of increased emission rates of specific compound sources. Separated by month, fluxes were largest from W>N>E$\geq$S in August and September, whereas during October, November and December fluxes followed the

pattern W>E≥N>S. The flux footprint in this study was relatively small compared to that of measurements previously made at 190 m height from the BT Tower in central London (Langford *et al.*, 2010b). Due to the relatively low measurement height in this study, flux measurements were always closely coupled with the surface layer, unlike measurements by Langford *et al.* (2010b) that were at times disconnected from the surface layer during stable night-time conditions.

The average length of the maximum flux footprint contribution ($X_{max}$) was around 330 m and 90% of all the fluxes ($X_{90}$) originated from within 900 m. The median footprint area was 1.8 $km^2$. This established that the majority of emission sources contributing to the measured fluxes must have been local. Additionally, the selected emission grid (cf Section 5.2.3.1 above) encompassed 97% of the footprint with S and W wind directions but only 80% and 84% during E and N winds. Grid square 5 represented the maximum contribution area because it encompassed the measurement point. Average footprint contributions (mean ± SD) comprised of grid squares 1 (2% ± 4%), 2 (5% ± 7%), 4 (4% ± 5%) and 5 (52% ± 31%) during S and W wind conditions, squares 6 (4% ± 9%) and 9 (4% ± 10%) indicated E wind conditions and square 8 (18% ± 27%) N wind conditions. During October contributions from square 9 increased to 10% and were more frequent at 30% in December. Squares 3 (0.6% ± 2%) and 7 (0.9% ± 2%) provided minimal average contributions.

The River Thames to the S may have caused the low fluxes associated with S winds (i.e. squares 1, 2 and 3). Contributions of traffic-related compound fluxes were statistically significant from the W (i.e. squares 4, 5, and 7), followed by the N (square 8) and E (squares 6 and 9) likely from the nearby heavily trafficked roads (Kingsway, Charing Cross, Strand and Blackfriars areas respectively). Biogenic compound fluxes were highest from the W and E, which coincides with significant nearby green areas within the flux footprint.

Correlations of fluxes with grid square contributions in the footprint can also give information on emission source strengths within the respective grid square (Figure 5.1). Generally positive correlations with fluxes across most compounds were seen from the W (squares 4, 5 and

7), confirming that high emission rates from sources within these grid squares were driving the large fluxes. The strongest correlations of fluxes with contributions from squares 4, 5 and 7 were seen during October and November ($R^2$ = 0.40-0.46, $p$ <0.001), especially for masses associated with biogenic sources ($m/z$ 33, 45, 59 and 69). Square 8 showed positive correlations for benzene and only in August for all compounds. Correlations of fluxes with contributions from squares 1, 2, 3, 6 and 9 were negative, indicating weaker emission sources in these squares or increased VOC deposition.

Highest mixing ratios with wind direction were from E>N≥W>S for traffic-related compounds, whereas oxygenated compounds/isoprene followed a similar pattern as the fluxes of W≥E>N≥S ($F$ statistic = 47.49-86.95, $p$ <0.001). Easterly winds in London are often associated with synoptic conditions that bring European continental air masses to the UK, resulting in higher background concentrations. Furthermore, since the boundary layer was on average more stably stratified and mixing heights were lowest (640 ± 80 m) with E wind conditions, it is likely that pollutant concentrations were allowed to build up, resulting in the observed higher concentrations to the E for the more ubiquitous compounds, whereas concentrations of compounds with biogenic contributions additionally had strong sources to the W, such as several green areas (St. James' Park, Hyde Park and Regents Park; total 331 ha).

### 5.3.4 Comparisons with LAEI and NAEI

The LAEI and NAEI produce yearly emission estimates over the 1 km$^2$ OS grid for a range of pollutants and emission sources. Total VOC emission estimates are provided, but only benzene and 1,3-butadiene are estimated separately. Measured emissions were compared with annual estimated emissions for the above OS grid area selection from 2012 for benzene using the LAEI and indirectly speciated VOCs of the NAEI. Using the average flux footprint, the grid square estimates were compared with the scaled flux measurements from the equivalent area (Figure 5.10).
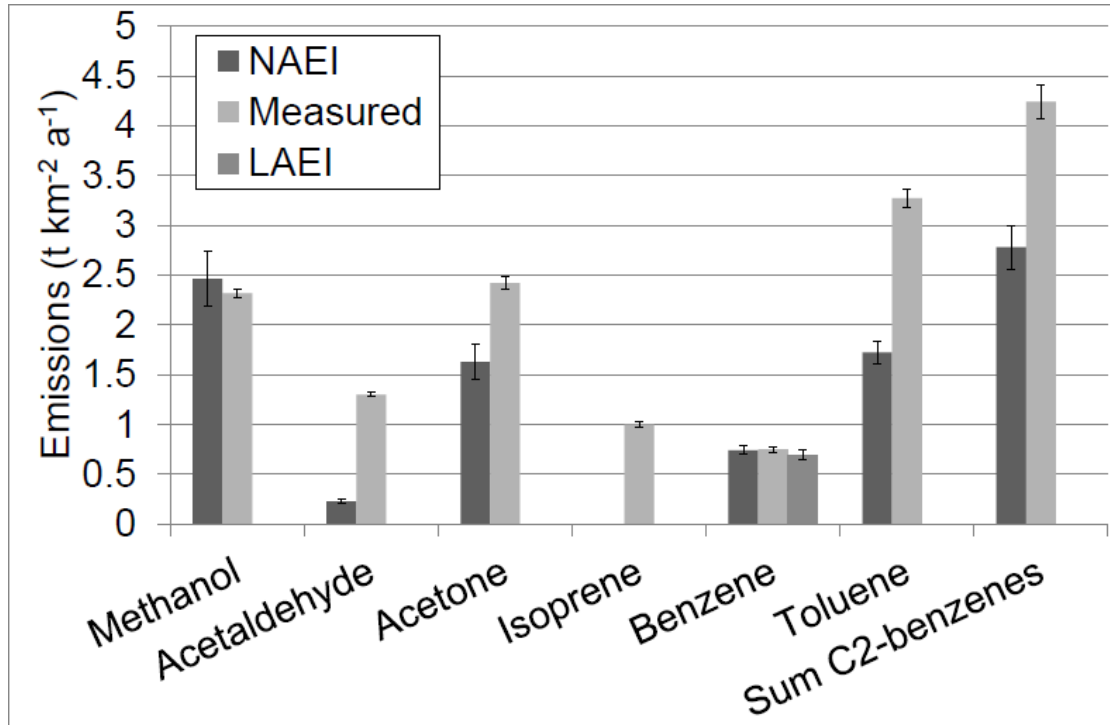
**Figure 5.10**. Bar chart showing scaled comparisons of LAEI and NAEI estimates against measured fluxes in t km$^{-2}$ a$^{-1}$ for speciated VOCs with error bars.

LAEI emission estimates included contributions from major (69%) and minor roads (4%) as well as evaporative emissions (27%). No data were available on cold start emissions for benzene. The calculated standard errors provided some uncertainty approximation. Measured fluxes compared well with emission estimates, although the LAEI predicted slightly smaller benzene fluxes. Comparisons of fluxes with wind directions (Section 5.3.3) agreed well with the LAEI emission estimates for the respective grid squares with highest emissions from squares 4, 5, 7 and 8 (i.e. W and N directions). This comparison assumes that the benzene fluxes during the measurement period were representative of annual emissions with any significant seasonal variation in benzene emission rates captured in this 5-month period. Section 5.3.1.2 confirmed that there was little month-to-month variability in the benzene flux.

Using speciated VOC emission contributions (percent of total VOC emissions) for 2006 (Bush *et al.*, 2006) and emission maps from 2012 for total non-methane VOC emissions, speciated estimates could be compared with observations (Figure 5.10). The NAEI includes a wide range

of emission sources divided into 11 SNAP (Selected Nomenclature for sources of Air Pollution) sectors including industrial, commercial and residential processes, transport, waste treatment, solvent use, point sources, agriculture and nature, although the latter two were unavailable for the London urban area. NAEI estimates for benzene exceed the LAEI due to the inclusion of a wider range of sources beyond traffic-related emissions. Total $C_2$-benzene emission estimates consisted of ethyl benzene, (*m+p*)-xylene and *o*-xylene. Benzene and methanol emissions agreed very well; however, for all the other compounds, estimated emissions were significantly lower than the measured fluxes. Uncertainties related to the measurements, such as isobaric interferences within the PTR-MS could have contributed to measurement overestimation, whereas uncertainties within the modelled emissions and the use of older speciation values may have impacted the estimates. In the case of isoprene, only minimal emissions are assumed, which do not include the biogenic sources that contributed to the measured fluxes. It is also likely that some of the *m/z* 69 signal could be attributed to cyclic alkenes, but Section 5.3.1.3 showed that biogenic isoprene provided a significant contribution during August and September in central London.

## 5.4 Conclusion

Our measurements show that vehicle emissions are the dominant source of the fluxes and concentrations of VOCs in central London, although biogenic sources and secondary atmospheric formation may make a significant contribution, particularly in summer for some compounds. There were observable spatial variations in flux rates, which result from the varying spatial distribution of emission types and strengths of emission sources, such as vegetation and traffic. Temporal variations in relative source strengths can be seen in the diurnal and seasonal profiles, reflecting the diurnality and seasonality of some of the driving factors. The measured VOC fluxes mostly originated from an area within a 1 km radius around the measurement site but some instances of pollution advection were seen to affect concentrations at the site. However many of the spatio-temporal differences in the observed mixing ratios were attributable to changes in emission sources and strengths combined with effects of meteorological conditions. The diurnal

and seasonal dynamics of the boundary layer mixing height are significant drivers of changes in observed VOC concentrations at the site.

The biogenic component of isoprene emissions was modelled using the G95 algorithm, and the calculated base emission rate closely matched previous published values for urban areas. Even in this central urban area with a temperate climate there is a detectable biogenic component to isoprene emissions. Because of the relative importance of isoprene in atmospheric chemistry, its inclusion in photochemical pollution models is essential.

Close agreement between the flux footprint contributions and the LAEI for benzene emissions, a compound which is thought to be accurately estimated in the inventory but associated with high measurement uncertainty, gives confidence in the PTR-MS measurements. Good agreement was also seen with methanol estimated from the NAEI, but other compounds were all greatly underestimated in the emissions inventory.

This study provides further evidence for the successful implementation of VOC flux measurements in heterogeneous urban landscapes when measurement sites fulfil basic eddy covariance criteria. Further VOC flux observations are essential for the validation of "bottom-up" emission inventories, especially as the latter are widely used for regulatory and compliance purposes.

## Author contributions

E. Nemitz and B. Langford planned the measurement campaign, A. Valach with the help of B. Langford and E. Nemitz made the measurements, A. Valach with the help of B. Langford processed the data and completed the analyses. C. N. Hewitt designed the study, obtained funding and supervised the work. A. Valach prepared the manuscript with support from all the co-authors.

## Acknowledgements

## 5.5 Supplementary information

### 5.5.A. Estimation of flux losses due to low frequency attenuation (from Section 5.2.3)

Attenuation from low frequency fluctuations for a 25 min flux period was investigated by re-analysing the sensible heat fluxes for longer averaging periods of 60, 90, 120 and 150 min. The coordinate rotation was applied to the joined files, which acted as a high pass filter to the three wind vectors, confirming that fluctuations of eddies with a longer time period than the averaging time did not contribute to the flux measurement. The fluxes were compared back to the 25 min average fluxes, which had the coordinate rotation applied before joining, again to ensure only turbulent fluctuations of ≤25 min contributed to the flux (Figure 5.A1). Flux losses due to low frequency attenuation were estimated to be <1.5% and, therefore, no corrections were deemed necessary.
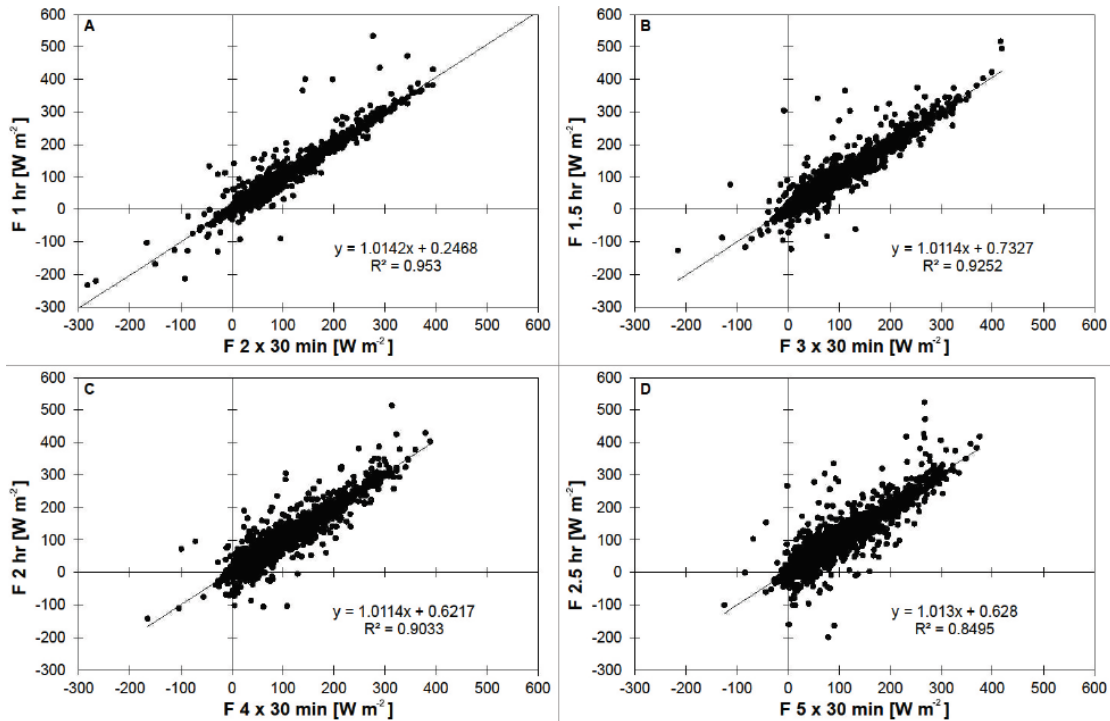
**Figure 5.A1**. Sensible heat fluxes (W m$^{-2}$) measured from the roof tower of the King's College London Strand building calculated using 1 to 2.5 h averaging periods and compared with fluxes calculated using the same 25 min averaging period as used for VOC fluxes.

## 5.5.B. Modelling the biogenic isoprene contribution in summer using the Guenther *et al.* (1995) algorithm

The base emission rate was determined from the slope of the linear regression of the measured total isoprene flux and activity adjustment factor for light and temperature ($\gamma$) (Figure 5.B1). This provided a base emission rate of 0.838 mg m$^{-2}$ h$^{-1}$, which was then divided by the estimated foliar density (*D*) and converted to produce an emission rate in units of µg g h$^{-1}$. The foliar density was calculated from the estimated leaf dry weight divided by the tree leaf area for trees located in the maximum flux footprint contribution area identified from visible satellite imagery. Using a foliar density of 0.129 kg dry matter m$^{-2}$, the final base emission rate of 6.5 µg g h$^{-1}$ was calculated, which compared well with the estimate of 5 µg g h$^{-1}$ for urban areas in a cold climate presented in Guenther *et al.*, (1995).
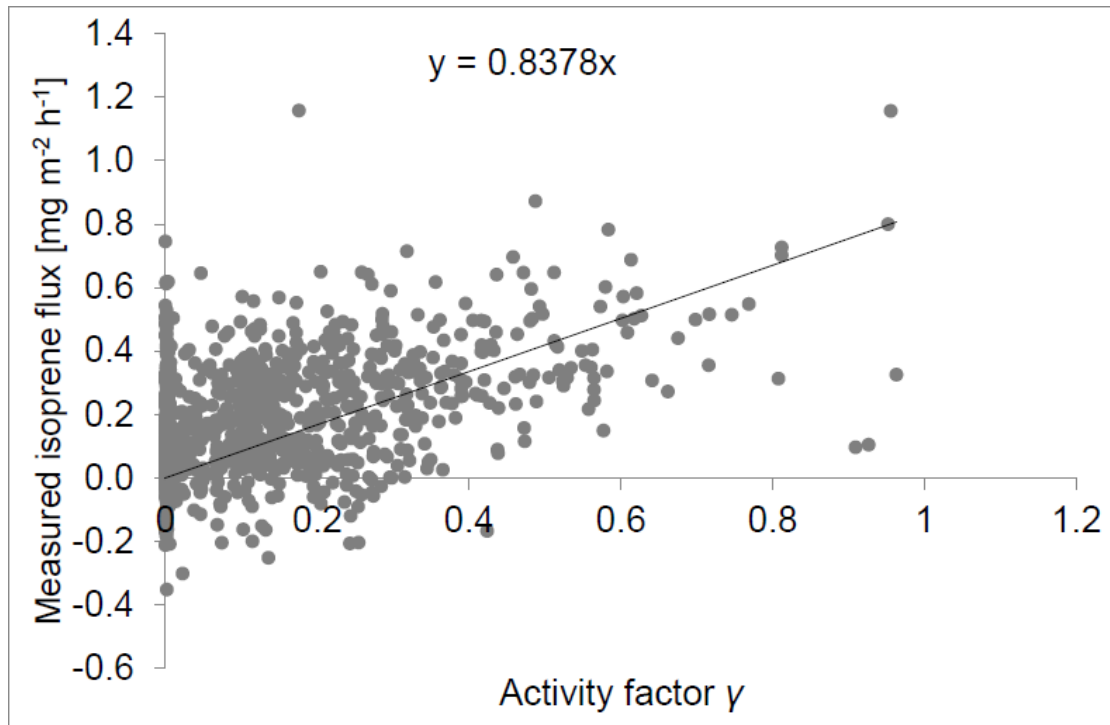
**Figure 5.B1.** The scatter plot of measured isoprene fluxes to the activity adjustment factor $\gamma$ with the linear regression used to determine the base emission rate in mg m$^{-2}$ h$^{-1}$.

# Chapter VI

# 6 Paper III: Seasonal variations in the fluxes and above-canopy concentrations of volatile organic compounds from a *terra firma* ecosystem in the pristine Amazonian rainforest

This chapter details the first long term VOC flux measurements over the Amazon forest using PTR-MS and virtual disjunct eddy covariance. Almost one year of continuous VOC flux and concentration measurements were made between 1 September 2013 and 20 June 2014 at a remote forest background site located approx. 60 km northwest of Manaus in Brazil. Analysis of fluxes and concentrations suggest strong seasonal variations during the dry and wet seasons, as well as changes in the atmospheric oxidation capacity determined from the concentration ratio of isoprene oxidation products to isoprene. The base canopy emission factor of isoprene was determined using the parameterized MEGAN algorithm (Guenther *et al.*, 2006) at different time resolutions, i.e. annual, seasonal, monthly and diurnal, and showed large variations. Isoprene emissions were modelled and compared with measured fluxes. The flux footprint of the tower was modelled showing a small local footprint extent and no anthropogenic interferences.

This chapter is a first draft of a paper to be submitted to Atmospheric Chemistry and Physics in the autumn of 2015. The authors' contributions are as follows:

**Emily R. House (Lancaster University):** Prepared, set up and operated the instrument during the field measurements, processed the data, and contributed to the manuscript.

**Amy C. Valach (Lancaster University and CEH):** Assisted in instrument preparation, setup, and operation during the field campaign, assisted with processing the data, assisted with the data analyses, carried out the modelling and analysis of isoprene emission, flux footprint and backward air mass trajectory, and wrote the first draft of the entire manuscript.

**Ben Langford (CEH):** Assisted with instrument preparation and set up, provided help with data processing and contributed to the manuscript.

**Eiko Nemitz (CEH):** Secured funding, assisted with instrument preparation and set up, provided help with data processing and contributed to the manuscript.

**A. Rob MacKenzie (University of Birmingham):** Devised the research, helped with interpretation of the results and compilation of the manuscript.

**Paulo Artaxo (University of Sao Paulo):** Coordinated and provided organisational and logistical support in Brazil.

**Joel de Brito (University of Sao Paulo):** Provided technical support and contributed to discussions.

**Kolby Jardine (Lawrence Berkley National Laboratory, National Institute of Amazonian Research):** contributed to discussions.

**Ana Maria Yañez-Serrano (National Institute of Amazonian Research, Max Planck Institute, University of Sao Paulo):** Provided on-site support with instrument operation and contributed to discussions.

**C. Nick Hewitt (Lancaster University):** Devised the research, secured funding, organised logistics and liaison, helped with interpretation of the results and compilation of the manuscript.

# Seasonal variations in the fluxes and above-canopy concentrations of volatile organic compounds from a *terra firma* ecosystem in the pristine Amazonian rainforest

E. R. House[1], A. C. Valach[1,2], B. Langford[2], E. Nemitz[2], A. R. MacKenzie[3], P. Artaxo[4], J. de Brito[4], K. Jardine[5,6], A. M.Yañez-Serrano[4,6,7], and C. N. Hewitt[1*]

[1]{Lancaster Environment Centre, Lancaster University, Lancaster, LA1 4YQ, United Kingdom

(ecrhouse@hotmail.com; a.valach@lancaster.ac.uk; n.hewitt@lancaster.ac.uk)}

[2]{Centre for Ecology & Hydrology, Bush Estate, Penicuik, Midlothian, EH26 0QB, United Kingdom

(benngf@ceh.ac.uk; en@ceh.ac.uk)}

[3]{Birmingham Institute of Forest Research, University of Birmingham, Edgbaston, Birmingham, B15 2TT, United Kingdom

(a.r.mackenzie@bham.ac.uk)}

[4]{Instituto de Física, Universidade de São Paulo, Rua do Matão, Travessa R, 187, CEP 05508-900, São Paulo, SP, Brazil

(artaxo@if.usp.br; joelbrito@gmail.com; ayanezserrano@yahoo.es)}

[5]{Lawrence Berkeley National Laboratory, Earth Science Division, One Cyclotron Rd, building 64-241, Berkeley, CA 94720, United States of America

(kjjardine@lbl.gov)}

[6]{ Instituto Nacional de Pesquisas da Amazônia, Clima e Ambiente, Av. André Araújo 2936, Manaus-AM, CEP 69083-000, Brazil}

[7]{Max Planck Institute for Chemistry, P. O. Box 3060, 55128, Mainz, Germany}

*Correspondence to: C. N. Hewitt (n.hewitt@lancaster.ac.uk, +44 1524 593931)

# Abstract

Of all ecosystems on Earth, tropical rainforests provide the largest contribution to annual global biogenic volatile organic compound (VOC) emissions, yet flux measurements from natural rainforests are scarce and usually only span short periods. Here we present the first long-term continuous measurements of fluxes and above-canopy volume mixing ratios of isoprene, isoprene oxidation products, and total monoterpenes, which were made at a remote primary forest site in the central Amazon Basin from September 2013 to July 2014. Mixing ratios were quantified by proton transfer reaction-mass spectrometry and fluxes calculated using the virtual disjunct eddy covariance technique. Median daytime fluxes were 2.21 mg m$^{-2}$ h$^{-1}$, -0.09 mg m$^{-2}$ h$^{-1}$, and 0.59 mg m$^{-2}$ h$^{-1}$ for isoprene, isoprene oxidation products, $i_{ox}$ (measured at $m/z$ 71), and total monoterpenes, respectively. Median above-canopy mixing ratios measured at 40 m above ground level, or about 10 m above the canopy top were 3.94 ppbv, 1.02 ppbv, and 0.46 ppbv, respectively. Strong seasonal trends were observed with increased net fluxes, and higher above-canopy mixing ratios, during the dry season and the dry-to-wet season transition periods in September - December 2013, and lower values during the wet season from January - July 2014. Much of the intra-diurnal variability in flux rates was linked to changes in light and temperature with strong correlations of VOC fluxes and mixing ratios with photosynthetically active radiation (PAR) and temperature.

Isoprene emissions were modelled using the Guenther *et al.* (2006) algorithm, and an annual canopy-scale base emission rate (the isoprene emission rate at standard conditions of 1500 μmol m$^{-2}$ s$^{-1}$ PAR and ambient air temperature of 30 °C) of 4.8 ± 0.1 mg m$^{-2}$ h$^{-1}$ was obtained. Base emission rates at higher time resolutions ranged from 2.9 ± 0.2 mg m$^{-2}$ h$^{-1}$ at 08:00 to 7 ± 0.9 mg m$^{-2}$ h$^{-1}$ at 10:00 and from 3.4 ± 0.3 mg m$^{-2}$ h$^{-1}$ in July to 6.3 ± 0.3 mg m$^{-2}$ h$^{-1}$ in October. Modelled isoprene emissions failed to accurately account for the observed seasonal variability in emissions when a constant base emission rate determined only from the current light, temperature and canopy loss factors was used. This points to significant seasonal variability in emissions, possibly associated with changes in tree phenology that have so far been ignored in the prediction of isoprene fluxes in chemistry and transport models. Flux footprints were calculated for the entire

measurement period and showed that 90% of the observed emissions originated from an area of 0.36 km$^2$ to the east of the measurement tower. Air mass back trajectories confirmed that the site experienced minimal anthropogenic contamination, any periods of which were excluded, and that air parcels had travelled considerable distances over mostly undisturbed primary forest before arriving at the site. The site is highly representative of large areas of lowland *terra firma* forest in Amazonia in terms of its species composition, climate, topography, etc. and hence the bVOC emissions data obtained at the site are expected to be representative of much of the Amazon rainforest ecosystem.

## 6.1 Introduction

Volatile organic compounds (VOC) affect atmospheric chemistry and climate through changing the oxidative capacity of the troposphere and contributing to secondary organic aerosol (SOA) formation (Atkinson, 2000; Kanakidou *et al.*, 2005). The fluxes of biogenic VOCs (bVOCs) are thought to outweigh those of anthropogenic origin by a factor of about 10 globally. The single most important bVOC is isoprene (2-methyl-1,3-butadiene) with estimated global emissions around 600 Tg a$^{-1}$, or about half of total global bVOC emissions (Guenther *et al.*, 2006). Isoprene emissions can be under circadian control, but are primarily driven by leaf temperature and the intensity of incident photosynthetically active radiation (PAR) and emission rates are therefore highest in areas of consistently high temperatures (Wilkinson *et al.*, 2006). Isoprene emissions are also highly plant species dependent, with many broadleaf tree and shrub species being major isoprene emitters. Consequently, tropical ecoregions provide the largest contribution of isoprene to the global flux of bVOCs.

Although the yield of SOA following isoprene oxidation in the atmosphere is probably small (Carlton *et al.*, 2009; Claeys *et al.*, 2004), the very large mass emission rate of isoprene leads to the formation of considerable quantities of SOA. Aerosols play an important role in tropical climate and ecology by affecting the radiative balance through direct and indirect radiative forcing, and influencing cloud condensation nuclei. Changes in aerosols have the potential to impact on regional precipitation regimes, which control the wet and dry seasonality,

on evapotranspiration, and therefore surface temperature. It has been postulated that bVOC emissions in general and isoprene emissions in particular may provide a feedback between tropical (Amazonian) rainforests and the climate system (Andreae *et al.*, 2002; Beerling *et al.*, 2007; Pacifico *et al.*, 2009).

Additionally, bVOCs play an important role in the chemistry and oxidation capacity of the troposphere. Oxidation of bVOCs by the hydroxyl (OH) radical leads to the formation of peroxy radicals. Under high VOC/$NO_x$ ratios, as is found in the Amazon (Lelieveld *et al.*, 2008), $O_3$ formation is $NO_x$-limited, peroxides represent the dominant radical sink and ozone is removed by photolysis resulting in no net formation. However, increasing $NO_x$ levels may lead to lower VOC/$NO_x$ ratios resulting in VOC-sensitive conditions, in which the formation and loss of radicals affect the rate of ozone formation. In this regime the peroxy radicals enhance the oxidation of NO to $NO_2$ and lead to net ozone formation. Mediation of the OH mixing ratio may also influence the lifetime of methane and other radiatively active gases in the atmosphere.

Recent studies have shown that tropical photochemistry and radical cycling are still poorly understood (Lelieveld *et al.*, 2008; Paulot *et al.*, 2009; Peeters *et al.*, 2009; Pugh *et al.*, 2010). Measurements of the flux rates of the primary isoprene oxidation products, methyl vinyl ketone (MVK) and methacrolein (MACR), as well as of isoprene itself, can help assess the photochemical evolution of bVOCs in the troposphere (Karl *et al.*, 2009b) and detailed quantification of bVOC fluxes are needed to constrain photochemistry schemes in atmospheric chemistry models (Pinho *et al.*, 2005; von Kuhlmann *et al.*, 2004) and to allow the role of bVOCs in the Earth system to be fully understood.

VOC emissions from tropical ecoregions are difficult to model due to the high biodiversity and biome heterogeneity. The semi-empirical models of Guenther *et al.* (1995) and Guenther *et al.* (2006) provide algorithms and base emission rates for a range of biomes, which urgently require testing and constraining by observations. Average isoprene mixing ratios and fluxes from observations in the tropics vary widely, depending on location, season and method used, e.g. Geron *et al.* (2002), Hewitt *et al.* (2010), Karl *et al.* (2004, 2007, 2009), Kesselmeier *et*

*al.* (2002, 2009), Kuhn *et al.* (2007), Langford *et al.* (2010b), Misztal *et al.* (2011), Rinne *et al.* (2002). Unfortunately, the number of studies quantifying bVOC fluxes in the tropics is limited due to inaccessibility, logistical and methodological difficulties.

Few measurements of VOCs have been made in the Amazon (Jacob and Wolfsy, 1988; Zimmermann *et al.*, 1988), although since the start of the Large Scale Biosphere-Atmosphere Experiment in Amazonia (LBA) in the mid 1990s, there has been a wealth of studies on understanding the functioning of several Amazonian ecosystems and the region's global importance (Betts and Silva Dias, 2010). These studies include several short-term VOC measurement campaigns using tethered balloons (Davis *et al.*, 1994; Greenberg *et al.*, 2004), but only limited and short term eddy covariance flux measurements during the different seasons (Karl *et al.*, 2007; 2009b; Kuhn *et al.*, 2007; Rinne *et al.*, 2002; Stefani *et al.*, 2000). A detailed understanding of the diurnal and seasonal changes in bVOC emission rates from a representative forest site in Amazonia was, until this current study, still lacking.

Here we present the first long-term, ecosystem-scale eddy covariance bVOC flux measurements from an Amazonian *terra firma* (non-flooded lowland humid tropical forest) ecosystem. Measurements commenced in September 2013 and lasted until July 2014 using the TT34 tower at the ZF2 site, a remote and undisturbed primary forest site in the Cuieiras Reserve approx. 60 km north of the city of Manaus, Brazil.

## 6.2 Methods

### 6.2.1 Measurement site and climate

Measurements were made at 40 m height from the triangular tower TT34 at the LBA ZF2 site (2.594637° S, 60.209519° W, altitude 67 m) located in the Reserva Biologica do Cuieiras in Central Amazonia, Brazil. The tower is surrounded by undisturbed, mature, *terra firma* tropical rainforest with a canopy height of 25-35 m and a single-sided leaf area index (LAI) of 4.3-6.5 $m^2$ $m^{-2}$ (NEO, 2014).

The ZF2 site in the north-western part of the Amazon is located in an equatorial rainforest with high precipitation (average annual rainfall around 3000 mm). Climatologically, there is a prolonged wet season from November to June, peaking in February and March (precipitation of 250 mm to 350 mm per month), and a short dry season (precipitation around 60 mm per month) in July to October (INMET Brazil, 2014). However, there is of course considerable year-to-year variability in timing and actual precipitation of the wet and dry seasons. The mean monthly relative humidity ranges between 72% (October) and 86% (March). The high annual precipitation and humidity is associated with low level convergence of moist air flowing from the east, as well as high rates of evapotranspiration, which recycles up to 30% of precipitation (Eltahir and Bras, 1996). Generally, the sea surface temperature of the tropical Atlantic to the east and the forcing produced by the Andes to the west are linked to the monsoon system, which is the main driver of precipitation across the Amazon basin (Nobre *et al.*, 2009).

Measurements at the ZF2 site during the period of observations showed average temperatures of $25 \pm 2.7$ °C peaking at the end of the dry season in October (27 °C) and midday median (and interquartile range, IQR) photosynthetically active radiation (PAR) of 930 (374 – 1430) $\mu mol\ m^{-2}\ s^{-1}$, which was highest during the dry season peaking in September. The years 2013 and 2014 exhibited less pronounced seasonality compared with the 1999-2012 average, with more precipitation during the dry season and less in the wet season (E. Alves, personal communication, 2015; Araújo *et al.*, 2002; Tanaka *et al.*, 2014). In particular, November 2013 was cooler and wetter than average, whereas April 2014 was warmer and drier than the long term mean. This means the seasonality observed in the results obtained from this study may be attenuated compared with the long-term mean behaviour. The mean ambient pressure was $997 \pm 5.6$ mbar with low average wind speeds of $1.9 \pm 0.9\ m\ s^{-1}$ from mostly easterly directions, i.e. trade winds from the equatorial Atlantic (52% frequency and monthly median directions between 84° and 144°).

The vegetation at the ZF2 site consists of evergreen broadleaf trees growing on well-drained, nutrient-poor yellow clay oxisols. The landscape is marked by lowlands interspersed by

small plateaux ranging from 50 m to 110 m altitude with dense tall trees on the plateau where the tower is located and open palm forests in the valley bottoms (Ribeiro *et al.*, 1999). The surrounding features of the reserve include a highway (BR-174) 20 km to the east, which is the only paved land connection to Manaus, and the Cuieiras river, which is a tributary to the Rio Negro, 13 km to the west. There are narrow strips of fragmented clearings through the forest, representing mosaic agriculture with degraded vegetation, 12 km to the south and 18 km to the north of the site. The plateau area around the tower and the reserve itself is very representative of undisturbed primary rainforest in central Amazonia (Andreae *et al.*, 2002; Pitman *et al.*, 2001).

## 6.2.2 Instrumentation and Data Acquisition

A proton transfer reaction-(quadrupole) mass spectrometer (PTR-MS) (Ionicon Analytik GmbH, Innsbruck, Austria) was deployed for mixing ratio and eddy flux measurements at TT34 from the 1 September 2013 to 20 July 2014 and a total of 4951 hours of concentration measurements were made. Air was sampled at ~80 L min$^{-1}$ through a 1/2" OD PFA (PFA-T8-062-100, Swagelok) sampling tube with the inlet located close to a sonic anemometer (Model R3-50, axis mode, 10 Hz, Gill Instruments, UK) at the top of the tower. The sampling tube was insulated and heated to 40 °C inside the air conditioned cabin, in which the PTR-MS was housed at the bottom of the tower, and for the first 2 m up the tower to prevent condensation occurring. The PTR-MS was operated with a drift tube temperature of 50 °C, pressure of 2.0 mbar and a voltage of 550 V (drift tube length ca. 9.5 cm) with a resultant *E/N* (*E*, electric field strength, *N*, buffer gas number density) of ~ 130 Td (1 Td = $10^{-17}$ V cm$^2$), which were maintained throughout the measurement period. The ion source current was 6.0 mA and the water flow rate was 6-8 sccm. The campaign average of the mean counts per second (cps) for the mass-to-charge ratio (*m/z*) of the first water cluster $H_3O^+(H_2O)$ (*m/z* 37) as a percentage of the cps of the primary ion (*m/z* 19) while recording in multiple ion detection (MID) mode was 3.4% (SD 0.4%, *n* = 4930). $O_2^+$ counts were <0.40% and $NO^+$ cps <0.15% of *m/z* 19 cps throughout the campaign as determined from mass scan measurements.

Flux measurements were made using the virtual disjunct eddy covariance (vDEC) technique, in which a covariance function between vertical wind velocity measurements ($w$) and VOC mixing ratios ($c$) is used to determine the flux for each selected compound ($F_c$), such that

$$F_C(\Delta t) = \frac{1}{n} \sum_{i=1}^{n} w' \left( i - \frac{\Delta t}{\Delta t_w} \right) \times c'(i), \tag{6.1}$$

where prime denotes the difference between the instantaneous and the 45 min mean vertical wind component or concentration. $\Delta t$ refers to the lag time between the concentration measurement and the vertical wind velocity measurement. $\Delta t_w$ is the sampling interval of the vertical wind velocity measurements (0.1 s) and $n$ gives the number of disjunct samples (approx. 1350) from the PTR-MS during each 45 min averaging period. A comprehensive description of this technique can be found in, e.g., Karl *et al.* (2002), Langford *et al.* (2009), and Rinne *et al.* (2001).

PTR-MS data were stored alongside the wind data from the sonic anemometer using a custom logging program written in LabVIEW (National Instruments, Austin, Texas, USA). This program switched the PTR-MS into MID mode for 45 min of each hour which generated the disjunct data used for the flux calculation. The remaining 15 min of each hour were used for a 5 min background measurement at the selected ions and dwells corresponding to the MID mode and two 5 min periods in which the PTR-MS scanned through a range of masses (*m/z* 21-141) whilst sampling ambient air and zero air alternately.

Here the measurements of three masses are presented to which the following compounds have been ascribed: *m/z* 69 (isoprene, plus any furan present), *m/z* 71 (isoprene oxidation products, $i_{ox}$ comprising methyl vinyl ketone, MVK, and methacrolein, MACR, plus a possible contribution of product ions from isoprene hydroxy hydroperoxides or ISOPOOH) and *m/z* 137 (total monoterpenes). ISOPOOH represents the dominant primary oxidation products of isoprene under low NO$_x$ conditions (Liu *et al.*, 2013). Although there is recent evidence that *m/z* 71 may suffer from interference by ISOPOOH product ions (Rivera-Rios *et al.*, 2014), we were unable to

quantify their contribution to the signal recorded at *m/z* 71 and the instrument was calibrated at this *m/z* value using MVK + MACR only. The selected masses were measured in the MID mode and corresponding background measurements in scan mode. In the MID mode *m/z* 69, *m/z* 71 and *m/z* 137 were measured alongside six other *m/z* with a dwell time of 0.2 s each. The primary ion was indirectly quantified via the isotopologue $H_3^{18}O^+$ at *m/z* 21, which together with the water cluster (*m/z* 37) was measured at a dwell of 0.1 s each, resulting in a total measurement cycle of 2 s.

Background measurements were made using a commercial platinum alumina-based zero air generator (Model 75-83-220, Parker Balston). The hourly mean background mixing ratio was subtracted from the ambient mixing ratio measurement at the corresponding hour. When no background measurement was available for a given hour, the median of the hourly backgrounds measured in the same month was applied. The mixing ratio limit of detection (LoD) was approximated from two standard deviations of the 5 min background measurement (in normalised counts per second, ncps) for a given hour divided by the corresponding sensitivity (ncps ppbv$^{-1}$). Here normalised cps refers to normalisation to $H_3O^+$ of $10^6$ cps and a drift tube pressure of 2.0 mbar. When no background measurement was available for a given hour the median of the hourly LoD (ppbv) values measured in the same month was applied. Ensemble averages of the applied background and LoD mixing ratios are given in Table 6.1, together with average sensitivities. Fluxes and mixing ratios below the LoD were included in the analysis of averaged data, as their removal can cause a bias towards high values, because when measurements are below the LoD they are indeed small (Helsel and Hirsch, 1992). Methods to substitute periods of data <LoD are available; however, these have also been shown to result in a significant bias, either high or low depending on the values used (Clarke, 1998). The percentage and number of data points which fail the LoD are given in Table 6.1.

*Table 6.1. Propagated averages of hourly applied sensitivities, background mixing ratios and limits of detection (LoD). Normalised counts $s^{-1}$ (ncps) refer to raw counts $s^{-1}$ normalised to $10^6$ cps $H_3O^+$ and drift tube pressure of 2.0 mbar. Mixing ratio LoDs were approximated from two standard deviations of hourly (5 min) background ncps divided by measured sensitivities (ncps $ppbv^{-1}$). The percentage and number of hours in which the mixing ratios measured in MID mode were below the LoD is shown.*

| | Sensitivity[a] (ncps $ppbv^{-1}$) Median (IQR) | Background (ppbv) Median (IQR) | LoD (ppbv) Median (IQR) | % of values <LoD (n) |
|---|---|---|---|---|
| Isoprene (m/z 69) | 3.78 (0.35) | 0.16 (0.11) | 0.50 (0.17) | 13 (644) |
| MVK+MACR+ ISOPOOH product ions (m/z 71) | 12.02 (2.08) | 0.08 (0.07) | 0.23 (0.11) | 22 (1066) |
| Monoterpenes (m/z 137) | 3.46 (0.36) | 0.02 (0.02) | 0.17 (0.07) | 35 (1721) |

[a]Average sensitivity uncertainties for VOC mixing ratios were 20-30% depending on compound.

Sensitivities were determined from automated calibrations performed from the end of October 2013 onward using a gravimetrically prepared standard containing 15 VOCs, including isoprene, MVK, MACR and $\alpha$-pinene, in ultrahigh purity nitrogen (Apel Riemer Environmental Inc., CO, USA) diluted with dry zero air. A 0.015-1 standard L $min^{-1}$ mass flow controller (MKS Instruments Limited, model 1259C) was used to control the zero air dilution flow and was automatically calibrated prior to each multipoint calibration using an electronic mass flow meter (model MAS1009AV2, Kobold) and logged in the program. To avoid losses and/or contamination the calibration unit was designed so that once in PTR-MS calibration mode the standard sampled by the PTR-MS did not flow though the mass flow meter. A 0-15 standard mL $min^{-1}$ mass flow controller (model F-200DV-AAD-22-V, Bronkhorst) was used to control the VOC flow and was manually calibrated at regular intervals using a mini-Buck flow calibrator (mini-Buck calibrator model M-5, A-P Buck, USA).

Multipoint calibrations in which selected *m/z* were monitored at the dwells employed in MID mode were interleaved by single-point calibrations undertaken in scan mode. To check for memory effects, multipoint calibrations were performed up and down the concentration range.

137

Mixing ratios of isoprene, $\alpha$-pinene, MVK and MACR sampled during calibrations were in the range of 2 to 20 ppbv each. Zero air measurements were performed before and after sampling at each VOC concentration. The secondary electron multiplier (SEM) voltage of the PTR-MS was optimised prior to calibrations. Calibrations were scheduled during the night when concentrations were low and when there frequently was insufficient turbulence for flux quantification. Humidified calibrations using either a bubbler or a dew point generator (Model LI610, LICOR) were performed off-line. A HMP60 probe (Vaisala) in the excess flow was used to monitor relative humidity and temperature. Humidity dependent sensitivities were applied to *m/z* 69 and *m/z* 71 in a method analogous to that described by Insomata *et al.* (2008) and Kameyama *et al.* (2009; 2010; 2014). The sensitivity of $\alpha$-pinene did not show a humidity dependence.

### 6.2.3 Flux calculations and quality assessment

Post-processing of fluxes was carried out in LabVIEW using a further development of the algorithm used by Langford *et al.* (2009). The applied flux limit of detection (termed Langford LoD hereafter) was calculated following the method outlined by Langford *et al.* (2015). Briefly, for each 45 min flux period an auto-covariance of *c'* was used to obtain the standard deviation of the instrument noise, $\varepsilon'$. A time series of white noise with this standard deviation was generated for each *m/z* and the cross-covariance function between *w'* and $\varepsilon'$ calculated for lag times of 0 to 300 cycles. The LoD was defined as three times the standard deviation of this cross-covariance for a given averaging period. For *m/z* 69, 71 and 137, 22%, 35% and 41%, respectively, of the otherwise unfiltered fluxes were below the Langford LoD. Alternate values of the LoD (e.g. Wienhold LoD) were estimated from three standard deviations of the covariance in the vertical wind velocity and VOC concentration at time lags of 150 to 180 s ($n = 300$ cycles) for comparison (Spirig *et al.*, 2005; Wienhold *et al.*, 1994).

Lag times between the vertical wind velocities and measured VOC concentrations were determined by the MAX, AVG and PRES methods outlined by Langford *et al.* (2015). A prescribed constant time lag of 8 s was applied to data presented here. This lag time was

determined from analysis of the histogram of lag times determined from the maximum in the cross-covariance of the isoprene concentration and vertical wind velocity (MAX method).

To identify non-stationary conditions the Foken and Wichura (1996) method was applied. The covariance of the vertical wind and VOC concentration was divided into nine intervals of 5 min and the average compared with the covariance for the whole 45 min period. When the difference between the covariances was greater than 60% the non-stationary data were rejected; this was the case for 17% of otherwise unfiltered fluxes. Data from periods of insufficient turbulence, i.e. when the friction velocity was less than 0.15 m s$^{-1}$ or the wind speed was less than 0.5 m s$^{-1}$, were removed. Around 39% of otherwise unfiltered data were rejected due to insufficient turbulence. The majority of these periods occurred during the night, and only 12% of the filtered data was from the hours between 07:00 to 17:00 local time. Application of both filtering periods of insufficient turbulence and non-stationarity resulted in a total loss of 52% of isoprene fluxes, 58% of $m/z$ 71 fluxes and 57% of $m/z$ 137 fluxes. Where averaging was applied to fluxes, the propagated LoD was used with resultant reduction in loss of flux (Langford *et al*., 2015). High frequency flux losses were corrected using the method of Horst (1997). The median increase in the flux was 1.3%, indicating that the high frequency flux range carried a minor proportion of the total flux at this measurement height.

Photosynthetically active radiation (PAR) fluxes were measured by the National Institute for Amazonian Research (Instituto Nacional de Pesquisas da Amazônia, INPA) at the nearby K34 tower. K34 is approximately 1.6 km south of TT34 and values are considered to be representative of both sites. PAR (W m$^{-2}$) was measured above the canopy at 51.6 m using a LI-190, SZ Li-COR sensor. Measurements were converted to photosynthetic photon flux density at 400 nm and 700 nm and the mean taken. 30 min values were averaged to provide hourly values for comparison with VOC fluxes.

Ambient temperature measurements were taken from the Gill R axis-mode sonic anemometer situated at TT34. These data were corrected by comparison with a weather station (DAVIS Vantage Pro 2) situated at 42 m on the TT34 tower and verified against temperatures

measured at K34 at 51.1 m (provided by INPA) with a Pt resistance (PT100) and Vaisala HMP45AC temperature and relative humidity probe.

## 6.3 Results and discussion

Table 6.2 shows the results and descriptive statistics of the fluxes and above-canopy volume mixing ratios of isoprene, primary isoprene oxidation products ($i_{ox}$), and sum of monoterpene measurements for all the data and split by daytime, wet and dry seasons. Annual median (with interquartile range, IQR) fluxes during the day (defined as 07:00 to 17:00 local time) for isoprene, $i_{ox}$, and monoterpenes were 2.21 (0.66 to 4.25) mg m$^{-2}$ h$^{-1}$, -0.13 (-0.22 to -0.05) mg m$^{-2}$ h$^{-1}$, and, 0.59 (0.23 to 1.07) mg m$^{-2}$ h$^{-1}$, respectively. Median (and IQR) above-canopy volume mixing ratios (measured at 40 m above ground-level) were 3.94 (2.02 to 6.12) ppbv, 1.02 (0.45 to 1.80) ppbv, and 0.46 (0.27 to 0.65) ppbv, respectively. Night-time fluxes were mostly rejected due to insufficient turbulence, therefore our analyses focus on the daytime values. Above-canopy mixing ratios of isoprene were around 1 ppbv during the night, whereas night-time monoterpene and, during the wet season, $i_{ox}$ mixing ratios were below the detection limit.

Observed fluxes and above-canopy mixing ratios are comparable to those from previous studies at similar sites in the central Amazon forest during the respective seasons (Andreae *et al.*, 2002; Kesselmeier *et al.*, 2002; Yañez-Serrano *et al.,* 2015), but higher than observations from tropical forests in Costa Rica (Karl *et al.*, 2004) and Borneo (Langford *et al.*, 2010a). Largest fluxes and highest mixing ratios were seen for isoprene. The oxidation products showed a net deposition to the canopy - about 3% of the carbon emitted as isoprene was deposited back to the canopy as oxidation products. However, the median volume mixing ratios of $i_{ox}$ were a quarter of those of isoprene. Monoterpene fluxes were four times lower than those of isoprene and above-canopy volume mixing ratios were a tenth of those of isoprene (see Section 6.3.3) and half of those of $i_{ox}$, presumably due to the higher gas-phase reactivity of monoterpene compounds.

*Table 6.2. Summary of VOC fluxes (mg m$^{-2}$ h$^{-1}$) and mixing ratios (ppbv) measured at 40 m above ground level (on average 10 m above the canopy top) of all the measurements taken during September 2013 to July 2014 and separated by daytime, dry and wet seasons.*

| | Fluxes (mg m$^{-2}$ h$^{-1}$) | | | Mixing ratios (ppbv) | | |
|---|---|---|---|---|---|---|
| | *Isoprene* | *Σ i$_{ox}$* | *Σ monoterpenes* | *Isoprene* | *Σ i$_{ox}$* | *Σ monoterpenes* |
| *Lifetime* | 1.4 h | 6.8 h[b], 4.1 h[b] | 2.6 h | 1.4 h | 6.8 h, 4.1 h | 2.6 h |
| *LoD[a]* | 0.03 | 0.04 | 0.06 | 0.50 | 0.23 | 0.17 |
| *All data* | | | | | | |
| *1st Quartile* | 0.03 | -0.12 | 0.05 | 0.91 | 0.25 | 0.13 |
| *Median* | 1.10 | -0.06 | 0.31 | 2.16 | 0.65 | 0.24 |
| *Mean* | 2.13 | -0.09 | 0.53 | 3.01 | 1.01 | 0.32 |
| *3rd Quartile* | 3.50 | -0.03 | 0.87 | 4.61 | 1.42 | 0.47 |
| *n* | 2390 | 2029 | 2591 | 4956 | 4852 | 4923 |
| *Daytime* | | | | | | |
| *1st Quartile* | 0.66 | -0.16 | 0.23 | 2.02 | 0.45 | 0.27 |
| *Median* | 2.21 | -0.09 | 0.59 | 3.95 | 1.02 | 0.46 |
| *Mean* | 2.87 | -0.11 | 0.72 | 4.26 | 1.27 | 0.48 |
| *3rd Quartile* | 4.25 | -0.04 | 1.07 | 6.12 | 1.80 | 0.65 |
| *n* | 1789 | 1364 | 1879 | 2269 | 2220 | 2229 |
| *Dry season* | | | | | | |
| *1st Quartile* | 1.37 | -0.18 | 0.39 | 3.07 | 1.03 | 0.41 |
| *Median* | 3.61 | -0.11 | 0.94 | 5.49 | 1.74 | 0.61 |
| *Mean* | 4.39 | -0.11 | 1.04 | 5.43 | 1.91 | 0.60 |
| *3rd Quartile* | 6.72 | -0.04 | 1.52 | 7.53 | 2.77 | 0.76 |
| *n* | 461 | 320 | 485 | 552 | 551 | 551 |
| *Wet season* | | | | | | |
| *1st Quartile* | 0.56 | -0.15 | 0.21 | 1.86 | 0.38 | 0.24 |
| *Median* | 1.88 | -0.09 | 0.51 | 3.54 | 0.83 | 0.41 |
| *Mean* | 2.35 | -0.11 | 0.61 | 3.89 | 1.06 | 0.44 |
| *3rd Quartile* | 3.64 | -0.04 | 0.93 | 5.69 | 1.45 | 0.59 |
| *n* | 1328 | 1044 | 1394 | 1717 | 1669 | 1678 |

[a] Limit of detection: Median flux detection limit calculated using Spirig *et al.* (2005) and concentration LoDs as by Taipale *et al.* (2008) are used respectively.

[b] Atmospheric lifetimes with regard to OH are for MVK and MACR respectively (Atkinson, 1997).

## 6.3.1 Temporal variability of bVOC fluxes and concentrations

### 6.3.1.1 Diurnal patterns

Diurnal profiles of concentrations and fluxes of isoprene, isoprene primary oxidation products, $i_{ox}$, and monoterpenes are shown in Figure 6.1. Isoprene and monoterpene fluxes showed emission throughout the day, with a strong diurnal pattern and a median midday peak (IQR) of 4.35 (0.89 to 8.42) mg m$^{-2}$ h$^{-1}$ and 1.08 (0.34 to 2.09) mg m$^{-2}$ h$^{-1}$, respectively. By contrast, $i_{ox}$ showed net deposition throughout the day with strongest median (IQR) deposition fluxes of -0.19 (-0.35 to -0.06) mg m$^{-2}$ h$^{-1}$ in the morning, which is earlier than the peak in the isoprene fluxes. Diurnal profiles of above-canopy mixing ratios for all compounds peaked in the early afternoon (13:00-15:00 local time) with median peak mixing ratios (IQR) of 5.52 (2.0 - 8.53) ppbv, 1.30 (0.43 - 2.88) ppbv, and 0.58 (0.28 - 0.88) ppbv for isoprene, $i_{ox}$, and monoterpenes, respectively. The total monoterpene volume mixing ratios were around one order of magnitude lower than those of isoprene, which is consistent with previous observations (Kesselmeier *et al.*, 2002).
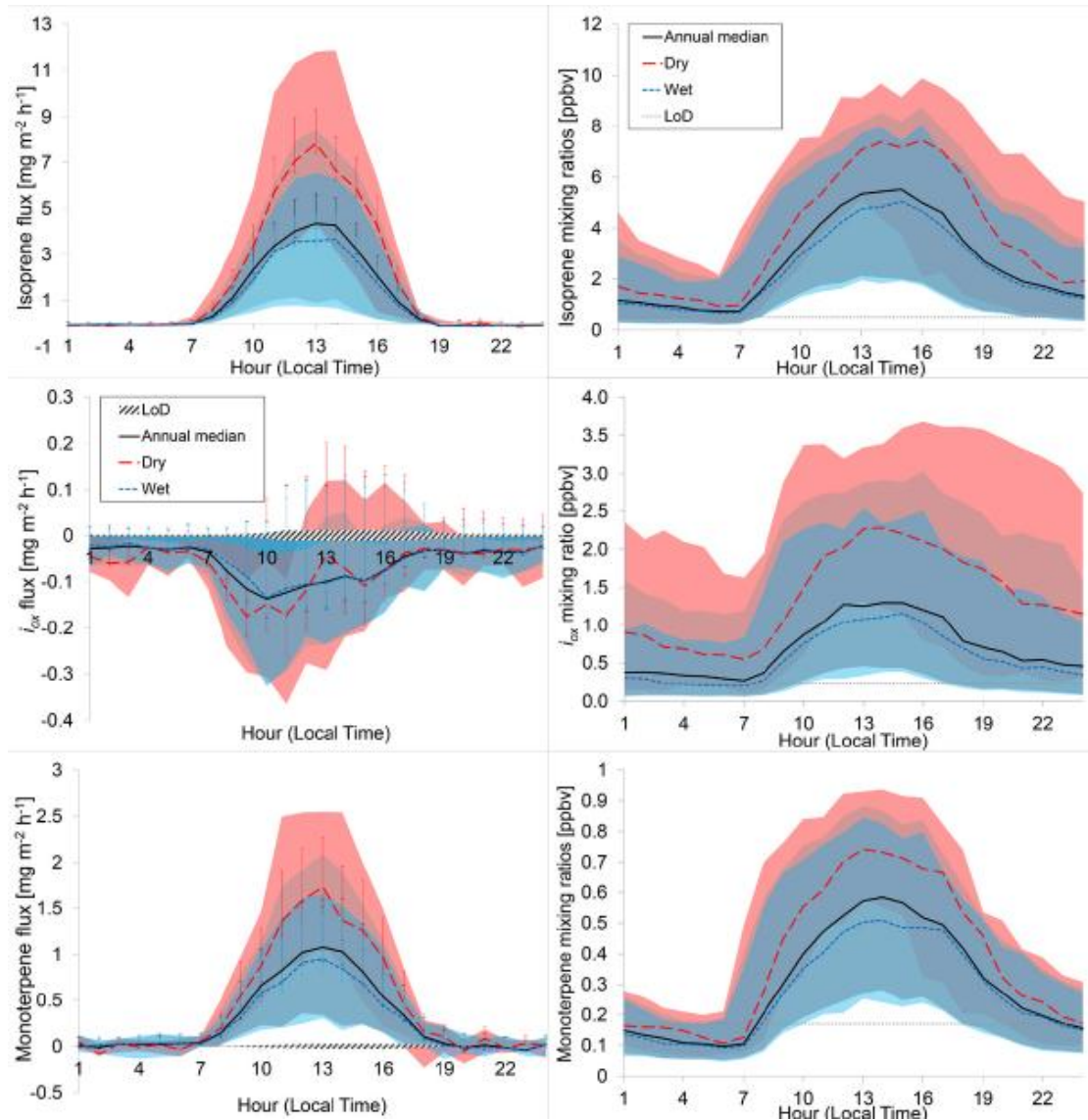
**Figure 6.1.** Diurnal profiles (in local time) of median fluxes (mg m$^{-2}$ h$^{-1}$) and mixing ratios (ppbv) for isoprene (*m/z* 69), isoprene oxidation products, $i_{ox}$ (*m/z* 71), and monoterpenes (*m/z* 137), interquartile ranges (shaded), flux precision (error bars), split by dry (dashed red) and wet (dotted blue) seasons and detection limits (pattern for fluxes and line for mixing ratios).

Mixing ratios of isoprene and monoterpenes dropped rapidly around sunset, whereas those of $i_{ox}$ continued to decline more slowly throughout the night, presumably due to their albeit reduced rates of formation from isoprene by nocturnal gas-phase chemistry and their continued deposition to the surface. Although data on boundary layer heights are not available for the site, and hence a detailed analysis of the role of boundary layer dynamics is not possible, it is likely that the diurnal dynamics of the boundary layer will contribute to the observed patterns of

compound mixing ratios. Minimum volume mixing ratios of all compounds were observed at dawn (06:00-07:00 local time) when the concentrations from emissions of the previous day had been degraded or deposited and before the morning emissions commenced.

The strong morning deposition fluxes of $i_{ox}$ are likely driven by the sharp increase in canopy-level $i_{ox}$ mixing ratios from the oxidation of rapidly increasing isoprene emissions, and/or the downward mixing of air from above as the boundary layer expands. Peak midday isoprene and monoterpene fluxes were greater by a factor of approx. two between the wet and the dry season, whereas peak morning $i_{ox}$ deposition was around 1.5 times greater during the dry than the wet season. The midday maxima were less pronounced during the wet season with an average difference of 2 ppbv and 0.2 ppbv (i.e. ca. 30-40% lower than the median value for the midday maximum during the dry season) for isoprene and monoterpene mixing ratios, respectively, and around 1 ppbv representing a 50% decrease between the dry and the wet season for median peak $i_{ox}$ mixing ratios. $I_{ox}$ showed elevated mixing ratios also during the evening in the dry season with an average difference around 1.5 ppbv between day and night during the dry season compared to a day/night difference of 1 ppbv during the wet season.

**6.3.1.2 Monthly variability**

Monthly median fluxes and above-canopy mixing ratios of bVOCs are shown in Figure 6.2. For isoprene, $i_{ox}$, and monoterpenes, monthly medians ranged from $1.09 \pm 0.3$ mg m$^{-2}$ h$^{-1}$ to $4.16 \pm 0.5$ mg m$^{-2}$ h$^{-1}$, $-0.06 \pm 0.05$ mg m$^{-2}$ h$^{-1}$ to $-0.16 \pm 0.07$ mg m$^{-2}$ h$^{-1}$, and $0.36 \pm 0.2$ mg m$^{-2}$ h$^{-1}$ to $1.04 \pm 0.3$ mg m$^{-2}$ h$^{-1}$ for fluxes and $2.8 \pm 0.1$ ppbv to $6.0 \pm 0.2$ ppbv, $0.5 \pm 0.1$ ppbv to $2.2 \pm 0.1$ ppbv, and $0.3 \pm 0.1$ ppbv to $0.7 \pm 0.1$ ppbv for mixing ratios, respectively. The results show that fluxes and mixing ratios of all compounds followed a clear seasonality with higher emissions, or, for $i_{ox}$, deposition, during the dry season when temperature and photosynthetically active radiation (PAR) are highest. Although July is considered the start of the dry season, VOC emissions and thus mixing ratios remained low, similar to levels during the wet season. Median fluxes during the dry season were greater than during the wet season by almost a factor of two for isoprene and monoterpenes, whereas $i_{ox}$ deposition was approx. 25% lower during the wet season.

Median isoprene and monoterpene mixing ratios were 35% lower during the wet season, and $i_{ox}$ concentrations presented the largest reduction of around 50% compared to the dry season. This resulted from reduced source emissions, as well as possibly a lower atmospheric oxidative capacity during the wet season. Monthly variability was in all cases statistically significant ($F$ statistics = 12.14-95.14, $p$ <0.001, total monthly sample sizes $n$ = 243-684). Generally fluxes and concentrations were higher, i.e. above the annual median, or in the case of $i_{ox}$ more negative, in September, October, November, December and January, although November seemed to be unseasonably cold and wet. Fluxes and above-canopy mixing ratios were lower than the annual median in February to July, or in the case of $i_{ox}$ fluxes showed less deposition.
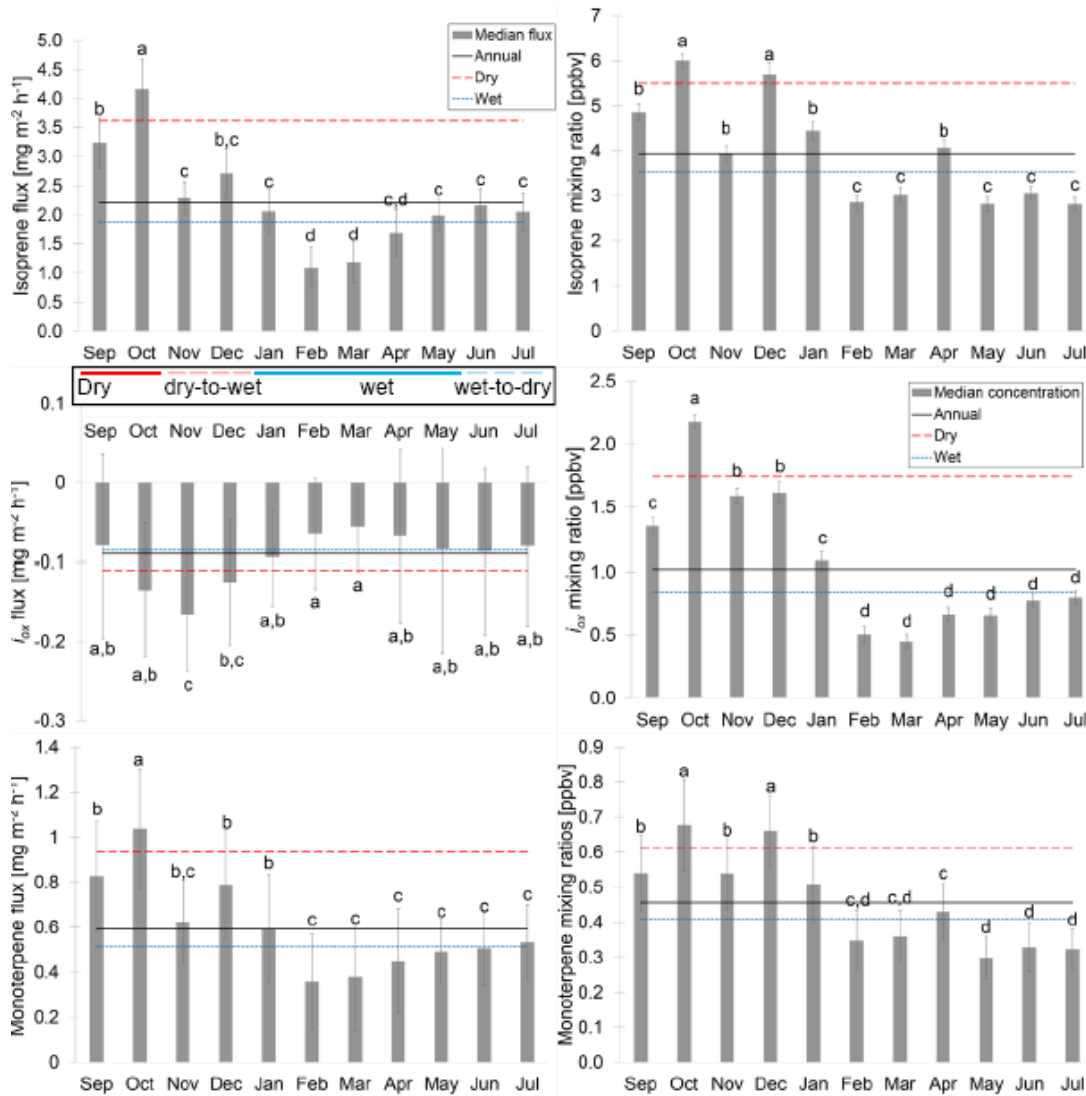
**Figure 6.2.** Bar chart showing monthly median fluxes (mg m$^{-2}$ h$^{-1}$) and mixing ratios (ppbv) of isoprene (*m/z* 69), isoprene oxidation products, $i_{ox}$ (*m/z* 71), and monoterpenes (*m/z* 137) with lines indicating the median annual (solid black), dry season (dashed red) and wet season (dotted blue) values respectively. Lowercase letters denote groups of statistically significant difference using Tukey's post hoc Honestly Significant Difference test and the coloured solid and dashed lines in the box indicate seasonality.

Emissions peaked at the end of the dry season in October, which coincided with highest median air temperatures and PAR. It has previously been suggested that the increase of fluxes and mixing ratios in October may result from increased amounts of active biomass after the dry season due to higher precipitation (Kesselmeier *et al.*, 2002). Measurements indicate that precipitation did increase from October onwards, however, leaf age and developmental stage may

have resulted in higher leaf emission capacities of isoprene at the end of the dry season when canopy flushing has been completed and young leaves have reached maturity (see Section 6.3.4). As well as phenological development of leaves, other factors such as the oxidative capacity of the atmosphere may affect the seasonality of emission rates of monoterpenes (Kuhn *et al.*, 2004a). MVK, MACR and ISOPOOH ($i_{ox}$) occur in the atmosphere as a result of, primarily, the gas-phase oxidation of isoprene above and within the forest canopy and production rates, therefore, depend on isoprene emission rates and the oxidative capacity of the troposphere (see Section 6.3.3). Direct emissions of MVK + MACR from within-leaf or on-leaf oxidation of isoprene may provide a minor contribution to $i_{ox}$ fluxes during peak temperatures (Jardine *et al.*, 2011), although we are not able to separate out these different sources in our data. The above-canopy flux is the net exchange composed of dry deposition, chemical formation/destruction below the measurement height as well as direct emission. In general, published observations of $i_{ox}$ fluxes tend to fall into one of two categories: over temperate ecosystems $i_{ox}$ tends to show emission that amounts to some 10% of the isoprene flux (Rinne *et al.*, 2012). By contrast, most tropical measurements have identified quite effective deposition at a rate approaching the limit imposed by turbulence (i.e. with a small canopy uptake resistance) (Misztal *et al.*, 2011). The reason for this is currently unclear: either tropical vegetation has a higher affinity for $i_{ox}$ compounds or the relative contributions of MVK, MACR and ISOPOOH differ between studies and these compounds behave very differently, possibly with ISOPOOH products adding the strong deposition behaviour.

### 6.3.2 Correlations with light and temperature

Emission rates of isoprene and monoterpenes plotted as a function of averaged temperature and photosynthetically active radiation (PAR) showed strong correlations with regression coefficients ($R^2$) of 0.94 and 0.94 ($p <0.001$) respectively for isoprene, and 0.92 and 0.85 ($p <0.001$), respectively, for monoterpenes (Figure 6.3). When plotted against temperature both compound fluxes indicated a threshold temperature of 26 °C before emissions increased in an exponential fashion, whereas when plotted against PAR, emissions increased linearly.

Averaged $i_{ox}$ fluxes were close to the averaged limit of detection and showed no correlation with temperature, but a weak trend was observed with PAR ($R^2 = 0.48$, $p < 0.05$), where increased deposition was related to increased PAR.
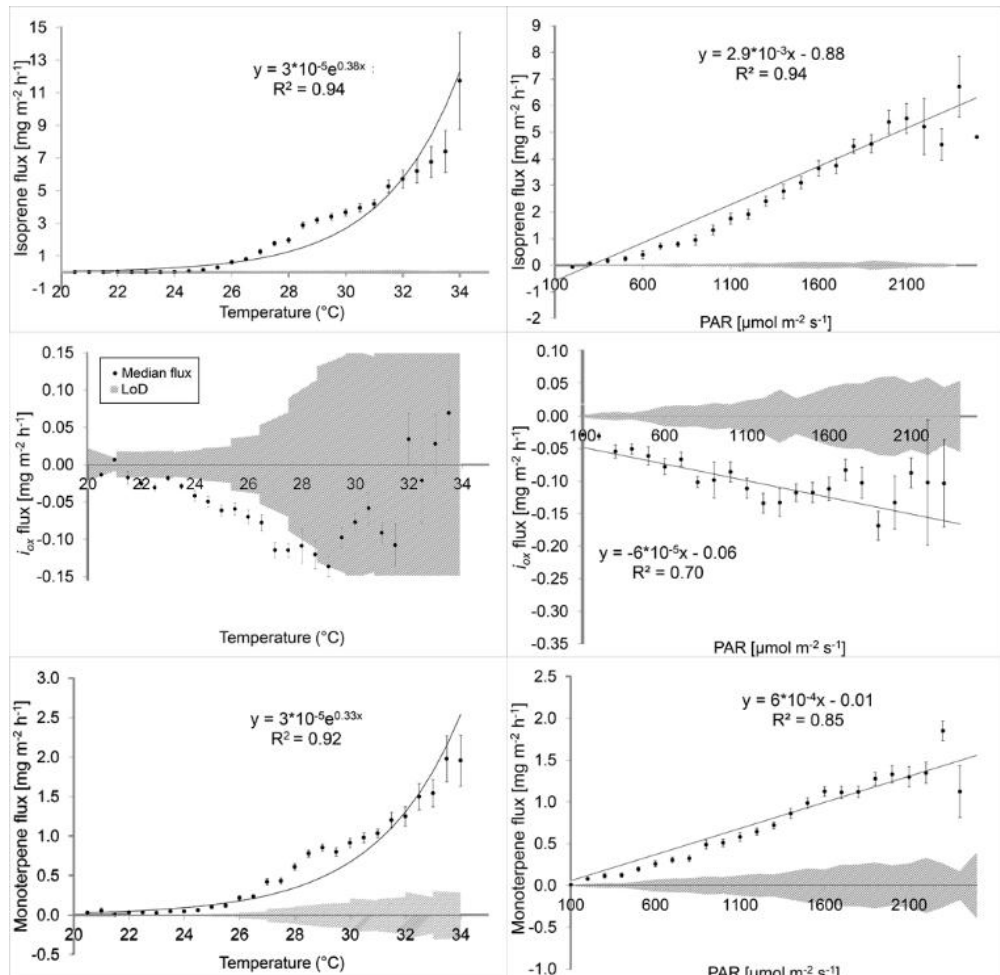


**Figure 6.3. Part I:** Plots showing VOC fluxes (mg m$^{-2}$ h$^{-1}$) plotted against averaged temperature (*left column*) and photosynthetically active radiation (PAR) (*right column*) measurements with standard errors, regression lines, formulae, regression coefficients ($R^2$), detection limits (pattern for fluxes and dotted line for mixing ratios). The range of data points (*n*) for each interval was between 1-297 for temperature and 1-1680 for PAR.
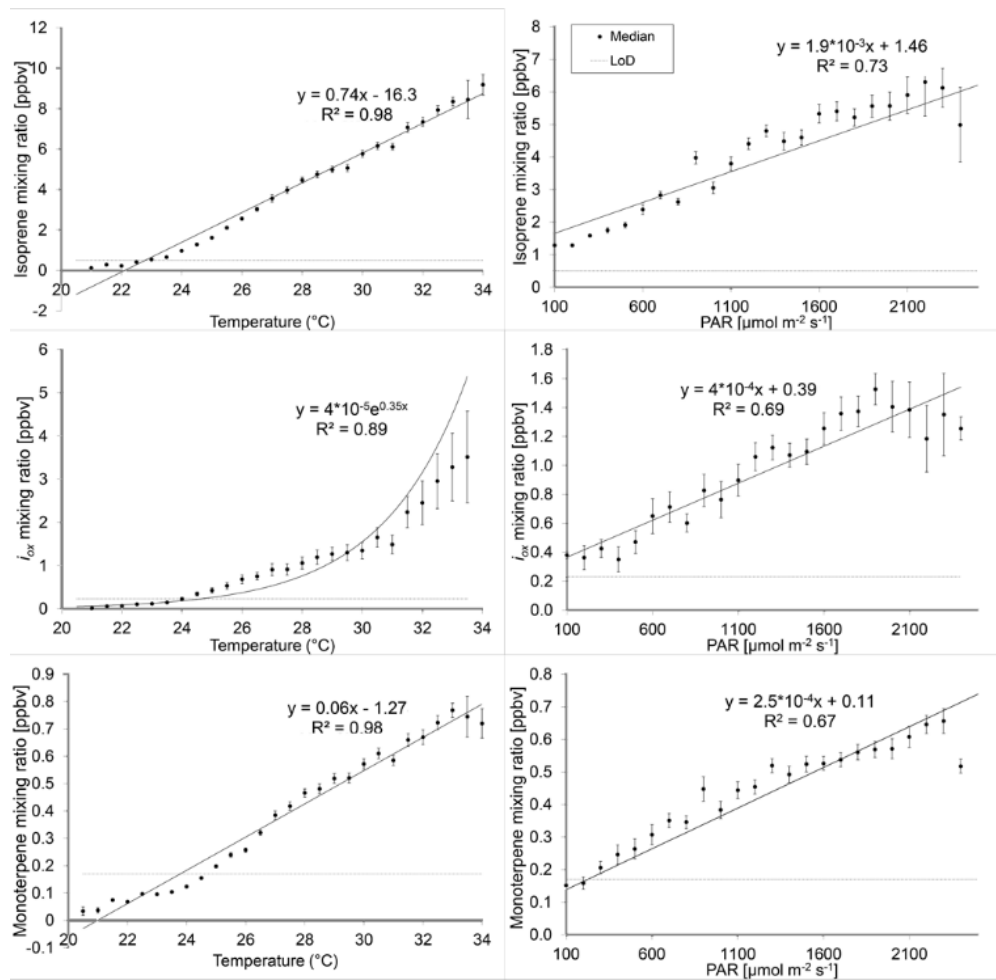
**Figure 6.3. Part II:** Plots showing VOC mixing ratios (ppbv) plotted against averaged temperature (*left column*) and photosynthetically active radiation (PAR) (*right column*) measurements with standard errors, regression lines, formulae, regression coefficients ($R^2$), detection limits (pattern for fluxes and dotted line for mixing ratios). The range of data points (*n*) for each interval was between 1-297 for temperature and 1-1680 for PAR.

Measurements of standardised responses of leaf-level isoprene emissions to temperature and PAR indicate initially exponential increases with temperature, which is seen in our measurements, until a peak threshold is reached, stated as 40 °C for tropical species. The response to PAR is assumed to be strongly logarithmic with a plateau at 1000 μmol m$^{-2}$ s$^{-1}$ PAR in many emissions models, but measurements have shown that the initial response of emission rates may not be as pronounced with a slower initial increase, but also show a lack of light saturation even beyond 1000 μmol m$^{-2}$ s$^{-1}$ (Harley *et al.*, 2004). The linear responses seen for canopy isoprene emissions in this study indicate a slower initial response, even slower than leaf measurements,

and no light saturation below 2000 μmol m$^{-2}$ s$^{-1}$. Leaf-level measurements are often made on sun-exposed leaves only, which are not representative of the whole canopy, which explains the reduced initial response. Sun-leaves show a lack of light saturation at high PAR levels, which may be species-specific and/or depend on the leaf adaptation to the ambient light environment (Harley *et al.*, 2004; Kuhn *et al.,* 2004b), but this is not expected to be seen for the whole canopy (Harley *et al.*, 1997; 2004; Kuhn *et al.*, 2002; Lerdau and Keller, 1997). Our measurements suggest a possible canopy saturation point around 2100 μmol m$^{-2}$ s$^{-1}$, although this remains speculation due to the low number of data points obtained at these high values.

Monoterpene emission responses are more complex as they depend on the compound species, as well as the source of the emissions, i.e. *de novo* emissions or from plant storage pools. Emissions from storage reservoirs were considered to be only temperature-dependent, but there is a wealth of evidence from the past 15 years showing that monoterpenes can be emitted in the same way as isoprene, e.g. Dindorf *et al.* (2006), Kuhn *et al.* (2002, 2004), Matsunaga *et al.* (2013), Rinne *et al.* (2002), Tarvainen *et al.* (2005). The total monoterpene flux in our measurements showed similar responses as seen with isoprene, i.e. an exponential increase with temperature, which is also assumed in monoterpene emission models (Kesselmeier and Staudt, 1999), but also a linear response to PAR, which only fairly recently has been added to emission models (Guenther *et al.*, 2012).

Strong correlations were seen between above-canopy volume mixing ratios and temperature with linear regressions and coefficients ($R^2$) of 0.98 ($p$ <0.001) and 0.99 ($p$ <0.001) for isoprene and monoterpenes, respectively, whereas $i_{ox}$ mixing ratios showed higher coefficients with an exponential fit ($R^2 = 0.89$, $p$ <0.001). Slightly weaker relationships were observed between above-canopy volume mixing ratios and PAR with $R^2$ of 0.73 ($p$ <0.001), 0.69 ($p$ <0.001), and 0.67 ($p$ <0.001), respectively for all compounds. In the case of $i_{ox}$, it is likely that the high temperature dependency of mixing ratios is an indirect driver, i.e. the temperature-dependency of isoprene emissions, and the linear regressions with PAR due to the photochemical

involvement in the formation of these compounds, which may also account for the observed pattern of increased $i_{ox}$ deposition with increasing PAR.

### 6.3.3 VOC/VOC ratios

The median (IQR) ratio of monoterpene to isoprene fluxes was 0.28 (0.20 to 0.41). For $i_{ox}$/isoprene fluxes it was -0.05 (-0.15 to 0.07). Median (IQR) ratios of monoterpene/isoprene mixing ratios above the canopy were 0.12 (0.10 to 0.15). The ratio of $i_{ox}$/isoprene mixing ratios was 0.29 (0.19 to 0.45). The fact that the monoterpene to isoprene ratio was greater for fluxes than for concentrations indicates that the total loss of monoterpenes takes place at a faster rate than for isoprene. No speciated measurements of monoterpenes were made as part of these measurements, but observations from the nearby K34 tower by Jardine *et al.* (2015) indicate large proportions of d-limonene and the presence of highly reactive compounds such as *cis-β*-ocimene, *trans-β*-ocimene, and terpinolene. Mixing ratios of $i_{ox}$ were ~30% of those of isoprene overall with 26% during the daytime and 34% at night.

In a well-mixed system near steady-state, the $i_{ox}$/isoprene ratio can provide information on the oxidant conditions during the day, as it depends on oxidation product yields from isoprene and the reaction rates of isoprene, MVK, MACR, and ISOPOOH with OH and $O_3$. In the presence of $NO_x$ the oxidation of isoprene by OH yields 32% and 23% MVK and MACR respectively (Tuazon and Atkinson, 1990). However, ozonolysis yields and reaction rates are reversed, such that isoprene produces more MACR than MVK. Under low $NO_x$ conditions the oxidation product yield of MVK + MACR can be significantly lower, i.e. a combined yield possibly as low as 7%, due to the dominant $HO_2$ pathway (Liu *et al.*, 2013). The measured $i_{ox}$/isoprene concentration ratio changed little during the day with 0.24 during the wet season compared with 0.32 in the dry season, whereas night-time ratios were 0.28 during the wet season and 0.52 during the dry season. The median ratio increased by a factor of 1.5 during the dry season indicating an increased atmospheric oxidation capacity. This increase was almost proportional with isoprene mixing ratios above the canopy increasing on average 1.5-fold and $i_{ox}$ 2.5-fold during the dry season, which is much lower than observed at a similar central Amazonian site (Yañez-Serrano *et al.*,

2015). The measurements from Yañez-Serrano *et al.* (2015) do not offer a direct comparison due to the different measurement heights used, which strongly affect $i_{ox}$/isoprene ratios, as well as the much shorter duration of the measurements of around two weeks during each season.

The diurnal profile of the $i_{ox}$/isoprene concentration ratio peaked before dawn at 0.43, decreased to around 0.24 throughout the day, and began to increase again after sunset (Figure 6.4). The day/night differences were more pronounced during the dry season with peak ratios around 0.65 at night and 0.35 during the day, but the diurnality was almost lost during the wet season when ratios remained constant throughout the day, at around 0.25. It must be noted that effects of boundary layer dynamics between seasons are not accounted for here, as boundary layer height measurements were not available, and may be affecting the diurnal patterns and ratios of compounds. Higher $i_{ox}$/isoprene mixing ratios during the night-time dry season are likely a result of larger relative differences in diurnal boundary layer heights between the dry and wet seasons resulting in less dilution in the nocturnal boundary layer.
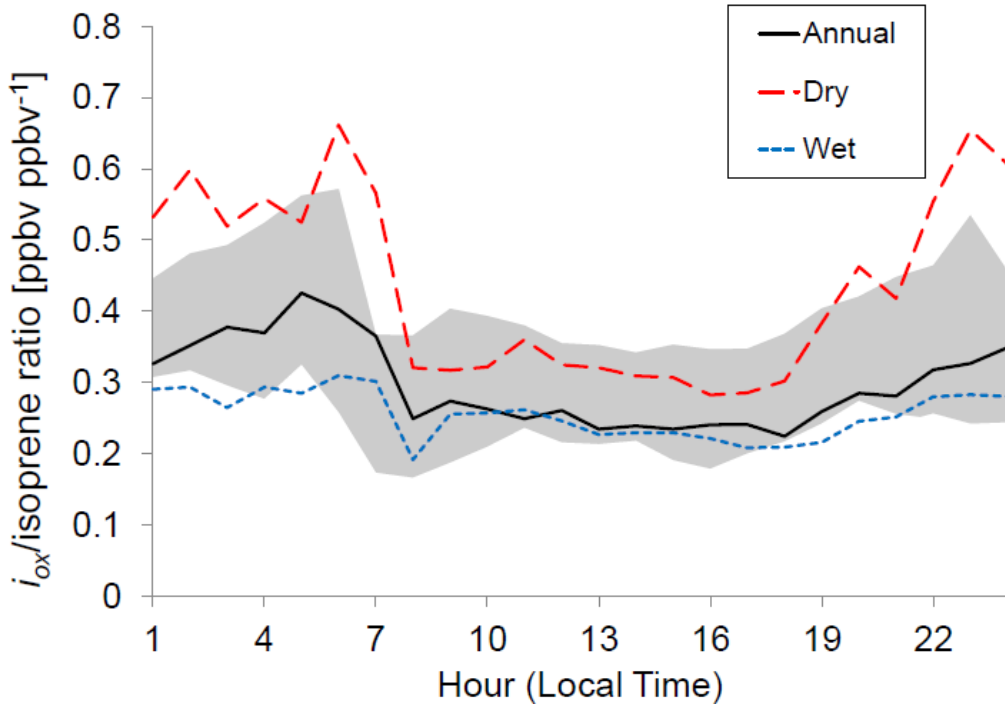
**Figure 6.4.** Diurnal profile of the median ratio of isoprene oxidation products ($i_{ox}$) to isoprene mixing ratios (ppbv ppbv$^{-1}$) for the dry season (dashed red), wet season (dotted blue), and for the entire period (solid black) with the interquartile range (shaded).

When compared with previous studies the measured $i_{ox}$/isoprene ratio of 0.29 (median) and 0.36 (mean) in this study was somewhat lower. For example mean ratios of 0.54 were found by Karl *et al.* (2004) at 42 m and 0.5-1.1 at 53 m at ZF2 by Andreae *et al.* (2002), but our results are consistent with a study in Rondonia, Brazil, which reported mean values of 0.23 ± 0.09 and 0.30 ± 0.16 during the wet and dry seasons, respectively (Kesselmeier *et al.*, 2002), as well as with a study at a nearby site showing ratios of 0.1 and 0.3 at 40 m during the wet and dry seasons, respectively (Yañez-Serrano *et al.*, 2015). These ratios will, to some extent, depend on the amount of vertical mixing and the measurement height above the canopy used. Because isoprene follows an emission profile where daytime isoprene mixing ratios decrease with height above the canopy (Yañez-Serrano *et al.*, 2015), while $i_{ox}$ shows a deposition gradient, the ratio $i_{ox}$/isoprene will increase with height, the effect being more pronounced at low turbulence, when the same flux induces a stronger gradient. Additionally, advected air masses — assumed to contain $NO_x$ emissions from increased seasonal biomass burning, as evident from black carbon mass

153

concentration measurements at the site — could have contributed to increased $O_3$ levels and thus higher oxidative capacity above the canopy during the dry season.

## 6.3.4 Modelling isoprene emissions using the Guenther algorithms (G95 and MEGAN)

The Guenther *et al.* (2006) Model of Emissions of Gases and Aerosols from Nature (MEGAN) was used to back-out isoprene base emission rates at standard conditions of temperature and PAR from the measurements. These were compared with those produced from the Guenther *et al.* (1995), termed G95, model to assess how well the model captures the temporal variability of the measured fluxes. The basic algorithm in MEGAN is an extension of the initial G95 model:

$$F = \varepsilon \times \gamma \times \rho, \tag{6.2}$$

where $\varepsilon$ is the base emission rate (mg m$^{-2}$ h$^{-1}$) of isoprene from a canopy at standard conditions of temperature and light intensity (30 °C and 1500 μmol m$^{-2}$ s$^{-1}$ PAR), $\gamma$ is a light and temperature dependent emission activity factor and $\rho$ accounts for production and loss within the canopy (Guenther *et al.,* 2006). The base emission rate, $\varepsilon$, can be considered to be the characteristic emission rate for a given ecoregion. In MEGAN, the base emission rate is modified by factors representing instantaneous and short-term variations from standard conditions (i.e., the emission activity, $\gamma$, and loss, $\rho$, factors). Any factors that can plausibly affect overall emissions but which are not captured by the $\gamma$ and $\rho$ functions will be incorporated into the base emission rate and will cause it to fluctuate on the time- and space-scales relevant to the un-modelled factors. Such un-modelled factors could include seasonal phenology, circadian control, and other long-term factors (Hewitt *et al.*, 2011). Both the G95 and the parameterised canopy environment emission activity (PCEEA) model of MEGAN were used to determine the annual base emission rate and model performance was compared (Section 6.3.4.2). The following results were determined using the PCEEA model.

The annual base emission rate at standard conditions of 30 °C and 1500 μmol m$^{-2}$ s$^{-1}$ PAR was calculated from the regression slope of all the measured hourly fluxes against hourly values of $\gamma \times \rho$, resulting in an annual canopy-scale base emission rate of 4.8 ± 0.3 mg m$^{-2}$ h$^{-1}$ (Figure 6.5a). This is 19% lower than the value of 5.9 ± 0.1 mg m$^{-2}$ h$^{-1}$ previously obtained at the ZF2 site from a limited data set during the dry season (Karl *et al.*, 2007). Generally, estimates of the base emission rate parameter are based on very limited data from short term observations and a summary is provided with comparisons with previous studies (see Table 6.3). Karl *et al.* (2007) took measurements during the late dry season only, and indeed the median emission factor for the dry season determined in this study of 5.4 ± 0.1 mg m$^{-2}$ h$^{-1}$ agrees more closely. The canopy base emission rate of this study was also provided for the wet season and was lower at 4.3 ± 0.1 mg m$^{-2}$ h$^{-1}$. The estimates are, however, well in the range of other measured and modelled emission rates using various techniques and model versions (see Table 6.3 or Holm *et al.,* 2014 and Sindelarova *et al.,* 2014 for an extensive review).
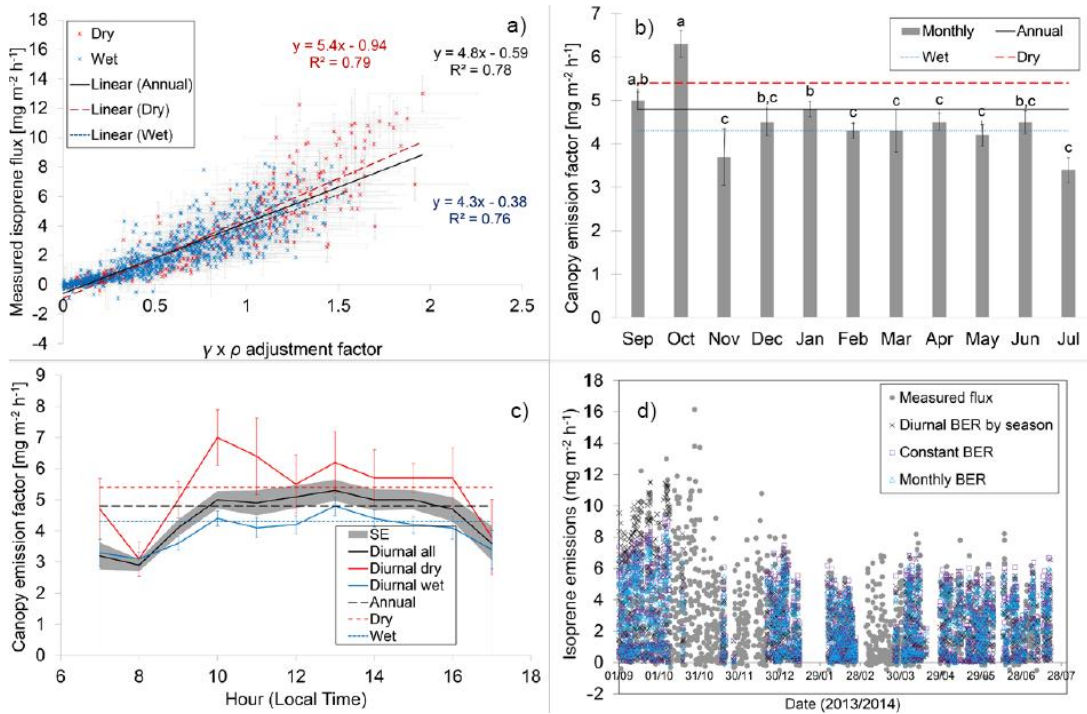
**Figure 6.5. a)** Scatter plot showing measured isoprene emissions (mg m$^{-2}$ h$^{-1}$) plotted against the environment and loss factors ($\gamma \times \rho$) of the Guenther *et al.* (2006) MEGAN algorithm with the linear regressions, coefficients ($R^2$), and formulae for all the data (black), the dry season (red), and the wet season (blue) only. **b)** Bar chart showing monthly median canopy base emission rates with standard errors and the annual (solid black), dry (dashed red) and wet (dotted blue) seasons medians. Lowercase letters denote groups of statistically significant difference using Tukey's post hoc Honestly Significant Difference test. **c)** Diurnal profile of base emission rates (mg m$^{-2}$ h$^{-1}$) during the daytime (07:00 – 17:00 local time) for the total period (solid black) with standard errors (shaded), dry (dashed red) and wet (dotted blue) seasons with error bars. **d)** Comparison of measured (grey dots) and modelled isoprene fluxes using the PCEEA model with base emission rates at different temporal resolutions: annual (purple squares), monthly (blue triangles), and diurnal (black cross).

### 6.3.4.1 Base emission rates of isoprene

The most decisive factor regarding the quantitative fit between the measurements and the PCEEA model estimated emissions was the base emission rate $\varepsilon$. Due to the method used to derive $\varepsilon$, the base emission rate represents the average canopy emission rate and this already includes many factors, such as canopy shading effects, as opposed to an aggregated emission rate based on individual species or genera, foliage mass, and canopy properties (Guenther *et al.*, 1994). Both

models underestimated the canopy average emissions as the environmental response factors in the models were based on leaves and branches lower in the canopy and are not representative of the entire canopy. Further differences can be seen when using hourly, daily or monthly average temperatures and PAR, which can show a difference in total modelled isoprene emissions of up to 70% (Ashworth *et al.*, 2010; Wang and Jacob, 1998).

In high biodiversity ecosystems such as the Amazon tropical forest, it is exceedingly difficult to compile inventories of individual plant species and distributions. Often genera or family level classifications are obtained. However, this information is insufficient as a basis to estimate bVOC emissions using a bottom-up inventory approach, since there is such high variability in the emission capacity even within individual plant species in terms of base emission rates, foliage properties, and environmental drivers (Harley *et al.*, 1999; Sharkey and Loreto, 1993). Furthermore, the high biodiversity at the site means that a large number of tree species are represented and separate leaf level emission measurements of each species would be required to identify isoprene emitting species and distributions to accurately determine the ecosystem level emission rates.

A study of species distributions in the Amazon forest has shown that there are often groups of common species with high frequency and abundance that form predictable oligarchies, which can dominate thousands of square kilometres of forest (Pitman *et al.*, 2001). A more recent study confirmed this by showing that regionally in the Amazon a small number of species can be hyperdominant (Ter Steege *et al.*, 2013). In terms of representativeness of the measurement site, these studies support the notion that the point measurements from TT34 presented here may be highly representative of large areas of lowland *terra firma* in the Amazon Basin.

The most abundant tree families at the site by both stem density (stems ha$^{-1}$) and basal area (m$^2$ ha$^{-1}$) are *Lecythidaceae*, *Sapotaceae*, *Euphorbiaceae* and *Caesalpinaceae* (Jardim and Hosokawa, 1987; Oliveira and Mori, 1999). These families each include several hundred to several thousand species and without species-level identification, this makes estimating isoprene

emissions from leaf-level measurements virtually impossible, given the known inter-species variability in isoprene emission rates.

The use of plant functional types (PFT) allows ecosystems to be divided into groups of plants depending on their function within the system. These groupings often reflect phylogenetic and phenological properties, as well as physical characteristics, and may not necessarily coincide with bVOC emission capacities. Guenther *et al.* (2006) suggest the use of isoprene emission factors for a range of PFTs based on the dominant species within Olson's 867 ecoregions (Olson *et al.*, 2001). Global averages of individual PFTs produce representative emission factors for each biome, however the accuracy of regional-level emission rates are strongly dependent on available measurements, which can differ greatly within the same PFT between regions. The dominant species within a PFT may vary, with one dominant being an isoprene emitter but another being a non-emitter. This can result in large uncertainties in estimated emission rates on a regional scale.

### 6.3.4.1.1 Base emission rates at higher temporal resolutions

The PCEEA algorithm used to determine annual average base emission rates at standard conditions can also be used to differentiate between monthly and diurnal, i.e. circadian-controlled, canopy emission factors, which are shown in Figures 6.5b and 6.5c respectively. Monthly base emission rates (Figure 6.5b) varied between $6.3 \pm 0.3$ mg m$^{-2}$ h$^{-1}$ in October and $3.4 \pm 0.3$ mg m$^{-2}$ h$^{-1}$ in July, which was statistically significant ($F$ statistic $= 7.94$, $p < 0.001$). These followed the seasonal pattern observed in isoprene emissions (Section 6.3.1.2), implying that not all the seasonal factors determining isoprene emissions have been removed in the derivation of the base emission rate. The time series is too short to allow any multi-month cycles to be characterised, but the fact that the variation around the mean is not random is suggestive of such cycles existing. The low base emission rate during July and resulting suppression of emissions may be due to leaf flushing at the beginning of the dry period and has been observed using indirect quantification by satellites (Barkley *et al.*, 2009).

Diurnal variability in base emission rates (Figure 6.5c) followed a similar profile as those in Hewitt *et al.* (2011) with a plateau between 10:00 and 15:00 local time, although rates varied

overall between $5.1 \pm 0.4$ mg m$^{-2}$ h$^{-1}$ at 12:00 local time and $2.9 \pm 0.2$ mg m$^{-2}$ h$^{-1}$ at 08:00 local time. Lowest hourly rates remained around 3 mg m$^{-2}$ h$^{-1}$ during both the wet and dry seasons, however peak emission rates reached $7 \pm 0.9$ mg m$^{-2}$ h$^{-1}$ during the dry season and only $4.4 \pm 0.3$ mg m$^{-2}$ h$^{-1}$ during the wet season. The observed diurnal plateau corresponded to the total seasonal emission rates of $6 \pm 0.9$ mg m$^{-2}$ h$^{-1}$ during the dry season and $4.3 \pm 0.3$ mg m$^{-2}$ h$^{-1}$ during the wet season.

Applying diurnal emission factors for the respective seasons improved the model slope fit ($R^2 = 0.78$, $p < 0.001$, slope = 0.92) and also greatly improved the reproduction of the seasonal variability of emissions in the model, especially during the dry season, which was not fully accounted for using a constant annual base emission rate using only light, temperature and canopy loss factors. However, the median modelled emissions using diurnal emission factors were closer to the measurements which represented a reduction of 18% compared with the median modelled emissions using a constant base emission rate. This indicates that using annual average base emission rates determined from the average of both seasons would underestimate dry season and overestimate wet season emissions. Hence, assuming that base emission rates measured during only one season are representative for the whole year can lead to a strong bias of modelled emissions, either high or low depending on the season during which the measurements were made. This would have consequences on the global or regional-scale modelling of secondary pollutant formation such as $O_3$ and bSOA. Using the example of $O_3$ formation, the modelled concentration ratio of VOC/NO$_x$ would be more variable under circadian-controlled isoprene emissions (Hewitt *et al.*, 2011).

### *6.3.4.1.2 Effects of phenology on model fit*

Any differences observed in the higher resolution base emission rates are due to effects not captured by the light, temperature and within canopy loss algorithms in the model. One variable unaccounted for may be phenological effects. Compared with temperate deciduous forests, there is less seasonal variation of LAI in tropical forests, despite the occurrence of leaf flushing events (Nelson *et al.*, 2014). The monthly LAI for the ZF2 study area obtained from the

Terra/MODIS database varied between 4.3 and 6.5 $m^2$ $m^{-2}$, which is comparable to other tropical forests (Maass *et al.*, 1995). During leaf flushes, many trees become deciduous or semi-deciduous prior to flushing. Completion of the crown flushing takes place within a month. This tends to happen during the driest months (June - October), although the timing varies widely between tree species and even between years. This may have a significant effect on bVOC emission rates, as young leaves do not emit isoprene and only begin to emit isoprene days to weeks into their development after acquiring photosynthetic competence (Sharkey *et al.*, 2008). At this point young mature leaves have the highest isoprene emission capacity at standard light and temperature conditions. The isoprene emission capacity then declines with leaf age (Alves *et al.*, 2014). Data from 2010 and 2011 show evidence that leaf flushing at this site occurs for a number of trees during June and July (Alves *et al.*, 2014; Nelson *et al.,* 2014), which would result in leaves reaching maturity and hence peak isoprene emission capacities in September and October.

Although the MEGAN model attempts to account for leaf age ($\gamma_{age}$) using this term did not greatly improve the model fit, presumably because seasonal foliage patterns can show high spatial and temporal variability. To improve the qualitative model fit of the term $\gamma_{age}$ for evergreen or semi-deciduous forests would require further integrated long-term measurements to provide information on inter-annual variability of bVOC emissions and links with tree phenology.

### *6.3.4.1.3 Comparisons of measured and modelled isoprene fluxes from different tropical forests*

Table 6.3 shows that the annual and seasonal isoprene emission rates measured at the site are comparable to previous studies at the same location in the Amazon, but higher than emission rates from natural rainforests in Borneo and other sites in Latin America. It is likely that differing species-specific base emission rates are the cause of lower isoprene emissions from the natural rainforest in Borneo, as average environmental drivers are similar (Langford *et al.*, 2010a). Measurements made from a monoculture oil palm plantation in Borneo showed very high emission rates due to the high emission capacity of this species (Misztal *et al.*, 2011). These, as well as the loose definition of base emission rates ($\varepsilon$) for the model algorithm, may account for

some of the differences in estimates. $\varepsilon$ is usually either aggregated from leaf-level emission rates of individual species or canopy-scale measurements, wherein $\varepsilon$ is calculated from the fit with the light and temperature parameter and canopy-loss factor. In the latter case, the entire dataset of flux measurements can be used or subsets thereof, such as daytime (07:00-17:00 local time) or midday (usually 10:00 – 15:00 local time) periods only, which greatly increases $\varepsilon$ (cf., Figure 6.5c). Furthermore, estimates derived from canopy-scale flux measurements are often lower than leaf-level emission estimates, as they already include terms for loss effects (Misztal *et al.*, 2011).

*Table 6.3. Measured isoprene fluxes (mean ± standard deviation) and base emission rates (ε) ± standard error at normalised conditions in mg m⁻² h⁻¹ where available, and regression coefficients of modelled fluxes using the Guenther algorithms to measurements for eddy covariance flux studies above lowland tropical forests.*

| Location (site) | Season | Measurement duration | Mean flux | Mean midday flux | $\varepsilon$ | $R^2$ | Method | Reference |
|---|---|---|---|---|---|---|---|---|
| Amazon, Brazil (Cuieiras Reserve) | W & D | 258 days | 2.87 ±2.7 | 4.79 ± 3.3 | 4.8 ±0.3 | 0.78 | vDEC, G06 | House *et al.*, this study |
| Amazon, Brazil (Cuieiras Reserve) | D | 61 days | 4.39 ±3.0 | 8.1 ±3.6 | 5.4 ±0.1 | 0.79 | vDEC, G06 | House *et al.*, this study |
| Amazon, Brazil (Cuieiras Reserve) | W | 197 days | 2.35 ±2.1 | 3.73 ±2.4 | 4.3 ±0.1 | 0.76 | vDEC, G06 | House *et al.*, this study |
| Amazon, Brazil (Cuieiras Reserve) | LD | 15 days | NA | 7.8 ±2.3 | 5.9 ±0.1 | 0.80 | vDEC, G06 | Karl *et al.*, 2007 |
| Amazon, Brazil (Cuieiras Reserve) | ED | 8 days | 2.38 ±1.6 | 6.12 | NA | NA | REA | Kuhn *et al.*, 2007 |
| Amazon, Brazil (Tapajós) | LW | 3 days | 1 | 2 | 2.4 | NA | DEA, G95 | Rinne *et al.*, 2002 |
| Costa Rica (La Selva) | D | 20 days | 1.35 | 2.9 | NA | NA | vDEC | Karl *et al.* 2004 |
| Borneo, SE Asia (Danum Valley) | LW, ED | 48 days | 0.93 ±1.3 | 1.9 | 1.6[a], 2.5[b] | 0.47[a], 0.50[b] | vDEC, G06 | Langford *et al.*, 2010a |
| Borneo, SE Asia (Oil palm plantation) | LW, ED | 11 days | 4.39 ±6.4 | 9.7 ±7.2 | 7.8[a], 18.8[b] | 0.75[a], 0.91[b] | vDEC, G06 | Misztal *et al.*, 2011[c] |

[a] G06 model using standard coefficients

[b] G06 model using optimised or fitted coefficients

[c] Fluxes are from an oil palm planation

NA, details are not available

D: dry season, W: wet season, ED: early dry, LD: late dry, EW: early wet, LW: late wet seasons.

## 6.3.4.2 Model details and comparisons between model versions

In order to determine the best fit between our observations and modelled fluxes the G95 and PCEEA MEGAN models were compared (Table 6.4). In all simulations the parameters were either taken from Guenther *et al.* (1995; 2006) or derived from ambient and satellite measurements. For the PCEEA the in-canopy loss parameter $\rho$ was calculated based on friction

velocity ($u_*$), canopy depth (15 m), and above canopy isoprene lifetime (s), which itself was estimated using measured average daytime OH concentrations from Vaughan *et al.* (2012). The calculated campaign average of $\rho$ was 0.95 (0.93-0.96), although a constant $\rho$ value of 0.96 can be assigned in the PCEEA model, since $\rho$ ranges from 0.93 to 0.99 for most conditions (Guenther *et al.*, 2006).

The use of additional algorithms to replace assumed constants in the PCEEA model, such as the calculation of leaf age ($\gamma_{age}$) and within-canopy isoprene loss ($\rho$), increased the regression coefficient ($R^2$) by <0.01, and in the G95 model, leaf temperature ($T_{leaf}$) decreased $R^2$ from 0.51 to 0.22 ($p$ <0.001). The leaf age algorithm is intended for deciduous canopies and is assumed to equal 1 for evergreen trees. However, rainforest canopies undergo leaf flushing, the effect of which may need to be taken into account via a different algorithm (see Section 6.3.4.1.2). Leaf temperatures were estimated using Nemitz *et al.* (2009) and when implemented in $\gamma$ and plotted against measured fluxes, it introduced a more linear fit, although at the expense of greatly increasing variability and hence reduced qualitative model fit.

Of all the model variations tested, the simple PCEEA most closely reproduced the time variability of the measurements, displaying a linear regression coefficient between the total measured and modelled fluxes of $R^2 = 0.78$ ($p$ <0.001). However, a slope (modelled/measured) of 0.78 implies that the constant emission factor used with this model would need to be 20% higher to accurately reproduce measured fluxes.

*Table 6.4. A comparison of Guenther 95 and MEGAN PCEEA algorithms used to determine base emission rates ($\varepsilon$) of isoprene emissions (mg m$^{-2}$ h$^{-1}$) at ZF2 with regression coefficients ($R^2$) of linear regressions of measurements to the environment adjustment and, for the PCEEA model, loss factors.*

| Model version | $\gamma$ algorithm | $\gamma_{CE}$ | $R^2$ | $\varepsilon$ |
|---|---|---|---|---|
| G95 | $C_L \times C_T$ | NA | 0.51 | 4.9 |
| MEGAN: PCEEA | $\gamma_{CE} \times \gamma_{age} \times \gamma_{SM}$ | $\gamma_{LAI} \times \gamma_P \times \gamma_T$ | 0.78 | 4.8 |

Mean calculated variables used in the determination of $\gamma$ for the MEGAN PCEEA version include $\gamma_{age} = 1.01$ and $\rho = 0.95$.

Parameters used in the MEGAN PCEEA version were taken from Guenther *et al.* (2006) and included $\gamma_{SM} = 1$, $C_{T1} = 80$, $C_{T2} = 200$, $A_{new} = 0.05$, $A_{gro} = 0.6$, $A_{mat} = 1.125$, $A_{old} = 1$, $\lambda = 0.3$.

Monthly averages of leaf area index (LAI) based on information of the leaf canopy spectral properties were retrieved from the NASA Earth Observations database for the $0.1 \times 0.1°$ area including the tower and ranged between 4.3 and 6.5 $m^2$ $m^{-2}$ (NEO, 2014). Variations in PAR and temperature accounted for much of the average variability, the dependence of which was evident from plots of averaged isoprene fluxes against ambient PAR and temperature measurements, which showed strong relationships (see Section 6.3.2), but the model failed to capture the full extent of increase during the dry season when using a constant annual or monthly base emission rate (Figure 6.5d). Only the diurnal base emission rates for the respective seasons reproduced the seasonal variability. This has potentially large implications as the seasonal periods of peak isoprene emissions are not accurately represented in emission models and that the seasonal increase may not entirely result from increased light and temperature.

In the PCEEA model, the parameter $\gamma$ is derived from light, temperature and LAI dependent terms, of which the former two parameters consider both instantaneous conditions and the environmental conditions averaged over the respective month. The comparison between models shows that the PCEEA MEGAN algorithms performed better than the original G95 model for estimating isoprene fluxes in the tropics, as the G95 algorithms were developed using data from temperate tree species.

### 6.3.4.3 Uncertainty estimation

An estimate of overall model uncertainty was attempted using total error propagation of contributing parameters to the models and resulted in <16% uncertainty for the PCEEA and <10% for the G95 model. The introduction of additional terms, which rely on estimates or observations associated with higher errors increased overall uncertainty of the PCEEA model. The G95 light and temperature adjustment factor stipulates the use of leaf temperature, however, as these were not available ambient air temperature was used. Estimating leaf temperature using algorithms from Nemitz *et al.* (2009) decreased the model fit markedly ($R^2 = 0.22$, $p$ <0.001). Detailed Monte Carlo uncertainty simulations of various MEGAN-based model output versions have shown that individual input parameters, especially those related to leaf temperature as used in the standard

MEGAN and G95 models, can cause up to 61% of model output uncertainty (Holm *et al.*, 2014). The PCEEA algorithm was used, as it showed a closer model fit than G95. Due to the lack of direct observations of estimated variables it is unclear whether the observed increase in uncertainty was a result of using additional algorithms in the estimation or poor predictive capacity of the model.

## 6.3.5 Flux footprint modelling

The flux footprint for each 45 min period for the whole measurement duration was calculated using the Microsoft Excel-based tool developed by Neftel *et al.* (2008), which employs the analytical footprint model of Kormann and Meixner (2001). The Kormann-Meixer model exclusively uses micrometeorological parameters from the eddy covariance measurements to determine the 2-D footprint density function. Individual footprints were calculated for each measurement period using the corresponding friction velocity ($u_*$), Obukhov length ($L$), measurement height ($z_m$), horizontal wind velocity at the measurement height ($u(z_m)$), and the standard deviation of the lateral wind ($\sigma_v$). The upwind surface flux $F_c$ *(x, y, 0)* determines the vertical turbulent flux $F_c$ *(0, 0, $z_m$-d)* at the measurement point, i.e. the measurement height ($z_m$) minus the zero-plane displacement height ($d = 2/3 \, x$ canopy height, $h$), leading to

$$F_c(0,0,z_m - d) = \int\limits_{\infty}^{-\infty} \int\limits_{0}^{\infty} F_c(x,y,z_m - d)\Phi(x,y,z_m - d)dxdy, \quad (6.3)$$

where the x-axis is aligned with the mean horizontal wind direction and $\phi(x, y, z_m\text{-}d)$ is the weighted footprint function describing the influence of a unit point source on an area flux from a specific surface location *(x, y)*. Boundary layer conditions were mostly unstable (63% frequency), defined as $\zeta = (z_m\text{-}d)/L < 0.2$, and stable conditions were mostly at night. User defined spatial elements were mapped as a 500 m resolution grid with nearest easterly grid squares being subdivided into 250 m long units (Figure 6.6) and footprint contributions (%) of each element were calculated. The gridded area included on average 96% (median) and 82% (mean) of the footprint area, which corresponded to a footprint size, defined as the area from which 99% of the flux originates, of 0.36 km$^2$ (median) and 0.56 km$^2$ (mean) during daytime periods of unstable

and near neutral stratification and 3.64 km$^2$ at night. Low wind speeds and stable stratification at night greatly increased the extent of the footprint area.
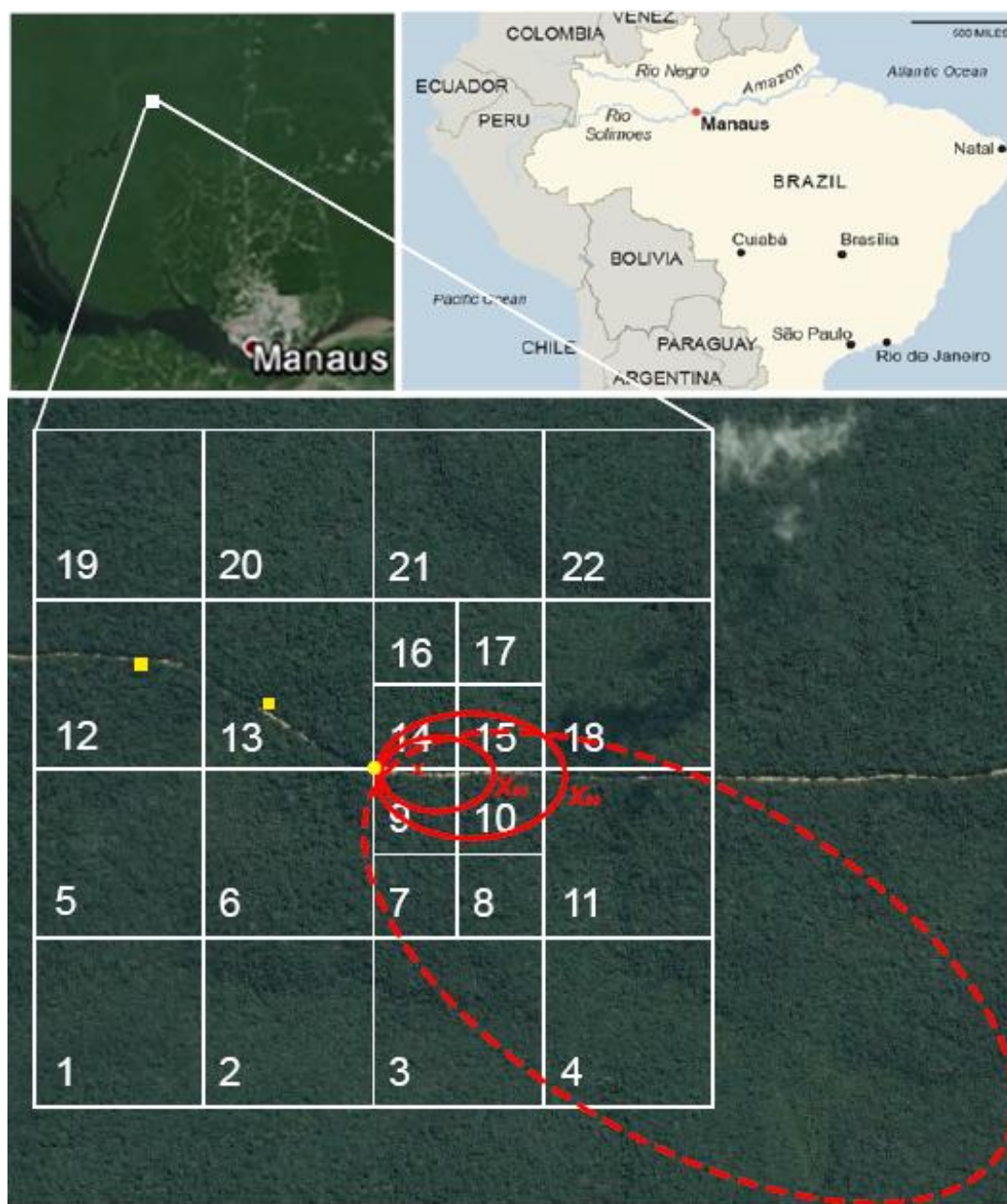


**Figure 6.6.** A visible satellite image showing the measurement site with the TT34 tower (yellow circle), generator and living quarters (yellow squares), a 500 m resolution grid overlaid (white) with numbered grid cells and subdivided cells of 250 m, and approximations of the calculated median flux footprint during stable night time periods (dashed red), the daytime median area contributing 99% to the flux ($X_{99}$), 90% ($X_{90}$), and the location of the daytime footprint peak ($X_{max}$) is indicated by the red cross with references to Manaus and Brazil. Imagery © 2015 Landsat, Map data © 2015 Google.

Comparisons with the Kljun *et al.* (2004) footprint parameterisation model using average daytime conditions and boundary layer heights from Fisch *et al.* (2004) showed that the footprint peak location ($X_{max}$) was at a distance of 120 m from the tower during the day and 194 m at night. The distance encompassing 90% of the footprint contributions ($X_{90}$) extended to 314 m during the day and 530 m at night. Due to the dominant easterly wind direction (52% frequency) with minor deviations to the N (18% frequency) and S (19% frequency), the easterly squares coinciding with $X_{max}$ contributed on average (mean $\pm$ SD) the most to the measured flux, i.e. squares 9 (18.5% $\pm$ 22%) and 14 (22% $\pm$ 26%), followed by the nearest surrounding squares 6 (9% $\pm$ 20%), 10 (3.6% $\pm$ 5%), 11 (2.6% $\pm$ 5%), 13 (7.5% $\pm$ 17%), 15 (3.7% $\pm$ 5%), and 18 (2.4% $\pm$ 4.8%), with the rest contributing on average <1%.

The forest to the E and upwind of the flux tower is located on a small plateau, which is flat and fairly homogeneous, providing almost ideal conditions for flux measurements. However, there are slopes to the W and S of the tower and these lower areas had slightly different canopy structures and heights. Wind direction analysis showed that largest fluxes were seen with E winds followed by N, S, and W directions for isoprene and monoterpenes (*F* statistic = 30.32, *p* <0.001 and *F* statistic = 40.04, *p* <0.001 respectively). Fluxes of $i_{ox}$ showed no statistical difference with wind direction (*F* statistic = 1.56, *p* = 0.18). Deposition was greatest from the E and N followed by S and W directions during the morning, but this was balanced by some afternoon emissions from the N and E. As the heterogeneous terrain in wind directions other than from the E introduces additional uncertainties and that the majority of the fluxes originated from the E, this analysis remains inconclusive in determining whether the differences in fluxes resulted from terrain effects on the micrometeorology or differing source strengths. However, the high frequency of E winds implied that any anthropogenic interferences on VOC fluxes from the nearby living quarters and power generators to the W were minor (Figure 6.6).

Correlating the percent contribution of each square with the measured flux can provide information on emission source strengths, distributions and vertical mixing within the flux

footprint, where high contributions from a square with correlating high fluxes indicate strong emission sources or emission drivers, including micrometeorological effects. Conversely, areas of high contributions with low corresponding fluxes reveal lower emission source strengths, emission drivers or negative fluxes through increased removal via photochemistry or deposition. Isoprene and monoterpenes showed a positive correlation with increasing contributions from squares 9 and 14 and negative correlations with the remaining squares. The inverse pattern was seen from $i_{ox}$ with negative correlations with increasing contributions from squares 9 and 14, and positive correlations with the rest of the squares. In this case, the source footprint area for the majority of fluxes coincided with the extensive *terra firma* plateau system to the E of the tower. This suggests that emission sources in this direction were relatively homogeneous and that the observed spatial and temporal patterns of bVOC fluxes probably arose from meteorological variations and photochemical processing.

The majority of photochemical conversion of isoprene to $i_{ox}$ takes place above the measurement height some distance above the canopy, causing the measured oxidation product flux to be overall negative as deposition occurred (Kesselmeier *et al.*, 2000). This was also shown from mixing ratio measurements at various heights within and above the canopy by Yañez-Serrano *et al.* (2015), where highest $i_{ox}$ mixing ratios were observed at 79 m above the canopy around noon coinciding with peak isoprene concentrations at 24 m resulting in estimated peak oxidative capacities at a height of 53 m determined from the $i_{ox}$/isoprene concentration ratio.

Due to the net deposition of $i_{ox}$ the correlation was negative, resulting in lower deposition when footprints were largest and greater deposition with small footprints. When the defined squares included most of the footprint area, i.e. smaller footprints, isoprene and monoterpene fluxes were larger (Spearman's correlation coefficient $r = 0.71$ and $r = 0.66$, $p < 0.01$ respectively) and $i_{ox}$ deposition was greater ($r = -0.37$, $p < 0.01$), due to the increased turbulence and hence vertical mixing.

In this study a minimum grid resolution of 250 m was required to map contributions for the squares around the tower due to the strong positive skew of the flux footprint density function,

with the majority of the emissions originated from these closest easterly squares. However, beyond a distance of 500 m from the tower this grid resolution was insufficient to produce clear trends or features of statistical significance due to the low number of data points from this area. Therefore, a 500 m grid resolution was implemented for the outermost squares. The low number of data points originating from most of the squares when grouped by month also caused a lack of observable trends. As a result, further detailed temporal analysis yielded no conclusive results.

### 6.3.6 Air mass back trajectories and land cover

The ZF2 site in the Cuieiras Reserve represents an ideal site to study bVOC emissions from a pristine primary tropical forest with no or minimal anthropogenic interferences. Many bVOCs have a relatively short atmospheric lifetime with respect to oxidation by OH, ranging from hours to several days. The combination of typically low wind speeds and distance of the site from primary anthropogenic emission sources such as urban areas, agriculture and major roads are sufficient to minimise contamination, as bVOC mixing ratios decline through photochemical processing and deposition before reaching the measurement site. Although the wind direction at this site is usually constrained to the east, calculating air mass back trajectories over several days and comparing them with land cover maps can highlight any possible periods where advection of pollution may have occurred as a result of the tracked air parcel passing over areas of anthropogenic activities. Therefore, back trajectories were calculated using the HYSPLIT (Hybrid Single Particle Lagrangian Integrated Trajectory) model (Draxler and Rolph, 2008), which was run at 3 h release intervals starting at a height of 10 m from the site and propagated 96 h backwards in time for the period of September 2013 to July 2014 (Figure 6.7).

Air mass back trajectories were limited to the area NE to SE of the site with some exceptions of southerly directions in October 2013. The heights of the air parcels remained within the boundary layer and passed over large areas of forest with some back trajectories reaching as far as the Atlantic Ocean. Figure 6.8 shows the land cover types of this area at a resolution of 1 km$^2$ per pixel (Eva *et al.*, 2002). Such maps may underestimate or overestimate land cover classes over fragmented areas depending on the spatial organisation of the respective class, but on a

continental scale can provide representative land cover estimates. Most of the area is covered by lowland evergreen tropical forest with some areas of freshwater flooded tropical forest and flooded savannah along the Amazon River. This area has limited land transport connectivity, so the river provides the main transport route for human communities. This is reflected by the areas of mosaic agriculture and degraded forests with some intensive agriculture and patches of shrub savannah with little or sparse vegetation along the river banks and towards the Amazon Delta. Urbanised areas (population size in millions) along the river are Manaus (1.8), Santarém (0.2), and Macapá (0.4). Back trajectories indicated several periods of multiple days when air masses passed over Manaus.
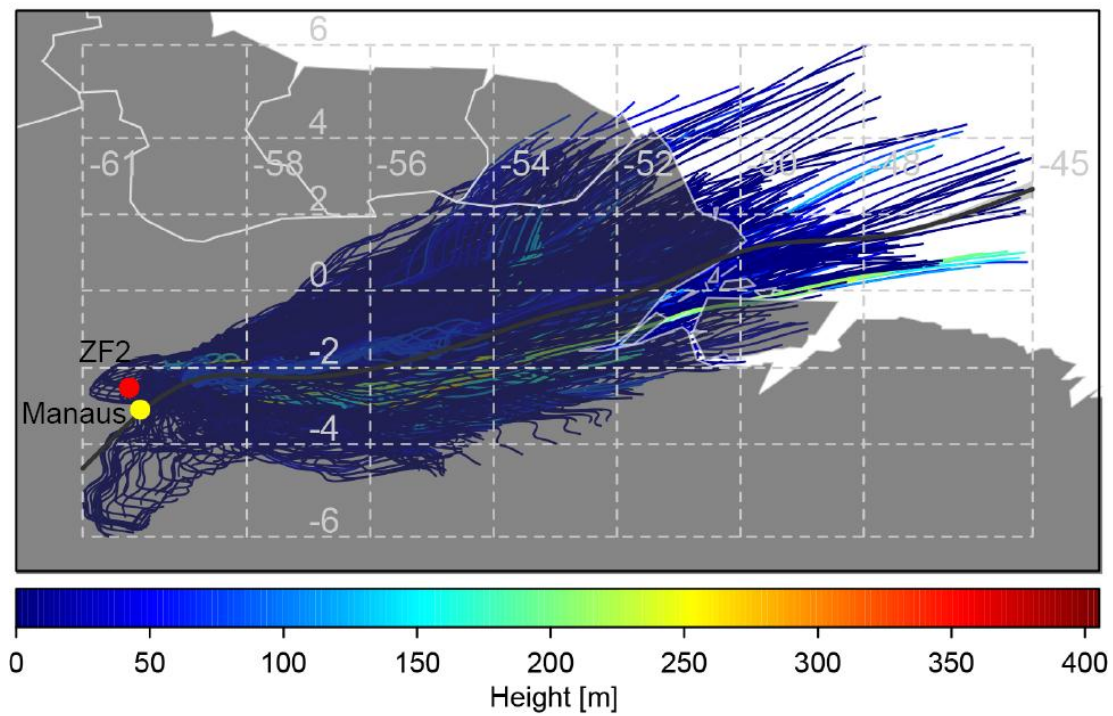


**Figure 6.7.** Plot showing all and the average of calculated back trajectories using the HYSPLIT model with the air mass height (m) within the boundary layer (colour bar), the measurement site (ZF2, red dot), Manaus (yellow dot). Particles were released from the site at ground level (10 m height) and propagated 96 h backwards. The thick black line represents the average trajectory.

Data available on local black carbon (BC) aerosol mass concentrations by Multi Angle Absorption Photometry were used to compare with the back trajectories, as well as to confirm and identify further periods of possible anthropogenic influences such as from biomass burning. The dry season is the peak fire season with increased slash and burn activities associated with mosaic agricultural systems as identified on the land cover map. This was reflected by increased BC concentrations during September and October 2013 somewhat extending through November, December 2013, and January 2014.
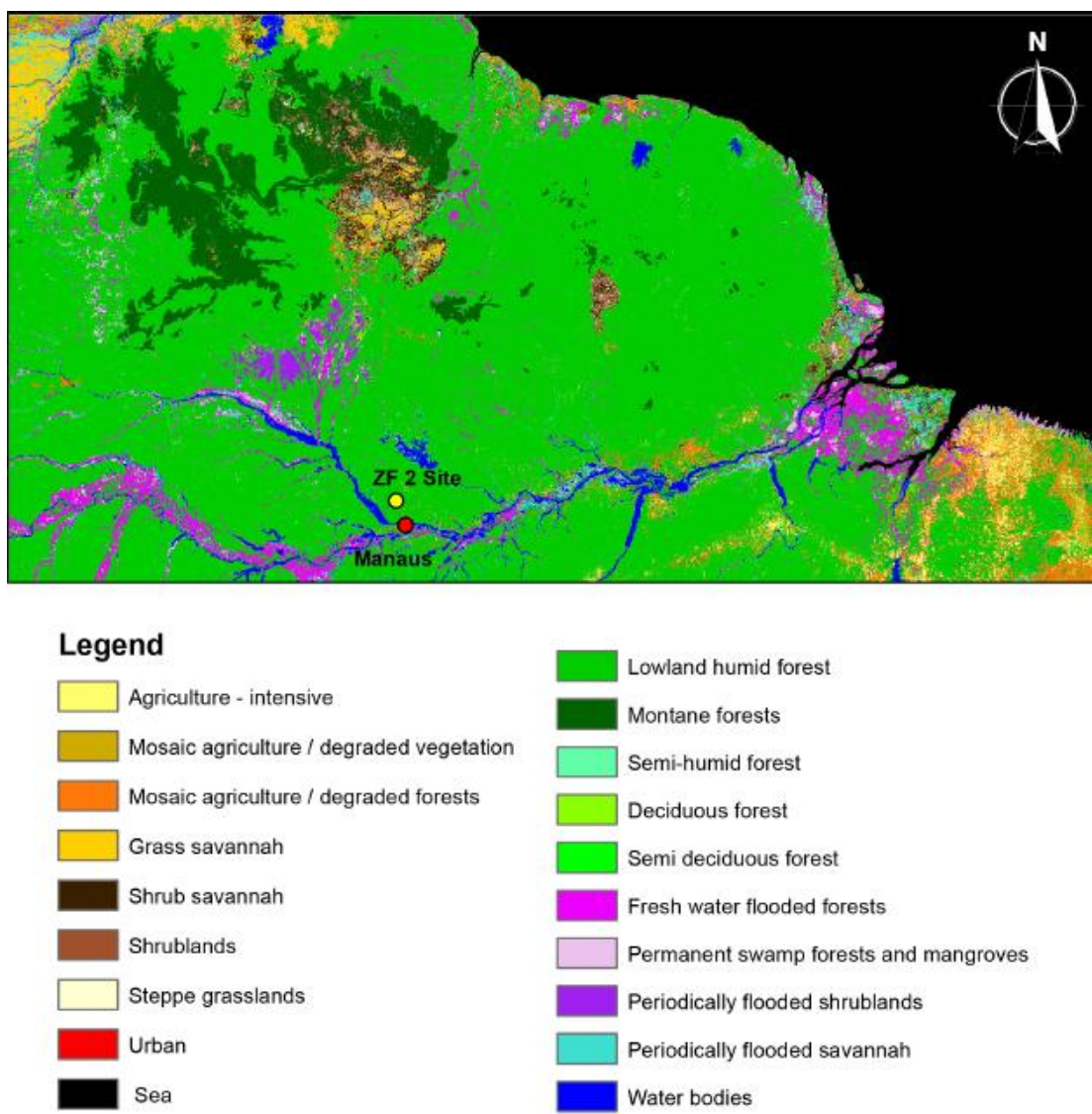


**Figure 6.8.** A map of northwestern South America showing land cover types where 1 pixel represents 1 km$^2$ with references to the ZF2 measurement site (yellow dot) and Manaus (red dot). Categories are given in the legend. Section reproduced from Eva *et al.* (2002).

In total the following periods were considered likely to have anthropogenic interferences: 16 - 25 September 2013, 15 - 28 October, 5 - 12 December, 1 - 4 January 2014, 19 March, and 5 - 7 May 2014. There were periods (1 - 5 November 2013 and 25 June – 4 July 2014) where back trajectories indicated a southerly course before reaching the site, however BC concentrations during those periods remained relatively low (<0.5 μg m$^{-3}$) suggesting little or no contamination from Manaus on those days. VOC concentrations of $m/z$ 69, 71 and 137 have short atmospheric lifetimes and showed no anomalies during these periods suggesting that measurements of the selected $m/z$ at this site were unaffected by anthropogenic influences. In general, wind direction analyses of these VOC mixing ratios followed those of fluxes, whereby isoprene and monoterpene mixing ratios were highest from the E, followed by N, S, and W ($F$ statistic = 1818 and $F$ statistic = 1295, $p$ <0.01 respectively), whereas $i_{ox}$ concentrations were highest from the E, followed by S, then W and N ($F$ statistic = 1429, $p$ <0.001).

## 6.4 Conclusions

The first long-term continuous measurements of bVOC fluxes and mixing ratios by virtual disjunct eddy covariance and proton transfer reaction mass spectrometry above a primary tropical rainforest have yielded detailed information on temporal variability of emissions, deposition and mixing ratios on seasonal and diurnal scales. Median emission rates of isoprene and monoterpenes and deposition rates of isoprene oxidation products ($i_{ox}$) were higher during the dry season than during the cooler wet season, by a factor of ~2 for isoprenoids and ~1.30, respectively. Median mixing ratios measured ~10 m above the canopy top during the dry season were higher by a factor ~1.5 for isoprenoids and ~2 for $i_{ox}$ than during the wet season. Compound fluxes and mixing ratios of isoprene and monoterpenes were highly correlated with photosynthetically active radiation (PAR) and temperature. Average and peak emissions and mixing ratios were comparable with those obtained by previous short-term measurements in the same area of the central Amazon forest, but were substantially higher than those measured in tropical forests in SE Asia (Langford *et al.*, 2010a) and in Costa Rica (Karl *et al.*, 2004). This difference was reflected in the base emission rates at normalised environmental conditions of 30

°C and 1500 μmol m$^{-2}$ s$^{-1}$ PAR, which were calculated for the whole year, for each season, for each month and for each hour of the day during the dry and wet seasons, respectively.

The base emission rates at 30 °C and 1500 μmol m$^{-2}$ s$^{-1}$ PAR and canopy level emissions of isoprene were best modelled using the PCEEA algorithm from Guenther *et al.* (2006). Base emission rates were determined at diurnal, monthly and seasonal time resolutions and these showed significant variability. For example, monthly base emission rates varied from $3.4 \pm 0.3$ mg m$^{-2}$ h$^{-1}$ to $6.3 \pm 0.3$ mg m$^{-2}$ h$^{-1}$ and hourly base emission rates varied from $2.9 \pm 0.2$ mg m$^{-2}$ h$^{-1}$ at 08:00 to $7 \pm 0.9$ at 10:00 local time. The use of diurnally-varying base emission rates to model annual isoprene emissions resulted in median annual emissions which matched measured emissions and were ~20% lower than emissions obtained using an annual average fixed base emission rate, but reproduced the seasonal variability more accurately than when using a constant or even monthly emission rates. Using increased temporal resolutions of the base emission rates gave some improvement to the overall model fit, but improvements were strongly biased depending on the season. The variations in isoprene base emission rates observed from sunrise to sunset and from one season to another indicate that using a single annual average value for the base emission rate will produce significant errors when estimating isoprene emissions during periods with increased seasonal variability. Hence, this has implications for the modelling of atmospheric chemistry on a regional or global scale. Where possible, time resolved base emission rates should be used for estimating isoprene emission rates.

Flux footprint and air mass back trajectory models showed that the observed emissions were of very local origin and that anthropogenic influences (on both local and regional scales) on the site were minimal. The site is surrounded by vast expanses of virtually undisturbed primary forest and the area within the flux footprint is likely highly representative of large areas of lowland tropical forests in the central Amazon.

This dataset is the first of its kind, consisting of continuous flux and above canopy volume mixing ratios during the dry and wet seasons, and will continue to provide further important

contributions to our understanding of the biosphere-atmosphere exchange of VOCs over tropical forests.

## Acknowledgements

# Chapter VII

## 7 Conclusions

In this thesis flux and mixing ratio measurements of volatile organic compounds (VOC) from two contrasting atmospheric environments were made – from a polluted urban environment in one of the world's largest cities (Paper I and Paper II) and from a pristine background site in the largest contiguous forest ecosystem on Earth (Paper III). In the first study the ground-level mixing ratios of a range of anthropogenic VOCs (aVOC) and in the second study, the fluxes and mixing ratios of aVOCs above the street canopy were quantified in central London, UK, during 4 weeks in winter 2012 and then over a period of five months beginning in August 2012. These studies captured the temporal variability in mixing ratios at different heights and, in the latter study, fluxes at different resolutions as well as the high spatial variability of emission sources in a complex urban environment. The third study investigated emissions of biogenic VOCs (bVOC) from the largest single source of VOCs globally, the Amazon rainforest. These represent the first long-term flux measurements from a rainforest and spanned eleven months during 2013-2014. Significant seasonalities in emission rates, fluxes and mixing ratios were observed. This chapter will compare the results of these studies and discuss the wider implications of the main findings.

### 7.1 Conclusions from London

Cities are known to emit a huge number and range of different VOCs (Lewis *et al.*, 2000), but here we focussed on a small selection of representative compounds with a multitude of emission sources and which are emitted with high spatio-temporal variability. The results showed that vehicle emissions were the dominant source of aromatic VOC fluxes and resulting mixing ratios. Oxygenated VOCs and isoprene originated from several different sources, some of which had strong light and temperature dependencies, indicating contributions from evaporative, biogenic or secondary atmospheric sources. The London Atmospheric Emissions Inventory

(LAEI) estimates that solvent use and road transport are the main contributors to VOC emissions in London and our results are consistent with this. The NAEI estimates that the selected VOCs quantified during the flux measurements contribute 15% of total VOC emissions from London (Bush *et al.*, 2006). Our data do not allow us to confirm this as we have no measurements of the total organic carbon emitted.

The combined VOC emission rate of measured species in the footprint area of central London ($\pm$ standard error) was $12.4 \pm 0.3$ t km$^{-2}$ a$^{-1}$, whereas the emission rate for the same species and area taken from the NAEI was $9.6 \pm 0.8$ t km$^{-2}$ a$^{-1}$, which is a difference of approx. 30%. There may be several reasons why the measured emission rates exceeded the NAEI estimated emission rates: i) the NAEI emissions may be underestimated, if the estimates are based on inaccurate activity information or on inaccurate emission factors, ii) the NAEI excludes specific sectors from the urban emissions profile, such as emissions from nature, which may in fact contribute to emissions in London; iii) the data used to speciate VOC emissions from specific sources is out of date, and/or iv) measured emissions may be overestimating VOCs due to isobaric interferences or other unidentified instrumental problems. Based on the measured emission rates and assuming that the measurement period was representative of annual emissions, total VOC emissions in central London (defined as the Congestion Charge Zone, CCZ, i.e. an area of 21 km$^2$) would equate to 2.1 kt a$^{-1}$. This estimate is again higher than the modelled emission estimate of 1.6 kt a$^{-1}$ from the NAEI for 2012, but lower than the previous estimate of 3.9 kt a$^{-1}$ from the LAEI 2010 database.

Clearly emission rates in the centre of London are higher per unit area than from the much larger Greater London Area (GLA, i.e. 1579 km$^2$). As traffic emissions represent a major source in the CCZ, imposing greater restrictions on traffic volume may provide the largest improvement in air quality.

In order to reduce the formation of ozone, it is necessary to achieve a VOC/NO$_x$ ratio that is removed from that of optimal O$_3$ formation. Therefore, the balance between VOC and NO$_x$ mixing ratios must be carefully considered when designing strategies to curb air pollution.

VOC/NO$_x$ ratios of ≤4:1 result in VOC-limited atmospheric chemistry, where greatest reductions in O$_3$ will result from reducing VOC emissions, but O$_3$ concentrations will increase with decreasing NO$_x$. The VOC/NO$_x$ ratio in London from measurements at 60 m above ground level and approx. 25-35 m above the surrounding roof height was 0.86. However, this ratio only includes VOC species in the measurement selection, which as discussed above probably only represent 15% of all VOC emissions. Additionally, the reactivity weighting of the photochemical ozone creation potential (POCP) of individual VOC species must be considered. When both factors are included, a VOC/NO$_x$ ratio of 1.9 is estimated from our measurements. This value compares relatively well with the weighted total VOC/NO$_x$ ratio of 2.49 from ground-level measurements at Marylebone Road made during the same five month period by the Automatic Hydrocarbon Network (AHN, http://naei.defra.gov.uk/data/data-selector). A VOC/NOx ratio of ~2 represents a strongly VOC-limited atmospheric environment (Sillman, 1999), which suggests that decreasing VOC emissions in central London would decrease the amount of O$_3$ formed. Further increasing NO$_x$ emissions and hence NO$_x$ mixing ratios would also lead to lower O$_3$ mixing ratios due to NO$_x$-titration (Bohnenstengel *et al.*, 2015). This is not to say that increasing NO$_x$ emissions would be a desirable air quality strategy, since NO$_2$ is itself harmful to human health and is a regulated pollutant, and current mixing ratios in central London exceed European Commission Directive limit values. However, decreasing NO$_x$ emissions without concomitant reductions in VOC emissions would increase O$_3$ formation.

Indications of a biogenic source contribution to isoprene emissions during the summer in central London are of interest, as although isoprene emissions are low, the high POCP of isoprene increases the weighting of the VOC/NO$_x$ ratio in favour of O$_3$ production. Urban biogenic VOC emissions are not currently included in air quality models, as they are assumed to be negligible. However, our measurements showed that up to 30% of the isoprene flux signal was temperature-dependent and likely of biogenic origin during the summer when emissions are higher. Biogenic isoprene emissions represent 0.3% of total VOC emissions or 2.2% of the measured VOC species in London during summer. The POCP weighting increases this contribution to total VOC

emissions to 0.4% and 2.5% of measured VOC species in summer. However, the mixing ratios of total isoprene in summer increases with the POCP from 7% to 14% of weighted VOC mixing ratios measured at the site.

Tree density is fairly low in the centre of London, but increases with the number and size of green areas in the GLA. Furthermore, street trees, which are common in London and other urban centres, are not normally included in tree inventories, even though they constitute up to 50% of urban tree crowns. Estimates of biogenic VOC emissions must take individual trees into account, since high isoprene emitting tree species, such as *Platanus x acerifolia* are often favoured as street trees due to their crown size and hardiness. When selecting species for urban trees the species specific VOC emission rates should be considered, focusing on low emitting species. Furthermore, air masses with high biogenic isoprene mixing ratios from suburban and peri-urban areas with extensive forests and green spaces can cause plumes of peak $O_3$ levels when advected over urban areas (MacKenzie *et al.*, 1991). It is therefore important to include bVOCs in urban air pollution models.

## 7.2 Conclusions from the Amazon forest

Fluxes and mixing ratios of isoprene, total monoterpenes, and the oxidation products of isoprene ($i_{ox}$), including methyl vinyl ketone (MVK), methacrolein (MACR), and isoprene hydroxy hydroperoxide (ISOPOOH) products, were measured at a pristine forest background site in the Amazon Basin over a period of eleven months. Emission variability during both the wet and dry seasons was clearly reflected in both measured VOC fluxes and above-canopy mixing ratios. Isoprene and monoterpene fluxes strongly correlated with temperature and photosynthetically active radiation (PAR) and were higher by a factor of two during the dry season, in September and October, than during the rest of the year when rainfall was higher and temperatures lower. Peak temperatures and PAR, and therefore peak emissions, were seen in October, although phenological effects may have also contributed to the timing of peak emissions (Alves *et al.*, 2014).

The base emission rate of isoprene determined from the MEGAN PCEEA algorithm from Guenther *et al.* (2006) showed an annual canopy base emission factor of $4.8 \pm 0.1$ mg m$^{-2}$ h$^{-1}$ at standard conditions (30 °C and 1500 μmol m$^{-2}$ s$^{-1}$) with large variations in monthly and diurnal base emission rates. During the dry season the base emission rate reached $5.4 \pm 0.1$ mg m$^{-2}$ h$^{-1}$, whereas it was $4.3 \pm 0.1$ mg m$^{-2}$ h$^{-1}$ during the wet season. These values compared well with those from previous studies in the same geographic region, but, especially during the dry season, were higher than from other tropical forests. The high variability in base emission rates indicates that not all seasonal emission variability can be accounted for using only the light, temperature and canopy loss factors in their current form in the parameterised MEGAN algorithm. The use of base emission rates at higher temporal resolutions increased the fit of modelled isoprene emissions, successfully reproducing the seasonal differences. The average diurnal base emission rates varied between $2.9 \pm 0.2$ mg m$^{-2}$ h$^{-1}$ during the early morning and peaking at $5.3 \pm 0.4$ mg m$^{-2}$ h$^{-1}$ around midday. Seasonal differences were more pronounced in diurnal base emission rates, ranging from around $3 \pm 0.3$ mg m$^{-2}$ h$^{-1}$ at 08:00 to midday peak values of $4.8 \pm 0.3$ mg m$^{-2}$ h$^{-1}$ during the wet season and $7 \pm 0.9$ mg m$^{-2}$ h$^{-1}$ during the dry season.

Total monoterpene mixing ratios were one order of magnitude lower than those of isoprene, but fluxes were around 25% of those of isoprene, which demonstrates a higher gas-phase reactivity of a large proportion of monoterpene compounds emitted at this site. Fluxes of $i_{ox}$ showed a net deposition to the canopy, which increased during the dry season. The ratio of the $i_{ox}$ mixing ratio to that of isoprene was 0.25 on average throughout the daytime, but increased to 0.35 at night and 0.65 during the night-time dry season respectively. Higher ratios of oxidation products to their isoprene parent compound indicate a greater atmospheric oxidative capacity, which changes with height within and above the canopy (Yañez-Serrano *et al.*, 2015), as well as environmental drivers and co-occurring compounds, such as NO$_x$. High dry season photochemistry was supplemented by NO$_x$ and additional VOC emissions from seasonal biomass burning for mosaic agriculture resulting in an enhanced oxidative capacity.

Flux footprints and modelled air mass back trajectories suggested that measured bVOC fluxes originated locally and generally with minimal contamination from anthropogenic sources throughout the year. Intensification of biomass burning and anthropogenic influences within the Amazon forest will likely have significant effects on tropospheric chemistry with a potential of large increases in ground level $O_3$ formation as $NO_x$ mixing ratios increase. Removal of large areas of forest may also increase regional temperatures and reduce precipitation and this in turn might lead to increases in bVOC emission rates.

The POCP-weighted sum of bVOC mixing ratios was estimated using the measurements made in this study for peak periods (12:00-15:00 local time) and assuming that the measured compounds comprise only 50% of total VOCs at the site (methanol, acetone and acetaldehyde mixing ratio measurements are not shown here). This fraction is in line with the mixing ratio measurements of Yañez-Serrano *et al.* (2015). If a $NO_x$ mixing ratio of 1 ppbv is assumed, this implies a VOC/$NO_x$ ratio of 11. However, if $NO_x$ mixing ratios are lower than 1 ppbv, then the VOC/$NO_x$ ratio would be even higher. This suggests that the atmospheric chemistry at the site is clearly within the $NO_x$-limited regime with respect to $O_3$ formation. Therefore, any increase in $NO_x$ emissions (e.g. from enhanced biomass burning, vehicle emissions or urbanisation) and thus increases in $NO_x$ mixing ratios at the site would lead to enhanced $O_3$ formation and hence higher $O_3$ mixing ratios.

Air masses generally passed over extensive areas of mostly undisturbed primary forest before reaching the site, which is likely to be highly representative of large expanses of lowland tropical forest in the central Amazon Basin. Therefore, an estimate of annual net VOC emissions from the Amazon tropical forest could be attempted. Assuming the seasonality of the measurement site is representative for the whole forest, the sum of measured average net fluxes of isoprene for each season (i.e. 3.6 and 1.9 mg m$^{-2}$ h$^{-1}$ for dry and wet seasons respectively) scaled up according to the duration of their respective seasons and to the total area of the rainforest (i.e. $5.5 \times 10^6$ km$^2$) would result in a net annual emission of $55 \pm 0.6$ Tg a$^{-1}$. The same method applied to monoterpenes would result in net annual monoterpene emissions from the Amazon of

around $14 \pm 0.6$ Tg a$^{-1}$, and $i_{ox}$ fluxes would result in a net annual deposition of $2.2 \pm 0.1$ Tg a$^{-1}$ of isoprene oxidation products to the canopy. Overall this leads to a net annual emission of reactive VOCs of $\sim 67 \pm 1.3$ Tg a$^{-1}$. This value only represents the direct emission of isoprene and monoterpenes and although these compounds are quantitatively dominant, many more compounds such as methanol, acetonitrile, acetaldehyde, acetone, are known to contribute to the overall bVOC flux. Although several of these compounds were included in our measurements, their emissions were mostly below the detection limit and hence were not shown in the analysis. However, due to the relatively long atmospheric lifetime of several oxygenated compounds, their contribution to the total VOC mixing ratio may be significant, albeit their small emissions. In light of this, it is unknown exactly how many different compounds in total are emitted from this site, and also therefore, what the flux of total organic carbon from the canopy may be.

The scaled up emission estimates from measurements compared well with those from a previous study, which estimated 60 Tg a$^{-1}$ isoprene emissions for a 5 x 10$^6$ km$^2$ area of the Amazon (Rasmussen and Khalil, 1988). Few studies have scaled up isoprene emissions from the Amazon forest individually, as many emission models use plant functional types instead of specific locations, as these are generally composed of several functional types. Generally, the Amazon is the single largest contributor of isoprene emissions from global tropical forests, which have been estimated to be 95 Tg a$^{-1}$, 12 Tg a$^{-1}$, and 39 Tg a$^{-1}$ for isoprene, monoterpene, and total other reactive compounds respectively (Guenther *et al.* 1995). Determining a representative annual emission rates specifically for the Amazon forest is therefore vital to ensure better model accuracy and performance.

The Guenther algorithms use a scaling factor to reproduce the variations of emissions from standard environmental conditions in conjunction with a constant base emission rate. Modelled total isoprene emission estimates using the Guenther algorithm with a constant annual base emission rate and assuming a 12 h emission period produce total annual emissions from Amazonia of $58 \pm 0.6$ Tg a$^{-1}$, which is 5% higher than the annual estimate derived from the measurements, whereas the estimated total emissions using base emission rates at higher temporal

resolutions such as diurnal rates lowers the emission to $52 \pm 0.5$ Tg a$^{-1}$. These figures do not reflect the seasonal variations, which using the constant base emission rate produces larger biases during both seasons, whereas a varying base emission rate by time of day and season reduces both biases. It must be noted that due to the method used to derive the base emission rates, this model does not provide an independent comparison to the measured emissions, hence the close match, but can be used to compare relative differences between model estimates using different base emission rates and the model fit at higher time resolutions (see Sindelarova *et al.,* 2014 for a more detailed model evaluation).

Median model outputs compared overall well with measured emissions regardless of the base emission rate used, however, determination of base emission rates at higher frequencies has shown that using a constant base emission rate results in a significant bias, positive or negative, between seasons. This bias is not always obvious when only considering annual model averages, which resulted in differences up to 30% (e.g. G95 algorithm) between total annual modelled and measured emissions. However, short-term, such as seasonal, variability can show seasonal peak variability up to a factor of 2, which has implications if base emission rates from one season are assumed to represent the annual average in the model. These results are consistent with previous estimates, whereby global isoprene emissions are estimated to be up to 50% of modelled emissions using various versions of the Guenther algorithm (Prather *et al.*, 2001; Sindelarova *et al.*, 2014).

This comparison shows that depending on the method used, annual isoprene emission estimates from the Amazon lowland forests may be over- or underestimated by up to a factor of ~2 and/or poorly reproduce seasonal differences resulting in seasonally biased estimates if employing a fixed annual base emission rate that does not capture the seasonal and diurnal variability. If only annual emission estimates are required then the use of either varying base emission rates at higher time resolutions or a fixed base emission rate would provide a fairly accurate estimate. However, if models are required to reproduce seasonal or diurnal emission variability, then the use of diurnally varying base emission rates by season is necessary to avoid

significant seasonal bias. These findings have large implications when isoprene emissions are required at higher time resolutions in atmospheric chemistry or climate models.

## 7.3 Overall conclusions

In Chapter 2, Table 2.1 compared global estimates of VOCs and their emissions from biogenic sources in a natural environment with those from anthropogenic sources in an urban environment. Table 7.1 compares the similarities and differences in VOCs using the example of the Amazon rainforest as a natural environment and London as an example of an urban environment. The table has been expanded using estimates derived from the flux measurements (in parenthesis and/or **bold** font) from this thesis and compares these with values taken from the literature. It is important to note that in both environmental domains VOC measurements consisted of only a few targeted compounds that were selected due to their importance (i.e. reactivity or toxicity) or quantitative dominance. Although isoprene is the most dominant VOC in the Amazon, there are many more species that contribute to total VOC emissions, such as methanol, acetaldehyde, and acetone that were not included in the measurements. Short-term measurements from a nearby site that include a wider range of compounds indicated that the sum of the additional compounds can represent up to 50% of total VOC mixing ratios above the forest canopy (Yañez-Serrano *et al.*, 2015). In an urban environment such as London, the VOC composition consists of a vast array of different species, with a majority of reactive carbon mass originating from $C_6$-$C_{14}$ compounds, including aromatics (Lewis *et al.*, 2000). The NAEI speciation database estimates that ethanol represents the largest contribution, i.e. 11%, to VOC emissions in the UK and the sum of measured compounds in London represent around 15% of total VOC emissions in the UK. There are no data available on VOC speciation at a regional level within the UK.

*Table 7.1. Comparison of biogenic and anthropogenic volatile organic compound species, emissions and effects based on measurements of VOC fluxes and mixing ratios from the Amazon tropical forest and London.*

| Category | Amazon, Brazil | London, UK |
|---|---|---|
| *Dominant compounds emitted* | Isoprene<br>Monoterpenes<br>$i_{ox}$ (MVK, MACR, ISOPOOH products) | $C_2$-benzenes<br>Toluene<br>Methanol<br>Acetone |
| *Measured emission rates* | **2.7** mg $m^{-2}$ $h^{-1}$<br>(**2.2** mg $m^{-2}$ $h^{-1}$ isoprene, **0.59** mg $m^{-2}$ $h^{-1}$ monoterpenes, **-0.09** mg $m^{-2}$ $h^{-1}$ $i_{ox}$) | **1.42** mg $m^{-2}$ $h^{-1}$<br>(**0.33** mg $m^{-2}$ $h^{-1}$ $C_2$-benzenes, **0.3** mg $m^{-2}$ $h^{-1}$ toluene, **0.27** mg $m^{-2}$ $h^{-1}$ methanol, **0.22** mg $m^{-2}$ $h^{-1}$ acetone) |
| *Emission estimates:* | | |
|   *Global* | 1150[a] TgC $a^{-1}$ | 110[h] Tg $a^{-1}$ |
|   *Regional* | 146[a] (**67**) Tg $a^{-1}$ global tropical rainforest (Amazon forest) (95[a] (**55**) Tg $a^{-1}$ isoprene, 12[a] (**14**) Tg $a^{-1}$ monoterpenes, 39[a] (**-2**) Tg $a^{-1}$ ORVOC ($i_{ox}$)) | 823[i] Gg $a^{-1}$ (UK)<br>1.6[j] (**2.1**) Gg $a^{-1}$ (central London) |
| *Typical chemical regime* | $NO_x$-limited | VOC-limited |
| *VOC/$NO_x$ [ppbv ppbv$^{-1}$]* | **11** | **1.9** |
| *Atmospheric lifetime[1]* | 1.4 h (isoprene)<br>2.6 h ($\alpha$-pinene)<br>4.1 h (MACR)<br>6.8 h (MVK)<br>12 d (methanol)<br>53 d (acetone) | 5.9 h (*m*-xylene)<br>1.9 d (toluene)<br>12 d (methanol)<br>53 d (acetone) |
| *POCP[2]* | 117.8 (isoprene)<br>18.2 (acetone) | 108.8 (*m*-xylene)<br>77.1 (toluene)<br>20.5 (methanol)<br>18.2 (acetone) |
| *Global SOA contribution* | Ca. 90%[e] 10-1820 [e,f,g] Tg $a^{-1}$<br>(19.1[e] Tg $a^{-1}$ (terpenes), 15[e] Tg $a^{-1}$ (other reactive VOCs), 2[m] Tg $a^{-1}$ (isoprene)) | 6 ± 2% 0.4-2.6[k] Tg $a^{-1}$<br>Or < 30% 3-25[l] Tg $a^{-1}$ |
| *Regional* | (**0.5-2.7** Tg $a^{-1}$)[n,o] Amazon rainforest | (**3-50** Gg $a^{-1}$)[n,o] Greater London |

[1] Atmospheric lifetimes with regard to OH using rate constants at 298 K taken from Atkinson (1997) and assuming a 12 h average daytime OH concentration of $2.0 \times 10^6$ molecule $cm^{-3}$.

[2] Integrated photochemical ozone creation potential (POCP) relative to ethylene from Derwent *et al.,* (1996).

References: a) Guenther *et al.* (1995), b) Guenther *et al.* (2000), c) Warneke *et al.* (1999), d) Lipari *et al.* (1984), e) Kanakidou *et al.* (2005), f) Goldstein and Gallbaly (2007), g) Hallqiust *et al.* (2009), h) Piccot *et al.* (1992), i) NAEI (2014), j) LAEI (2013), k) Tsigaridis and Kanakidou (2003), l) Volkamer *et al.* (2006), m) Claeys *et al.* (2004), n) Hao *et al.* (2011), o) Wood *et al.* (2010).

VOC emissions from the Amazon are higher both in terms of emission rates by land surface area, as well as total source area. On a land surface area basis, emission rates are higher by almost a factor of 2 compared to central London, and the POCP-weighted emission rates are higher in the Amazon on an area basis by almost a factor of 4, due to the high emissions of reactive isoprene from the Amazon rainforest. On a regional scale annual bVOC emissions from the Amazon are 2 orders of magnitude higher than the total national aVOC emissions from the UK.

The chemical regimes of the atmosphere for the two regions present a clear contrast. The VOC/NO$_x$ concentration ratio is very low in central London, i.e. 1.9, calculated using both ambient above-canopy VOC and NO$_x$ measurements, compared with a ratio of 11 above the forest canopy in the Amazon, which used above-canopy VOC mixing ratio measurements, but assumed a NO$_x$ mixing ratio of 1 ppbv. These chemical regimes represent two extremes in the "Sillman" continuum – central London is strongly VOC-limited and Amazonia is strongly NO$_x$-limited. This clearly points to the effects that changing primary emissions will have on ozone mixing ratios. In London, increasing VOC emissions, or reducing NO$_x$ emissions, will lead to increasing ozone concentrations. Hence, care is needed in the implementation of air quality control measures as reductions in NO$_x$ emissions must be accompanied by appropriate reductions in VOC emissions. In Amazonia, increasing VOC emissions (due to warming of the atmosphere) will not lead to increases in O$_3$, but increases in NO$_x$ emissions (from biomass burning or other anthropogenic activities) will lead to increases in O$_3$ concentrations.

In terms of secondary organic aerosol (SOA) formation, the compound-dependent SOA mass yields depend on VOC emissions and ambient NO$_x$ mixing ratios. Assuming the discussed chemical regimes in each area, the SOA yields were estimated from measured compound emissions and showed that total annual SOA yields from the Amazon forest would be 2-3 orders

of magnitude higher than from the Greater London Area. This is due to the larger emission source area, the emission of compounds with high SOA forming potentials such as monoterpenes, many of which produce a high aerosol yield, but also the large emissions of isoprene even though their relative yield is lower. Using an average yield of a range of the most common monoterpene species (i.e. $10 \pm 2\%$) (Hao *et al.*, 2011) and the mass yield of isoprene (i.e. 0.4%) (Claeys *et al.*, 2004) under low $NO_x$ conditions, the contribution of isoprene to the overall bSOA yield is estimated to be ~13%.

SOA yields from aVOCs were determined using estimated speciated yields under high $NO_x$ conditions taken from Wood *et al.* (2010) and showed that especially aromatic and higher carbon compounds contributed the most to SOA yields. Overall emissions of precursor VOCs were lower than from the Amazon forest and thus the total SOA yield was lower.

In terms of total carbon, even though the Amazon forest emits higher amounts of VOCs and $CO_2$, London represents a net source of carbon due to the massive emissions of $CO_2$ from fossil fuel combustion in the city. The Amazon is a large sink of $CO_2$, although observations of strong droughts in recent years have shown that increased tree mortality can release large amounts of carbon and turn the Amazon forest into a net $CO_2$ source (Lewis *et al.*, 2011; Phillips *et al.*, 2009). The majority (70-80%) of carbon in isoprene and monoterpene emissions results from recent photosynthesis of atmospheric $CO_2$, assuming sufficient soil moisture, temperature and PAR levels to drive photosynthesis and thus VOC emissions. Elevated atmospheric $CO_2$ concentrations up to around 500 ppmv due to the net emissions of anthropogenic $CO_2$ may increase the amount of carbon sequestered by plants via the carbon fertilisation effect (Ciais *et al.*, 2013), which in turn provides carbon for bVOC synthesis(Figure 7.1). However, there is evidence that increased $CO_2$ concentrations may inhibit isoprene synthesis (Young et al., 2009). Additionally, increased global mean surface temperatures and early shifts in regional climates are generally causing more environmental stress on plants, which produce and emit bVOCs to mitigate the effects of abiotic stress assuming sufficient nutrients are available. Furthermore, higher contributions of bVOCs to bSOA formation may provide a negative, stabilising feedback

in terms of global warming. Therefore, it is important to understand and be able to quantify the effects of each element in order to determine the net ecosystem response.
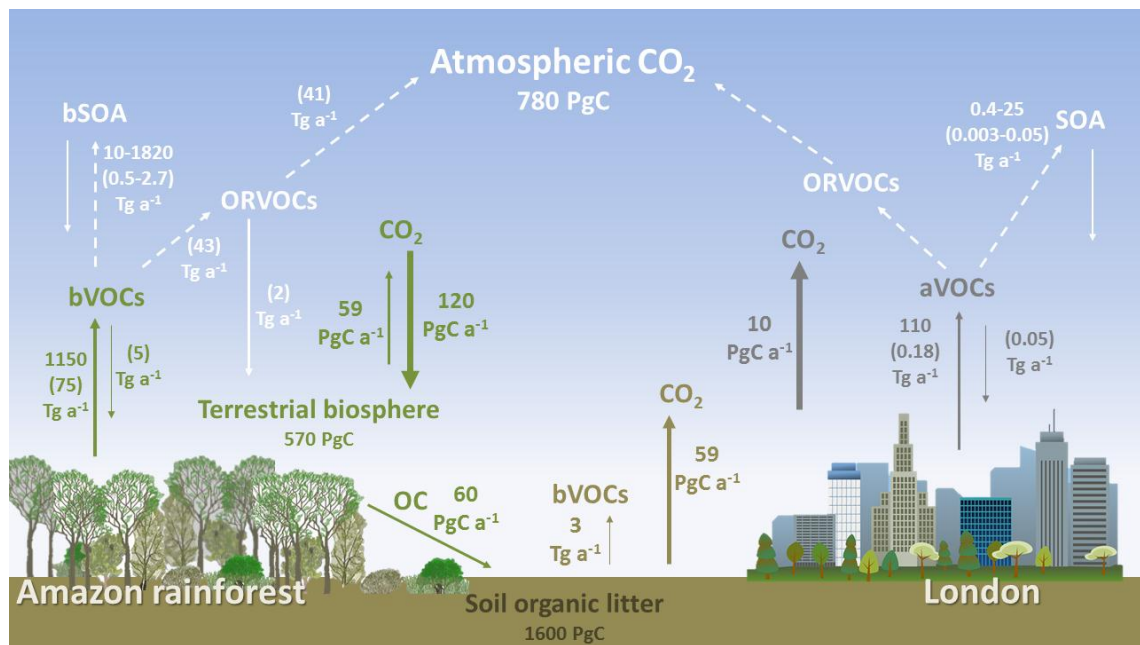


**Figure 7.1.** Diagram showing the global terrestrial carbon cycle of $CO_2$ emissions (taken from Drenzek, 2007 and Le Quéré *et al.*, 2013) supplemented by global emission estimates of VOCs from terrestrial vegetation (taken from Guenther *et al.*, 1995, Sawada and Tutsuka, 1986, and Warneck, 1988) and anthropogenic sources (taken from Piccot *et al.*, 1992) and estimated emissions of global secondary organic aerosols (taken from Goldstein and Gallbaly, 2007, Hallqiust *et al.*, 2009, Kanakidou *et al.*, 2005, Tsigaridis and Kanakidou, 2003, and Volkamer *et al.*, 2006) with scaled up emissions and depositional fluxes of VOCs in parenthesis representative of the Greater London Area and the Amazon rainforest using scaled measurements taken from Papers II and III. Estimates of further oxidation products and SOA formation in parenthesis were calculated from scaled measurements using yields taken from the literature (Claeys *et al.*, 2004, Guenther *et al.,* 1995, Hao *et al.*, 2011, and Wood *et al.*, 2010). Contributions from methane are not included.

To date there are only few direct measurements of VOC fluxes above the street canopy in urban environments. Legislation to curb air pollution strongly depends on estimated emission inventories which studies, including this thesis, have shown can greatly underestimate VOC emissions. Increased spatial and temporal resolution of VOC flux measurements are needed to validate and verify VOC emission estimates. Emission estimates must be updated accordingly

and enforcement of air quality policies must be based on the combined information from direct measurements, emission inventories and robust models. These observations overall help to improve the predictive capabilities of air quality models on a regional and local scale at high time resolutions, as well as provide a more reliable foundation on which legislation can be based.

Although there are several studies of direct canopy measurements of VOC fluxes in the tropics, the study presented in this thesis is the first that provides measurements of above-canopy fluxes and mixing ratios during all seasons at a high temporal resolution (1 h). These measurements give robust information on net VOC emissions, deposition of oxidation products, and canopy base emission rates of isoprene at a high temporal resolution throughout an 11 month period, which includes the wet and dry seasons. Generally, the results can help to constrain VOC emission budgets, which are used in global and regional models of atmospheric chemistry and climate. More specifically, these data are very valuable to future research, as they hold detailed information useful to a variety of disciplines, examples of which are mentioned below.

Information on emission and deposition budgets, as well as on the oxidative capacity of the troposphere taken from this dataset can be included in chemical box models and used to determine surface deposition and VOC reaction and radical cycling mechanisms in the tropics, as detailed chemical degradation mechanisms in clean environments are still not fully understood. Further long-term measurements are needed to capture inter-annual variability, including phenological effects, and the number of flux sites expanded to encompass the spatial variability not just throughout the Amazon rainforest, but also from other tropical forests around the world, which have been shown to possess very different VOC emission characteristics. The importance of general and species-specific phenological effects on VOC emissions are largely unknown in the Amazon forest and will require further integrated measurements of VOC fluxes and ecological monitoring in addition to the dataset presented here to isolate their individual effects. More detailed investigations using ecological measurements from the ZF2 site can be integrated with the results of this study to identify possible key periods of emission related plant activity. These data also provide information on canopy-scale light and temperature responses of VOC emissions,

188

which seem to plateau at higher levels than expected from leaf level measurements under controlled light and temperature conditions. This effect could be contributing to the underestimation of dry season emissions by current environment adjustment algorithms in emission models. Further investigation of leaf level VOC synthesis and leaf emission capacity under comparable conditions recreated in the laboratory may improve emission algorithms.

Overall both datasets present measurements of VOC fluxes by virtual disjunct eddy covariance and proton transfer reaction mass spectrometry made over periods of several months each and provide vital knowledge to constrain bottom-up inventories, emission budgets and thus models of atmospheric chemistry and climate.

# Bibliography

Alves, E. G., Harley, P., Gonçalves, J. F. de C., Moura, C. E. da S., and Jardine, K. (2014). Effects of light and temperature on isoprene emission at different leaf developmental stages of eschweilera coriacea in central Amazon. *Acta Amaz., 44*(1), 9-18.

Andreae, M. O., and Merlet, P. (2001). Emission of trace gases and aerosols from biomass burning, *Global Biogeochem. Cy., 15*(4), 955–966.

Andreae, M. O., Artaxo, P., Brandao, C., Carswell, F. E., Ciccioli, P., da Costa, A. L., Culf, A. D., EstevesJ. L., Gash, J. H. C., Grace, J., Kabat, P., Lelieveld, J., Malhi, Y., Manzi, A. O., Meixner, F. X., Nobre, A. D., Nobre, C. Ruivo, M. d. L. P., Silva-Dias, M. A., Stefani, P., Valentini, R., von Jouanne, J., and Waterloo, M. J. (2002). Biogeochemical cycling of carbon, water, energy, trace gases, and aerosols in Amazonia: The LBA-EUSTACH experiments. *J. Geophys. Res., 107*(D20), 8066.

Araújo, A. C., Nobre, A. D., Kruijt, B., Elbers, J. A., Dallarosa, R., Stefani, P., von Randow, C., Manzi, A. O., Culf, A. D., Gash, J. H. C., Valentini, R., and Kabat, P. (2002). Comparative measurements of carbon dioxide fluxes from two nearby towers in a central Amazonian rainforest: The Manaus LBA site. *J. Geophys. Res., 107*(D20), 8090.

Arneth, A., Miller, P., Scholze, M., Hickler, T., Smith, B., and Prentice, I. C. (2007a). CO2 inhibition of global terrestrial isoprene emissions: Potential implications for atmospheric chemistry. *Geophys. Res. Lett., 34*, L18813. doi: 18810.11029/12007GL030615.

Arneth, A., Niinemets, Ü., Pressley, S., Bäck, J., Hari, P., Karl, T., Noe, S., Prentice, I. C., Serca, D., Hickler, T., Wolf, A., and Smith, B. (2007b). Process-based estimates of terrestrial ecosystem isoprene emissions: incorporating the effects of a direct CO2-isoprene interaction. *Atmos. Chem. Phys., 7*, 31–53. doi:10.5194/acp-7-31-2007.

Arneth, A., Monson, R.K., Schurgers, G., Niinemets, Ü., and Palmer, P.I. (2008). Why are estimates of global terrestrial isoprene emissions so similar (and why is this not so for monoterpenes)? *Atmos. Chem. Phys., 8*, 4605–4620.

Arneth, A., Schurgers, G., Lathière, J., Duhl, T., Beerling, D. J., Hewitt, C. N., Martin, M., and Guenther, A. (2011). Global terrestrial isoprene emission models: sensitivity to variability in climate and vegetation. *Atmos. Chem. Phys., 11*, 8037–8052. doi:10.5194/acp-11-8037-2011.

Ashworth, K., Wild, O., and Hewitt, C. N. (2010). Sensitivity of isoprene emissions estimated using MEGAN to the time resolution of input climate data. *Atmos. Chem. Phys.,10,* 1193-1201.

Atkinson, R. (1997). Gas-Phase Tropospheric Chemistry of Volatile Organic Compounds: 1. Alkanes and Alkenes. *J. Phys. Chem. Ref. Data, 26*, 215. doi: 10.1063/1.556012.

Atkinson, R. (2000). Atmospheric chemistry of VOCs and NOx. *Atmos. Environ., 34*, 2063–2101.

Aubinet, M., Grelle, A., Ibrom, A., Rannik, Ü., Moncrieff, J., Foken, T., Kowalski, A. S., Martin, P. H., Berbigier, P., Bernhofer, Ch., Clement, R., Elbers, J., Granier, A., Grünwald, T., Morgenstern, K., Pilegaard, K., Rebmann, C., Snijders, W., Valentini, R., and Vesala, T. (1999). Estimates of the Annual Net Carbon and Water Exchange of Forests: The EUROFLUX Methodology. *Adv. Ecol. Res., 30*, 113-175.

Baldocchi, D. (2003). Assessing the eddy covariance technique of evaluating carbon dioxide exchange rates of ecosystems: past, present and future. *Glob. Change Biol., 9*, 479-492.

Baker, A.K., Beyersdorf, A.J., Doezema, L.A., Katzenstein, A., Meinardi, S., Simpson, I.J., Blake, D.R., and Rowland, F.S. (2008). Measurements of non-methane hydrocarbons in 28 United States cities. *Atmos. Environ*. 42 (1), 170-182.

Barkley, M. P., Palmer, P. I., De Smedt, I., Karl, T., Guenther, A., and Van Roozendael, M. (2009). Regulated large-scale annual shutdown of Amazonian isoprene emissions? *Geophys. Res. Lett., L04803*, 1-5.

Beerling, D. J., Hewitt, C.N., Pyle, J.A., and Raven, J.A. (2007). Critical issues in trace gas biogeochemistry and global change. *Phil. Trans. R. Soc. A, 365*, 1629-1642. doi: 10.1098/rsta.2007.2037.

Betts, A. K. and Silva Dias, M. A. F. (2010). Progress in Understanding Land-Surface-Atmosphere Coupling from LBA Research. *J. Adv. Model. Earth Syst., 2*, 1-20.

Blunden, J. and Arndt, D. S. (2014). State of the Climate in 2013. *Bull. Amer. Meteor. Soc., 95*, S1–S279.

Bohnenstengel, S. I., Belcher, S. E., Allan, J. D., Allen, G., Bacak, A., Bannan, T. J., Barlow, J. F., Beddows, D. C. S., Bloss, W. J., Booth, A. M., Chemel, C., Coceal O., Di Marco, C. F., Faloon, K. H. , Fleming, Z. L., Furger, M., Geitl, J. K., Graves, R. R., Green, D. C., Grimmond, C. S. B., Halios, C., Hamilton, J. F., Harrison, R. M., Heal, M. R., Heard, D. E., Helfter, C., Herndon, S. C., Holmes, R. E., Hopkins, J. R., Jones, A. M., Kelly, F. J., Kotthaus, S., Langford, B., Lee, J. D., Leigh, R. J., Lewis, A. C., Lidster, R. T., Lopez-

Hilfiker, F. D., McQuaid, J. B., Mohr, C., Monks, P. S., Nemitz, E., Ng, N. L., Percival, C. J., Prévôt, A. S. H., Ricketts, H. M. A., Sokhi, R., Stone, D., Thornton, J. A., Tremper, A. H., Valach, A. C., Visser, S., Whalley, L. K., Williams, L. R., Xu, L., Young, D. E., and Zotter, P. (2015). Meteorology, air quality, and health in London: The ClearfLo project. *Bull. Amer. Meteor. Soc.,* 96, 779–804.

Borbon, A., Fontaine, H., Veillerot, M., Locoge, N., Galloo, J. C., and Guillermo, R. (2001). An investigation into the traffic-related fraction of isoprene at an urban location. *Atmos. Environ., 35*, 3749-3760.

Brégonzio-Rozier, L., Siekmann, F., Giorio, C., Pangui, E., Morales, S. B., Temime-Roussel, B., Gratien, A., Michoud, V., Ravier, S., Tapparo, A., Monod, A., and Doussin, J.-F. (2015). Gaseous products and Secondary Organic Aerosol formation during long term oxidation of isoprene and methacrolein. *Atmos. Chem. Phys., 15*, 2953–2968. doi:10.5194/acp-15-2953-2015.

Broadway, G., and Tipler, A. (2008). Gas Chromatography: Ozone Precursor Analysis Using a Thermal Desorption- GC System (White Paper), pp. 1-13.

Bush, T., Tsagatakis, I., King, K., and Passant, N. (2006). *NAEI UK Emission, Mapping Methodology.*, AEA, Didcot, Oxfordshire, UK.

Cady-Pereira, K.E., Shephard, M.W., Millet, D.B., Luo, M., Wells, K.C., Xiao, Y., Payne, V.H., and Worden, J., (2012). Methanol from TES global observations: retrieval algorithm and seasonal and spatial variability. *Atmos. Chem. Phys.,* 12 (17), 8189-8203.

Canadell, J. G., Mooney, H. A., Baldocchi, D. D., Berry, J. A., Ehleringer, J. R., Field, C. B., Gower, S. T., Hollinger, D. Y., Hunt, J. E., Jackson, R. B., Running, S. W., Shaver, G. R., Steffen, W., Trumbore, S. E., Valentini, R., and Bond, B. Y. (2000). Commentary: Carbon Metabolism of the Terrestrial Biosphere: A Multitechnique Approach for Improved Understanding. *Ecosystems, 3*(2), 115-130.

Carbon Dioxide Information Analysis Center. (2012). *CO$_2$ emissions (kt).* Oak Ridge National Laboratory, Tennessee, USA.

Carlton, A. G., Wiedinmyer, C., and Kroll, J. H. (2009). A review of Secondary Organic Aerosol (SOA) formation from isoprene. *Atmos. Chem. Phys., 9*, 4987–5005.

Carslaw, D. (2012). The Openair Manual: Open-source Tools for Analysing Air Pollution Data. *Manual for version 0.5-16*. King's College, London.

Carslaw, D. C. and Ropkins, K. (2012). Openair - an R package for air quality data analysis. *Environ. Model. Softw*. 27-28, 52-61.

Chan, C., Ozkaynak, H., Spengler, J. D., and Sheldon, L. (1991). Driver exposure to volatile organic compounds, CO, ozone, and NO, under different driving conditions. *Environ. Sci. Technol.,* (5), 964-972.

Chan, C. Y., Chan, L. Y., Wang, X. M., Liu, Y. M., Lee, S. C., Zou, S. C., Sheng, G. Y., and Fu, J. M. (2002). Volatile organic compounds in roadside microenvironments of metropolitan Hong Kong. *Atmos. Environ.*, *36*, 2039-2047.

Ciais, P., Sabine, C., Bala, G., Bopp, L., Brovkin, V., Canadell, J., Chhabra, A., DeFries, R., Galloway, J., Heimann, M., Jones, C., Le Quéré, C., Myneni, R.B., Piao S., and Thornton, P. (2013). Carbon and Other Biogeochemical Cycles. In: T. Q.-K. Stocker, *Climate Change 2013: The Physical Science Basis. Contribution of Working Group I to the Fifth Assessment Report of the Intergovernmental Panel on Climate Change* (p. 465). Cambridge University Press, Cambridge, UK.

City of Westminster. (2009). *Trees and the Public Realm (Draft).* City Planning Delivery Unit, City of Westminster, London, UK.

Claeys, M., Graham, B., Vas, G., Wang, W., Vermeylen, R., Pashynska, V., Cafmeyer, J., Guyon, P., Andreae, M. O., Artaxo, P., and Maenhaut, W. (2004). Formation of Secondary Organic Aerosols Through Photooxidation of Isoprene. *Science, 303*, 1173–1176.

Clarke, J. U. (1998). Evaluation of censored data methods to allow statistical comparisons among very small samples with below detection limit observations. *Environ. Sci. Technol,.32*, 177–183.

Corrêa, S. M. and Arbilla, G. (2006). Aromatic hydrocarbons emissions in diesel and biodiesel exhaust, *Atmos. Environ.*, *40*, 6821–6826.

Dabberdt, W. F., Lenschow, D. H., Horst, T. W., Zimmerman, P. R., Oncley, S. P. and Delany, A. C. (1993). Atmosphere-Surface Exchange Measurements. *Science, 260*(5113), 1472-1481.

Dalponte, M., Gianelle, D., and Bruzzone L. (2007). *Use of hyperspectral and LIDAR data for classifi cation of complex forest areas.* Canopy Analysis and Dynamics of a Floodplain Forest, pp. 25-37.

Drenzek, N. J. (2007). *The temporal dynamics of terrestrial organic matter transfer to the oceans: Initial assessment and application* (PhD Thesis). MIT Woods Hole Oceanographic Institution, Woods Hole, MA, USA.

Davis, J. M. and Giddings, J.C. (1983). Statistical theory of component overlap in multicomponent chromatograms. *Anal. Chem., 55*, 418–424.

Davis, K. J., Lenschow, D. H., and Zimmermann, P. R. (1994). Biogenic nonmethane hydrocarbon emissions from tethered balloon observations. *J. Geophys. Res., 99*, 25587-25598.

Davison, B. Taipale, R. Langford, B. Misztal, P. Fares, S. Matteucci, G. Loreto, F. Cape, J. N. Rinne, J., and Hewitt, C. N. (2009). Concentrations and fluxes of biogenic volatile organic compounds above a Mediterranean macchia ecosystem in western Italy. *Biogeosciences, 6*, 1655-1670.

de Gouw, J. A. and Warneke, C. (2007). Measurements of volatile organic compounds in the earth's atmosphere using proton-transfer-reaction mass spectrometry. *Mass. Spectrom. Rev., 26*(2), 223–257. doi: 10.1002/mas.20119.

de Gouw, J. A.,Warneke, C., Karl, T., Eerdekens, G., van der Veen, C., and Fall, R. (2003). Sensitivity and specificity of atmospheric trace gas detection by proton-transfer-reaction mass spectrometry. *Int. J. Mass. Spectrom., 223*, 365–382.

de Gouw, J. A., Middlebrook, A. M., Warneke, C., Goldan, P. D., Kuster, W. C., Roberts, J. M., Fehsenfeld, F. C., Worsnop, D. R., Canagaratna, M. R., Pszenny, A. A. P., Keene, W. C., Marchewka, M., Bertman, S. B., and Bates, T. S. (2005). Budget of organic carbon in a polluted atmosphere: Results from the New England Air Quality Study in 2002. *J. Geophys. Res., 110*, D16305.

De Oliveira, A. A. and Mori, S.A. (1999). A central Amazonian terra firme forest. I. High tree species richness on poor soils. *Biodivers. Conserv., 8*(9), 1219-1244.

Denmead, O. T., Dunin, F. X., Wong, S. C., and Greenwood, E. A. N. (1993). Measuring water-use efficiency of eucalypt trees with chambers and micrometeorological techniques. *J. Hydrol., 150*, 649-664.

Department of Energy and Climate Change. (2015). *2013 UK Greenhouse Gas Emissions, Final Figures.* National Statistics, Newport, UK.

Department for Transport (2012). Retrieved 22 11 2012, www.dft.gov.uk/traffic-counts/.

Department for Transport (2014). Retrieved 5 11 2014, http://www.dft.gov.uk/traffic-counts/area.php? region=London.

Derwent, R. G., Jenkin, M. E., and Saunders, S. M. (1996). Photochemical ozone creation potentials for a large number of reactive hydrocarbons under European conditions. *Atmos. Environ., 30*(2), 181-199.

Derwent, R. G. (1995). *Sources, Distributions, and Fates of VOCs in the Atmosphere.* Issues in Environmental Science and Technology, pp. 1-16.

Dewick, P. (1999). The biosynthesis of C-5-C-25 terpenoid compounds. *Nat. Prod. Rep., 16*, 97–130.

Dindorf, T., Kuhn, U., Ganzeveld, L., Schebeske, G., Ciccioli, P., Holzke, C., Köble, R., Seufert, G., and Kesselmeier, J. (2006). Significant light and temperature dependent monoterpene emissions from European beech (Fagus sylvatica L.) and their potential impact on the European volatile organic compound budget. *J. Geophys. Res., 111*, D16305.

Donovan, R., Hope, E., Owen, S., Mackenzie, A., and Hewitt, C. N. (2005). Development and application of an urban tree air quality score for photochemical pollution episodes using the Birmingham, United Kingdom, area as a case study. *Environ. Sci. Technol., 39*, 6730–6738.

Dorsey, J. R., Nemitz, E., Gallagher, M. W., Fowler, D., Williams, P. I., Bower, K. N., and Beswick, K. M. (2002). Direct measurements and parameterisation of aerosol flux, concentration and emission velocity above a city. *Atmos. Environ., 36*, 791-800.

Draxler, R. R. and Rolph, G. D. (2008). *HYSPLIT (HYbrid Single-Particle Lagrangian Integrated Trajectory) Model*. Retrieved 12 8, 2014, from NOAA ARL READY Website: http://ready.arl.noaa.gov/HYSPLIT_traj.php.

EC Directive 1999/13/EC. European Commission. *Solvents Emssions Directive.*

Eiceman, G. (2000). Gas Chromatography. In R. M. (Ed), *Encyclopedia of Analytical Chemistry: Applications, Theory, and Instrumentation* (p. 10627). Wiley, Chichester, UK.

Eltahir, E. A. B. and Bras, R. L. (1996). Precipitation recycling. *Rev. Geophys., 34*, 367-378.

EPA (2014). *Semi-volatile organic compounds fact sheet.* Environmental Protection Agency, Washington, D.C., US.

Erickson, M. H., Gueneron, M., and Jobson, B. T. (2014). Measuring long chain alkanes indiesel engine exhaust by thermal desorption PTR-MS. *Atmos. Meas. Tech.*, *7*(1), 225-239.

Eva, H. D., de Miranda, E. E., Di Bella, C. M., Gond, V., Huber, O., Sgrenzaroli, M., Jones, S., Coutinho, A., Dorado, A., Guimarães, M., Elvidge, C., Achard, F., Belward, A. S., Bartholomé, E., Baraldi, A., De Grandi, G., Vogt, P., Fritz, S., and Hartley, A. (2002). *A vegetation map of South America,* European Commision, Luxembourg.

Fernando, H. J. S., Lee, S. M., Anderson, J., Princevac, M., Pardyjak, E., and Grossman-Clarke, S. (2001). Urban Fluid Mechanics: Air Circulation and Contaminant Dispersion in Cities. *Environ. Fluid Mech., 1*, 107–164.

Fisch, G., Tota, J., Machado, L. A. T., Silva Dias, M. A. F., da Lyra, R. F., Nobre, C. A., Dolman, A. J., and Gash, J. H. C. (2004). The convective boundary layer over pasture and forest in Amazonia. *Theor. Appl. Climatol., 78*(1-3), 47–59. doi:10.1007/s00704-004-0043-x.

Foken, T., and Wichura, B. (1996). Tools for quality assessment of surface-based flux measurements. *Agr. Forest Meteorol., 78*, 83-105.

Foken, T., Göckede, M., Mauder, M., Mahrt, L., Amiro, B., and Munger, W. (2004). Post-field data quality control. In X. M. Lee, *Handbook of micrometeorology* (pp. 181-208). Kluwer Academic Publishers, Dordrecht, The Netherlands.

Forster, P., Ramaswamy, V., Artaxo, P., Berntsen, T., Betts, R., Fahey, D.W., Haywood, J., Lean, J., Lowe, D.C., Myhre, G., Nganga, J., Prinn, R., Raga, G., Schulz, M., and Van Dorland, R. (2007). Changes in Atmospheric Constituents and in Radiative Forcing. In S. D. Solomon, *Climate Change 2007: The Physical Science Basis. Contribution of Working Group I to the Fourth Assessment Report of the Intergovernmental Panel on Climate Change* (pp. 131-217). Cambridge University Press. Cambridge, UK and New York, NY, USA.

Fortin, T. J., Howard, B. J., Parrish, D. D., Goldan, P.D., Kuster, W. C., Atlas, E. L., and Harley, R. A. (2005). Temporal changes in US benzene emissions inferred from atmospheric measurements, *Envion. Sci. Technol.*, *39*(6), 1403-1408, doi:10.1021/es049316n.

Fowler, D., Coyle, M., Flechard, C., Hargreaves, K., Nemitz, E., Storeton-West, R., Sutton, M., and Erisman, J. W. (2001). Advances in micrometeorological methods for the measurement and interpretation of gas and particle nitrogen fluxes. *Plant Soil, 228*, 117-129.

Fowler, D., Nemitz, E., Misztal, P., Di Marco, C., Skiba, U., Ryder, J., Helfter, C., Cape, J. N., Owen, S., Dorsey, J., Gallagher, M. W., Coyle, M., Phillips, G., Davison, B., Langford, B., MacKenzie, A. R., Muller, J., Siong, J., Dari-Salisburgo, C., Di Carlo, P., Aruffo, E., Giammaria, F., Pyle, J. A., and Hewitt, C. N. (2011). Effects of land use on surface–atmosphere exchanges of trace gases and energy in Borneo: comparing fluxes over oil palm plantations and a rainforest. *Phil. Trans. R. Soc. B, 366*, 3196–3209.

Fujita, E. M., Croes, B. E., Bennett, C. L., Lawson, D. R., Lurmann, F. W., Main, H. H. (1992). Comparison of emission and ambient concentration ratios of CO, NOx, and NMOG in Californias south coast air basin. *J. Air Waste M. A., 42*, 264-276.

Garrat, J. (1992). *The Atmospheric Boundary Layer.* Cambridge University Press, Cambridge, UK.

Geider, R. J., Delucia, E. H., Falkowski, P. G., Finzi, A. C., Grime, J. P., Grace, J., Kana, T. M., La Roche, J., Long, S. P., Osborne, B. A., Platt, T., Prentice, I. C., Raven, J. A., Schlesinger, W. H., Smetacek, V., Stuart, V., Sathyendranath, S., Thomas, R. B., Vogelmann, T. C., Williams, P., and Woodward, F. I. (2001). Primary productivity of planet earth: biological determinants and physical constraints in terrestrial and aquatic habitats. *Glob. Change Biol., 7*(8), 849-882.

Geron, C. D., Guenther, A. B., and Pierce, T. E. (1994). An improved model for estimating emissions of volatile organic compounds from forests in the eastern United States, *J. Geophys. Res., 99*(D6), 12773–12791.

Geron, C., Guenther, A., Greenberg, J., Loescher, H. W., Clark, D., and Baker, B. (2002). Biogenic volatile organic compound emissions from a lowland tropical wet forest in Costa Rica. *Atmos. Environ., 36*, 3793–3802.

Ghirardo, A., Koch, K., Taipale, R., Zimmer, I., Schnitzler, J.-P., and Rinne, J. (2010). Determination of de novo and pool emissions of terpenes from four common boreal/alpine trees by $^{13}CO_2$ labelling and PTR-MS analysis. *Plant Cell Environ., 33*, 781–792.

Goldstein, A. H. and Galbally, I. E. (2007). Known and unexplored organic constituents in the earth's atmosphere. *Environ. Sci. Technol., 41*, 1514–1521.

Grabmer, W., Graus, M., Lindinger, C., Wisthaler, A., Rappenglück, B., Steinbrecher, R., and Hansel, A. (2004). Disjunct eddy covariance measurements of monoterpene fluxes from a Norway spruce forest using PTR-MS. *Int. J. Mass Spectrom., 239*(2-3), 111-115.

Greenberg, J. P., Guenther, A. B., Petron, G., Wiedinmyer, C., Vega, O., Gatti, L. V., Tota, J., and Fisch, G. (2004). Biogenic VOC emissions from forested Amazonian landscapes. *Glob. Change Biol., 10*(5), 651-662.

Grimmond, C. S. B., and T. R. Oke (1999). Aerodynamic properties of urban areas derived from analysis of surface form. *J. Appl. Meteorol., 38*, 1262– 1292.

Grimmond, C. S. B., King, T. S., Cropley, F. D., Nowak, D. J., and Souch, C. (2002). Local-scale fluxes of carbon dioxide in urban environments: methodological challenges and results from Chicago. *Environ. Pollut., 116*, 243–254.

Gros, V., Sciare, J., and Yu, T. (2007). Air-quality measurements in megacities: focus on gaseous organic and particulate pollutants and comparison between two contrasted cities, Paris and Beijing. *C. R. Geosci., 339*, 764–774.

Guenther, A. and Hills, A. J. (1998). Eddy covariance measurement of isoprene fluxes. *J. Geophys. Res. - Atmos., 103*(D11), 13145–13152.

Guenther, A., Zimmerman, P., and Wildermuth, M. (1994). Natural volatile organic compound emission rate estimates for U.S. woodland landscapes. *Atmos. Environ., 28*(6), 1197-1210.

Guenther, A. , Hewitt, C. N., Erickson, D., Fall, R., Geron, C., Graedel, T., Harley, P., Klinger, L., Lerdau, M., McKay, W. A., Pierce, T., Scholes, B., Steinbrecher, R., Tallamraju, R., Taylor, J., and Zimmerman, P. (1995). A global model of natural volatile organic compound emissions. *J. Geophys. Res.- Atmos., 100*(D5), 8873–8892.

Guenther, A., Geron, C., Pierce, T., Lamb, B., Harley, P., and Fall., R. (2000). Natural emissions of non-methane volatile organic compounds; carbon monoxide, and oxides of nitrogen from North America. *Atmos. Environ., 34*, 2205–2230.

Guenther, A., Hewitt, C. N., Erickson, D., Fall, R., Geron, C., Graedel, T., Harley, P., Klinger, L. Lerdau, M., McKay, W. A., Pierce, T., Scholes, B., Steinbrecher, R., Tallamraju, R., Taylor, J., and Zimmerman, P. (2006). Estimates of global terrestrial isoprene emissions using MEGAN (Model of Emissions of Gases and Aerosols from Nature). *Atmos. Chem. Phys., 6*, 3181–3210.

Guenther, A. B., Jiang, X., Heald, C. L., Sakulyanontvittaya, T., Duhl, T., Emmons, L. K., and Wang, X. (2012). The Model of Emissions of Gases and Aerosols from Nature version 2.1 (MEGAN2.1): an extended and updated framework for modeling biogenic emissions. *Geosci. Model Dev., 5*, 1471–1492.

198

Hakola, H., Tarvainen, V., Bäck, J., Ranta, H., Bonn, B., Rinne J., and Kulmala, M. (2006). Seasonal variation of mono- and sesquiterpene emission rates of Scots pine. *Biogeosciences, 3*, 93–101.

Hallquist, M., Wenger, J. C., Baltensperger, U., Rudich, Y., Simpson, D., Claeys, M., Dommen, J., Donahue, N. M., George, C., Goldstein, A. H., Hamilton, J. F., Herrmann, H., Hoffmann, T., Iinuma, Y., Jang, M., Jenkin, M. E., Jimenez, J. L., Kiendler-Scharr, A., Maenhaut, W., McFiggans, G., Mentel, Th. F., Monod, A., Prévôt, A. S. H., Seinfeld, J. H., Surratt, J. D.,Szmigielski, R., and Wildt, J. (2009). The formation, properties and impact of secondary organic aerosol: current and emerging issues. *Atmos. Chem. Phys., 9*, 5155–5236.

Hamilton, A. J. May, R. M. and Waters, E. K. (2015). Zoology: Here be dragons. *Nature*, *520*, 42-43.

Hamilton, J. and Lewis, A. (2003). Monoaromatic complexity in urban air and gasoline assessed using comprehensive GC and fast GC-TOF/MS. *Atmos. Environ., 37*, 589–602.

Hao, L. Q., Romakkaniemi, S., Yli-Pirilä, P., Joutsensaari, J., Kortelainen, A., Kroll, J. H., Miettinen, P., Vaattovaara, P., Tiitta, P., Jaatinen, A., Kajos, M .K., Holopainen, J. K., Heijari, J., Rinne, J., Kulmala, M., Worsnop, D. R., Smith, N. J., and Laaksonen, A. (2011). Mass yields of secondary organic aerosols from the oxidation of α-pinene and real plant emissions. *Atmos. Chem. Phys., 11*, 1367–1378.

Harley, R. A. and Cass, G. R. (1994). Modeling the concentrations of gas-phase toxic organic air pollutants : Direct emissions and atmospheric formation. *Environ. Sci. Technol.*, 28*(1),* 88–98.

Harley, P., Guenther, A., and Zimmerman, P. (1997). Environmental controls over isoprene emission in deciduous oak canopies. *Tree Physiol., 17*(11), 705-714, doi:10.1093/treephys/17.11.705.

Harley, P.C., Monson, R. K., and Lerdau, M. T. (1999). Ecological and evolutionary aspects of isoprene emission from plants. *Oecologia, 118*(2), 109-123.

Harley, P., Vasconcellos, P., Vierling, L., Pinheiro, C. C. d. S., Greenberg, J., Guenther, A., Klinger, L., Almeida, S. S. d., Neill, D., Baker, T., Phillips, O., and Malhi, Y. (2004). Variation in potential for isoprene emissions among Neotropical forest sites. *Glob. Change Biol., 10*, 630–650.

Hastie, T. J. and Tibshirani, R. (1990). Generalized Additive Models. Chapman and Hall, London, UK.

Hayward, S., Hewitt, C. N., Sartin, J. H., and Owen, S. M. (2002). Performance characteristics and applications of a proton transfer reaction-mass spectrometer for measuring volatile organic compounds in ambient air. *Environ. Sci. Technol.*, *36*(7), 1554–60.

Heald, C. L., Jacob, D. J., Park, R. J., Russell, L. M., Huebert B. J., Seinfeld, J. H., Liao, H., and Weber, R. J. (2005). A large organic aerosol source in the free troposphere missing from current models. *Geophys. Res. Lett., 32*, L18809. doi:10.1029/2005GL023831

Heald, C. L., Henze, D. K., Horowitz, L. W., Feddema, J., Lamarque, J. F., Guenther, A., Hess, P. G., Vitt, F., Seinfeld, J. H., Goldstein, A. H., and Fung, I. (2008). Predicted change in global secondary organic aerosol concentrations in response to future climate, emissions, and land use change. *J. Geophys. Res.-Atmos., 113*, D05211. doi:10.1029/2007JD009092.

Heald, C. L., Ridley, D. A., Kreidenweis, S. M., and Drury, E. E. (2010). Satellite observations cap the atmospheric organic aerosol budget. *Geophys. Res. Lett., 37*, L24808.

Heeb, N. V, Forss, A., Bach, C., Reimann, S., Herzog, A., and Ja, H. W. (2000). A comparison of benzene , toluene and C -benzenes mixing ratios in automotive exhaust and in the suburban atmosphere during the introduction of catalytic converter technology to the Swiss Car Fleet. *Atmos. Environ.*, *34*, 3103–3116.

Helfter, C., Famulari, D., Phillips, G. J., Barlow, J. F., Wood, C. R., Grimmond, C. S. B., and Nemitz, E. (2011). Controls of carbon dioxide concentrations and fluxes above central London. *Atmos. Chem. Phys., 11*, 1913–1928. doi:10.5194/acp-11-1913-2011.

Helmig, D. , Ortega, J., Duhl, T., Tanner, D., Guenther, A., Harley, P., Wiedinmyer, C., Milford, J., and Sakulyanontvittaya, T. (2007). Sesquiterpene Emissions from Pine Trees − Identifications, Emission Rates and Flux Estimates for the Contiguous United States. *Environ. Sci. Technol., 41*(5), 1545–1553.

Helsel, D. R. and Hirsch, R. M. (1992). *Statistical methods in water resources.* Elsevier, New York, USA.

Hewitt, C. N. and Jackson, A. (2003). *Handbook of Atmospheric Science.* Blackwell Publishing company, Oxford, UK.

Hewitt, C. N., Hayward, S., and Tani, A. (2003). The application of proton transfer reaction-mass spectrometry (PTR-MS) to the monitoring and analysis of volatile organic compounds in the atmosphere. *J. Environ. Monit., 5*, 1-7. doi: 10.1039/B204712H.

Hewitt, C. N., MacKenzie, A. R., Di Carlo, P., Dorsey, J. R., Evans, M., Fowler, D., Gallagher, M. W., Helfter, C., Hopkins, J., Jones, H., Langford, B., Lee, J. D., Lewis, A. C., Lim, S. F., di Marco, C., Misztal, P., Moller, S., Monks, P. S., Nemitz, E., Oram, D.E., Owen, S. M., Phillips, G., Pugh, T., Pyle, J. A., Reeves, C. E., Ryder, J., Siong, J., Skiba, U., Stewart, D. J., and Thomas, R. (2009). Nitrogen management is essential to prevent tropical oil palm plantations from causing ozone pollution. *Proc. Natl. Acad. Sci., 106*, 18447-18451.

Hewitt, C. N., Lee, J. D., MacKenzie, A. R., Barkley, M. P., Carslaw, N., Carver, G. D., Chappell, N. A., Coe, H., Collier, C., Commane, R., Davies, F., Davison, B., DiCarlo, P., Di Marco, C. F., Dorsey, J. R., Edwards, P. M., Evans, M. J., Fowler, D., Furneaux, K. L., Gallagher, M., Guenther, A., Heard, D. E., Helfter, C., Hopkins, J., Ingham, T., Irwin, M., Jones, C., Karunaharan, A., Langford, B., Lewis, A. C., Lim, S. F., MacDonald, S. M., Mahajan, A. S., Malpass, S., McFiggans, G., Mills, G., Misztal, P., Moller, S., Monks, P. S., Nemitz, E., Nicolas-Perea, V., Oetjen, H., Oram, D. E., Palmer, P. I., Phillips, G. J., Pike, R., Plane, J. M. C., Pugh, T., Pyle, J. A., Reeves, C. E., Robinson, N. H., Stewart, D., Stone, D. , Whalley, L. K., and Yin, X. (2010). Overview: oxidant and particle photochemical processes above a south-east Asian tropical rainforest (the OP3 project): introduction, rationale, location characteristics and tools. *Atmos. Chem. Phys., 10*, 169-199.

Hewitt, C. N., Ashworth, K., Boynard, A., Guenther, A., Langford, B., MacKenzie, A. R., Misztal, P. K., Nemitz, E., Owen, S. M., Possell, M., Pugh, T. A. M., Ryan, A. C., and Wild, O. (2011). Ground-level ozone influenced by circadian control of isoprene emissions. *Nat. Geosci., 4*, 671–674. doi:10.1038/ngeo1271

Hoerger, C. C., Werner, A., Plass-Duelmer, C., Reimann, S., Eckart, E., Steinbrecher, R., Aalto, J., Arduini, J., Bonnaire, N., Cape, J. N., Colomb, A., Connolly, R., Diskova, J., Dumitrean, P., Ehlers, C., Gros, V., Hakola, H., Hill, M., Hopkins, J. R., Jäger, J., Junek, R., Kajos, M. K., Klemp, D., Leuchner, M., Lewis, A. C., Locoge, N., Maione, M., Martin, D., Michl, K., Nemitz, E., O'Doherty, S., Pérez Ballesta, P., Ruuskanen, T. M., Sauvage, S., Schmidbauer, N., Spain, T. G., Straube, E., Vana, M., Vollmer, M. K., Wegener, R., and Wenger, A. (2014). ACTRIS non-methane hydrocarbon intercomparison experiment in Europe to support WMO-GAW and EMEP observation networks. *Atmos. Meas. Tech. Discus., 7*, 10423–10485.

Holloway, T., Fiore, A., and Hastings, M. G. (2003). Intercontinental Transport of Air Pollution: Will Emerging Science Lead to a New Hemispheric Treaty? *Environ. Sci. Technol., 37*, 4535-4542.

Holm, J. A., Jardine, K., Guenther, A. B., Chambers, J. Q., and Tribuzy, E. (2014). Evaluation of MEGAN-CLM parameter sensitivity to predictions of isoprene emissions from an Amazonian rainforest. *Atmos. Chem. Phys. Discuss., 14*, 23995–24041.

Holzinger, R., Jordan, A., and Hansel, A. (2001). Automobile emissions of acetonitrile: assessment of its contribution to the global source. *J. Atmos. Chem.,* 38, 187-193.

Horst, T. (1997). A simple formula for attenuation of eddy fluxes measured with first-order-response scalar sensors. *Bound.-Lay. Meteorol., 82*(2), 219-233.

INMET Brazil. (2014). Instituto Nacional de Meteorologia. Brasília, Federal District, Brazil. Retrieved 19 5 2015, from Climatologicas: http://www.inmet.gov.br/portal/index.php?r=clima/normaisClimatologicas.

Inomata, S., Tanimoto, H., Kameyama, S., Tsunogai, U., Irie, H., Kanaya, Y., and Wang, Z. (2008). Technical note: determination of formaldehyde mixing ratios in air with PTR-MS: laboratory experiments and field measurements. *Atmos. Chem. Phys., 8*, 273–284.

Jacob, D.J. and Wolfsy, S.C. (1988). Photochemistry of biogenic emissions over the Amazon forest. *J. Geophys. Res., 93*, 1477-1486.

Jacobson, M. Z. (2000). Physically-based treatment of elemental carbon optics: Implications for global direct forcing of aerosols. *Geophys. Res. Lett., 27*(2), 217– 220.

Jardim, F. C. S. and Hosokawa R. T. (1987). Estrutura da floresta equatorial umida da estacao experimental de silvicultura tropical do INPA. *Acta Amaz., 16/17*, 411–508.

Jardine, A., Jardine, K. J., Fuentes, J. D., Martin, S. T., Martins, G., Durgante, F., Carneiro, V., Higuchi, N., Manzi, A. O., and Chambers, J. Q. (2015). Highly reactive light-dependent monoterpenes in the Amazon. *Geophys. Res. Lett., 42*(5), 1576-1584.

Jardine, K. J., Monson, R. K., Abrell, L., Saleska, S. R., Arneth, A., Jardine, A., Ishida, F. Y., Serrano, A. M. Y., Artaxo, P., Karl, T., Fares, S., Goldstein, A., Loreto, F., and Huxman, T. (2011). Within-plant isoprene oxidation confirmed by direct emissions of oxidation products methyl vinyl ketone and methacrolein. *Glob. Change Biol., 18*, 973–984.

Jimenez, J. L., Canagaratna, M. R., Donahue, N. M., Prevot, A. S. H., Zhang, Q., Kroll, J. H., De Carlo, P. F., Allan, J. D., Coe, H., Ng, N. L., Aiken, A. C., Docherty, K. S., Ulbrich, I.

M., Grieshop, A. P., Robinson, A. L., Duplissy, J., Smith, J. D., Wilson, K. R., Lanz, V. A., Hueglin, C., Sun, Y. L., Tian, J., Laaksonen, A., Raatikainen, T., Rautiainen, J., Vaattovaara, P., Ehn, M., Kulmala, M., Tomlinson, J. M., Collins, D. R., Cubison, M. J., Dunlea, E. J., Huffman, J. A., Onasch, T. B., Alfarra, M. R., Williams, P. I., Bower, K., Kondo, Y., Schneider, J., Drewnick, F., Borrmann, S., Weimer, S., Demerjian, K., Salcedo, D., Cottrell, L., Griffin, R., Takami, A., Miyoshi, T., Hatakeyama, S., Shimono, A., Sun, J. Y., Zhang, M. Y., Dzepina, K., Kimmel, J. R., Sueper, D., Jayne, J. T., Herndon, S. C., Trimborn, A. M., Williams, L. R., Wood, E. C., Middlebrook, A. M., Kolb, C. E., Baltensperger, U., and Worsnop, D. R. (2009). Evolution of Organic Aerosols in the Atmosphere. *Science, 326* (5959), 1525-1529.

Jobson, B. T., Volkamer, R. A., Velasco, E., Allwine, G., Westberg, H., Lamb, B. K., Alexander, M. L., Berkowitz, C. M., and Molina, L. T. (2010). Comparison of aromatic hydrocarbon measurements made by PTR-MS, DOAS and GC-FID during theMCMA 2003 Field Experiment. *Atmos. Chem. Phys., 10* (4), 1989-2005.

Jones, A. R., Thomson, D. J., Hort, M., and Devenish, B. (2007). The U.K. Met Office's next-generation atmospheric dispersion model, NAME III. In B. C. A.-L., *Air Pollution Modeling and its Application XVII: Proceedings of the 27th NATO/CCMS International Technical Meeting on Air Pollution Modelling and its Application* (pp. 580-589). Springer, London, UK.

Jordan, A., Haidacher, S., Hanel, G., Hartungen, E., Märk, L., Seehauser, H., Schottkowsky, R., Sulzer, P., and Märk, T. D. (2009). A high resolution and high sensitivity proton-transfer-reaction time-of-flight mass spectrometer (PTR-TOF-MS). *Int. J. Mass. Spectrom., 286*(2-3), 122–128.

Kameyama, S., Tanimoto, H., Inomata, S., Tsunogai, U., Ooki, A., Yokouchi, Y., Takeda, S., Obata, H., and Uematsu, M. (2009). Equilibrator inlet-proton transfer reaction-mass spectrometry (EI-PTRMS) for sensitive, high-resolution measurement of dimethyl sulfide dissolved in sea water. *Anal. Chem., 81*(21), 9021–9026.

Kameyama, S., Tanimoto, H., Inomata, S., Tsunogai, U., Ooki, A., Takeda, S., Obata, H., Tsuda, A., and Uematsu, M. (2010). High-resolution measurement of multiple volatile organic compounds dissolved in seawater using equilibrator inlet-proton transfer reaction-mass spectrometry (EI-PTR-MS). *Mar. Chem., 122*, 59–73.

Kameyama, S., Yoshida, S., Tanimoto, H., Inomata, S., Suzuki, K., and Yoshikawa-Inoue, H. (2014). High-resolution observations of dissolved isoprene in surface seawater in the Southern Ocean during austral summer 2010–2011. *J. Oceanogr., 70*, 225–239.

Kanakidou, M., Seinfeld, J. H., Pandis, S. N., Barnes, I., Dentener, F. J., Facchini, M. C., Van Dingenen, R., Ervens, B., Nenes, A., Nielsen, C. J., Swietlicki, E., Putaud, J. P., Balkanski, Y., Fuzzi, S., Horth, J., Moortgat, G. K., Winterhalter, R., Myhre, C. E. L., Tsigaridis, K., Vignati, E., Stephanou, E. G., and Wilson, J. (2005). Organic aerosol and global climate modelling: a review. *Atmos. Chem. Phys., 5*, 1053–1123.

Kansal, A. (2009). Sources and reactivity of NMHCs and VOCs in the atmosphere: A review. *J. Hazard. Mater., 166*, 17-26.

Karakitsios, S. P., Delis, V. K., Kassomenos, P. A., and Pilidis, G. A. (2007). Contribution to ambient benzene concentrations in the vicinity of petrol stations: Estimation of the associated health risk. *Atmos. Environ., 41*(9), 1889-1902.

Karl, T., Fall, R., Crutzen, P.J., Jordan, A., and Lindinger, W. (2001a). High concentrations of reactive biogenic VOCs at a high altitude site in late autumn. *Geophys. Res. Lett., 28*, 507–510.

Karl, T., Guenther, A., Lindinger, C., Jordan, A., Fall, R., and Lindinger, W. (2001b). Eddy covariance measurements of oxygenated volatile organic compound fluxes from crop harvesting using a redesigned proton-transfer-reaction mass spectrometer. *J. Geophys. Res.- Atmos., 106*(D20), 24157–24167.

Karl, T. G., Spirig, C., Rinne, J., Stroud, C., Prevost, P., Greenberg, J., Fall, R., and Guenther, A. (2002). Virtual disjunct eddy covariance measurements of organic compound fluxes from a subalpine forest using proton transfer reaction mass spectrometry. *Atmos. Chem. Phys., 2*, 279-291.

Karl, T., Potosnak, M., Guenther, A., Clark, D., Walker, J., Herrick, J. D., and Geron, C. (2004). Exchange processes of volatile organic compounds above a tropical rain forest: Implications for modeling tropospheric chemistry above dense vegetation. *J. Geophys. Res. - Atmos., 109*, D18306. doi:10.1029/2004JD004738.

Karl, T., Guenther, A., Yokelson, R. J., Greenberg, J., Potosnak, M., Blake, D. R., and Artaxo, P. (2007). The tropical forest and fire emissions experiment: Emission, chemistry, and transport of biogenic volatile organic compounds in the lower atmosphere over Amazonia. *J. Geophys. Res.- Atmos., 112*, D18302. doi:10.1029/2007JD008539.

Karl, T., Apel, E., Hodzic, A., Riemer, D. D., Blake, D. R., and Wiedinmyer, C. (2009a). Emissions of volatile organic compounds inferred from airborne flux measurements over a megacity. *Atmos. Chem. Phys., 9*, 271–285.

Karl, T., Guenther, A., Turnipseed, A., Tyndall, G., Artaxo, P., and Martin, S. (2009b). Rapid formation of isoprene photo-oxidation products observed in Amazonia. *Atmos. Chem. Phys., 9*, 7753–7767. doi:10.5194/acp-9-7753-2009.

Kato, S., Miyakawa, Y., Kaneko, T., and Kajii, Y. (2004). Urban air measurements using PTRMS in Tokyo area and comparison with GC-FID measurements. *Int. J. Mass. Spectrom., 235* (2), 103-110.

Kesselmeier, J. and Staudt, M. (1999). Biogenic Volatile Organic Compounds (VOC): An Overview on Emission, Physiology and Ecology. *J. Atmos. Chem., 33*, 23-88.

Kesselmeier, J., Kuhn, U., Wolf, A., Andreae, M. O., Ciccioli, P., Brancaleoni, E., Frattoni, M., Guenther, A., Greenberg, J., De Castro Vasconcellos, P., de Oliva, T., Tavares, T., and Artaxo, P. (2000). Atmospheric volatile organic compounds (VOC) at a remote tropical forest site in central Amazonia. *Atmos. Environ., 34*(24), 4063–4072.

Kesselmeier, J., Kuhn, U., Rottenberger, S., Biesenthal, T., Wolf, A., Schebeske, G., Andreae, M. O., Ciccioli, P., Brancaleoni, E., Frattoni, M., Oliva, S. T., Botelho, M. L., Silva, C. M. A., and Tavares, T.M. (2002). Concentrations and species composition of atmospheric volatile organic compounds (VOCs) as observed during the wet and dry season in Rondonia (Amazonia). *J. Geophys. Res. - Atmos., 107*, 8053. doi:10.1029/2000JD000267.

Kesselmeier, J., Guenther, A., Hoffmann, T., Piedade, M. T. F., and Warnke, J. (2009). Natural volatile organic compound emissions from plants and their roles in oxidant balance and particle formation. In M. B. Keller, *Amazonia and Global Change, Geophys. Monogr. Ser.* (pp. 183–206). American Geophysical Union. Washington, DC, USA. doi:10.1029/2008GM000717.

Kim, Y. M., Harrad, S., and Harrison, R. M. (2001). Concentrations and sources of VOCs in urban domestic and public microenvironments. *Environ. Sci. Technol.*, *35*(6), 997–1004.

Kleindienst, T. E., Jaoui, M., Lewandowski, M., Offenberg, J. H., Lewis, C. W., Bhave, P. V., Edney, E. O. (2007). Estimates of the contributions of biogenic and anthropogenic hydrocarbons to secondary organic aerosol at a southeastern US location. *Atmos. Environ., 41*(37), 8288–8300.

Kleindienst, T. E., Lewandowski, M., Offenberg, J. H., Jaoui, M., and Edney, E. O. (2009). The formation of secondary organic aerosol from the isoprene plus OH reaction in the absence of NOx. *Atmos. Chem. Phys., 9*, 6541–6558. doi:10.5194/acp-9-6541-2009.

Kljun, N., Calanca, P., Rotachhi, M. W., and Schmid, H. P. (2004). A simple parameterisation for flux footprint predictions. *Bound.-Lay. Meteorol., 112*, 503–523.

Kormann, R. and Meixner, F. X. (2001). An Analytical Footprint Model For Non-Neutral Stratification. *Bound.-Lay. Meteorol., 99*(2), 207-224.

Kotthaus, S. and Grimmond, C. S. B. (2012). Identification of Micro-scale Anthropogenic CO2, heat and moisture sources – Processing eddy covariance fluxes for a dense urban environment. *Atmos. Environ.*, *57*, 301–316. doi:10.1016/j.atmosenv.2012.04.024.

Kotthaus, S. and Grimmond, C. S. B. (2014a). Energy exchange in a dense urban environment – Part I: Temporal variability of long-term observations in central London. *Atmos. Environ., 10*(2), 261-280.

Kotthaus, S. and Grimmond, C. S. B. (2014b). Energy exchange in a dense urban environment – Part II: Impact of spatial heterogeneity of the surface. *Atmos. Environ., 10*(2), 281-307.

Kroll, J. H., Ng, N. L., Murphy, S. M., Flagan, R. C., and Seinfeld, J. H. (2005). Secondary organic aerosol formation from isoprene photooxidation under high-NOx conditions. *J. Geophys. Res., 32*, L18808. doi:10.1029/2005GL023637.

Kuhn, U., Rottenberger, S., Biesenthal, T., Wolf, A., Schebeske, G., Ciccioli, P., Brancaleoni, E., Frattoni, M., Tavares, T. M., and Kesselmeier, J. (2002). Isoprene and monoterpene emissions of Amazonian tree species during the wet season: Direct and indirect investigations on controlling environmental functions. *J. Geophys. Res., 107*(D20), 8071.

Kuhn, U., Rottenberger, S., Biesenthal, T., Wolf, A., Schebeske, G., Ciccioli, P., Brancaleoni, E., Frattoni, M., Tavares, T., M., and Kesselmeier, J. (2004a). Seasonal differences in isoprene and light-dependent monoterpene emission by Amazonian tree species. *Glob. Chang. Biol., 10*, 663–682.

Kuhn, U., Rottenberger, T., Biesenthal, T., Wolf, A., Schebeske, G.,Ciccioli, P., and Kesselmeier, J. (2004b). Strong correlation between isoprene emission and gross photosynthetic capacity during leaf phenology of the tropical tree species Hymenaea courbaril with fundamental changes in volatile organic compounds emission composition during early leaf development. *Plant, Cell Environ., 27*, 1469-1485.

Kuhn, U., Andreae, M. O., Ammann, C., Araújo, A. C., Brancaleoni, E., Ciccioli, P., Dindorf, T., Frattoni, M., Gatti, L. V., Ganzeveld, L., Kruijt, B., Lelieveld, J., Lloyd, J., Meixner, F. X., Nobre, A. D., Pöschl, U., Spirig, C., Stefani, P., Thielmann, A., Valentini, R., and

Kesselmeier, J. (2007). Isoprene and monoterpene fluxes from Central Amazonian rainforest inferred from tower-based and airborne measurements, and implications on the atmospheric chemistry and the local carbon budget. *Atmos. Chem. Phys., 7*, 2855–2879. doi:10.5194/acp-7-2855-2007.

Kuster, W. C., Jobson, B. T., Karl, T., Riemer, D., Apel, E., and Goldan, P. D. (2004). Intercomparison of volatile organic carbon measurement techniques and data at La Porte during the TexAQS2000 air quality study. *Environ. Sci. Technol.* 38 (1), 221-228.

LAEI. (2013). London Atmospheric Emissions Inventory. Greater London Authority, London, UK. Retrieved 26 6 2015, from Data selector: http://data.london.gov.uk/dataset/london-atmospheric-emissions-inventory-2010.

Lamsal, L. N., Martin, R. V., Padmanabhan, A., van Donkelaar, A., Zhang, Q., Sioris, C. E., Chance, K., Kurosu, T. P., and Newchurch, M. J. (2011). Application of satellite observations for timely updates to global anthropogenic NO x emission inventories. *Geophys. Res. Lett.*, *38*(5). doi:10.1029/2010GL046476.

Langford, B., Davison, B., Nemitz, E., and Hewitt, C. N. (2009). Mixing ratios and eddy covariance flux measurements of volatile organic compounds from an urban canopy (Manchester, UK). *Atmos. Chem. Phys., 9*, 1971–1987.

Langford, B., Misztal, P. K., Nemitz, E., Davison, B., Helfter, C., Pugh, T. A. M., MacKenzie, A. R., Lim, S. F., and Hewitt, C. N. (2010a). Fluxes and concentrations of volatile organic compounds from a South-East Asian tropical rainforest. *Atmos. Chem. Phys., 10*, 8391-8412.

Langford, B., Nemitz, E., House, E., Phillips, G. J., Famulari, D., Davison, B., Hopkins, J. R., Lewis, A. C., and Hewitt, C.N. (2010b). Fluxes and concentrations of volatile organic compounds above central London, UK. *Atmos. Chem. Phys., 10*, 627–645.

Langford, B., Acton, W. J., Ammann, C., Valach, A. C., and Nemitz, E. (2015). Eddy-covariance data with low signal-to-noise ratio: time-lag determination, uncertainties and limit of detection. *Atmos. Meas. Tech. Discuss., 8*, 2913–2955.

Laothawornkitkul, J., Taylor, J. E., Paul, N. D., and Hewitt, C. N. (2009). Biogenic volatile organic compounds in the earth system. *New Phytol., 183*, 27–51.

Le Quéré, C. (2006). The unknown and the uncertain in earth system modeling . *Eos T Am. Geophys. Un., 87*, 496–496.

Le Quéré, C., Andres, R. J., Boden, T., Conway, T., Houghton, R. A., House, J. I., Marland, G., Peters, G P., van der Werf, G. R., Ahlström, A., Andrew, R. M., Bopp, L., Canadell, J. G., Ciais, P., Doney, S. C., Enright, C., Friedlingstein, P., Huntingford, C., Jain, A. K., Jourdain, C., Kato, E., Keeling, R. F., Klein Goldewijk, K., Levis, S., Levy, P., Lomas, M., Poulter, B., Raupach, M. R., Schwinger, J., Sitch, S., Stocker, B. D., Viovy, N., Zaehle, S., and Zeng, N. (2013). The global carbon budget 1959–2011. *Earth Syst. Sci. Data, 5*, 165–185.

Lelieveld, J., Butler, T.M., Crowley, J.N., Dillon, T.J., Fischer, H., Ganzeveld, L.,Harder, H., Lawrence, M.G., Martinez, M., Taraborrelli, D., and Williams, J. (2008). Atmospheric oxidation capacity sustained by a tropical forest. *Nature, 452*, 737–740.

Lemieux, P. M., Lutes, C. C., and Santoianni, D. A. (2004). Emissions of organic air toxics from open burning: a comprehensive review. *Prog. Energ. Combust., 30*, 1–32.

Lerdau, M. and Keller, M. (1997). Controls on isoprene emission from trees in a subtropical dry forest. *Plant, Cell Environ., 20*(5), 569-578.

Levis, S., Wiedinmyer, C., Bonan, G. B., and Guenther. A. (2003). Simulating biogenic volatile organic compound emissions in the Community Climate System Model. *J. Geophys. Res.- Atmos., 108*, 659(D4). doi:10.1029/2002JD003203.

Lewis, A. C., Carslaw, N., Marriott, P. J., Kinghorn, R. M., Morrison, P., Lee, A. L., Bartle, K. D., and Pilling, M. J. (2000). Alarger pool of ozone-forming carbon compounds in urban atmospheres. *Nature, 405*, 778-781.

Lewis, S. L., Brando, P. M., Phillips, O. L., van der Heijden, G. M. F., and Nepstad, D. (2011). The 2010 Amazon Drought. *Science, 331*(6017), 554.

Lin, Y. H., Zhang, Z., Docherty, K. S., Zhang, H., Budisulistiorini, S. H., Rubitschun, C. L., Shaw, S. L., Knipping, E. M., Edgerton, E. S., Kleindienst, T. E., Gold, A., and Surratt, J. D. (2012). Isoprene Epoxydiols as Precursors to Secondary Organic Aerosol Formation: Acid-Catalyzed Reactive Uptake Studies with Authentic Compounds. *Environ. Sci. Technol., 46*, 250-258. doi:10.1021/es202554c, 2012.

Lindinger, W., Hirber, J., and Paretzke, H. (1993). An ion/molecule-reaction mass spectrometer used for on-line trace gas analysis. *Int. J. Mass. Spectrom. Ion Proc., 129*, 79.

Lindinger, W., Hansel, A., and Jordan, A. (1998). On-line monitoring of volatile organic compounds at pptv levels by means of proton-transfer-reaction mass spectrometry (PTR-

MS): Medical applications, food control and environmental research. *Int. J. Mass. Spectrom. Ion Proc., 173*(3), 191-241.

Lipari, F., Dasch, J. M., and Scruggs, W. F. (1984). Aldehyde emissions from wood-burning fireplaces. *Environ. Sci. Technol., 18*, 326-330.

Lippman, M. (1993). Health effects of tropospheric ozone: review of recent research findings and their implications to ambient air quality standards. *J. Expo. Anal. Env. Epid., 3*(1), 103-129.

Liu, Y. J., Herdlinger-Blatt, I., McKinney, K. A., and Martin, S. T. (2013). Production of methyl vinyl ketone and methacrolein via the hydroperoxyl pathway of isoprene oxidation. *Atmos. Chem. Phys., 13*, 5715–5730.

Maass, J. M., Vose, J. M., Swank, W. T., and Martinez-Yrizar, A. (1995). Seasonal changes of leaf area index (LAI) in a tropical deciduous forest in west Mexico. *Forest Ecol. Manag., 74*, 171-180.

MacKenzie, A. R., Harrison, R. M., Colbeck, I., and Hewitt, C. N. (1991). The role of biogenic hydrocarbons in the production of ozone in urban plumes in southeast England. *Atmos. Env., 25*(2), 351–359. doi:10.1016/0960-1686(91)90306-R.

Maleknia, S. D., Bell, T .L., and Adams, M. A. (2007). PTR-MS analysis of reference and plant emitted volatile organic compounds. *Int. J. Mass Spectrom.*, 262 (3), 203-210.

Massman, W. (2000). A simple method for estimating frequency response corrections for eddy covariance systems. *Agr. Forest Meteorol., 104*(3), 185-198.

Matsunaga, S., Niwa, S., Mochizuki, T., Tani, A., Kusumoto, D., Utsumi, Y., Enoki, T., and Hiura, T. (2013). Seasonal variation in basal emission rates and composition of mono- and sesquiterpenes emitted from dominant conifers in Japan. *Atmos. Environ., 69*, 124-130.

Met Office UK (2012). *Climate summaries.* Retrieved 6  8 2013, from Met Office UK: www.metoffice.gov.uk/climate/uk/summaries/2012.

Met Office UK (2013). *Climate summaries, UK*. Retrieved 9 10 2013, from Met Office UK: http://www.metoffice.gov.uk/climate/uk/summaries/2013.

Milford, J., Gao, D., Sillman, S., Blossey, P., Russell, A. G. (1994). Total reactive nitrogen (NOy) as an indicator for the sensitivity of ozone to NOx and hydrocarbons. *J. Geophys. Res., 99*, 3533-3542.

Millet, D. B., Jacob, D. J., Custer, T. G., de Gouw, J. A., Goldstein, A. H., Karl, T., Singh, H. B., Sive, B. C., Talbot, R.W.,Warneke, C., and Williams, J. (2008). New constraints on terrestrial and oceanic sources of atmospheric methanol. *Atmos. Chem. Phys., 8*, 6887–6905. doi:10.5194/acp-8-6887-2008.

Misztal, P. K., Owen, S. M., Guenther, A. B., Rasmussen, R., Geron, C., Harley, P., Phillips, G. J., Ryan, A., Edwards, D. P., Hewitt, C. N., Nemitz, E., Siong, J., Heal, M. R., and Cape, J. N. (2010). Large estragole fluxes from oil palms in Borneo. *Atmos. Chem. Phys., 10*, 4343–4358.

Misztal, P. K., Nemitz, E., Langford, B., Di Marco, C. F., Phillips, G. J., Hewitt, C. N., MacKenzie, A. R., Owen, S. M., Fowler, D., Heal, M. R., and Cape, J. N. (2011). Direct ecosystem fluxes of volatile organic compounds from oil palms in South-East Asia. *Atmos. Chem. Phys., 11*, 8995–9017. doi:10.5194/acp-11-8995-2011.

Misztal, P. K., Heal, M. R., Nemitz, E., and Cape, J. N. (2012). Development of PTR-MS selectivity for structural isomers: Monoterpenes as a case study. *Int. J. Mass. Spec., 310*, 10-19.

Moncrieff, J., Finnigan, R. C. J., and Meyers, T. (2004). Averaging, detrending, and filtering of eddy covariance time series. In W. Lee, *Handbook of Micrometeorology* (pp. 7-30). Kluwer Academic Publishers, Dordrecht, The Netherlands.

Monks, P.S., Granier, C., Fuzzi, S., Stohl, A., Williams, M.L., Akimoto, H., Amann, M., Baklanov, A., Baltensperger, U., Bey, I., Blake, N., Blake, R.S., Carslaw, K., Cooper, O.R., Dentener, F., Fowler, D., Fragkou, E., Frost, G.J., Generoso, S., Ginoux, P., Grewe, V., Guenther, A., Hansson, H.C., Henne, S., Hjorth, J., Hofzumahaus, A., Huntrieser, H., Isaksen, I.S.A., Jenkin, M.E., Kaiser, J., Kanakidou, M., Klimont, Z., Kulmala, M., Laj, P., Lawrence, M.G., Lee, J.D., Liousse, C., Maione, M., McFiggans, G., Metzger, A., Mieville, A., Moussiopoulos, N., Orlando, J.J., O'Dowd, C.D., Palmer, P.I., Parrish, D.D., Petzold, A., Platt, U., Pöschl, U., Prévôt, A.S.H., Reeves, C.E., Reimann, S., Rudich, Y., Vautard, R., Vestreng, V., Vlachokostas, Ch., and von Glasow, R. (2009). Atmospheric composition change – global and regional air quality. *Atmos. Environ., 43*, 5268–5350.

Monson, R. K., Grote, R., Niinemets, Ü., and Schnitzler, J.-P. (2012). Modeling the isoprene emission rate from leaves. *New Phytol., 195*, 541–559.

Na, K., Kim, Y. P., Moon, I., and Moon, K.-C. (2004). Chemical compo- sition of major VOC emission sources in the Seoul atmosphere. *Chemosphere, 55*, 585–594.

Na, K., Moon, K. C., and Kim, Y. P. (2005). Source contribution to aro- matic VOC concentration and ozone formation potential in the atmosphere of Seoul. *Atmos. Environ., 39*, 5517–5524.

NAEI. (2014). *National Atmospheric Emissions Inventory*. Retrieved 2015, from Department for Environment, Food and Rural Affairs: http://naei.defra.gov.uk/.

Neftel, A., Spirig, C., and Ammann, C. (2008). Application and test of a simple tool for operational footprint evaluations. *Environ. Pollut., 152*(3), 644–652. doi:10.1016/j.envpol.2007.06.062.

Nelson, B. W., Tavares, J. V., Wu, J., Valeriano, D. M., Lopes, A. P., Marostica, S. F., Martins, G., Prohaska, N., Albert, L., De Araujo, A. C., Manzi, A. O., Saleska, S. R., and Huete, A. R. (2014). Seasonality of Central Amazon Forest Leaf Flush Using Tower-Mounted RGB Camera. *AGU Fall Meeting.* American Geophysical Union. San Francisco, California, USA.

Nemitz, E., Hargreaves, K. J., McDonald, A. G., Dorsey, J. R., and Fowler, D. (2002). Meteorological measurements of the urban heat budget and CO2 emissions on a city scale. *Environ. Sci. Technol., 36*, 3139-3146.

Nemitz, E., Hargreaves, K. J., Neftel, A., Loubet, B., Cellier, P., Dorsey, J. R., Flynn, M., Hensen, A., Weidinger, T., Meszaros, R., Horvath, L., Dämmgen, U., Frühauf, C., Löpmeier, F. J., Gallagher, M. W., and Sutton, M. A. (2009). Intercomparison and assessment of turbulent and physiological exchange parameters of grassland. *Biogeosciences, 6*, 1445–1466.

Nemitz, E., Coyle, M., Langford, B., Gerosa, G., Marzuoli, R., Stella, P., Loubet, B., Potier, E., Joensuu, J., Altimir, N., Ammann, C., Vuolo, R., Pilegaard, K., and Weidinger, T. (in preparation 2015 for *Atmos. Meas. Tech. Discuss.*). Eddy-covariance flux measurements of ozone deposition: review and development of a common methodology.

NEO. (2014). *Leaf Area Index (TERRA/MODIS)*. Retrieved 15 10 2014 from NASA Earth Observations: http://neo.sci.gsfc.nasa.gov/view.php?datasetId=MOD15A2_M_LAI.

Ng, N. L., Chhabra, P. S., Chan, A. W. H., Surratt, J. D., Kroll, J. H., Kwan, A. J., McCabe, D. C., Wennberg, P. O., Sorooshian, A., Murphy, S. M., Dalleska, N. F., Flagan, R. C., and Seinfeld, J.H. (2007a). Effect of NOx level on secondary organic aerosol (SOA) formation from the photooxidation of terpenes. *Atmos. Chem. Phys., 7*, 5159–5174.

Ng, N. L., Kroll, J. H., Chan, A. W. H., Chhabra, P. S., Flagan, R. C., and Seinfeld, J. H. (2007b). Secondary organic aerosol formation from *m*-xylene, toluene, and benzene. *Atmos. Chem. Phys., 7*, 3909–3922.

Niinemets, Ü., Tenhunen, J. D., Harley, P. C., and Steinbrecher, R. (1999). A model of isoprene emission based on energetic requirements for isoprene synthesis and leaf photosynthetic properties for Liquidambar and Quercus. *Plant. Cell. Environ., 22*, 1319–1335.

Nobre, C. A., Obergon, G. O., Marengo, J. A., Fu, R., and Poveda, G. (2009). Characteristics of Amazonian Climate: Main Features. In M. B. Keller, *Amazonia and global change* (pp. 149-162). American Geophysical Union. Washington, DC, USA.

Odum, J. R., Jungkamp, T. P. W., Griffin, R. J., Forstner, H. J. L., Flagan, R. C., Seinfeld, J. H. (1997). Aromatics, reformulated gasoline, and atmospheric organic aerosol formation. *Environ. Sci. Technol., 31*, 1890–1897.

Oke, T. R. (2006). Towards better scientific communication in urban climate. *Theor. Appl. Climatol., 84*, 179–190.

Olson, D. M., Dinerstein, E., Wikramanayake, E. D., Burgess, N. D., Powell, G. V. N., Underwood, E. C., D'amico, J. A., Itoua, I., Strand, H. E., Morrison, J. C., Loucks, C. J., Allnutt, T. F., Ricketts, T. H., Kura, Y., Lamoreux, J. F., Wettengel, W. W., Hedao, P., and Kassem, R. (2001). Terrestrial Ecoregions of the World: A New Map of Life on Earth: A new global map of terrestrial ecoregions provides an innovative tool for conserving biodiversity. *BioScience, 51*(11), 933-938.

Ortega, J., Helmig, D., Guenther, A., Harley, P., Pressley, S., and Vogel, C. (2007). Flux estimates and OH reaction potential of reactive biogenic volatile organic compounds (BVOCs) from a mixed northern hardwood forest. *Atmos. Environ., 41*(26), 5479–5495.

Owen, S. M. and Hewitt, C. N. (2000). Extrapolating branch enclosure measurements to estimates of regional scale biogenic VOC fluxes in the northwestern Mediterranean basin. *J. Geophys. Res. - Atmos., 105*, 11573-11583.

Pacifico, F., Harrison, S. P., Jones, C. D., and Sitch, S. (2009). Isoprene emissions and climate. *Atmos. Environ., 43*, 6121–6135.

Park, C., Schade, G. W., and Boedeker, I. (2010). Flux measurements of volatile organic compounds by the relaxed eddy accumulation method combined with a GC-FID system in urban Houston, Texas. *Atmos. Environ., 44*, 2605-2614.

Park, C., Schade, G. W., and Boedeker, I. (2011). Characteristics of the flux of isoprene and its oxidation products in an urban area. *J. Geophys. Res. - Atmos., 116(*D21*)*, D21303.

Passant, N. (2002). *Speciation of UK emissions of non-methane volatile organic compounds.* AEA Technology, Abingdon, Oxfordshire, UK.

Paulot, F., Crounse, J. D., Kjaergaard, H. G., Kurten, A., St. Clair, J. M., Seinfeld, J. H., and Wennberg, P. O. (2009). Unexpected Epoxide Formation in the Gas-Phase Photooxidation of Isoprene. *Science, 325*, 730–733.

Pavia, D. L., Lampman, G. M., Kritz, G. S., and Engel, R. G. (2006). *Introduction to Organic Laboratory Techniques (4th Ed.).* Thomson Brooks/Cole, Pacific Grove, California, USA.

Peeters, J., Nguyen, T. L., and Vereecken, L. (2009). HOx radical regeneration in the oxidation of isoprene. *Phys. Chem. Chem. Phys., 11*(28), 5935–5939.

Perry, D. (1994). *Forest Ecosystems.* The Johns Hopkins University Press, Baltimore, USA.

Phillips, O. L., Aragão, L. E. O. C., Lewis, S. L., Fisher, J. B., Lloyd, J., López-González, G., Malhi, Y., Monteagudo, A., Peacock, J., Quesada, C. A., van der Heijden, G., Almeida, S., Amaral, I., Arroyo, L., Aymard, G., Baker, T. R., Bánki, O., Blanc, L ., Bonal, D., Brando, P., Chave, J., de Oliveira, A. C. A., Cardozo, N. D., Czimczik, C. I., Feldpausch, T. R., Freitas, M. A., Gloor, E., Higuchi, N., Jiménez, E., Lloyd, G., Meir, P., Mendoza, C., Morel, A., Neill, D. A., Nepstad, D., Patiño, S., Peñuela, M. C. , Prieto, A., Ramírez, F., Schwarz, M., Silva, J., Silveira, M., Thomas, A. S., ter Steege, H., Stropp, J., Vásquez, R., Zelazowski, P., Dávila, E. A., Andelman, S., Andrade, A., Chao, K. J, Erwin, T., Di Fiore, A., Honorio C., E., Keeling, H., Killeen, T. J., Laurance, W. F., Cruz, A. P., Pitman, N. C. A., Vargas, P. N., Ramírez-Angulo, H., Rudas, A., Salamão, R., Silva, N., Terborgh, J., and Torres-Lezama, A. (2009). Drought Sensitivity of the Amazon Rainforest., *Science, 323*, 1344-1347.

Piccot, S. D. , Watson. J. J., and Jones, J. W. (1992). A global inventory of volatile organic compound emissions from anthropogenic sources. *J. Geophys. Res.- Atmos., 97*(D9), 9897–9912.

Pinho, P. G., Pio, C. A., and Jenkin, M. E. (2005). Evaluation of isoprene degradation in the detailed tropospheric chemical mechanism, MCM v3, using environmental chamber data. *Atmos. Environ., 39*, 1303–1322.

Pitman, N. C. A., Terborgh, J. W., Silman, M. R., Núñez V, P., Neill, D. A., Cerón, C. E., Palacios, W. A., and Aulestia, M. (2001). Dominance and distribution of tree species in upper Amazonian Terra Firme forests. *Ecology, 82*, 2101–2117.

Plantaz, M. (1998). *Surface/atmosphere exchange of ammonia over grazed pasture.* PhD Thesis, Wageningen, The Netherlands.

Prather, M., Ehhalt, D., Dentener, F. J., Derwent, R., Dlugokencky, E. J., Holland, E., Isaksen, I., Katima, J., Kirchhoff, V., Matson, P., Midgley, P., and Wang, M. (2001). Atmospheric chemistry and greenhouse gases. In J. T. Houghton, *Climate Change 2001, The Scientific Basis, Contribution of Working Group I to the Third Assessment Report of the Intergovernmental Panel on Climate Change* (pp. 238–287). Cambridge University Press, Cambridge, UK.

Presto, A. A., Huff Hartz, K. E., and Donahue, N. M. (2005). Secondary organic aerosol production from ozonolysis: 2. Effect of NOx concentration. *Environ. Sci. Technol., 39*, 7046–7054.

Pugh, T. A. M., MacKenzie, A. R., Hewitt, C. N., Langford, B., Edwards, P. M., Furneaux, K. L., Heard, D. E., Hopkins, J. R., Jones, C. E., Karunaharan, A., Lee, J., Mills, G., Misztal, P., Moller, S., Monks, P. S., and Whalley, L. K. (2010). Simulating atmospheric composition over a South-East Asian tropical rainforest: performance of a chemistry box model. *Atmos. Chem. Phys., 10*, 279-298. doi:10.5194/acp-10-279-2010.

Pugh, T. A. M., MacKenzie, A. R. , Whyatt, J. D., and Hewitt, C. N. (2012). Effectiveness of Green Infrastructure for Improvement of Air Quality in Urban Street Canyons. *Environ. Sci. Technol., 46*(14), 7692–7699.

Räisänen, T., Ryyppö, A., and Kellomäki, S. (2009). Monoterpene emission of a boreal Scots pine (Pinus sylvestris L.) forest. *Agr. Forest Meteorol., 149*(5), 808–819.

Ramanathan, V., Crutzen, P. J., Kiehl, J. T., and Rosenfeld, D. (2001). Aerosols, climate, and the hydrological cycle. *Science, 294*(5549), 2119–2124.

Rasmussen, R. A. and Khalil, M. A. K. (1988). Isoprene over the Amazon Basin. *J. Geophys. Res.*, *93*(D2), 1471-1421.

Reissell, A., Harry, C., Aschmann, S. M., Atkinson, R., and Arey, J. (1999). Formation of acetone from the OH radical- and $O_3$-initiated reactions of a series of monoterpenes. *J. Geophys. Res*., *104*, 13869-13879.

Ribeiro, J. D. S., Hopkins, M., Vicentini, A., Sothers, C. A., Costa, M. A. d. S., de Brito, J. M., de Souza, M. A. D., Martins, L. H. P., Lohmann, L. G., Assuncao, P. A. C. L., Pereira, E. d. C., da Silva, C. F., Mesquita, M. R., and Procópio, L. C. (1999). *Flora da Reserva Ducke: Guia de identificacao das plantas vasculares de uma floresta de terra-firme na Amazonia Central.* INPA, Manaus, Brazil.

Rinne, H. J. I., Guenther, A. B., Warneke, C., de Gouw, J. A., and Luxembourg, S. L. (2001). Disjunct eddy covariance technique for trace gas flux measurements. *Geophys. Res. Lett., 28*(16), 3139–3142. doi: 10.1029/2001GL012900.

Rinne, H. J. I., Guenther, A. B., Greenberg, J. P., and Harley, P. C. (2002). Isoprene and monoterpene fluxes measured above Amazonian rainforest and their dependence on light and temperature. *Atmos. Environ., 36*, 2421–2426.

Rinne, H. J. I., Markkanen, T., Ruuskanen, T. M., Petäjä, T., Keronen, P., Tang, M. J., Crowley, J. N., Rannik, Ü., and Vesala, T. (2012). Effect of chemical degradation on fluxes of reactive compounds – a study with a stochastic Lagrangian transport model. *Atmos. Chem. Phys., 12*, 4843-4854.

Rivera-Rios, J. C., Nguyen, T. B., Crounse, J. D., Jud, W., St. Clair, J. M., Mikoviny, T., Gilman, J. B., Lerner, B. M., Kaiser, J.B., de Gouw, J., Wisthaler, A., Hansel, A., Wennberg, P. O., Seinfeld, J. H., and Keutsch, F. N. (2014). Conversion of hydroperoxides to carbonyls in field and laboratory instrumentation: observational bias in diagnosing pristine versus anthropogenically-controlled atmospheric chemistry. *Geophys. Res. Lett., 41*(23), 8645–8651.

Robinson, A. L., Donahue, N. M., Shrivastava, M. K., Weitkamp, E. A., Sage, A. M., Grieshop, A. P., Lane, T. E., Pierce, J. R., and Pandis, S. N. (2007). Rethinking Organic Aerosols: Semivolatile Emissions and Photochemical Aging. *Science, 315* (5816 ), 1259-1262. doi: 10.1126/science.1133061.

Rubin, J. I., Kean, A. J., Harley, R. A., Millet, D. B., and Goldstein, A. H. (2006). Temperature dependence of volatile organic com- pound evaporative emissions from motor vehicles. *J. Geophys. Res.- Atmos., 111*, D03305. doi:10.1029/2005JD006458.

Running, S. W., Baldocchi, D. D., Turner, D. P., Gower, S. T., Bakwin, P. S., and Hibbard, K. A. (1999). A Global Terrestrial Monitoring Network Integrating Tower Fluxes, Flask Sampling, Ecosystem Modeling and EOS Satellite Data. *Remote Sens. Environ., 70*(1), 108–127.

Sawada, S. and Tutsuka, T. (1986). Natural and anthropogenic sources of atmospheric ethylene. *Atmos. Environ., 20*, 821–832.

Schade, G. W. and Goldstein, A. H. (2001). Fluxes of oxygenated volatile organic compounds from a ponderosa pine plantation. *J. Geophys. Res.*, *106*, 3111–3123.

Seaton, A., Godden, D., MacNee, W., and Donaldson, K. (1995). Particulate air pollution and acute health effects. *Lancet, 345*(8943), 176–178. doi:10.1016/S0140-6736(95)90173-6.

Sharkey, T. D. and Loreto, F. (1993). Water stress, temperature, and light effects on the capacity for isoprene emission and photosynthesis of kudzu leaves. *Oecologia, 95*(3), 328-333.

Sharkey, T. D., Wiberley, A. E., and Donohue, A. R. (2008). Isoprene Emission from Plants: Why and How. *Ann. Bot-London, 101*, 5-18.

Shindell, D. T., Faluvegi, G., Bell, N., and Schmidt, G. A. (2005). An emissions-based view of climate forcing by methane and tropospheric ozone. *Geophys. Res. Lett., 32*, L04803. doi:10.1029/2004GL021900.

Sillman, S., He, D., Pippin, M., Daum, P., Kleinman, L., Lee, J.H., and Weinstein-Lloyd, J. (1998). Model correlations for ozone, reactive nitrogen and peroxides for Nashville in comparsion with measurements: implications for $NO_x$-hydrocarbon sensitivity. *J. Geophys. Res., 103*, 22,629-22,644.

Sillman, S. (1999). The relation between ozone, NOx and hydrocarbons in urban and polluted rural environments. *Atmos. Environ., 33*, 1821- 1845.

Simpson, D., Guenther, A., Hewitt, C. N., and Steinbrecher, R. (1995). Biogenic emissions in Europe: 1. Estimates and uncertainties. *J. Geophys. Res., 100*(D11), 22875–22890. doi:10.1029/95JD02368.

Sindelarova, K., Granier, C., Bouarar, L., Guenther, A., Tilmes, S., Stavrakou, T., Müller, J.-F., Kuhn, U., Stefani, P., and Knorr, W. (2014). Global data set of biogenic VOC emissions calculated by the MEGAN model over the last 30 years. *Atmos. Chem. Phys., 14*, 9317–9341.

Singh, H. B., O'Hara, D., Herlth, D., Sachsse, W., Blake, D. R., Bradshaw, J. D., Kanakidou, M., and Crutzen, P. J. (1994). Acetone in the atmosphere: Distribution, source, and sinks. *J. Geophys. Res., 99*, 1805-1819.

Sitch, S., Smith, B., Prentice, I. C., Arneth, A., Bondeau, A., Cramer, W., Kaplan, J. O., Levis, S., Lucht, W., Sykes, M. T., Thonicke, K., and Venevsky, S. (2003). Evaluation of

ecosystem dynamics, plant geography and terrestrial carbon cycling in the LPJ dynamic global vegetation model. *Glob. Change Biol., 9*, 161–185.

Spaněl, P. and Smith, D. (2000). Influence of water vapour on selected ion flow tube mass spectrometric analyses of trace gases in humid air and breath. *Rapid Commun. Mass Sp., 14*(20), 1898–906.

Spirig, C., Neftel, A., Ammann, C., Dommen, J., Grabmer, W., Thielmann, A., Schaub, A., Beauchamp, J., Wisthaler, A., and Hansel, A. (2005). Eddy covariance flux measurements of biogenic VOCs during ECHO 2003 using proton transfer reaction mass spectrometry. *Atmos. Chem. Phys., 5*, 465-481.

Spracklen, D. V., Jimenez, J. L., Carslaw, K. S., Worsnop, D. R., Evans, M. J., Mann, G. W., Zhang, Q., Canagaratna, M. R., Allan, J., Coe, H., McFiggans, G., Rap, A., and Forster, P. (2011). Aerosol mass spectrometer constraint on the global secondary organic aerosol budget. *Atmos. Chem. Phys., 11*, 12109–12136.

Srivastava, A., Joseph, A. E., More, A., and Patil, S. (2005). Emissions of vocs at urban petrol retail distribution centres in India (Delhi and Mumbai). *Environ. Monit. Assess., 109*, 227–242.

Staudt, M. and Seufert, G. (1995). Light-dependent emission of monoterpenes by holm oak (Quercus ilex L.). *The Science of Nature, 82*(2), 89-92.

Stefani, P., Valentini, R., Ciccioli, P., Brancaleoni, E., Frattoni, M., Nobre, A., and De Araujo, A. (2000). Preliminary assessment of VOC fluxes from a primary rain forest performed at the LBA site in Manuas. In: Artaxo, P. (Ed.), *Proceedings of the First LBA Scientific Conference* (p. 106). MCT. Belem, Brazil.

Stewart, I. D. and Oke, T. R. (2012). Local Climate Zones for Urban Temperature Studies, *B. Am. Meteorol. Soc.*, 93, 1879–1900.

Stull, R. (1988). A reevaluation of two dispersal theories. *J. Atmos. Sci., 45*(14), 2082-2091.

Taipale, R., Ruuskanen, T. M., Rinne, J., Kajos, M. K., Hakola, H., Pohja, T., and Kulmala, M. (2008). Technical Note: Quantitative long-term measurements of VOC concentrations by PTR-MS − measurement, calibration, and volume mixing ratio calculation methods. *Atmos. Chem. Phys., 8*, 6681–6698.

Taipale, R., Ruuskanen, T. M., and Rinne, J. (2010). Lag time determination in DEC measurements with PTR-MS. *Atmos. Meas. Tech., 3*, 853-862.

Taipale, R., Kajos, M. K., Patokoski, J., Rantala, P., Ruuskanen, T. M., and Rinne, J. (2011). Role of de novo biosynthesis in ecosystem scale monoterpene emissions from a boreal Scots pine forest. *Biogeosciences, 8*, 2247–2255.

Tanaka, L. M. d. S., Satyamurty, P., and Machado, L. A. T. (2014). Diurnal variation of precipitation in central Amazon Basin. *Int. J. Climatol., 34*, 3574–3584.

Tani, A., Hayward, S., Hansel, A., and Hewitt, C. N. (2004). Effect of water vapour pressure on monoterpene measurements using proton transfer reaction-mass spectrometry (PTR-MS). *Int. J. Mass. Spectrom., 239*, 161–169.

Tarvainen, V., Hakola, H., Hellén, H., Bäck, J., Hari, P., and Kulmala, M. (2005). Temperature and light dependence of the VOC emissions of Scots pine. *Atmos. Chem. Phys., 5*, 989–998.

Ter Steege, H., Pitman, N. C. A., Sabatier, D., Baraloto, C., Salomão, R. P., Guevara, J. E., Phillips, O. L., Castilho, C. V., Magnusson, W. E., Molino, J.-F., Monteagudo, A., Núñez Vargas, P., Montero, J. C., Feldpausch, T. R., Coronado, E. N. H., T. J., Killeen, Mostacedo, B., Vasquez, R., Assis, R. L., Terborgh, J., Wittmann, F., Andrade, A., Laurance, W. F., Laurance, S. G. W., Marimon, B. S., Marimon, B.-H., Guimarães Vieira, I. C., Amaral, I. L., Brienen, R., Castellanos, H., Cárdenas López, D., Duivenvoorden, J. F., Mogollón, H. F., Matos, F.D. de A., Dávila, N., García-Villacorta, R., Stevenson Diaz, P.R., Costa, F., Emilio, T., Levis, C., Schietti, J., Souza, P., Alonso,A., Dallmeier, F., Montoya, A. J. D., Fernandez Piedade, M.T., Araujo-Murakami, A., Arroyo, L., Gribel, R., Fine, P. V. A., Peres, C. A., Toledo, M., Aymard C, G. A., Baker, T. R., Cerón,C., Engel, J., Henkel, T. W., Maas, P., Petronelli, P., Stropp, J.,Zartman, C. E., Daly, D., Neill, D., Silveira, M., Paredes, M. R., Chave, J., Lima Filho, D. de A., Jørgensen, P. M., Fuentes, A.,Schöngart, J., Cornejo Valverde, F., Di Fiore, A., Jimenez, E.M., Peñuela Mora, M. C., Phillips, J. F., Rivas, G., van Andel,T. R., von Hildebrand, P., Hoffman, B., Zent, E. L., Malhi, Y., Prieto, A., Rudas, A., Ruschell, A. R., Silva, N., Vos, V., Zent,S., Oliveira, A. A., Schutz, A. C., Gonzales, T., Trindade Nascimento, M., Ramirez-Angulo, H., Sierra, R., Tirado, M., UmañaMedina, M. N., van der Heijden, G., Vela, C. I. A., Vilanova Torre, E., Vriesendorp, C., Wang, O., Young, K. R., Baider, C., Ferreira, C., Mesones, I., Torres-Lezama, A., Urrego Giraldo, L. E., Zagt, R., Alexiades, M. N., Hernandez, L., Huamantupa-Chuquimaco, I., Milliken, W., Palacios Cuenca, W., Pauletto, D., Valderrama Sandoval, E., Valenzuela Gamarra, L., Dexter, K.G., Feeley, K., Lopez-Gonzalez, G., and Silman, M. R. (2013). Hyperdominance in the Amazonian tree flora. *Science, 342(6156)*, 1243092. doi:10.1126/science.1243092.

Theloke, J. and Friedrich, R. (2007). Compilation of a database on the composition of anthropogenic VOC emissions for atmospheric modeling in Europe. *Atmos. Environ., 41*, 4148–4160.

Tsigaridis, K. and Kanakidou, M. (2003). Global modelling of secondary organic aerosols in the troposphere: A sensitivity study. *Atmos. Chem. Phys., 3*, 1849–1869.

Tuazon, E. C. and Atkinson, R. (1990). A product study of the gas-phase reaction of isoprene with the OH radical in the presence of $NO_x$. *Int. J. Chem. Kinet., 22*, 1221– 1236.

Turnipseed, A. A., Pressley, S. N., Karl, T., Lamb, B., Nemitz, E., Allwine, E., Cooper, W. A., Shertz, S., and Guenther, A. B. (2009). The use of disjunct eddy sampling methods for the determination of ecosystem level fluxes of trace gases. *Atmos. Chem. Phys., 9*, 981– 994.

Valach, A. C., Langford, B., Nemitz, E., MacKenzie, A. R., and Hewitt, C. N. (2014). Concentrations of selected volatile organic compounds at kerbside and background sites in central London. *Atmos. Environ.*, *95*, 456–467. doi:10.1016/j.atmosenv.-2014.06.052.

Valencia, R., Foster, R. B., Villa, G., Condit, R., Svenning, J.-C., Hernández, C., Romoleroux, K., Losos, E., Magård, E., and Balslev, H. (2004). Tree species distributions and local habitat variation in the Amazon: large forest plot in eastern Ecuador. *J. Ecol., 92*, 214– 229.

van Loon, M., Vautard, R., Schaap, M., Bergström, R., Bessagnet, B., Brandt, J., Builtjes, P.J.H., Christensen, J.H., Cuvelier, C., Graff, A., Jonson, J.E., Krol, M., Langner, J., Roberts, P., Rouil, L., Stern, R., Tarrasón, L., Thunis, P., Vignati, E., White, L. and Wind, P. (2007). Evaluation of long-term ozone simulations from seven regional air quality models and their ensemble. *Atmos. Environ.*, *41*(10), 2083–2097.

Vardoulakis, S., Valiantis, M., Milner, J., and ApSimon, H. (2007). Operational air pollution modelling in the UK—Street canyon applications and challenges. *Atmos. Environ., 41*, 4622–4637.

Vaughan, S., Ingham, T., Whalley, L. K., Stone, D., Evans, M. J., Read, K. A., Lee, J. D., Moller, S. J., Carpenter, L. J., Lewis, A. C., Fleming, Z. L., and Heard, D. E. (2012). Seasonal observations of OH and $HO_2$ in the remote tropical marine boundary layer. *Atmos. Chem. Phys., 12*, 2149–2172.

Velasco, E., Lamb, B., Pressley, S., Allwine, E., Westberg, H., Jobson, B. T., Alexander, M., Prazeller, P., Molina, L., and Molina, M. (2005). Flux measurements of volatile organic compounds from an urban landscape. *Geophys. Res. Lett., 32*, L20802.

Velasco, E., Lamb, B.,Westberg, H., Allwine, E., Sosa, G., Arriaga-Colina, J. L., Jobson, B. T., Alexander, M. L., Prazeller, P., Knighton, W. B., Rogers, T. M., Grutter, M., Herndon, S. C., Kolb, C. E., Zavala, M., de Foy, B., Volkamer, R., Molina, L. T., Kolb, C. E., Zavala, M., de Foy, B., Volkamer, R., Molina, L. T., and Molina, M. J. (2007). Distribution, magnitudes, reactivities, ratios and diurnal patterns of volatile organic compounds in the Valley of Mexico during the MCMA 2002 & 2003 field campaigns. *Atmos. Chem. Phys.*, 7, 329–353.

Velasco, E., Pressley, S., Grivicke, R., Allwine, E., Coons, T., Foster, W., Jobson, B. T., Westberg, H., Ramos, R., Hernández, F., Molina, L. T., and Lamb, B. (2009). Eddy covariance flux measurements of pollutant gases in urban Mexico City. *Atmos. Chem. Phys., 9*, 7325–7342.

Vilà-Guerau de Arellano, J., van den Dries, K., and Pino, D. (2009). On inferring isoprene emission surface flux from atmospheric boundary layer concentration measurements. *Atmos. Chem. Phys., 9*, 3629–3640.

Volkamer, R., Jimenez, J. L., San Martini, F., Dzepina, K., Zhang, Q., Salcedo, D., Molina, L. T., Worsnop, D. R., and Molina, M. J. (2006). Secondary organic aerosol formation from anthropogenic air pollution: Rapid and higher than expected. *Geophys. Res. Lett., 33*, L17811. doi:10.1029/2006GL026899.

von Kuhlmann, R., Lawrence, M. G., Pöschl, U., and Crutzen, P. J. (2004). Sensitivities in global scale modeling of isoprene. *Atmos. Chem. Phys., 4*, 1–17.

Wagner, W., Nemecek-Marshall M., and Fall, R. (1999). Three Distinct Phases of Isoprene Formation during Growth and Sporulation of Bacillus subtilis. *J. Bacteriol., 181*(15), 4700–4703.

Wang, Y. and Jacob, D. J. (1998). Anthropogenic forcing on tropospheric ozone and OH since preindustrial times. *J. Geophys. Res., 103*, 31123–31135.

Warneck, P. (1988). *Chemistry of the Natural Atmosphere.* Academic Press, San Diego, California, USA.

Warneke, C., Karl, T., Judmaier, H., Hansel, A., Jordan, A., Lindinger, W., and Crutzen, P. J. (1999). Acetone, methanol, and other partially oxidized volatile organic emissions from

dead plant matter by abiological processes: Significance for atmospheric $HO_x$ chemistry. *Global Biogeochem. Cy., 13*, 9–17.

Warneke, C., van der Veen, C., Luxembourg, S., de Gouw, J. A., and Kok, A. (2001). Measurements of benzene and toluene in ambient air using proton-transfer-reaction mass spectrometry: calibration, humidity dependence, and field intercomparison. *Int. J. Mass. Spectrom., 207*(3), 167–182.

Warneke, C., Luxembourg, S. L., de Gouw, J. A., Rinne, H. J. I., Guenther, A. B., and Fall, R. (2002). Disjunct eddy covariance measurements of oxygenated volatile organic compounds fluxes from an alfalfa field before and after cutting. *J. Geophys. Res.- Atmos., 107*(D8), 4067. doi:10.1029/2001JD000594.

Warneke, C., de Gouw, J. A., Kuster, W. C., Goldan, P. D., and Fall, R. (2003). Validation of atmospheric VOC measurements by proton-transfer-reaction mass spectrometry using a gas-chromatographic preseparation method. *Environ. Sci. Technol., 37*, 2494–2501.

Warneke, C., McKeen, S. A., de Gouw, J. A., Goldan, P. D., Kuster, W. C., Holloway, J. S., Williams, E. J., Lerner, B. M., Parrish, D. D., Trainier, M., Fehsenfeld, F. C., Kato, S., Atlas, E. L., Baker, A., and Blake, D. R. (2007). Determination of urban volatile organic compound emission ratios and comparison with an emissions database. *J. Geophys. Res., 112*(D10), D10S47. doi:10.1029/2006JD007930.

Weber, R. O. (1999). Remarks on the definition and estimation of friction velocity. *Bound.-Lay. Meteorol., 93*(2), 197-209.

Wei, W., Wang, S., Chatani, S., Klimont, Z., Cofala, J., and Hao, J. (2008). Emission and speciation of non-methane volatile organic compounds from anthropogenic sources in China. *Atmos. Environ., 42*(20), 4976–4988.

Wienhold, F. G., Frahm, H., and Harris, G. W. (1994). Measurements of N2O fluxes from fertilized grassland unsing a fast-response tunable diode-laser spectrometer. *J. Geophys. Res.- Atmos., 99*, 16557-16567.

Wilkinson, M. J., Owen, S. M., Possell, M., Hartwell, J., Gould, P., Hall, A., Vickers, C., and Hewitt, C. N. (2006). Circadian control of isoprene emissions from oil palm (Elaeis guineensis). *Plant J., 47*, 960-968.

Williams, M., Barrowcliffe, R., Laxen, D., and Monks, P. (2011). Review of air quality modelling in DEFRA. Air Quality Modelling Review Steering Group, London, UK.

Wood, E. C., Canagaratna, M. R., Herndon, S. C., Onasch, T. B., Kolb, C. E., Worsnop, D. R., Kroll, J. H., Knighton, W. B., Seila, R., Zavala, M., Molina, L. T., DeCarlo, P. F., Jimenez, J. L., Weinheimer, A. J., Knapp, D. J., Jobson, B. T., Stutz, J., Kuster, W. C., and Williams, E. J. (2010). Investigation of the correlation between odd oxygen and secondary organic aerosol in Mexico City and Houston. *Atmos. Chem. Phys., 10*, 8947–8968.

Wood, S. (2006). Generalized Additive Models: an Introduction with R. Chapman & Hall, CRC Press, London, UK.

Wyche, K. P., Ryan, A. C., Hewitt, C. N., Alfarra, M. R., McFiggans, G., Carr, T., Monks, P. S., Smallbone, K. L., Capes, G., Hamilton, J. F., Pugh, T. A. M., and MacKenzie, A. R. (2014). Emissions of biogenic volatile organic compounds and subsequent photochemical production of secondary organic aerosol in mesocosm studies of temperate and tropical plant species. *Atmos. Chem. Phys., 14*, 12781–12801.

Yañez-Serrano, A. M., Nölscher, A. C., Williams, J., Wolff, S., Alves, E., Martins, G. A., Bourtsoukidis, E., Brito, J., Jardine, K., Artaxo, P., and Kesselmeier, J. (2015). Diel and seasonal changes of biogenic volatile organic compounds within and above an Amazonian rainforest. *Atmos. Chem. Phys., 15*, 3359–3378.

Yardley, R., Dernie, J., and Dumitrean, P. (2012). UK Hydrocarbon Network Annual Report for 2011.

Young, P. J., Arneth, A., Schurgers, G., Zeng, G., and Pyle, J. A. (2009). The CO2 inhibition of terrestrial isoprene emission significantly affects future ozone projections. *Atmos. Chem. Phys., 9*, 2793-2803.

Yuan, B., Warneke, C., Shao, M., and de Gouw, J. A. (2014). Interpretation of volatile organic compound measurements by proton-transfer-reaction mass spectrometry over the deepwater horizon oil spill. *Int. J. Mass. Spectrom., 358*, 43–48. doi:10.1016/j.ijms.2013.11.006.

Zavala, M., Herndon, S. C., Slott, R. S., Dunlea, E. J., Marr, L. C., Shorter, J. H., Zahniser, M., Knighton, W. B., Rogers, T. M., Kolb, C. E., Molina, L. T., and Molina, M. J. (2006). Characterization of on-road vehicle emissions in the Mexico City Metropolitan Area using a mobile laboratory in chase and fleet average measurement modes during the MCMA-2003 field campaign, *Atmos. Chem. Phys., 6*, 5129–5142.

Zaveri, R. A., Voss, P. B., Berkowitz, C. M., Fortner, E., Zheng, J., Zhang, R., Valente, R. J., Tanner, R. L., Holcomb, D., Hartley, T. P., and Baran, L. (2010). Overnight atmospheric transport and chemical processing of photochemically aged Houston urban and petrochemical industrial plume. *J. Geophys. Res., 115*, D23303.

Zhang, X., Cappa, C. D., Jathar, S. H., McVay, R. C., Ensberg, J. J., Kleeman, M. J., and Seinfeld, J. H. (2014). Influence of vapor wall loss in laboratory chambers on yields of secondary organic aerosol. *P. Natl. A. Sci, 111*(16), 5802-5807.

Zimmermann, P. R., Greenberg, J. P., and Westberg, C. E. (1988). Measurements of atmospheric hydrocarbons and biogenic emission fluxes in the Amazon boudary layer. *J. Geophys. Res., 93*(D2), 1407-1416.

# Appendix I

## A1.1 Conservation equation

The conservation equation parameterises the four major transport processes: turbulent exchange, horizontal advection, chemical reaction and molecular diffusion.

$$\frac{\partial \bar{c}}{\partial t} = -\underbrace{\frac{\bar{u}\partial \bar{c}}{\partial x} - \frac{\bar{v}\partial \bar{c}}{\partial y} - \frac{\bar{w}\partial \bar{c}}{\partial z}}_{\text{Advection}} - \underbrace{\frac{\partial \overline{u'c'}}{\partial x} - \frac{\partial \overline{v'c'}}{\partial y} - \frac{\partial \overline{w'c'}}{\partial z}}_{\text{Divergence}} + D + S, \qquad (A1.1)$$

where the scalar is ($c$), $u$, $v$, and $w$ are the 3D wind components, $D$ is molecular diffusion, and $S$ represents source and sink terms for the chemical reactions.

## A1.2 Sonic data processing

Coordinate rotations of the sonic data to correct for instrument tilting were applied using the following equations:

$$U_{hor} = \sqrt{(V^2 + U^2)} \qquad (A1.2)$$

$$U_{tot} = \sqrt{(W^2 + U_{hor}{}^2)} \qquad (A1.3)$$

$$\cos(\eta) = \frac{U}{U_{hor}} \qquad (A1.4)$$

$$\sin(\eta) = \frac{V}{U_{hor}} \qquad (A1.5)$$

$$\cos(\theta) = \frac{U_{hor}}{U_{tot}} \qquad (A1.6)$$

$$\sin(\theta) = \frac{W}{U_{tot}} \qquad (A1.7)$$

$$U_{cor} = u\cos(\theta)\cos(\eta) + v\cos(\theta)\sin(\eta) + w\sin(\theta) \qquad (A1.8)$$

$$V_{cor} = -u\sin(\eta) + v\cos(\eta) \qquad (A1.9)$$

$$W_{cor} = -u\sin(\theta)\cos(\eta) - v\sin(\theta)\sin(\eta) + w\cos(\theta), \qquad (A1.10)$$

where $U$, $V$, and $W$ represent the average wind components over the flux averaging period and $u$, $v$, and $w$ are their instantaneous values. Wind direction is dependent on the type of sonic anemometer used, but wind speed is calculated as

$$ws = \sqrt{(U^2 + V^2 + W^2)} \qquad (A1.11)$$

Additional variables were then calculated:

Sensible heat flux:

$$H = c_P\rho_0\overline{w'T'} \qquad (A1.12)$$

where $c_P$ is the specific heat capacity of air, $\rho_0$ is the density of air, and $T$ is the temperature taken from the sonic anemometer calculated from measuring the speed of sound.

Momentum flux:

$$\tau = \rho_0\overline{u'w'} \qquad (A1.13)$$

A common method to calculate the friction velocity is:

$$u^* = \sqrt{\left|\left(\frac{\tau}{\rho_0}\right)\right|} = \sqrt{|\overline{u'w'}|} \qquad (A1.14)$$

However, the theoretical requirements of this method are not always met (Weber, 1999) and therefore $u_*$ should be calculated as follows:

$$u^* = \left(\overline{u'w'}^2 + \overline{v'w'}^2\right)^{1/4} \qquad (A1.15)$$

Obukhov length:

$$L = \frac{-c_P \rho_0 u^{*3} T}{K g H} \qquad (A1.16)$$

where $K$ is the von Karman's constant (0.40) and $g$ is the acceleration due to gravity.

## A1.3 Isoprene emission model algorithms

The light and temperature adjustment factor $\gamma_0$ in the isoprene emission model based on Guenther *et al.* (1995) is calculated from light and temperature factors as

$$\gamma_0 = C_L C_T, \qquad (A1.17)$$

whereby $C_L$ is calculated by

$$C_L = \frac{\alpha c_{L1} Q}{\sqrt{1 + \alpha^2 Q^2}}, \qquad (A1.18)$$

where $Q$ is the PAR flux ($\mu$mol m$^{-2}$ s$^{-1}$), $\alpha = 0.0027$ and $c_{L1} = 1.066$ are empirically derived coefficients, and $C_T$ is calculated by

$$C_T = \frac{exp\frac{c_{T1}(T_L - T_S)}{RT_S T_L}}{1 + exp\frac{c_{T2}(T_L - T_M)}{RT_S T_L}}, \qquad (A1.19)$$

where $T$ is the leaf temperature (K), $T_S$ is the temperature at standard conditions (303 K), $R = 8.314$ J K$^{-1}$ mol$^{-1}$ is a constant, and $c_{T1} = 95000$ J mol$^{-1}$, $c_{T2} = 230000$ J mol$^{-1}$, and $T_M = 314$ K are empirical coefficients. There are a number of ways to calculate or estimate the foliar density ($D_0$) depending on the climate and seasonality of the ecosystem, which are listed in detail elsewhere (Guenther *et al.,* 1995).

The MEGAN algorithm provides different versions of $\gamma$. The PCEEA algorithm was used, which calculates $\gamma$ as follows

$$\gamma = \gamma_{CE} \gamma_{age} \gamma_{SM}, \qquad (A1.20)$$

where leaf age $\gamma_{age}$ and soil moisture $\gamma_{SM}$ factors can be assumed to equal 1, and the canopy environment factor $\gamma_{CE}$ is calculated by

$$\gamma_{CE} = \gamma_{LAI}\gamma_P\gamma_T, \tag{A1.21}$$

where the leaf area index variations are from

$$\gamma_{LAI} = \frac{0.49LAI}{\sqrt{(1 + 0.2LAI^2)}}, \tag{A1.22}$$

where LAI is the leaf area index of the canopy. The factor accounting for variations in PAR flux $\gamma_P = 0$ if $\sin(a) < 0$ where $a$ is the solar angle (°), for $\sin(a) > 0$ it is calculated from

$$\gamma_P = \sin(a)\left[2.46\left(1 + 0.0005(P_{daily} - 400)\right)\phi - 0.9\phi^2\right], \tag{A1.23}$$

where $P_{daily}$ is the daily average above-canopy PAR flux ($\mu$mol m$^{-2}$ s$^{-1}$) and $\varphi$ is the non-dimensional above-canopy PAR transmission from

$$\phi = \frac{P_{ac}}{(\sin(a)\,P_{toa})}, \tag{A1.24}$$

where $P_{ac}$ is the above-canopy PAR and $P_{toa}$ is the PAR flux ($\mu$mol m$^{-2}$ s$^{-1}$) at the top of the atmosphere estimated using

$$P_{toa} = 3000 + 99\cos\left(6.28\frac{(DOY - 10)}{365}\right), \tag{A1.25}$$

where DOY is the day of the year. Finally the factor accounting for temperature variations $\gamma_T$ is calculated by

$$\gamma_T = \frac{E_{opt}C_{T2}\exp(C_{T1}x_1)}{(C_{T2} - C_{T1}(1 - \exp(C_{T2}x_1)))}, \tag{A1.26}$$

where $C_{T1} = 80$ and $C_{T2} = 200$ are empirical coefficients, $E_{opt}$ is calculated from

$$E_{opt} = 1.75\exp\left(0.08(T_{daily} - 297)\right), \tag{A1.27}$$

where $T_{daily}$ is the daily average air temperature (K) representative of the simulation period, and $x$ from $\gamma_T$ is calculated by

$$x_1 = \frac{[\left(\frac{1}{T_{opt}}\right) - \left(\frac{1}{T_{hr}}\right)]}{0.00831}, \tag{A1.28}$$

where $T_{hr}$ is the hourly average air temperature (K), and $T_{opt}$ is calculated from

$$T_{opt} = 313 + \left(0.6\left(T_{daily} - 297\right)\right). \tag{A1.29}$$

## A1.4 Basic reactions of ozone formation and loss

The basic synthesis and decomposition of $O_3$ using the example of $NO_x$, where $O(^3P)$ represents ground-state atomic oxygen, is as follows:

$$NO_2 + hv \xrightarrow{\lambda < 400\ nm} NO + O(^3P) \tag{A1.31}$$

$$O(^3P) + O_2 + M \rightarrow O_3 + M \tag{A1.32}$$

$$NO + O_3 \rightarrow NO_2 + O_2. \tag{A1.33}$$

The degradation reaction of VOCs initiated by the hydroxyl radical (OH) produces $HO_2$ and $RO_2$ radicals as shown below using a generic hydrocarbon ($RCH_3$). Sources of OH radicals include from the reaction of water with excited atomic oxygen from the photolysis of $O_3$ (A1.34) or from the reaction of $HO_2$ with NO in polluted environments (A1.40):

$$O_3 + hv \xrightarrow{\lambda < 315\ nm} O_2 + O(^1D) \tag{A1.34}$$

$$O(^1D) + H_2O \rightarrow 2OH. \tag{A1.35}$$

The OH radical then oxidises the hydrocarbon:

$$OH + RCH_3 \rightarrow H_2O + R\dot{C}H_2 \tag{A1.36}$$

$$R\dot{C}H_2 + O_2 + M \rightarrow RCH_2O\dot{O} + M \tag{A1.37}$$

$$RCH_2O\dot{O} + NO \rightarrow RCH_2\dot{O} + NO_2 \tag{A1.38}$$

$$RCH_2\dot{O} + O_2 \rightarrow HO_2 + RCHO \tag{A1.39}$$

$$HO_2 + NO \rightarrow OH + NO_2, \tag{$A$1.40}$$
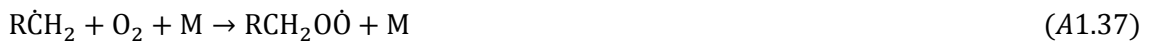
wherein the $HO_2$ and $RO_2$ radicals convert NO to $NO_2$ without using $O_3$ (Equations A1.38 and A1.40). As per Equation A1.31, $NO_2$ then photolyses to form additional $O_3$, which overall results in a net $O_3$ production.

# Appendix II

Additional papers are listed below to which A. Valach has contributed.

## A2.1 Meteorology, air quality, and health in London: The ClearfLo project

The work presented in Papers I and II was made as part of the Clean Air for London campaign funded by NERC during 2011/2012. The measurements are summarised along with additional trace gas measurements in the gas-phase section of this paper. This paper was submitted to the Bulletin of the American Meteorological Society, accepted on 30 Jul 2014 and published in May 2015.

**Amy C. Valach (Lancaster University):** Provided data, results and contributed to the manuscript.

# METEOROLOGY, AIR QUALITY, AND HEALTH IN LONDON
## The ClearfLo Project

BY S. I. BOHNENSTENGEL, S. E. BELCHER, A. AIKEN, J. D. ALLAN, G. ALLEN, A. BACAK, T. J. BANNAN, J. F. BARLOW, D. C. S. BEDDOWS, W. J. BLOSS, A. M. BOOTH, C. CHEMEL, O. COCEAL, C. F. DI MARCO, M. K. DUBEY, K. H. FALOON, Z. L. FLEMING, M. FURGER, J. K. GIETL, R. R. GRAVES, D. C. GREEN, C. S. B. GRIMMOND, C. H. HALIOS, J. F. HAMILTON, R. M. HARRISON, M. R. HEAL, D. E. HEARD, C. HELFTER, S. C. HERNDON, R. E. HOLMES, J. R. HOPKINS, A. M. JONES, F. J. KELLY, S. KOTTHAUS, B. LANGFORD, J. D. LEE, R. J. LEIGH, A. C. LEWIS, R. T. LIDSTER, F. D. LOPEZ-HILFIKER, J. B. MCQUAID, C. MOHR, P. S. MONKS, E. NEMITZ, N. L. NG, C. J. PERCIVAL, A. S. H. PREVOT, H. M. A. RICKETTS, R. SOKHI, D. STONE, J. A. THORNTON, A. H. TREMPER, A. C. VALACH, S. VISSER, L. K. WHALLEY, L. R. WILLIAMS, L. XU, D. E. YOUNG, AND P. ZOTTER

The Clean Air for London (ClearfLo) project provides integrated measurements of the meteorology, composition, and particulate loading of the urban atmosphere in London, United Kingdom, to improve predictive capability for air quality.

## A2.2 Eddy-covariance data with low signal-to-noise ratio: time-lag determination, uncertainties and limit of detection

VOC flux measurements from central London (Paper II) were used to develop and test a new method of processing eddy covariance data with low signal-to-noise ratios in order to reduce the uncertainty and avoid significant bias of the fluxes. This method was applied to calculate the fluxes for both Paper II and III.

This paper was submitted on 26 Jan 2015, published in Atmospheric Measurement Techniques Discussions on 18 Mar 2015 and is currently undergoing the review process.

**Amy C. Valach (Lancaster University):** Provided data, assisted in method testing and contributed to the manuscript.

Atmospheric Measurement Techniques
Open Access
Discussions

AMTD

8, 2913–2955, 2015

# Eddy-covariance data with low signal-to-noise ratio: time-lag determination, uncertainties and limit of detection

Eddy-covariance data with low signal-to-noise ratio

B. Langford et al.

B. Langford[1], W. Acton[2], C. Ammann[3], A. Valach[2], and E. Nemitz[1]

[1]Centre for Ecology and Hydrology, Bush Estate, Penicuik, EH26 0QB, UK
[2]Lancaster Environment Centre, Lancaster University, Lancaster, LA1 4YQ, UK
[3]Agroscope Research Station, Climate and Air Pollution Group, Zürich, Switzerland

Discussion Paper | Discussion Paper | Discussion Paper | Discussion Paper

| Title Page | |
| --- | --- |
| Abstract | Introduction |
| Conclusions | References |
| Tables | Figures |
| I◀ | ▶I |
| ◀ | ▶ |
| Back | Close |
| Full Screen / Esc | |
| Printer-friendly Version | |
| Interactive Discussion | |

## A2.3 Canopy-scale flux measurements and bottom-up emission estimates of volatile organic compounds from a mixed oak and hornbeam forest in northern Italy

This paper reports the fluxes and mixing ratios of biogenic volatile organic compounds above a mixed oak and hornbeam forest in Bosco Fontana, northern Italy. Mixing ratios were measured by proton transfer reaction mass spectrometer (PTR-MS) and fluxes calculated using the method of virtual disjunct eddy covariance. Measurements were made as part of the ECLAIRE campaign (1 Jun to 11 Jul 2012) of the European Framework Programme 7. BVOC fluxes and mixing ratios were also recorded using a proton transfer reaction-time of flight-mass (PTR-ToF-MS) spectrometer and comparisons of PTR-MS with PTR-ToF-MS results showed that isoprene fluxes had very good agreement while monoterpene fluxes were slightly overestimated by the PTR-MS. A basal isoprene emission rate was calculated using the MEGAN isoprene emissions algorithms (Guenther *et al.* 2006). Leaf level emissions of isoprene and monoterpenes recorded using GC-MS combined with a detailed tree species distribution map for the site (Dalponte *et al.*, 2007) allowed scaled up fluxes (bottom-up method) to be compared with the top-down canopy scale flux measurements. For monoterpenes, the two methods compared well, but the bottom-up approach significantly underestimated the isoprene flux, compared with the top-down measurements.

This work will shortly be submitted to Atmospheric Chemistry and Physics for publication.

**Amy C. Valach (Lancaster University):** Independently operated the instrument in Bosco Fontana for a period of 3 weeks and assisted with site setup, maintenance and data collection of additional measurements within the campaign, as well as contributed to the manuscript.